STRAIGHTFORWARD SYNTHESIS OF POLYCARBONATE MATERIALS FROM GLUCOSE TOWARDS BIOMEDICAL AND ENGINEERING APPLICATIONS

A Dissertation

by

SIMCHA E. FELDER

Submitted to the Office of Graduate and Professional Studies of
Texas A&M University
in partial fulfillment of the requirements for the degree of

DOCTOR OF PHILOSOPHY

Chair of Committee,	Karen L. Wooley
Committee Members,	Janet Blümel
	Lei Fang
	Melissa A. Grunlan
Head of Department,	Simon W. North

December 2018

Major Subject: Chemistry

ABSTRACT

Carbohydrates are fundamental building blocks for natural polymers; their bioavailability, chemical functionality, and stereochemical diversity make them attractive starting materials for the development of new synthetic polymers. This dissertation describes the development of polycarbonate materials from derivatives of one such carbohydrate, D-glucopyranoside. Several novel monofunctional and multifunctional monomers were synthesized to produce linear and branched/crosslinked polymers. The regiochemical and stereochemical sophistication inherent to carbohydrates was harnessed in each project to study the effects on chemical reactivity of the monomers and on physicochemical properties of the resulting polymers.

A library of linear poly(glucose carbonate)s (PGCs) was synthesized from a single monomer, methyl 4,6-*O*-benzylidene-2,3-*O*-carbonyl-α-D-glucopyranoside (MBGC), *via* ring-opening polymerization (ROP) followed by post-polymerization reactions, to determine the effect of repeat unit structure and molar mass on polymer properties. Beyond the production of homopolymers, MBGC was further employed to afford amphiphilic copolymers and block copolymers *via* ROP with a small molecule initiator and a macroinitiator, respectively. Within these different polymeric systems, a wide range of thermal decomposition temperatures (221-339 °C), glass transition temperatures (-48-222 °C, T_g), and water contact angles (38-128°) were achieved. Further, assembly of the amphiphilic copolymers and block copolymers under aqueous conditions revealed interesting morphological differences as a function of composition.

In efforts to produce multifunctional monomers for branched/crosslinked polymeric materials, a difunctional cyclic carbonate monomer methyl 2,3:4,6-di-*O*-carbonyl-α-D-glucopyranoside (MGDC) for ROP, as well as a synthetic methodology for multifunctional alkene-containing monomers for thiol-ene photopolymerization were developed. ROP of MGDC was studied by varying the conditions to produce branched and linear homopolymers. In addition to homopolymerization, MGDC was also used as a comonomer to create branched/crosslinked PGCs. The multifunctional alkene-containing monomers were copolymerized with a variety of multifunctional thiols to produce networks with a range of thermal and physical properties depending on the comonomer composition, with T_gs from -17 to 58 °C and storage moduli from 0.4 to 30 MPa.

This dissertation focuses on the development of monomers that will allow for the straightforward synthesis of glucose-based polycarbonates. Multiple monomers and polymerization techniques were utilized in this work to produce polymers with varied architectures. Throughout, the effect of different functionalities and regiochemistries of the monomers were correlated to the properties of the resultant polymers. Overall these highly tunable, glucose-based degradable polymeric platforms hold great promise for the sustainable production of advanced engineering materials, biomaterials, and composites for implementation in a diverse range of applications, from medicine to electronics, and many others.

DEDICATION

To the family, friends, and educators who have always believed in me and pushed me to reach my highest potential.

ACKNOWLEDGEMENTS

I would first like to thank my advisor, Professor Karen Wooley. Her encouragement and support have allowed me to pursue my passions in chemistry and molded me into the scientist I am today. Karen has taught me to always dig into my chemistry and push to really understand the data and to never be satisfied with a weak understanding. I have been fortunate to learn from her and in being a part of the research group I have grown not only as a scientist, but as a person.

Secondly, I would like to thank my committee Professors Janet Blümel, Lei Fang, and Melissa A. Grunlan. Their technical expertise, advice, and questioning, particularly during the milestone events of my study have provided me with new manners to view my work and directions of useful study. I would also like to thank my all my collaborators for their help guiding and producing this work. With special thanks to Professor Scott M. Grayson, and McKenna Redding (Tulane University) for their help and insight into the chemistry of the polymers developed. I am extremely grateful to the Wooley group as a whole, it has been my great honor to learn from and with you during my time in the lab. I would like to offer particular thanks to those current and former members who left an indelible mark on myself and my science Amandine Noel, Yannick Borguet, Phil Imbesi, Ritu Shrestha, Marco Giles, Rachel Letteri, Lu Su, Soon-Mi Lim, Kevin Wacker, Peter Wang, Richen Li, Mei Dong, Yue Song, Brooke Versaw, Dan Dobbins, and Jessica Huang. Your friendship and advice are truly appreciated. I would like to thank the current and past Wooley lab staff and managers (Justin Smolen, Sherry Melton, Andy Moutray, and Jeff Raymond) for all they do to keep Wooley lab going and producing. Finally, I would like to

thank my team in the NSF Innovation Corps project, Dr. William Howell, Dr. Ashlee Jahnke, and Dr. Karen Wooley. Your support in that endeavor and all others has been greatly appreciated.

It would be remiss of me to not acknowledge all of the Administrative and Support Staff in the Chemistry Department, particularly the Graduate Office (Sandy Horton, Valerie McLaughlin, Dr. Joanna Goodey-Pellois, and Dr. Simon North), Business Operations (Ron Carter, Curtis Lee, Angie Stickley, Judy Ludwig, Julie Zercher, Angie Medina, and Melvin William), NMR facilities (Drs. Greg Wylie, Vladimir Bakhmoutov, Doug Elliott), Mass Spectrometry (Drs. Bo Wang, Doyong Kim, Yohannes Rezenom, Mr. Michael Raulerson, and Ms. Vanessa Santiago), Electronics (Tim Pehl), Glass Blowing (Bill Merka), Machine Shops (Bill Seward), and IT (Steve Tran, Daven Kostroun, Mike Green) – I am grateful for all that you have done, especially the work that often goes unnoticed by the students but keeps the Chemistry Department at Texas A&M functioning.

Finally I would like to thank my family and friends – your support during the trials and tribulations of life, and particularly graduate school, have given me great strength and allowed me to pursue my passions. I appreciate your constant belief in me, particularly when I did not believe in myself or my abilities. I will be forever indebted to you for your love, friendship, and guidance.

CONTRIBUTORS AND FUNDING SOURCES

Contributors

This dissertation was supervised by a committee of researchers at Texas A&M: Prof. Karen L. Wooley (advisor) of the Departments of Chemistry, Chemical Engineering, and Materials Science and Engineering; Prof. Janet Blümel (committee member) of the Department of Chemistry; Prof. Lei Fang (committee member) of the Departments of Chemistry, and Materials Science and Engineering; Prof. Melissa A Grunlan (committee member) of the Departments of Biomedical Engineering, Chemistry, and Materials Science and Engineering.

In Chapter II, synthesis of the monomers and polymers was performed with the help of Dr. Amandine Noel of the Department of Chemistry. All matrix-assisted laser desorption ionization time-of-flight mass spectrometry experiments were performed by Ms. McKenna J. Redding of Tulane University under the supervision Prof. Scott M. Grayson of Tulane University, both of the Department of Chemistry.

In Chapter III, synthesis of monomers and polymers were performed with the help of Mr. Shota Osumi, of the Nippon Soda Co., Ltd. Dynamic light scattering, transmission electron microscopy, and atomic force microscopy measurements were assisted by Mr. Shota Osumi, Mr. Yen-Nan Lin, Mr. Hai Peter Wang, and Ms. Mei Dong, all of the Department of Chemistry.

In Chapter IV, the monofunctional monomer in the copolymerization study was synthesized by Ms. Yue Song of the Department of Chemistry. All matrix-assisted laser

desorption ionization time-of-flight mass spectrometry experiments were performed by Dr. Yohannes Rezenom of the Department of Chemistry.

In Chapter V, design and synthesis of the monomers and polymers was performed with the help of Dr. Ashlee A. Jahnke and Dr. William Howell of the Department of Chemistry. Differential scanning calorimetry was also run in part by Dr. Ashlee Jahnke.

In Chapter VI, synthesis of methyl 2,3-*O*-dibenzyl-4,6-*O*-carbonyl-α- D-glucopyranoside was performed with the help of Dr. Amandine Noel. The cell experiments were run by Dr. Soon-Mi Lim of the Department of Chemistry.

All other experiments were carried out independently by the student.

Funding Sources

The work in Chapter II was made possible by financial support from the National Science Foundation (grant numbers CHE-1410272, CHE-1610311, CHE-1412439, CHE-0619770 and the Graduate Research Fellowship Program), and the Welch Foundation through the W. T. Doherty-Welch Chair in Chemistry (A-0001).

The work in Chapter III was supported by the National Science Foundation (grant numbers CHE-1610311, DMREF-1629094, DMR-1507429), the Welch Foundation through the W. T. Doherty-Welch Chair in Chemistry (A-0001), and the Nippon Soda Co.

The work in Chapters IV and V was funded by the National Science Foundation (grant numbers CHE-1410272, CHE-1610311 and the Graduate Research Fellowship Program), and the Welch Foundation through the W. T. Doherty-Welch Chair in Chemistry (A-0001).

Graduate study was supported by a graduate merit fellowship from Texas A&M University.

The contents are solely the responsibility of the authors and do not necessarily represent the official views of the National Science Foundation, the Welch Foundation, Texas A&M University, or the Nippon Soda Co.

NOMENCLATURE

AC	Allyl chloroformate
AFM	Atomic force microscopy
BDBMA	1,4-Butanediol bis(mercaptoacetate)
BDT	2,3-Butanedithiol
COSY	Homonuclear correlation spectroscopy
Đ	Dispersity index
DBU	1,8-Diazabicyclo[5.4.0]undec-7-ene
DCM	Dichloromethane
DLS	Dynamic light scattering
DMA	Dynamic mechanical analysis
DMAP	4-Dimethylaminopyridine
DMF	*N*,*N*-Dimethylformamide
DMPA	2,2-Dimethoxy-2-phenylacetophenone
DMSO	Dimethyl sulfoxide
DP	Degree of polymerization
DPEHMP	Dipentaerythritol hexakis(3-mercaptoproprionate)
DSC	Differential scanning calorimetry
E'	Storage moduli
EDT	1,2-Ethane dithiol
FTIR	Fourier-transform infrared
GCEPC	Methyl 4,6-*O*-carbonyl-2-*O*-ethyloxycarbonyl-3-*O*-propargyloxycarbonyl-α-D-glucopyranoside

HDT	1,6-Hexanedithiol
HMQC	Heteronuclear multiple quantum coherence
HSQC	Heteronuclear single quantum coherence or heteronuclear single quantum correlation
LALS	Low-angle light scattering
MALDI-TOF MS	Matrix-assisted laser desorption ionization time-of-flight mass spectrometry
MBA	4-Methylbenzyl alcohol
MBGC	Methyl 4,6-*O*-benzylidene-2,3-*O*-carbonyl-α-D-glucopyranoside
$MGC_{2,3}$	Methyl 2,3-*O*-carbonyl-α-D-glucopyranoside
MGDC	Methyl 2,3:4,6-di-*O*-carbonyl-α-D-glucopyranoside
M_n	Number average molar mass
mPEG	Monomethoxy-monohydroxy-terminated poly(ethylene glycol)
M_w	Weight average molar mass
NMR	Nuclear magnetic resonance
PETMP	Pentaerythritol tetrakis(3-mercaptopropionate)
PGC	Poly(glucose carbonate)
PGCEPC	Poly(methyl 4,6-*O*-carbonyl-2-*O*-ethyloxycarbonyl-3-*O*-propargyloxycarbonyl-α-D-glucopyranoside)
$PMAc_2GC$	Poly(methyl 4,6-di-*O*-acetyl-2,3-*O*-carbonyl-α-D-glucopyranoside)
PMBGC	Poly(methyl 4,6-*O*-benzylidene-2,3-*O*-carbonyl-α-D-glucopyranoside)
PMGC	Poly(methyl 2,3-*O*-carbonyl-α-D-glucopyranoside)

RALS	Right-angle light scattering
RI	Refractive index
ROP	Ring-opening polymerization
SEC	Size exclusion chromatography
tBBA	4-*t*-Butylbenzyl alcohol
TBD	1,5,7-Triazabicyclo[4.4.0]dec-5-ene
T_d	Thermal decomposition temperatures
TEGBMP	Tetraethylene glycol bis(3-mercaptoproprionate)
TEM	Transmission electron microscopy
TFA	Trifluoroacetic acid
T_g	Glass transition temperature
TGA	Thermogravimetric analysis
THF	Tetrahydrofuran
TLC	Thin-layer chromatography
T_m	Melting transition temperature
TMPTMP	Trimethylolpropanyl tris(3-mercaptopropionate)
TU	N-[3,5-bis(Trifluoromethyl)phenyl]-N'-[(1R,2R)-2-(dimethylamino)cyclohexyl]-thiourea
UV	Ultraviolet

TABLE OF CONTENTS

Page

LIST OF FIGURES

Page

LIST OF TABLES

Page

CHAPTER I

INTRODUCTION

Polymeric materials have enabled many of the major technological advances of the last 50 years. Polymers are used in a variety of important applications including electronics, engineering materials, transportation, biomedical devices, and packaging. In these applications, plastics have provided significant improvements over previous materials used, allowing for more efficient production and robust, tunable properties through varying the polymeric architectures and structures. Because of these advantages, in the past 50 years there has been > 20× increase in the amount of virgin plastic produced each year using petroleum-based feedstocks.[1,2] Approximately 40% of these newly produced polymers are used in single-use packaging, such as drink bottles, household good containers, or food containers.[2] Following the end of the useful lifetime of these materials, they are disposed by the consumers and enter waste streams. It is estimated that, of these materials, 40% are landfilled, 15% are recycled into new materials, 15% are incinerated for energy recovery, and 30% do not enter regulated waste streams.[1-4] The materials that do not enter regulated waste streams are either inappropriately disposed, or are left to litter the environment. Approximately 8 million tons of this plastic material will enter the Earth's waterways each year,[1,4] and can cause significant damage to the ecosystem, humans, and animals that rely on these waterways. Eventually the plastics in local waterways, such as rivers and streams, enter the open ocean, where they tend to aggregate and form what are generally referred to as garbage patches. One of the most well know of these is the "Great Pacific Garbage Patch"

in the Pacific Ocean.[5] It is estimated that 80,000 metric tons of trash is in the Pacific garbage patch, and that it spans 1.6 million square kilometers (roughly 3 times the size of France, or 2 times the size of Texas).[5] The majority of the plastic materials in the patch are not anticipated to degrade over time to small molecules, but will breakdown physically into smaller particulates.[6,7] Depending on the size of these particles, they are referred to as microplastics or nanoplastics. The effects of these small plastic particulates on the ecosystem is not fully understood, but several studies have demonstrated that these particulates accumulate in the flesh of various aquatic animals and may be a source of persistent organic pollutants.[3,8-11]

To alleviate the negative effects of plastic accumulation in the environment and provide materials for high value applications such as biomedical devices, research has been undertaken into the development of polymers with labile chemical bonds within the polymer chain. For applications that require degradability under general environmental conditions, chemical linkages sensitive to aqueous environments hold important potential as linkages along the polymer backbone. Several different types of chemical bonds are able to degrade under hydrolytic conditions, such as acetals, esters, carbonates, phosphoesters, and others. Significant work has been completed to include these linkages into the backbones of various polymers.[12-18] Monomers amenable to traditional radical polymerization techniques have been developed to insert these different linkages into polymers,[17,19,20] while other polymerization methodologies have also been developed that allow for the direct incorporation of these linkages into the polymer backbone.[21,22] Using these various types of polymer materials allows for not only physical degradation of the plastic materials, but also chemical degradation into small molecules that may be more readily cleared from the

environment. The ability of these polymers to degrade into small molecules adds different challenges and factors to the choice and development of new polymeric materials. One of these factors is the small molecules produced upon degradation of the polymer, and ensuring that these degradation products cause minimal damage to the environment and exhibit negligible toxicity as the polymer degrades.

An attractive characteristic of both natural and synthetic polymers derived from renewable feedstocks is that they can undergo degradation by photochemical, thermal, enzymatic, or hydrolytic processes into small molecules that are presumed to be relatively non-toxic to the environment. Currently many chemicals that are vital to industrial and academic research are traditionally produced from petrochemical sources, and as the scarcity of petroleum increases, there is a need to identify new sources for commodity chemicals. A variety of target molecules have been identified as high-value added chemicals that can be derived from biomass, with many being targeted as "drop-in" replacements for current commodity chemicals produced from petroleum sources.[23-29] In the past 20 years, hundreds of companies have been formed with the focus of producing commodity chemicals and materials from biosources. The commodity chemicals that are produced from natural sources by these companies can in many cases be directly used as monomers to produce traditional polymeric materials. One well known example of this is from the Coca-Cola® Company and their use of biosourced ethylene glycol in the production of polyethylene terephthalate used in the PlantBottle®. As the field of sustainably sourced chemicals increases, naturally-derived polymers will have significant potential to address the desire of the public for more sustainable, but still fully functional polymeric materials. Biosourced polymers can be generated in two main methods: they can be isolated directly from Nature

(*e.g.*, polysaccharides, polynucleic acids, polypeptides, *etc*.) or used to produce naturally sourced monomers amenable to a variety of polymerizations. Natural products can be isolated from plants, animals, fungi, bacteria, *etc*. and include a variety of classes of chemicals including saccharides, amino acids, neolignans, cyclitols, flavinoids, and many others.

A Department of Energy report on "Top Value Added Chemicals from Biomass" identified 30 target molecules from biosources; from these 30, a further set of 12 molecules were identified as molecules that can serve as drivers for the development new biorefinery operations. All 12 molecules were derived from saccharide starting materials. Saccharides, also called carbohydrates or sugars (these three names will be used interchangeably throughout this dissertation), are a class of natural products with the general chemical formula $C_nH_{2n}O_n$, and can range from simple monosaccharides (glucose, fructose, *etc*.) to complex polymeric architectures (starch, DNA, *etc*.). Sugars play a variety of different roles in living organisms, including energy storage, transmission of genetic information, as well as structural formation. Saccharides are attractive starting materials in the production of renewable materials; as the fundamental building blocks of different natural polymers, they have several biomass sources including potatoes, rice, beets, sugar cane and wood.[30-32] In addition, the industrial fermentation of saccharides yields several renewable chemicals on commodity scales, such as lactic acid, succinic acid and ethanol.[15,31,32] Beyond their ability to be used as precursors for a range of different molecules, the wide range of stereochemical diversity, regioselectivity, and high degree of functionality of carbohydrates make them attractive starting materials in the synthesis of functional molecules. Carbohydrate linkages have been included in the backbones and side chains of a variety of different polymeric

architectures, to make use of their structural diversity and favorable bioactivity.[24,33-40] Polymers synthesized *via* radical polymerization techniques include sugars as side chain functionalities to act as targeting moieties for various biomedical applications.[41,42] These materials, however, have non-degradable polymer backbones, hindering clearance from the body or environment. Therefore, significant efforts have been put towards the development of monomers and polymerization methods that allow for the inclusion of the sugar molecules in the backbones of well-defined polymeric materials.

Combining the advantageous properties of polycarbonates with natural product-based monomers has great potential for the production of benign degradable polymers. Upon degradation of a polycarbonate, the small molecule by-products will be CO_2 and a diol, these are expected to be more easily tolerated by the environment than the degradation products of some other classes of degradable polymers which can cause inflammation. Polycarbonates are widely used materials in a range of technically challenging and demanding applications, from impact resistant materials to commodity goods to biomedical devices.[43-46] Multiple polymerization techniques can be used to synthesize polycarbonates in a straightforward manner. Most commonly used are condensation polymerizations (such as those involving phosgene analogs and diols),[40,47,48] transesterification of a carbonate comonomer with a diol monomer,[49] copolymerization of CO_2 with ring-opening of an epoxide,[50-54] or ring-opening polymerizations (ROP) of cyclic carbonate monomers.[37,55-60] Of these polymerization techniques, ROP of currently provides the greatest control over the molar mass, selectivity of the reaction and, ultimately, over the properties of the final materials.

ROP is a powerful controlled polymerization technique that allows for the straightforward inclusion of heteroatoms into the backbone of polymer chains. Several different types of polymers can be synthesized *via* ROP, including polyesters, polyamides, polyethers, polycarbonates, and others.[61] In recent years, a large variety of catalysts has been developed for ROP of cyclic monomers.[55,62,63] Organocatalysts are becoming competitive with inorganic catalysts, both in price and reactivity, overcoming toxicity concerns and difficulties with the availability of metal-based catalysts.[21,22,55,57,63-65] Further, the ability of ROP to include heteroatoms in the polymer backbone makes it a powerful tool not only for the inclusion of degradable chemical linkages, but also saccharides into polymer backbones. The combination of a degradable polymer backbone having biocompatible sugars as part of the repeat unit offers high potential of hydrolytic degradation into easily metabolized by-products. Although there is interest in the use of sugars in a variety of polymeric architectures and morphologies, this dissertation will focus on the production of poly(saccharide carbonate)s, which have been produced from several different carbohydrates and their derivatives, including xylose,[47,66,67] deoxyadenosine,[68] isosorbide,[49] and pyranosides.[37,40,48,56,59,60,69-74] Glucose is of particular interest to include in polymeric materials, since as the main component of cellulose it is able to be isolated commercially in large quantities. The Wooley laboratory has a significant interest in the development of synthetic methodologies for the preparation of well-defined poly(glucose carbonate)s, tuning their properties and investigating their implementation in a diverse range of applications.[48,75-78]

This dissertation will describe the design of scalable and robust synthetic methodologies for the production of cyclic glucose carbonate monomers for ROP as well as

a carbonate-containing monomer for a thiol-ene photopolymerization (Figure I.1). Several guidelines have encompassed the synthesis of the glucose carbonate monomers and polymers, including the use of simple, scalable and translatable chemistries. The monomers and polymers are designed such that the resulting material properties are easily manipulated by further functionalization. Additionally, each study was designed to understand the effect of different repeat unit structures, molar masses, and polymeric architectures on the final polymer properties. It was an aim of this work to increase the understanding and usefulness of glucopyranosides in the field of polymer science and lay a foundation from which new chemistries, engineering, and biomedical applications may be explored.

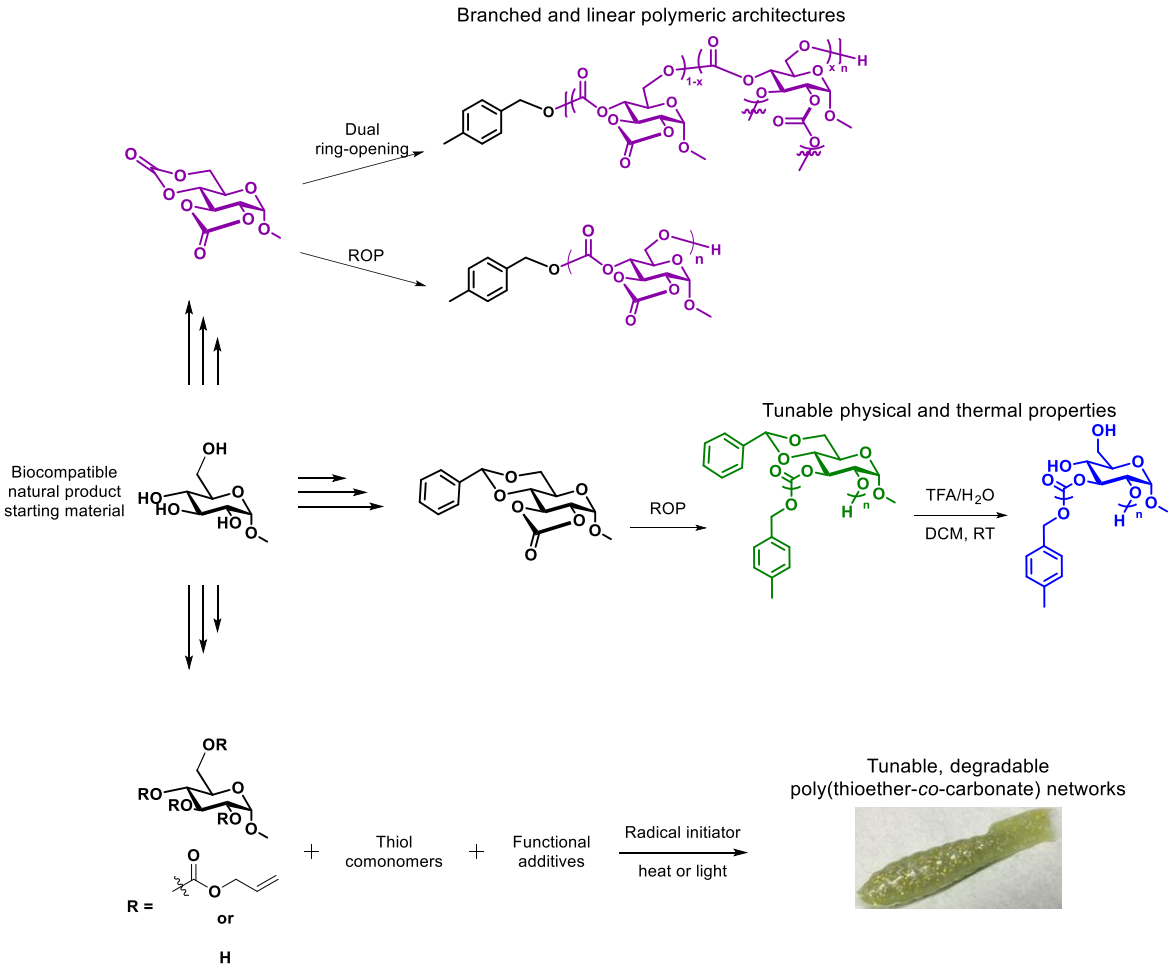

Figure I.1. Synthesis of carbonate monomers from methyl α-D-glucopyranoside.

CHAPTER II

ORGANOCATALYZED ROP OF A GLUCOPYRANOSIDE DERIVED 5-MEMBERED CYCLIC CARBONATE[1]

2.1 Introduction

Polycarbonates, predominantly composed of phenolic-type monomers, *e.g*. bisphenol A, are fundamental mainstay materials that serve broad purposes in technically demanding conditions, for instance automotive components and commodity materials. However, aliphatic polycarbonates are also of significant value. Over the past decade, aliphatic polycarbonates have garnered increasing interest for use in biomedical applications, primarily because of their tissue compatibility, potential degradation *in vivo*, and benign degradation products.[43-45] The wide range of stereochemical diversity and high degree of functionality of carbohydrates, as well as the ability to perform functional group transformations and combine different carbohydrates, make them attractive starting materials in the synthesis of monomers that can be converted into polymer materials with a diversity of structures and properties. Moreover, due to the extensive bioavailability of carbohydrates, their use as feedstocks for the synthesis of polycarbonates can reduce the dependence on petrochemical starting materials and offers a high potential of hydrolytic degradation into easily metabolized byproducts. Significant work has been done to produce

[1]Adapted with permission from "Organocatalyzed ROP of a Glucopyranoside Derived Five-Membered Cyclic Carbonate" by Felder, S. E.; Redding, M. J.; Noel, A.; Grayson, S. M.; Wooley, K. L., *Macromolecules*, **2018**, *51*(5), 1787-1797. Copyright 2018 American Chemical Society

poly(saccharide carbonate)s from various carbohydrates and their derivatives, including xylose,[47,66,67] deoxyadenosine,[68] isosorbide,[49] and pyranosides.[37,40,48,56,59,60,69-74]

Polycarbonates are most commonly synthesized by condensation polymerizations (such as those with phosgene analogs and a diol),[40,47,48] transcarbonation of a carbonate comonomer with a diol monomer,[49] copolymerization of carbon dioxide with the ring opening of an epoxide,[50-52] or ring-opening of cyclic carbonate monomers.[37,55-60] Among these methods, ring-opening polymerization (ROP) provides the greatest control over the molar mass, selectivity of the reaction and, ultimately, over the properties of the final materials. In recent years, a large variety of catalysts has been developed for the ROP of cyclic carbonates.[55,62] Organocatalysts are becoming competitive with inorganic catalysts, both in price and reactivity, overcoming the toxicity, and difficulties with the availability of metal-based catalysts.[55,57,63] However, their application in certain ROPs are still limited by monomer reactivity. For instance, the polymerization of 5-membered cyclic carbonate monomers is challenging under common catalytic conditions. Monomers of this ring size, for esters or carbonates, generally do not undergo polymerization,[79] or even ring opening to produce acyclic molecules under common catalytic conditions.[80-84] In cases where polymerization was achieved, side reactions, such as the elimination of CO_2 during the polymerization leading to a poly(carbonate-*co*-ether) rather than the desired polycarbonate, were also a main issue.[85-87] One of the early examples of an efficient 5-membered ROP leading to a polycarbonate was the anionic polymerization of methyl 4,6-*O*-benzylidene-2,3-*O*-carbonyl-α-D-glucopyranoside (MBGC), a fused *trans*-cyclic carbonate.[69] In this anionic ROP, the effect of solvent, monomer concentration, and initiator were studied thoroughly by the Endo and Haba groups.[69,72,73,88] The selective ROP of other *trans*-fused ring carbonate

monomers has been investigated further by Guillame and Carpentier *et al.*, using several catalysts, including an organocatalyst.[89-91] The additional strain from the cyclic carbonates being in a *trans*-fused bicyclic conformation was likely the driving force for these polymerizations. These interesting results guided us to examine the ability of MBGC to undergo organocatalyzed ROP.

Herein, we report a study of the organocatalytic scope and a kinetic analysis of the MBGC polymerization to confirm its controlled nature. Optimized experimental conditions were then applied to the synthesis of several molar masses of PMBGC to explore the thermophysical properties. The acid sensitivity of the benzylidene protecting group was then used to generate the deprotected, polyhydroxyl-presenting polycarbonates, which were further functionalized. Finally, the physical properties and hydrolytic stabilities of the synthesized polymers were analyzed and compared in terms of molar mass and side chains (benzylidene acetal, hydroxyl, or acetyl), which revealed interesting mechanistic differences under acidic vs basic aqueous conditions.

2.2 Results and Discussion

On the basis of our interest in the production of well-defined poly(glucose carbonate)s,[48,56,58,71] and reported ROPs of 5-membered cyclic carbonates,[69,72,73,81,88-90] we investigated the polymerization of a five-membered cyclic carbonate of glucose under a range of organocatalytic conditions, the post-polymerization modification of the polymers produced, and their thermophysical and degradation properties

2.2.1 Monomer synthesis

The methyl 4,6-*O*-benzylidene-2,3-*O*-carbonyl-α-D-glucopyranoside (MBGC) monomer may be synthesized from the commercially available methyl 4,6-*O*-benzylidene-α-D-glucopyranoside by establishment of a five-membered cyclic carbonate through the hydroxyl groups at positions 2 and 3. This carbonylation reaction has been reported to proceed by using excess (30 equivalents) ethyl chloroformate[92] or 2 equivalents of phosgene.[93] To overcome the safety hazards associated with gaseous phosgene, we chose to employ equivalent phosgene, generated *in situ* from triphosgene, as the carbonylation agent. Several other carbonylation agents were tested, and none was able to produce the cyclic product in an acceptable isolated yield (Table II.3 and Figure II.28). Although, the use of triphosgene requires additional safety precautions, as it degrades into phosgene, the nearly quantitative yield and ease of purification made this route our favored method of synthesis. All relevant NMR and IR spectra for the monomer and polymers can be found in Figures II.10-27.

2.2.2 Organocatalytic scope of polymerization and kinetic study

Literature precedent suggested the five-membered cyclic carbonate would require highly active catalyst regimes.[69,85,87,90] Consequently, the polymerization of MBGC (initiator:monomer, 1:50) was initially tested using a range of organocatalysts among the most active organobase catalysts (1,8-diazabicyclo[5.4.0]undec-7-ene (DBU), a mixture of DBU and *N*-[3,5-bis(trifluoromethyl)phenyl]-*N*′-[(1*R*,2*R*)-2-(dimethylamino)cyclohexyl]thiourea (TU), a mixture of DBU and TBD, or TBD)[55,57] Surprisingly, all the conditions tested were able to polymerize MBGC with reasonable molar masses (2.9–5.8 kDa, as measured by $CHCl_3$ SEC), narrow dispersities (*Đ*, 1.19–1.29), and

good yields (63–78%, Table II.1 and Figure II.1). The *trans*-fused bicyclic configuration of the cyclic carbonate generates strain energy and was likely responsible for the feasibility of the ROPs. As expected, higher catalyst loadings (4 mol % *vs*. 2 mol %) gave slightly higher molar masses over the same reaction time, as did more active catalyst regimes (TBD *vs.* DBU). The highest M_ns and lowest $Đ$ were achieved with TBD as the catalyst. The molar masses and $Đ$ were initially measured *via* SEC with $CHCl_3$ eluent (this was necessary to ensure separation between the SEC signals for the eluent injection and the lowest molar mass polymers). While the M_ns determined by this SEC were lower than anticipated, the trend in MW is valid, indicating that TBD produced the largest polymers at the 5 h time point, relative to the other organobase catalyst systems. Therefore, the kinetics of the polymerization were studied using TBD.

Table II.1. Effect of organocatalyst system on the ROP of MBGC, each measured at a time point of 5 h.[a]

Catalyst	Catalyst loading (mol%)	M_n[b] (kDa)	$Đ$[b]	Yield[c] (%)
DBU	2	3.8	1.23	63
	4	5.0	1.25	70
DBU/TU	2	2.9	1.24	63
	4	3.1	1.23	78
TBD/DBU	2	4.8	1.29	74
	4	5.7	1.20	68
TBD	2	4.5	1.20	78
	4	5.8	1.19	65

[a]$[MBGC]_0$ = 0.50 M, MBGC:MBA = 50:1, 30 °C, 5 h, in DCM. [b]Measured with SEC ($CHCl_3$ eluent) calibrated with polystyrene standards. [c]After three precipitations into methanol, no monomer detected by SEC.

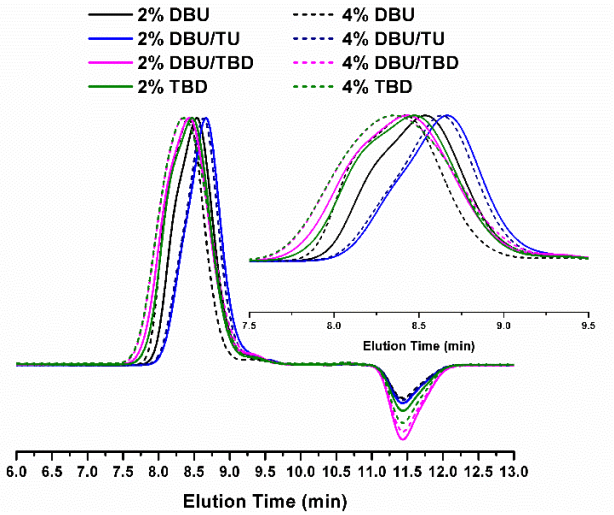

Figure II.1. SEC traces ($CHCl_3$ eluent) for the polymerization of MBGC with various organocatalysts. $[MBGC]_0$ = 0.50 M, MBGC:Initiator = 50:1, 30 °C, 5 h, in DCM. Inset shows the same traces.

The kinetics of the ring-opening of MBGC were studied using 4-methylbenzyl alcohol (MBA) as an initiator (initiator:monomer, 1:50), and TBD as a catalyst (2 mol % to MBGC, Figure II.3 and Table II.4). The monomer conversion was monitored by SEC using an internal standard because significant overlap between monomer and polymer proton resonance frequencies was responsible for inaccurate conversion values by ^{1}H NMR. Naphthalene was chosen as an internal standard because of its compatibility with the reaction conditions and its unique signal in the SEC from monomer and oligomers. The polymerization had reached 50% conversion after 90 min and full conversion after 180 min. The SEC traces revealed monomodal signals during the polymerization, which progressed to lower elution times as the monomer was consumed. The polymer molar mass grew linearly with the conversion of monomer, while maintaining relatively low $Đ$. As expected, a kinetic plot of $ln\frac{[M]_0}{[M]}$ *versus* time confirmed the controlled nature of the polymerization and indicated the polymerization was pseudo-first-order with respect to the monomer

(Figure II.2). Comparing these data to the polymerizations described by our group of six-membered glucose carbonate monomers, the polymerization overall required significantly longer time to reach full conversion, supporting the lower reactivity of the five-membered glucose carbonate monomer.[71] As with the investigation of the organocatalytic scope, the molar mass values determined are lower than expected; however, use of the SEC with $CHCl_3$ eluent was necessary as it was the only instrument accessible that provided separation between the retention volumes for the monomer, internal standard, and the growing polymer chain, without overlap with the eluent injection negative peak. The conversion values were determined independently and are not subject to potential errors from the artificially reduced MWs determined; therefore, the trends determined from these data are valid (Figure II.2). Absolute molar mass determination was attempted using matrix-assisted laser desorption ionization time-of-flight mass spectrometry (MALDI-TOF MS, Figures II.5, 23, 32, 33); however, the data were not accurate because of the relatively high *Đ*s and the resulting non-Gaussian distributions observed in the MALDI-TOF spectra for several of the samples.

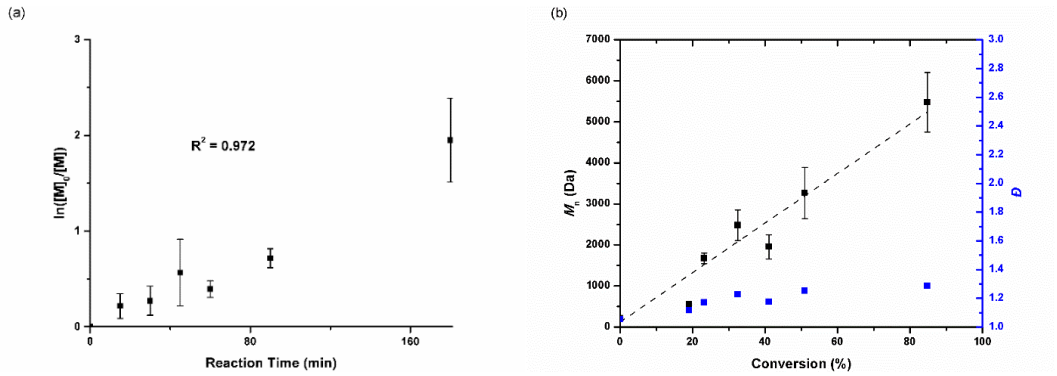

Figure II.2. (a) Kinetic plot of $\boldsymbol{ln\frac{[M]_0}{[M]}}$ *vs.* reaction time. (b) M_n (left axis, black) and *Đ* (right axis, blue) *vs.* monomer conversion of MBGC using TBD (catalyst), MBA (initiator), and naphthalene (internal standard). Data for both plots were obtained using SEC (UV detector, $CHCl_3$ eluent), n = 3.

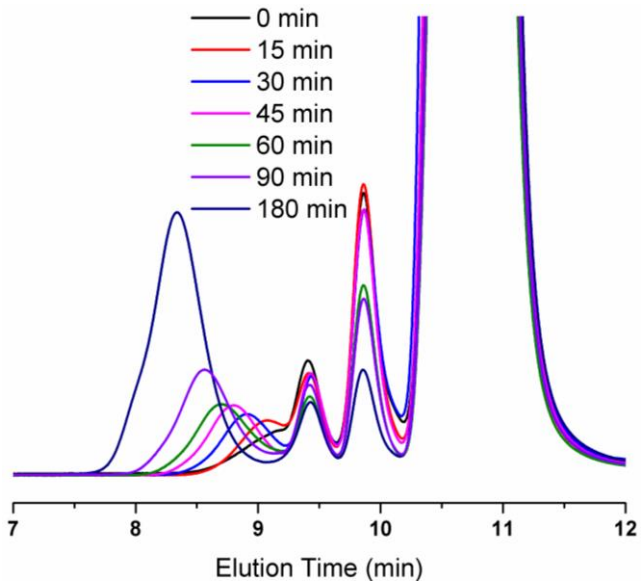

Figure II.3. SEC traces ($CHCl_3$ eluent, UV detector) for the kinetic analysis of the MBGC polymerization. $[MBGC]_0$ = 0.50 M, MBGC:Initiator = 50:1, 30 °C, in DCM.

2.2.3 Polymer synthesis and post-polymerization modification

A series of PMBGCs with different degrees of polymerization were synthesized using MBA as initiator and TBD as catalyst (Table II.2). The breadth of PMBGC molar masses was then used to investigate the effect of the degree of polymerization on the thermophysical properties. Three of the PMBGC syntheses were conducted on a gram scale to allow for post-polymerization modification reactions and further investigations (Figure II.36). For these large-scale reactions, each polymer was obtained in good yield (>75%), with $Đ < 1.36$ (**2**, **3**, and **5**).

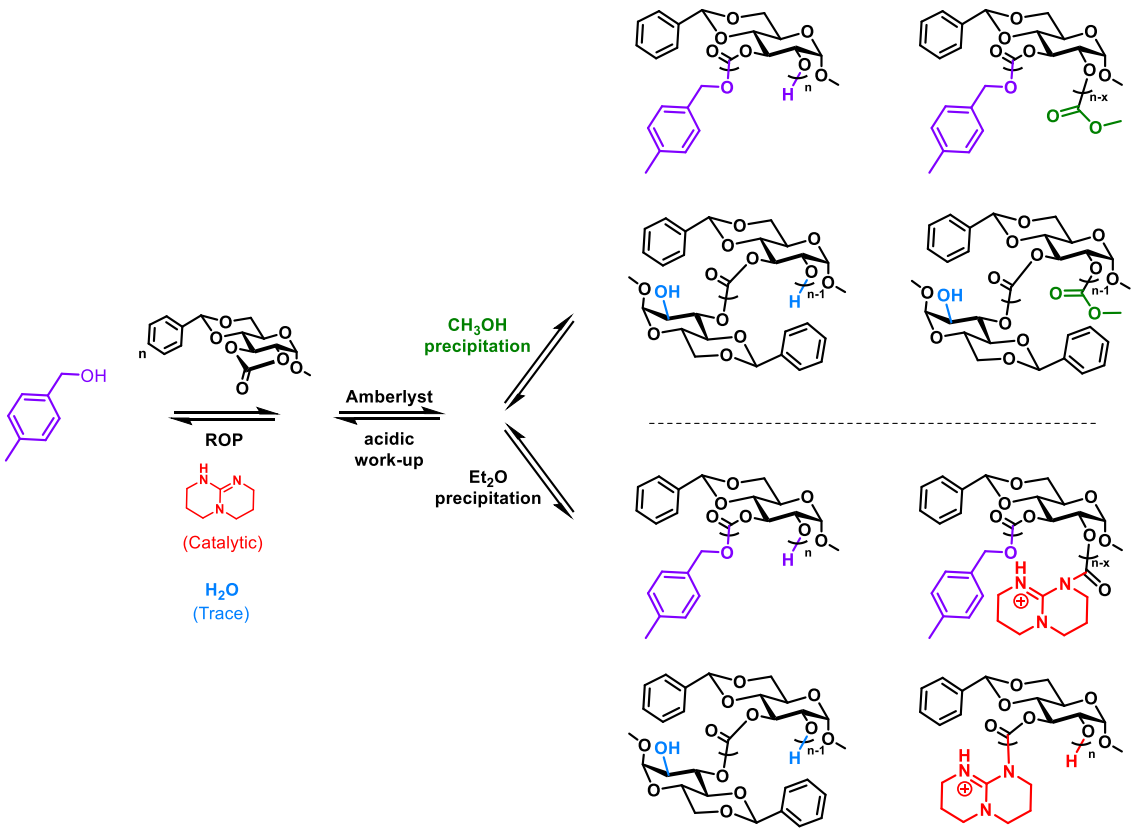

Figure II.4. Synthesis and purification *via* precipitation of PMBGC with MBA as intended initiator and TBD catalyst. Polymer structures shown are all supported by MALDI-TOF MS, Figures II.29-33, and are colored to match the initiating or terminating species (MBA – purple, water impurity – blue, TBD – red, methanol – green.

Analysis of the PMBGC samples by MALDI-TOF MS provided further insight into the mechanism of the polymerization. The mass spectra of the PMBGC samples exhibited narrow polymer distributions with the expected monoisotopic repeating unit of 308.10 Da (RU_{theor} = 308.09),[94] confirming CO_2 was not eliminated during the polymerization, and the benzylidene protecting groups were retained throughout the polymerization and acidic work-up (Figure II.5). Further examination of the data (Figure II.29) revealed the presence of multiple distributions, each with a 308.1 Da repeat unit, resulting from different initiating and terminating events (Figure II.4, 30, 31). The major distribution corresponded to the

expected polymer species, with MBA as the initiating end group and a free hydroxyl on either the 2- or 3-position of the glucopyranoside as the terminating functionality. The second series of signals was consistent with PMBGC polymers with water as the initiating group and an alcohol terminating group, resulting in a −147.9 Da mass shift with respect to the main distribution. Unlike the polymers initiated from MBA, this product undergoes a single decarboxylation to yield a free hydroxyl group on the initiating end (Figure II.30). This peak series represents ~10% of the total peak area relative to that of the main distribution. While these MALDI-TOF MS data cannot be considered as accurate for quantification purposes, they do qualitatively suggest this species is a minor component. There are no ^{1}H NMR signals unique to this initiating species that would allow for a more accurate quantitation of this species. Finally, in some samples, a third series of signals was identified that was consistent with the MBA initiation, but termination with a methyl carbonate end group rather than the expected 2- or 3-free hydroxyl group. This distribution exhibited a +58.0 Da shift with respect to the main distribution and is proposed to have originated from a competing termination during the methanolic purification, wherein the TBD present would allow methanol to react with the carbonate backbone (Figure II.4, 31). This side reaction is similar to the previously reported intentional organocatalytic depolymerizations in the presence of alcohols.[83,95-97] The use of dendritic calibrants in the mass range of interest enable sufficient mass accuracy (generally ±0.1 Da) to make these assignments with confidence.[98] Further confirmation of these proposed mass spectral assignments was gained by analyzing an alternative initiation with 4-*tert*-butylbenzyl alcohol (tBBA, Figure II.29c,d). As expected, analogous series to the first and third distributions described in the MBA initiated polymers were observed, but shifted +42.0 Da,

corresponding to the mass increase for the tBBA initiator. The distribution which was identified in the MBA initiated polymerization as the water-initiated series, on the other hand, showed no shift in molar mass, confirming that this species originated from adventitious initiation with water.

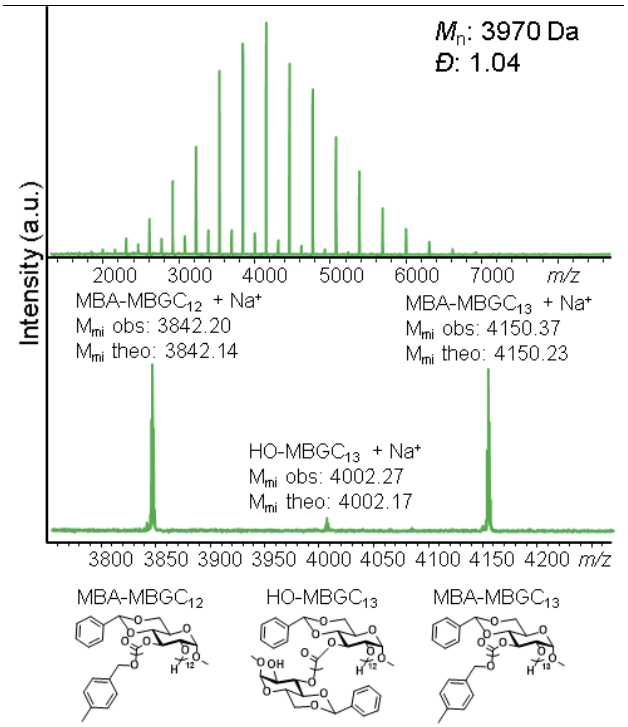

Figure II.5. Entire MALDI-TOF mass spectrum of PMBGC (above) and expanded inset (below) showing the monoisotopic masses (M_{mi}) observed for PMBGC with the proposed chemical structures of each individual species identified.

The presence of competing termination chemistry during the purification with methanol led to the investigation of alternative work-up procedures, and the products of these alternative protocols were subsequently analyzed by MALDI-TOF MS. The substitution of a non-nucleophilic solvent, diethyl ether, for methanol in the purification did cause the disappearance of the methyl carbonate chain ends; however, a new polymer species

was identified as the major distribution with a −5.0 Da mass shift relative to the main polymer distribution observed as a result of the methanolic purification (Figure II.32). A cation competition study, comparing the mass spectra of samples prepared with added lithium, sodium, and potassium salts, was explored to confirm the ionizing species for this distribution. During this study, regardless of the added cation, there was no shift in the distribution. It was therefore verified that the polymer species included a preionized cationic end group, which was determined to be the TBD cation (Figure II.32). This study showed two polymer populations: one with initiation by the TBD catalyst during the polymerization and a second with both a MBA chain end and a TBD cation chain end (Figure II.4). There was no presence of the expected MBA-initiated hydroxyl-terminated polymer by MALDI-TOF MS; however, ^{1}H NMR spectroscopy showed the expected signal of the MBA initiator. This observation may result from the amplification of mass spectral signals from the TBD-functionalized chains, owing to their inherent cationic nature and therefore increased ionization efficiency. To probe this inconsistency, an additional precipitation into methanol was performed after the ether precipitation (Figure II.33). This final methanol precipitation caused the MS signals of the TBD chain end populations to disappear, as the TBD cation is an excellent leaving group and would be removed upon exposure to nucleophilic methanol. The resultant PMBGC samples exhibited only two distributions in their mass spectra, the expected MBA initiated product, and a minor water-initiated distribution (Figure II.2).

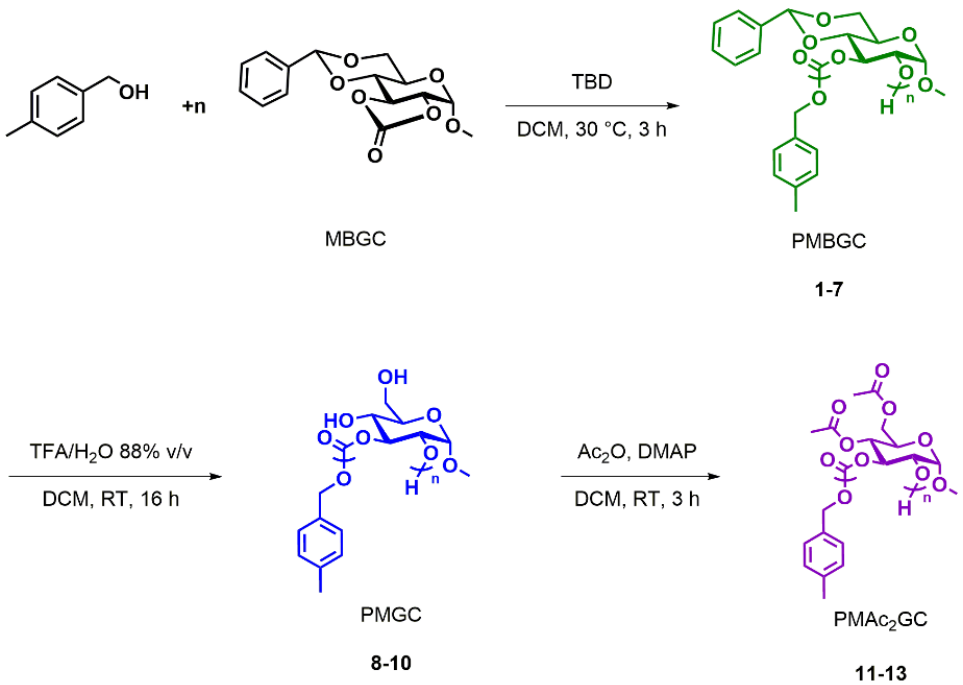

Figure II.6. Synthesis and post-polymerization modification of poly(methyl 4,6-O-benzylidene-2,3-O-carbonyl-α-D-glucopyranoside)s (PMBGC). Although preliminary data suggest that the polymerization is not regioregular (Figures II.12-20); only one repeat unit connectivity is shown for simplicity.

The benzylidene protecting group on MBGC was chosen specifically for its ease of removal in acidic conditions to produce free hydroxyl groups, allowing for a switching of the polymer chain character, from hydrophobic to hydrophilic, through a straightforward post-polymerization modification. The PMBGCs that were synthesized on a gram scale were therefore deprotected to generate polyhydroxyl polymers (**8**, **9**, and **10**, synthesized from **2**, **3**, and **5**, respectively; Figure II.6). The deprotection was achieved under acidic conditions (trifluoroacetic acid/water in DCM). The completion of these reactions (>78% yield) was confirmed through the disappearance of ^{1}H and ^{13}C NMR signals corresponding to the benzylidene group (Figures II.21-24) as well as the appearance of an IR signal at 3600–3200 cm^{-1} corresponding to the O–H stretch (Figure II.27). Upon deprotection,

the M_n of the precipitated polymer sample, measured by SEC (DMF), was larger than the protected precursor polymer (Table II.2). Examination of the reaction supernatant suggested transcarbonation reactions between the deprotected hydroxyl groups and the carbonate units in the backbones may have contributed to the larger than expected M_n. Intra- and intermolecular transcarbonation reactions could explain the observation of cleaved chains appearing at longer retention times in the SEC of the reaction supernatant (Figure II.36d) and could also produce the observed longer polymeric chains by intermolecular transcarbonations (Figure II.35). Alternatively, the shorter retention times for the deprotected polymer precipitant could also be attributed to a more flexible monocyclic repeat unit of PMGC vs the bicyclic repeats of PMBGC, with the PMGC being better solvated by DMF than were the PMBGC precursors, giving them larger hydrodynamic volumes, even at comparable degrees of polymerization. Examination of the ^{1}H NMR spectra of **3** and **8** also supports transcarbonation reactions occurring during the deprotection. In sample **3**, the DP value is calculated to be 30, whereas in sample **8**, the DP value calculated is 70, suggesting that not every polymer chain retained its initiator. The deprotected polymers were further analyzed by MALDI-TOF MS to probe the completeness of the deprotection as well as the presence of polymer species caused by transcarbonation (Figure II.34). Although the protected PMBGC precursors exhibited a relatively narrow molar mass distribution in their mass spectra, the PMGC product signal patterns were consistent with an increased dispersity, further supporting transcarbonation occurred under the acidic reaction conditions. Meaningful average molar mass and dispersity data could not be gained from these samples; however, analyses of the distributions did give information about the repeat unit and end group structure. For example, at least four different distributions were observed in these

samples, but all exhibited a 220.1 Da spacing, consistent with complete removal of the benzylidene protecting groups on each repeat unit. Furthermore, end group analysis confirmed the two major distributions corresponded to water initiated polymer chains with a hydroxyl end group and water initiated chains with a methyl carbonate end, from the PMBGC precursor. The expected product, the MBA-initiated polymer with a hydroxyl end group, was also observed, though the signals were less intense. The fact that the MBA distribution appeared to have been significantly attenuated relative to the protected starting material provides further evidence of transcarbonation reactions during the benzylidene removal. Finally, a fourth distribution is observed which is consistent with cyclic polymers having no end groups. Again, this observation is consistent with transcarbonation occurring during the deprotection reaction.

Table II.2. Properties of PMBGC, PMGC, and $PMAc_2GC$.

Polymer	Sample	M:I[a]	M_n[b] (kDa)	M_n[c] (kDa)	$Đ$[c]	T_d[d] onset (°C)	T_g[e] midpoint (°C)	Water contact angle[f] (°)
PMBGC	**1**	20	4.1	6.4	1.22	-	87	-
	2	25	7.8	8.6	1.32	296	104	108 ± 13
	3	40	9.7	11.5	1.36	307	134	116 ± 7
	4	50	10.3	12.4	1.28	-	172	-
	5	55	12.5	13.7	1.27	339	220	128 ± 9
	6	100	18.6	16.8	1.38	347	232	-
	7	200	-	18.2	1.41	346	233	-
PMGC	**8**	-	-	9.6	1.34	279	132	38 ± 3
	9	-	-	12.6	1.26	247	148	58 ± 10
	10	-	-	16.4	1.23	233	158	40 ± 8
$PMAc_2GC$	**11**	-	-	16.0	1.15	264	140	110 ± 4
	12	-	-	17.4	1.16	247	149	103 ± 11
	13	-	-	20.7	1.19	290	156	94 ± 5

[a]MBGC:MBA. [b]Measured by NMR comparing the aromatic signals of the polymer to the methyl signal of the initiator. [c]Measured with SEC (DMF eluent) calibrated with polystyrene standards. [d]Measured by TGA. [e]Measured by DSC. [f]Measured with a droplet of water, average of 4 droplets with measurements taken over 10 s. Polymers **8**, **9**, and **10**, were synthesized from **2**, **3**, and **5** respectively, and **11**, **12**, and **13**, were synthesized from **8**, **9**, and **10** respectively.

Further reaction of the hydroxyl side chains was also conducted to probe the SEC behaviors without the significant solubility difference. The PMGCs were functionalized with acetic anhydride to facilitate SEC characterization, confirming the apparent higher degree of polymerization after the deprotection reaction, and demonstrating the reactivity of the resulting hydroxyl groups (**11**, **12**, and **13** synthesized from **8**, **9**, and **10**, respectively). Additionally, this functionalization would allow for differentiation between the changes in the thermophysical properties of the polymers caused by the presentation of hydroxyl groups and those caused by the transcarbonation that may have occurred during the benzylidene removal. The success of the acetylation was confirmed through the disappearance of the OH stretch in the IR spectrum, the appearance of the methyl signals in both the ^{1}H (2.17–1.85 ppm) and ^{13}C (21.1–19.8 ppm) NMR spectra, and the appearance of the ^{13}C signal of the ester carbonyls (Figures II.25, 26). As expected, the SEC (DMF) traces for the PMAc$_2$GCs shifted to shorter elution times than their PMGC and PMBGC precursors.

2.2.4 Thermal and Physical Properties of the PMBGCs, PMGCs, and PMAc$_2$GCs

The thermal and physical properties were examined by thermogravimetric analysis (TGA), differential scanning calorimetry (DSC), and contact angle measurements (Table II.2). The analyses performed on the polymers highlighted the correlation between the repeat unit structure and thermal properties. For the protected polymers, PMBGCs and PMAc$_2$GCs, higher numbers of repeat units resulted in higher thermal decomposition temperatures (T_d, Figure II.37); between the smallest polymer and the largest (8.6 to 18.2 kDa, as measured by SEC, DMF eluent), the T_d rose ca. 50 °C. The deprotected materials (PMGC),

however, demonstrated the opposite trend: as the molar mass increased, a ca. 50 °C decrease was observed in the T_d. We do not have an explanation for the observed dependence of T_d on molar mass. However, contributions of the hydroxyls to these changes in T_d are supported by the general increase in T_d with molar mass upon capping of those hydroxyl groups by two different protecting groups, as seen in the $PMAc_2GC$ and PMBGC series of polymers.

The polymers were then examined by DSC to determine their glass transition temperatures (T_gs). Inconsistencies in the T_g values determined from the polymers led us to the hypothesis that water was being absorbed by the polymer samples and having an effect on the glass transition. The effect of water on the polymers was confirmed by monitoring the changes in T_g for two polymer samples (**5** and **10**) as a function of added water (0, 5, and 10 wt %, Figures II.41, 42, Table II.5). Therefore, because of the changes in T_g caused by water, all samples were dried under reduced pressure with mild heating prior to analysis by DSC. As expected, the T_gs of all the dried samples of polymers increased with the molar mass. The observed changes in T_g with increasing MW were most pronounced in the PMBGC polymers with a ca. 150 °C change vs a change of 15–30 °C in the PMGCs and $PMAc_2GC$s (Figures II.38-40). This significant change in T_g for the PMBGC series over the 3-fold range of M_n, from below to above an expected entanglement molar mass, is in accordance with the classical dependence of T_g on M_n of linear homopolymers, with an apparent $(T_g)_\infty$ of ca. 230 °C (Figure II.7). In contrast, the PMGCs and $PMAc_2GC$s were each of higher and narrower ranges of molar masses. The relatively high T_gs in the PMBGC series are likely due to the rigidity of the bicyclic backbone repeat unit. Upon deprotection, the changes in the T_gs are presumably caused by the removal of the benzylidene acetal to give a monocyclic repeat unit, rather than the transesterification that occurred during the

deprotection. This hypothesis is supported by the similar T_g values observed in both PMGC and $PMAc_2GC$ (Figures II.39, 40).

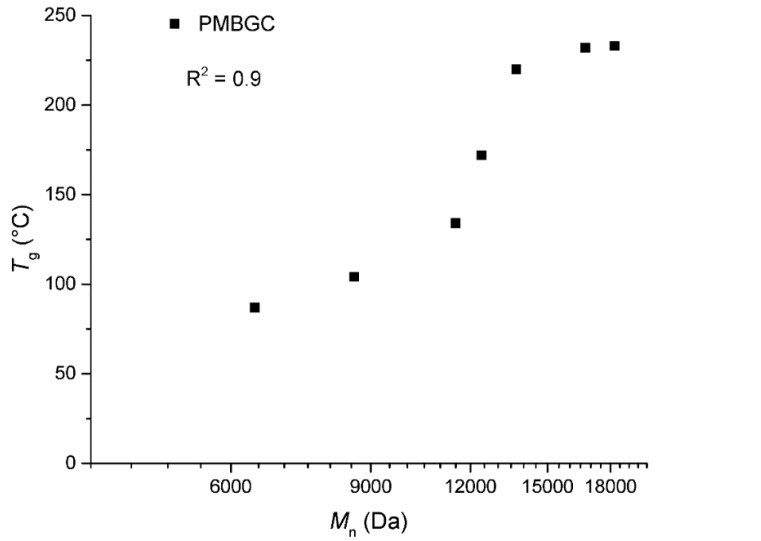

Figure II.7. Dependence of the glass transition temperature on the molar mass of PMBGC. M_n values were measured by SEC (DMF eluent) calibrated with polystyrene standards.

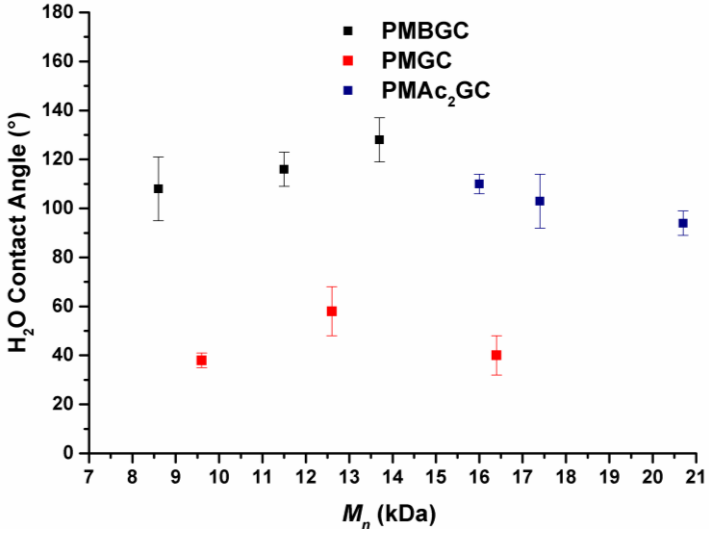

Figure II.8. Static water contact angle vs. M_n of the PMBGC (black), PMGC (red), and $PMAc_2GC$ (blue), where each sample was analyzed using four 5 µL-drops of nanopure water and twenty images were collected per drop. M_n values were measured by SEC (DMF eluent) calibrated with polystyrene standards.

Water contact angles, as expected, revealed significant differences in the wettabilities (Figure II.8, 43, Table II.2). The benzylidenated and acetylated polymers were hydrophobic (contact angles between 94° and 128°) while PMGC was hydrophilic (38°–58°). PMGC is, in fact, moderately water-soluble. This observation did not affect the contact angle measurements, as several hours were required for PMGC to dissolve in buffer or water, and intact films were observed after the measurement. In addition, the polymer length had little to no effect on the polymer hydrophilicity.

2.2.5 PMBGC Bulk Degradation and Identification of the Degradation Products

The bulk degradation of **2**, **3**, and **5** as polymer pellets was investigated under acidic, basic, and neutral aqueous conditions. When the polymer was exposed to physiological conditions (PBS, pH = 7, 37 °C), no significant bulk degradation or pellet swelling was observed over several months (Figure II.44). More rigorous aqueous conditions (1 M HCl or 1 M NaOH) were then used to examine the bulk hydrolytic degradation, revealing differing degradation kinetics and profiles (Figures II.45, 46). Under acidic conditions, an incubation period was observed, between 0 and 40 days, where no significant degradation ($\geq$ 90% mass remaining) or swelling occurred ($\leq$ 5%). This initial period was followed by a rapid loss of pellet weight, increased swelling as the pellet degraded, and complete degradation within 4 months total for all samples. However, under basic conditions, no incubation period was observed; instead, a gradual weight loss occurred, with 0-10% of the pellet weight being lost in 2 days, followed by 10–20% in the first week, and complete degradation in 9 months. These differing degradation profiles and kinetics suggested that

acidic and basic conditions proceeded *via* different degradation mechanisms, which was further investigated by NMR spectroscopy.

^{1}H NMR spectroscopy was used to identify the degradation products and, thereby, the likely degradation mechanisms, for PMBGC and PMGC. Pristine polymer samples were added to either 1 M DCl or 1 M NaOD in D_2O, and the portions of the materials that underwent dissolution into the aqueous solutions were, subsequently, examined over time. In basic solutions, both PMBGC and PMGC degraded into their monomeric repeat units, methyl 4,6-*O*-benzylidene-α-D-glucopyranoside and methyl α-D-glucopyranoside, respectively (Figure II.9, 50, 51). PMBGC showed sharp signals matching in chemical shift and integration with methyl 4,6-*O*-benzylidene-α-D-glucopyranoside within 7 days, with solid remaining in the NMR tube, whereas PMGC degraded even more rapidly, undergoing full dissolution with the appearance of sharp ^{1}H resonance signals corresponding to methyl α-D-glucopyranoside within 1 day. However, in acidic conditions (Figure II.9, 47, 48), no significant degradation of the polymer backbone appeared to occur over 30 weeks. The PMBGC sample released the benzylidene protecting group after 40 days. The presence of benzaldehyde was confirmed by the aldehyde ^{1}H resonance frequency at 9.89 ppm and the aromatic signals at 7.93, 7.72, and 7.60 ppm. After removal of the benzylidene, the resulting PMGC was soluble in the acidic aqueous solution; however, it did not appear to degrade further into methyl α-D-glucopyranoside (Figure II.49), as no sharp signals appeared in the ^{1}H NMR spectrum consistent with saccharide chemical shifts (4.5–3.0 ppm).

Applying this knowledge of the degradation products to the bulk degradation of PMBGC, the incubation period in 1 M HCl is likely the acidic solution removing the benzylidene acetal, supported by a strong scent of almond in the degradation solution, and

the pellet lost weight as the polymer became water-soluble as more hydroxyl groups were released. In 1 M NaOH, the carbonate backbone itself was cleaved and the small molecule diol was released, causing the pellet to lose weight. Taken together, these experiments support the hypothesis that the difference in kinetics observed in the bulk degradation is caused by a difference in degradation mechanisms occurring under acidic and basic conditions.

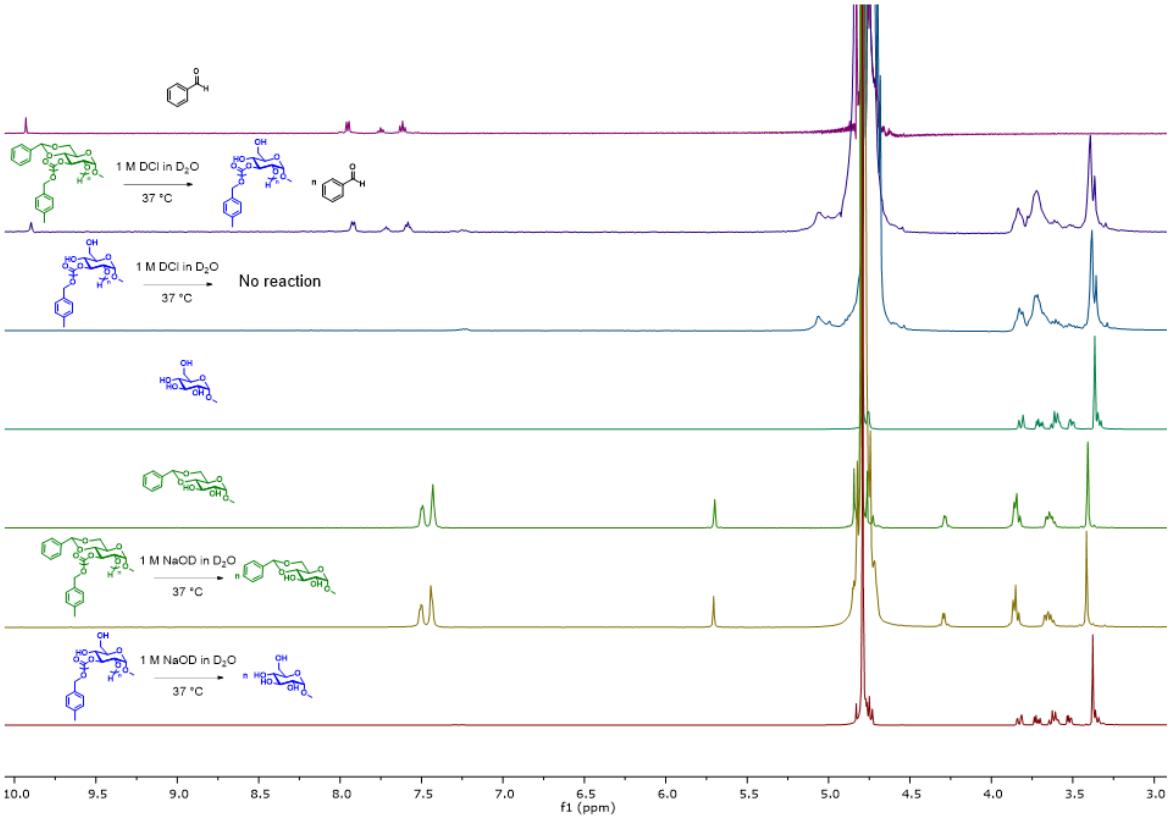

Figure II.9. ^{1}H NMR spectra of PMBGC and PMGC, each collected as the latest time point from acidic (1 M DCl/D_2O) and basic (1 M NaOD/D_2O) degradation experiments (Figures II.47-51), and the identified small molecule degradation products. The reactions shown with each spectrum indicates the polymeric sample, reaction conditions, and degradation products.

2.3 Experimental Section

2.3.1 Materials

All materials were purchased from VWR or Sigma-Aldrich. Unless noted; all reagents were used as received. Dichloromethane (DCM) was purified and dried by a solvent purification system (J. C. Meyer Solvent System). 4-Methylbenzyl alcohol (MBA) and TBD were dried over CaH_2, dried under vacuum, and stored under an argon atmosphere. DBU was dried over CaH_2, distilled, and stored under an argon atmosphere. TU and MBGC were dried under reduced pressure over P_2O_5 and stored under an atmosphere of argon. *Caution: When working with phosgene precursors, including triphosgene, special precautions should be taken as they are highly toxic by inhalation or ingestion.*

2.3.2 Instrumentation

^{1}H, ^{13}C, COSY, and HMQC NMR spectra were recorded on an Inova500 spectrometer; chemical shifts were referenced to the resonance signals of the deuterated solvent.

IR spectra were recorded on a Shimadzu IR Prestige attenuated total reflectance Fourier-transform infrared spectrophotometer and analyzed using IR solution v. 1.40 software.

Size exclusion chromatography was performed with (1) $CHCl_3$ as eluent on a Tosoh EcoSEC for the organocatalytic scope and kinetic studies and (2) DMF as eluent on a Waters chromatography system for the molar mass determinations across the polymer samples having challenging solubilities due to the different side chain groups.

Instrumental details: (1) Tosoh Co. (Tokyo, Japan) model HLC-8320 EcoSEC system with a two-column set of TOSOH bioscience TSKgel columns (Super HM-M 6.0 mm i.d × 15 cm columns) and a guard column (Super H-H 4 μm) with chloroform as the eluent (0.300 mL/min) at 30 °C. Polymer solutions were prepared at ca. 3 mg/mL and an injection volume of 200 μL was used. The system was calibrated with Polymer Laboratories, Inc. (Amherst, MA) polystyrene standards (580–271 800 Da). (2) A Waters Chromatography, Inc. (Milford, MA) system with an isocratic pump model 1515, a differential refractometer model 2414, and a four-column set of 5 μm Guard (50 × 7.5 mm), Styragel HR 4 5 μm DMF (300 × 7.5 mm), Styragel HR 4E 5 μm DMF (300 × 7.5 mm), and Styragel HR 2 5 μm DMF (300 × 7.5 mm) with DMF (0.05 M LiBr) as the eluent (1.00 mL/min) at 70 °C. Polymer solutions were prepared at ca. 5 mg/mL, with toluene as a flow marker, and an injection volume of 200 μL was used. The system was calibrated with Polymer Laboratories, Inc. (Amherst, MA) polystyrene standards (580–1 233 000 Da).

Mass spectral data were collected using a Bruker-Daltonics matrix assisted laser desorption ionization time-of-flight (MALDI-TOF) Autoflex III mass spectrometer in reflector mode with positive ion detection. Typical sample preparation for MALDI-TOF MS data acquisition was performed by making stock solutions in THF of matrix (20 mg/mL), polymer analyte (2 mg/mL), and an appropriate cation source (2 mg/mL). The stock solutions were mixed in a 25/5/1 ratio (matrix/analyte/cation), deposited onto the MALDI target plate and allowed to evaporate *via* the dried droplet method. *trans*-2-[3-(4-*tert*-Butylphenyl)-2-methyl-2-propenylidene]malononitrile (DCTB) and α-cyano-4-hydroxycinnamic acid (α-cyano) were used as matrices for PMBGC and PMGC, respectively. Sodium trifluoroacetate was used as the primary cation. Lithium iodide and

potassium trifluoroacetate were used as cations for additional ionization studies. MALDI-TOF MS data were calibrated against SpheriCal dendritic calibrants from Polymer Factory (Stockholm, Sweden).

Glass transition temperatures were measured by differential scanning calorimetry with a Mettler-Toledo DSC822^e under N_2, as the midpoint of the inflection tangent on the third heating scan, with a 10 °C/min heating and cooling rate. Melting points were measured as the onset of the inflection tangent of the first heating scan with a heating rate of 10 °C/min. Measurements were analyzed using Mettler-Toledo Star^{e}v.10.00 software.

Thermogravimetric analysis (TGA) was performed under an Ar atmosphere using a Mettler-Toledo model TGA/DSC 1, with a heating rate of 10 °C/min. Measurements were analyzed using Mettler-Toledo Star^e v.10.00 software.

Contact angles were measured as static contact angles with an Attension Theta optical tensiometer (Biolin Scientific). The static contact angle was calculated with the Theta software (Biolin Scientific), using a Young–Laplace fit to the drops of liquid (water).

2.3.3 Synthesis

Synthesis of methyl 4,6-*O*-benzylidene-2,3-*O*-carbonyl-α-D-glucopyranoside (MBGC). To a solution of methyl 4,6-*O*-benzylidene-α-D-glucopyranoside (6.0677 g, 21.5 mmol) in DCM (100 mL), pyridine was added (8.7 mL, 110 mmol). A solution of triphosgene (2.3130 g, 7.79 mmol, 23.4 mmol of carbonylation agent generated *in situ*) in DCM (75 mL) was added dropwise to the glucopyranoside solution. The reaction was monitored using TLC and was stirred at RT until no starting material was present; a stain of 5% HCl in methanol was used for visualization. Any remaining triphosgene was quenched

by the addition of a saturated solution of sodium bicarbonate; this mixture was stirred until no bubbles were visible in the reaction vessel. The organic layer was then collected and washed with saturated sodium bicarbonate, a 5% HCl solution, and finally a sodium chloride brine solution. The organic layer was then dried over sodium sulfate, filtered, and concentrated to yield 6.6102 g (99.8% yield) of a white powder. FTIR (ATR): 3000–2800, 1807, 1454, 1385, 1275, 1213, 1169, 1097, 1065, 1038, 976, 951, 924, 785, 762, 698, 648 cm^{-1}. ^{1}H NMR (500 MHz, DMSO-d_6): δ 7.43 (overlapping, 2 H), 7.39 (overlapping, 3 H), 5.76 (s, 1 H), 5.36 (d, J = 3 Hz, 1 H), 4.84 (t, J = 11 Hz, 1 H), 4.66 (dd, J = 3 Hz, 11 Hz, 1 H), 4.31 (t, J = 9.5 Hz, 1 H), 4.24 (dd, J = 4.6 Hz, J = 10 Hz, 1 H), 3.90 (t, J= 10 Hz, 1 H), 3.67 (td, J = 4.6 Hz, J = 9.5 Hz, 1 H), 3.46 (s, 3 H) ppm. ^{13}C NMR (125 MHz, DMSO-d_6): δ 153.2, 136.9, 129.1, 128.1, 126.2, 100.3, 95.9, 78.2, 77.0, 76.0, 67.4, 64.7, 55.3 ppm. MS (ESI^+): calculated $[M + H]^+$ for $C_{15}H_{17}O_7$ 309.0974; found 309.0973; m_p = 110 °C.

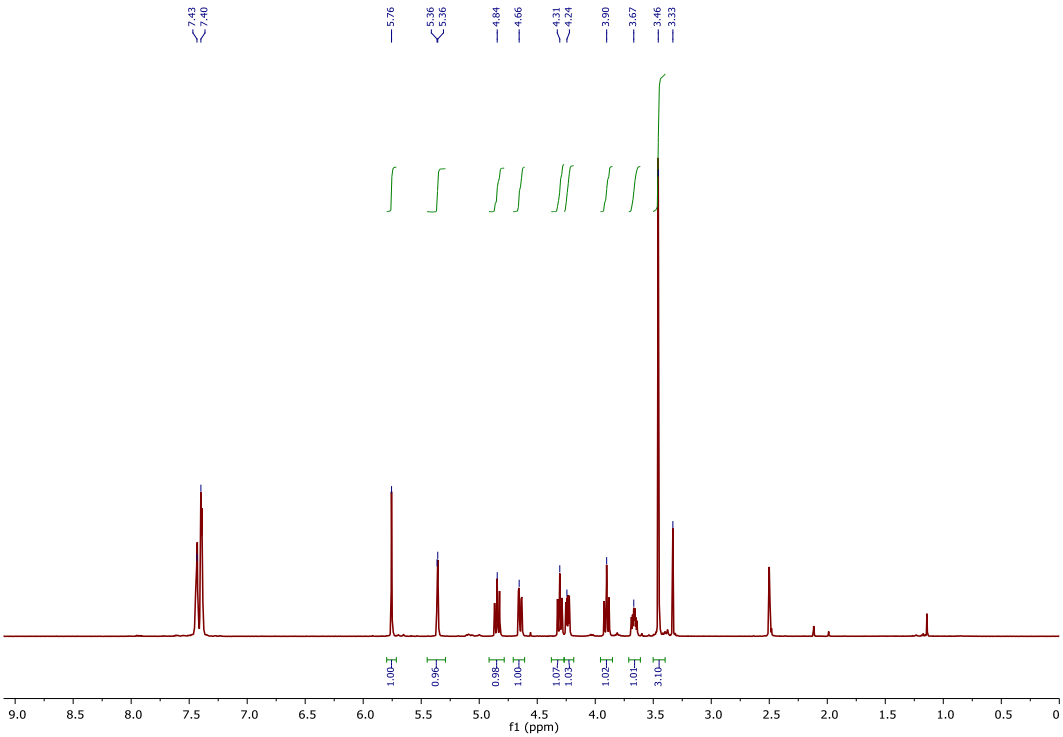

Figure II.10. ^{1}H NMR (500 MHz) spectrum of MBGC in DMSO-*d*$_6$.

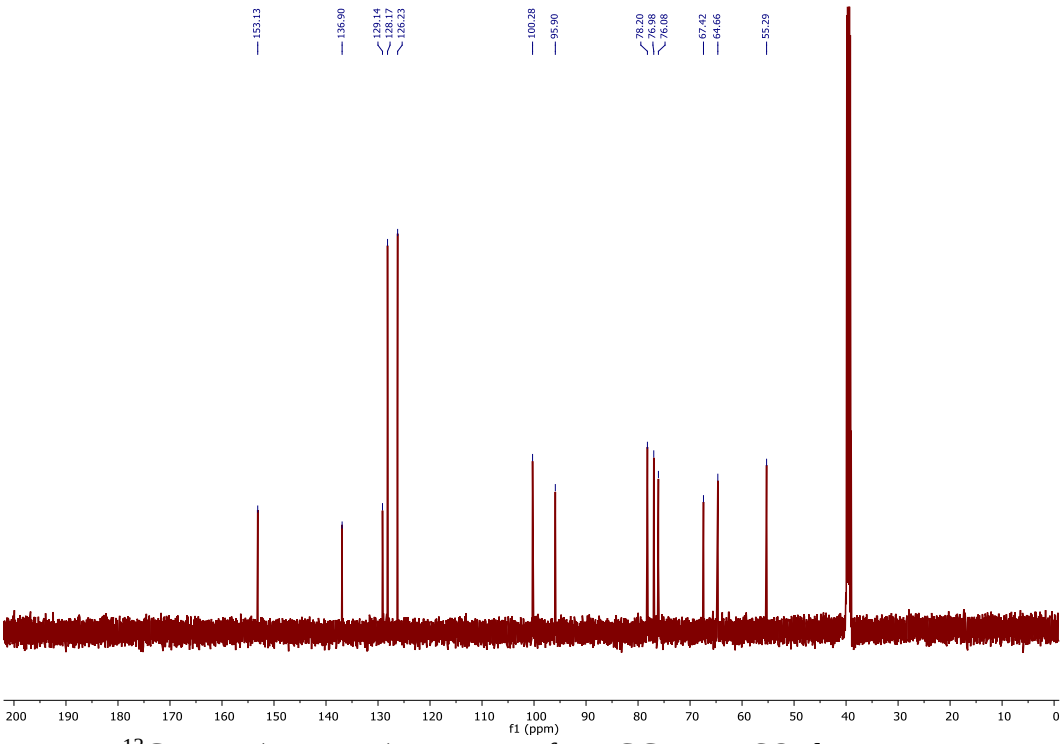

Figure II.11. ^{13}C NMR (125 MHz) spectrum of MBGC in DMSO-*d*$_6$.

General procedure for determining the organocatalytic scope for the polymerization of MBGC. In a glovebox, to a solution of MBGC (100 mg, 0.32 mmol) in DCM (enough to reach a final monomer concentration of 0.5 M, after the addition of all reagents), was added a solution of 4-methylbenzyl alcohol (MBA, 0.79 mg, 6.5 μmol) in DCM (80 μL). The reaction mixture was stirred for 2-3 min. A solution of organocatalyst in DCM (either 1,8-diazabicyclo[5.4.0]undec-7-ene (DBU), DBU and N-[3,5-bis(trifluoromethyl)phenyl]-N'-[(1R,2R)-2-(dimethylamino)cyclohexyl]-thiourea (TU), DBU and 1,5,7-Triazabicyclo[4.4.0]dec-5-ene (TBD), or TBD), was added (2 or 4 mol% to MBGC). The reaction mixture was stirred in the glovebox for 5 h, and was then quenched by the addition of Amberlyst 15 H-form resin. The polymers obtained were purified by precipitation from DCM into methanol three times to give PMBGCs as white powders (63-78 % yield). The materials were analyzed by $CHCl_3$ SEC to determine the M_n and $Đ$ (Table II.1, Figure II.1).

Kinetic analysis of MBGC polymerization, in a glovebox, to a solution of MBGC (220 mg, 0.71 mmol) in DCM (530 μL) was added a solution of naphthalene (36 mg) in DCM (526 μL), and a solution of MBA (1.75 mg, 14.3 μmol) in DCM (175 μL). The reaction mixture was stirred for 2-3 min. A solution of TBD (1.99 mg, 14.3 μmol) in DCM (200 μL) was added, to give a final monomer concentration of 0.50 M. At different times after the addition of TBD (0, 15, 30, 45, 60, 90, and 180 min), an aliquot (200 μL) of the reaction mixture was quenched using Amberlyst 15 H-form resin. The monomer conversion was then determined with $CHCl_3$ SEC using a UV detector, (naphthalene was used as an internal standard, a representative set of SEC data are shown in Figure II.3). The signals in the SEC traces were integrated to determine their areas, and monomer conversion was measured by normalizing the monomer signal to the naphthalene signal in each trace and

then comparing the normalized monomer signals at the different time points to the normalized monomer signal at t = 0. The signals in Figure II.3 from higher to lower elution times are naphthalene, MBGC, benzaldehyde, and the growing polymer. The naphthalene signal is relatively intense compared to the other signals because both the RI and UV detectors were examined, and to have appreciable RI signal a larger amount of naphthalene was required than in the UV. The UV detector was used to examine monomer conversion as it gave more reproducible data, and had no solvent signal which could overlap with the naphthalene signal by RI. The acidic quenching conditions for the polymerization produced a trace amount of benzaldehyde (<5%) as a side product; to correct for any error this release may have caused in the conversion or MW calculations these experiments were completed in triplicate. The monomer conversions, M_n, and $Đ$ from the triplicate experiments were averaged and displayed in Figure II.21 and Table II.4.

Procedure for a single ring-opening of MBGC, in a glovebox, MBGC (50 mg, 0.16 mmol) and MBA (20mg, 0.16 mmol) were dissolved in DCM (320 µL), the reaction mixture was stirred for 2-3 min. A solution of TBD was added (22 mg, 0.16 mmol) in 320 µL of DCM, and the reaction was allowed to proceed for 12 h. TBD was removed from the reaction mixture by running through a silica plug, the reaction mixture was further purified to isolate the single ring-opened products *via* column chromatography (acetone/hexanes eluent). See below for full NMR characterization.

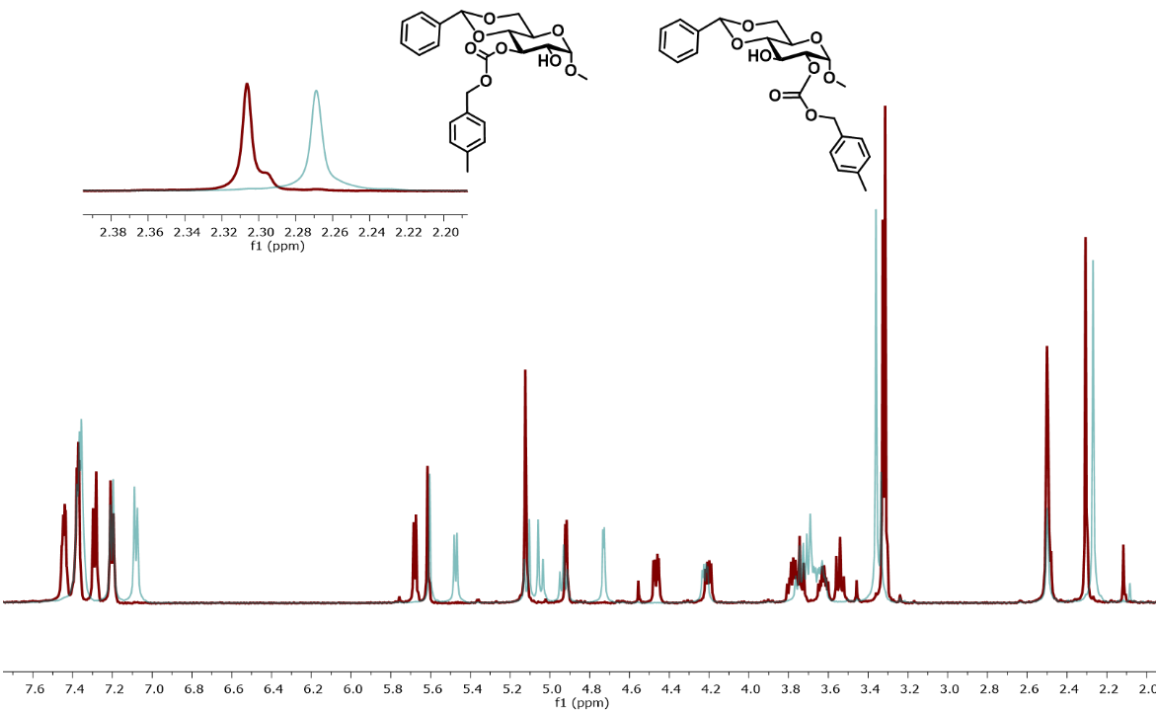

Figure II.12. ^{1}H NMR (500 MHz) overlayed spectra of a single ring-opening of MBGC using MBA in DMSO-d_6. Suggesting a non-regioregular ROP, and the shift of the methyl signal (inset) of the MBA initiator based on the directionality of the RO. The maroon trace is 2 to 3 ring-opening and teal trace is 3 to 2 ring-opening, Figures II.13-20 show individual NMR spectra for each structure.

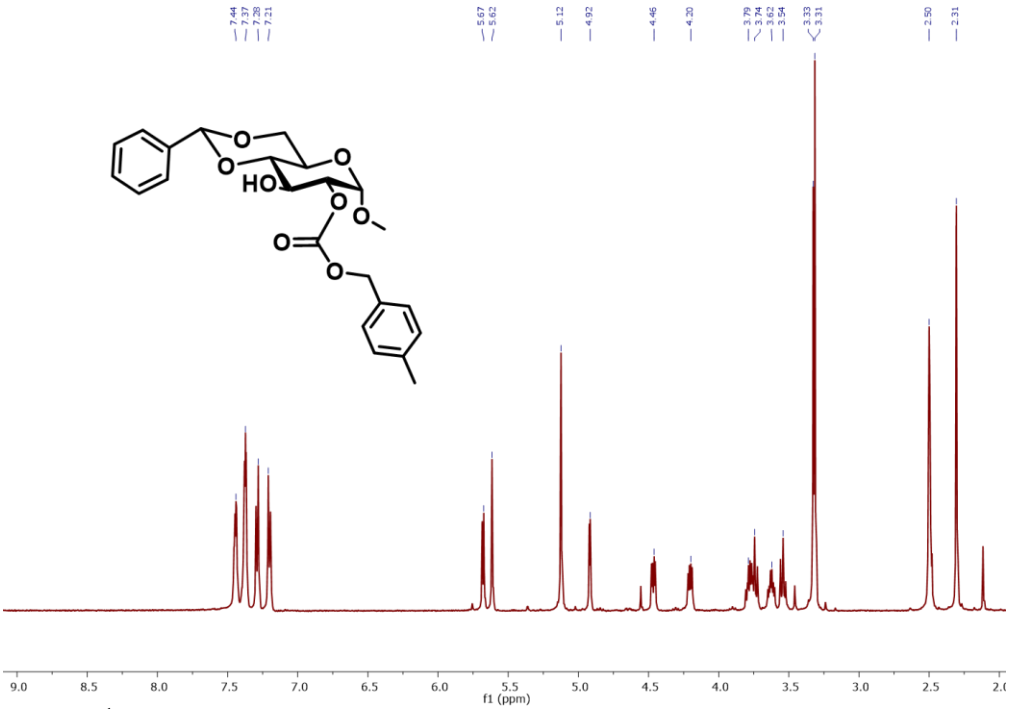

Figure II.13. ^{1}H NMR (500 MHz) spectrum of a single ring-opening of MBGC using MBA in DMSO-d_6. Ring-opening was observed in the 2 to 3 direction, as shown in the structure.

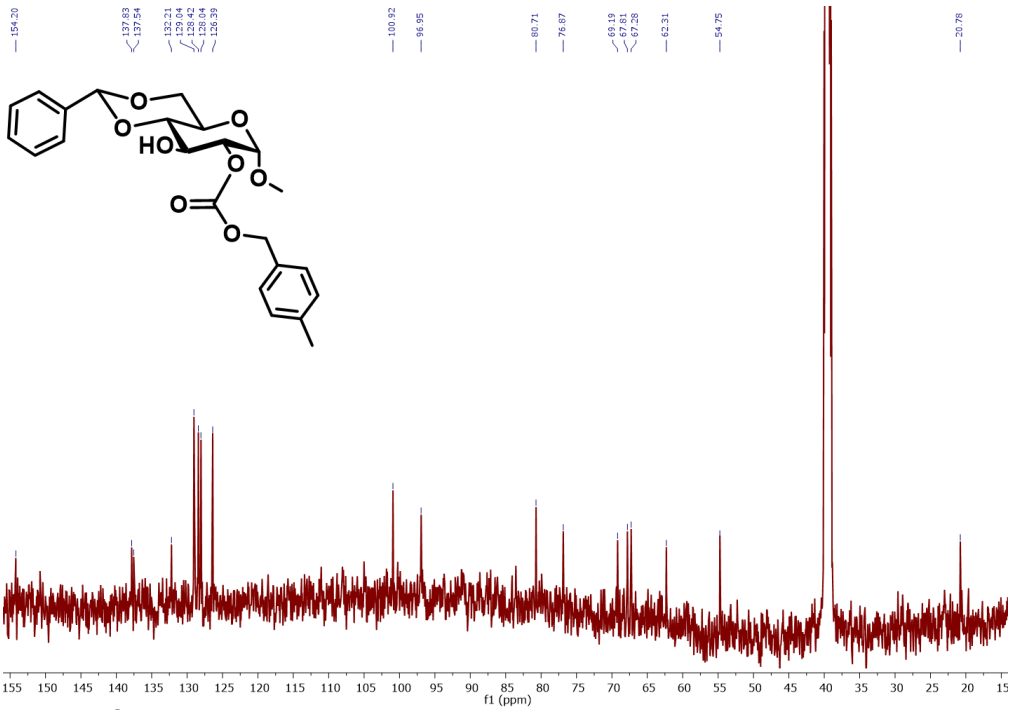

Figure II.14. ^{13}C NMR (125 MHz) spectrum of a single ring-opening of MBGC using MBA in DMSO-d_6. Ring-opening was observed in the 2 to 3 direction, as shown in the structure.

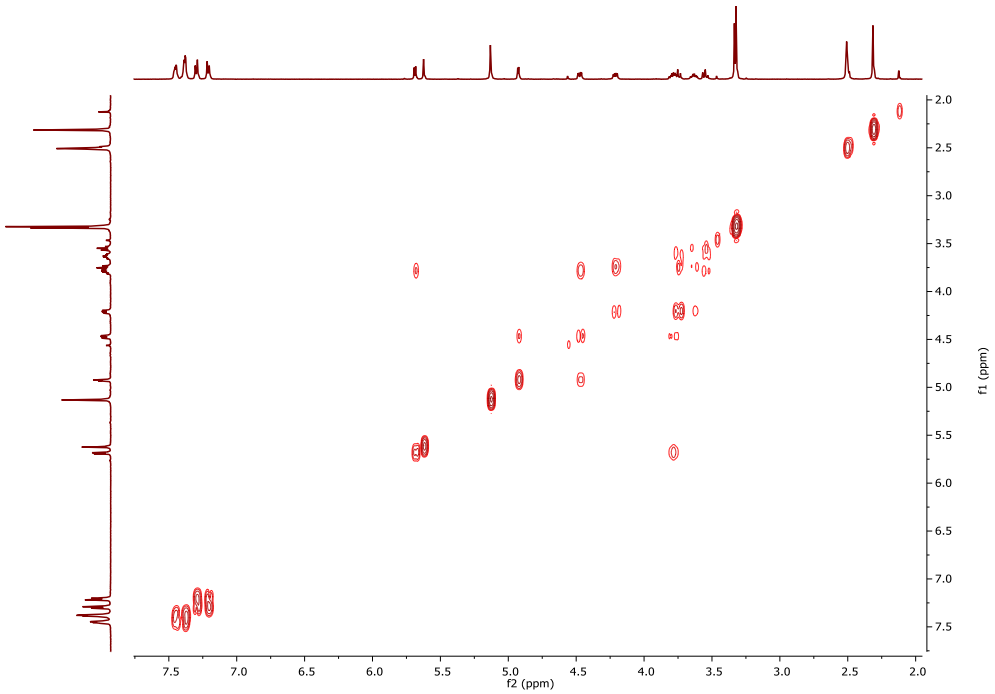

Figure II.15. COSY NMR spectrum of a single ring-opening of MBGC using MBA in DMSO-d_6. Ring-opening was observed in the 2 to 3 direction.

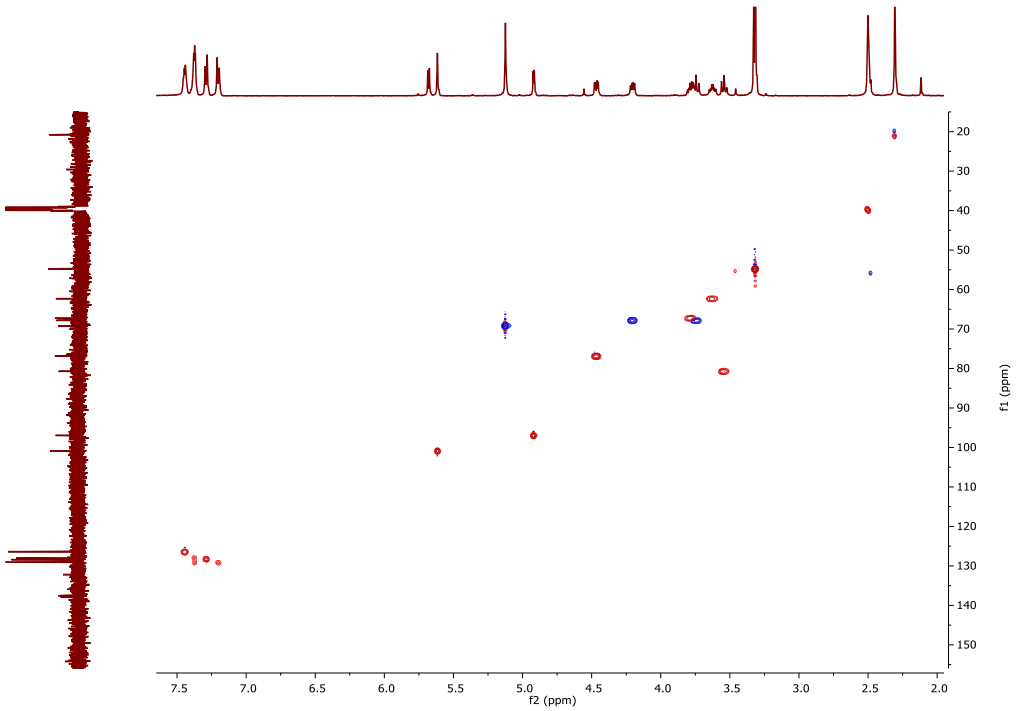

Figure II.16. HSQC NMR spectrum of a single ring-opening of MBGC using MBA in DMSO-d_6. Ring-opening was observed in the 2 to 3 direction.

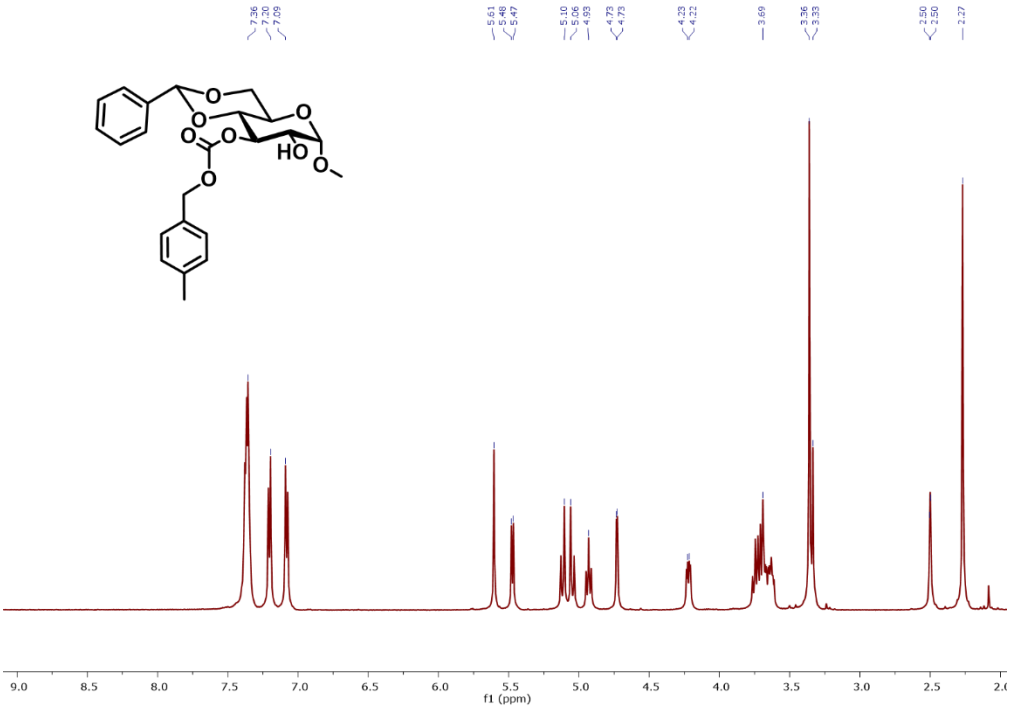

Figure II.17. ^{1}H NMR (500 MHz) spectrum of a single ring-opening of MBGC using MBA in DMSO-d_6. Ring-opening was observed in the 3 to 2 direction, as shown in the structure.

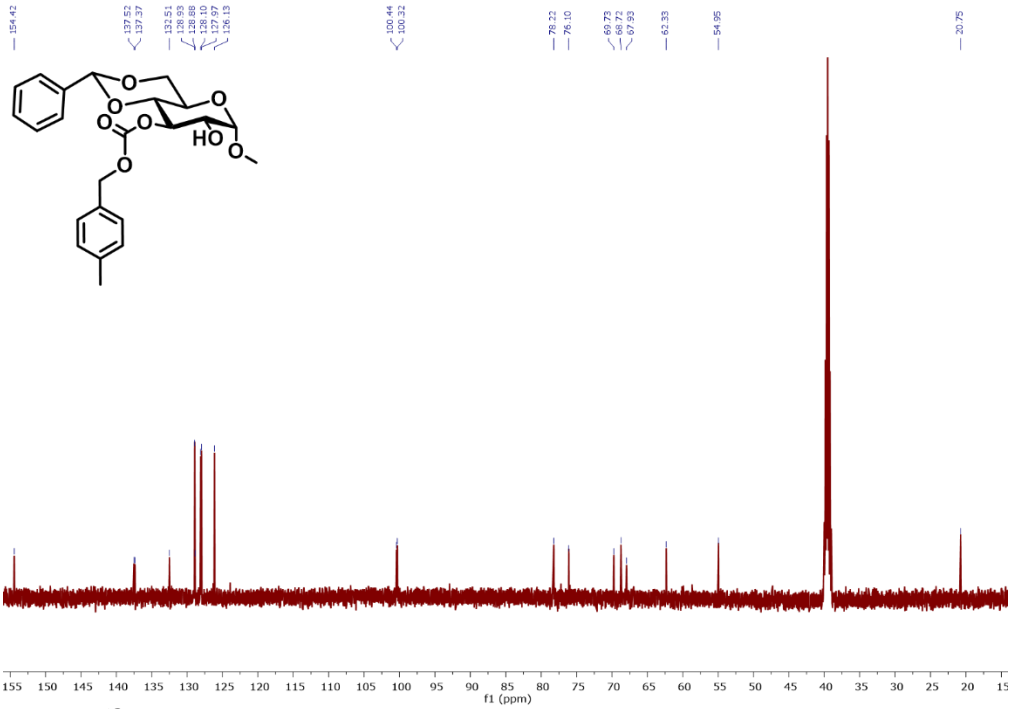

Figure II.18. ^{13}C NMR (125 MHz) spectrum of a single ring-opening of MBGC using MBA in DMSO-d_6. Ring-opening was observed in the 3 to 2 direction, as shown in the structure.

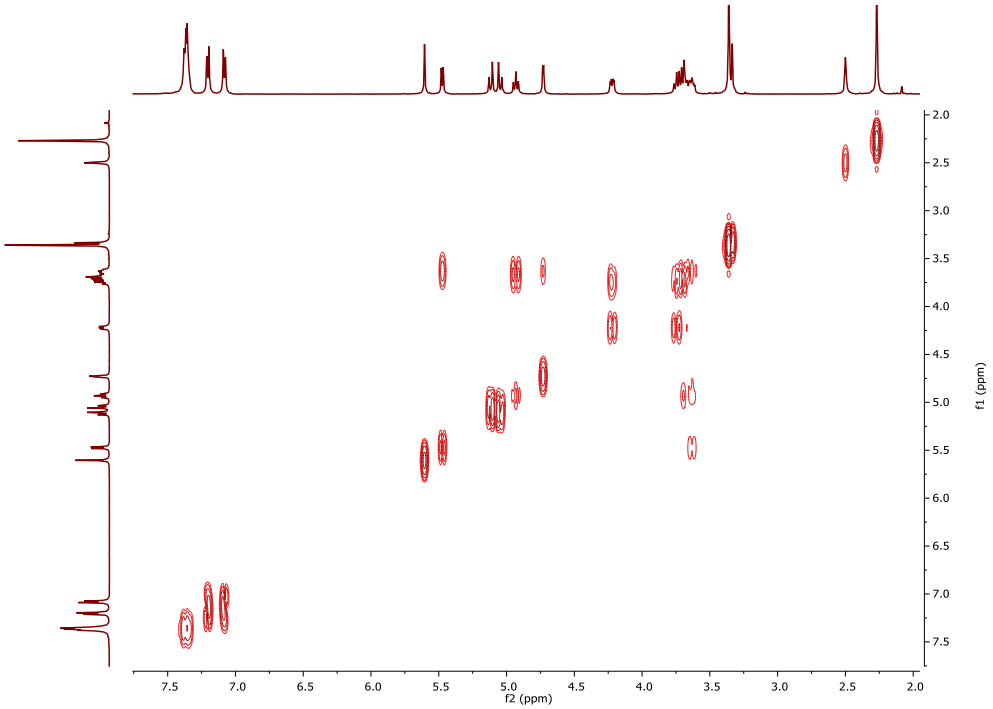

Figure II.19. COSY NMR spectrum of a single ring-opening of MBGC using MBA in DMSO-d_6. Ring-opening was observed in the 3 to 2 direction.

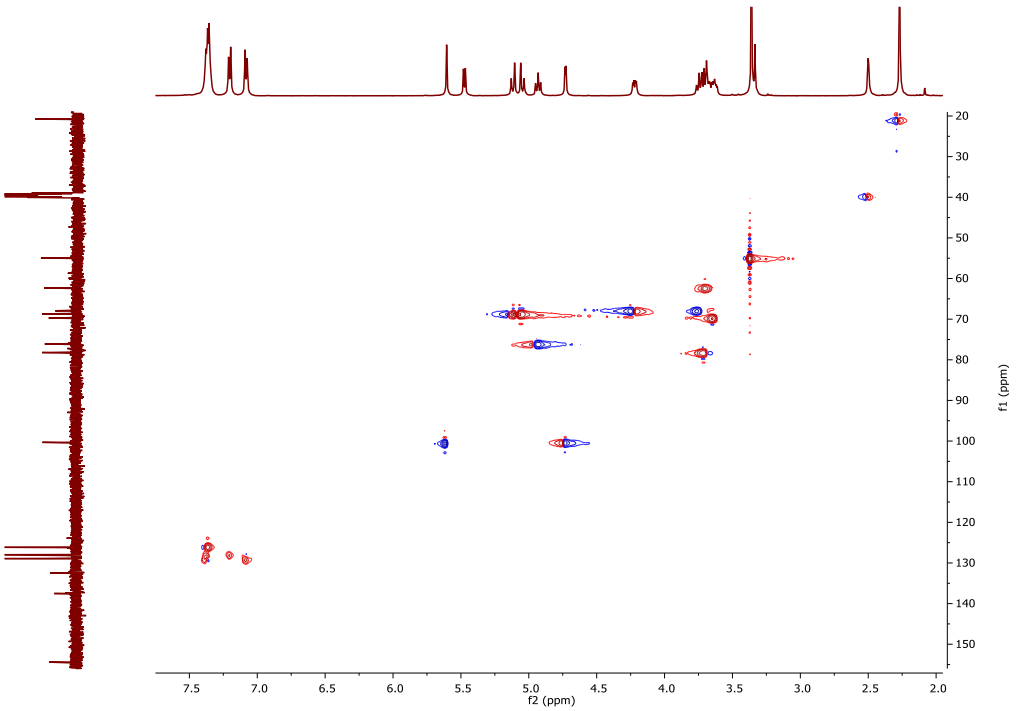

Figure II.20. HSQC NMR spectrum of a single ring-opening of MBGC using MBA in DMSO-d_6. Ring-opening was observed in the 3 to 2 direction.

General procedure for the synthesis of poly(methyl 4,6-*O*-benzylidene-2,3-*O*-carbonyl-α-D-glucopyranoside) (PMBGC). In a glovebox, MBGC (1.00 g, 3.24 mmol) was dissolved in 4.8 mL of DCM. A solution of MBA (9.3 mg, 0.076 mmol) in 668 μL of DCM was added, followed by a solution of TBD (9.5 mg, 0.068 mmol) in 1.0 mL of DCM. The reaction was monitored by SEC ($CHCl_3$ eluent) and was quenched when there was no visible monomer signal or change in MW of the polymer signal in the trace (2–9 h, for **1**–**7** depending on the polymerization), by adding Amberlyst 15 H-form resin. The reaction mixture was purified by precipitation into methanol from DCM (three times) to give **3** as a white powder. FTIR (ATR): 3100–2750, 1759, 1454, 1373, 1277, 1234, 1215, 1092, 1049, 988, 752, 698, 656 cm^{-1}. ^1H NMR (500 MHz, DMSO-d_6): δ 7.50–7.26 (br), 5.73–5.53 (br), 5.22–5.03 (br), 5.08–4.87 (br), 4.78–4.66 (br), 4.41–4.13 (br), 3.91–3.61 (br), 3.41–3.19 (br) ppm. ^{13}C NMR (125 MHz, DMSO-d_6): δ 153.0, 137.0, 130.1–127.3, 127.0–125.2, 101.4–99.5, 97.3–95.4, 78.0–76.3, 75.1–72.1, 68.0–66.9, 62.9–61.3, 56.8–54.3 ppm.

During MALDI-TOF MS analysis of these materials, it was determined that an undesired side reaction occurred between the polymer backbone and methanol during the precipitation, which was estimated to occur in approximately 10% of the polymer chains, primarily caused by free TBD present during the first precipitation. This reaction could be avoided by changing the precipitation procedure to use a non-nucleophilic solvent, such as ether, followed by a final precipitation into methanol. Mechanistic explanation and MALDI-TOF MS data are given on pages 49-54. **2**: 79% yield, M_n(DMF SEC) = 8600 g/mol, $Đ$(DMF SEC) = 1.32, T_g(midpoint) = 104 °C, TGA in Ar: 296–338 °C, 62% weight loss, 14% mass remaining at 500 °C. **3**: 97% yield, M_n(DMF SEC) = 11 500 g/mol, $Đ$(DMF SEC) = 1.36, T_g(midpoint) = 134 °C, TGA in Ar: 307–346 °C, 71% weight loss, 0% mass

remaining at 500 °C. **5**: 75% yield, M_n(DMF SEC) = 13 700 g/mol, $Đ$(DMF SEC) = 1.27, T_g(midpoint) = 220 °C, TGA in Ar: 339–370 °C, 70% weight loss, 5% mass remaining at 500 °C.

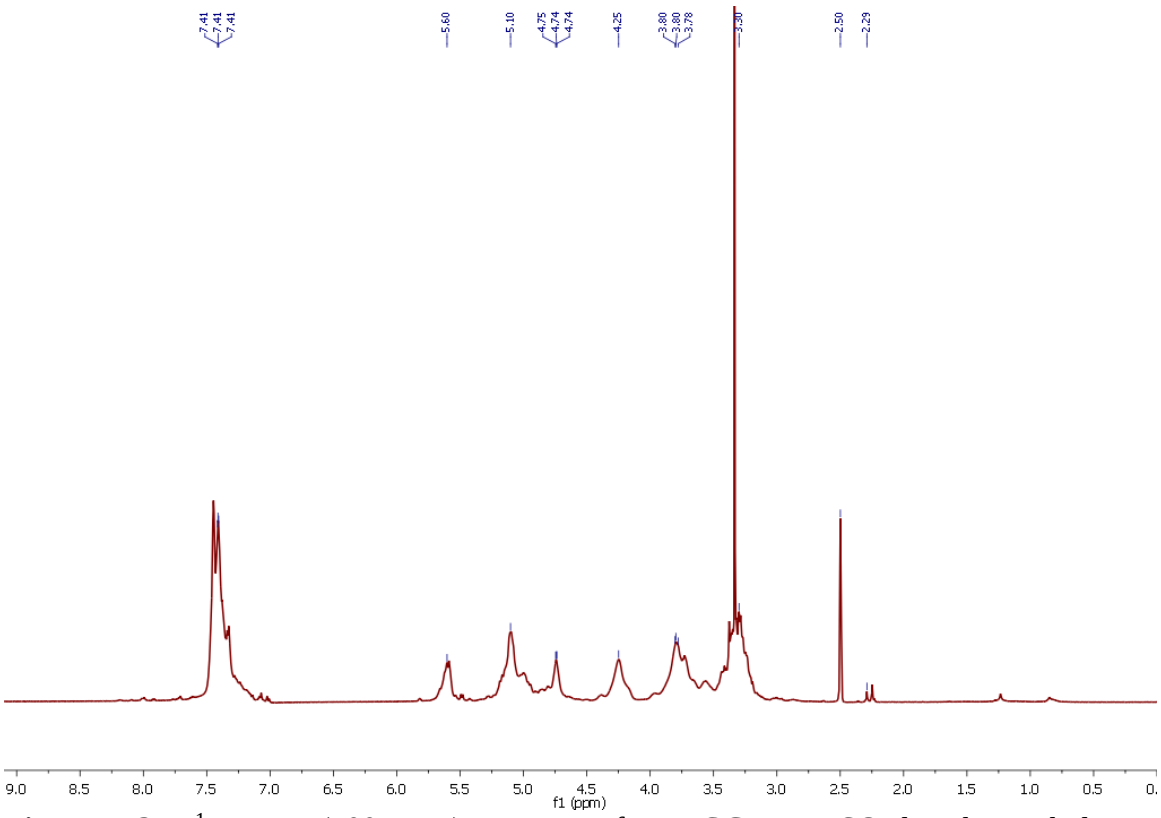

Figure II.21. ^{1}H NMR (500 MHz) spectrum of PMBGC in DMSO-d_6. The methyl signal of the initiator is broader than anticipated based on the differences in proton environment based on the directionality of the RO during the initiation. See pages 33-37 for NMR spectroscopic confirmation.

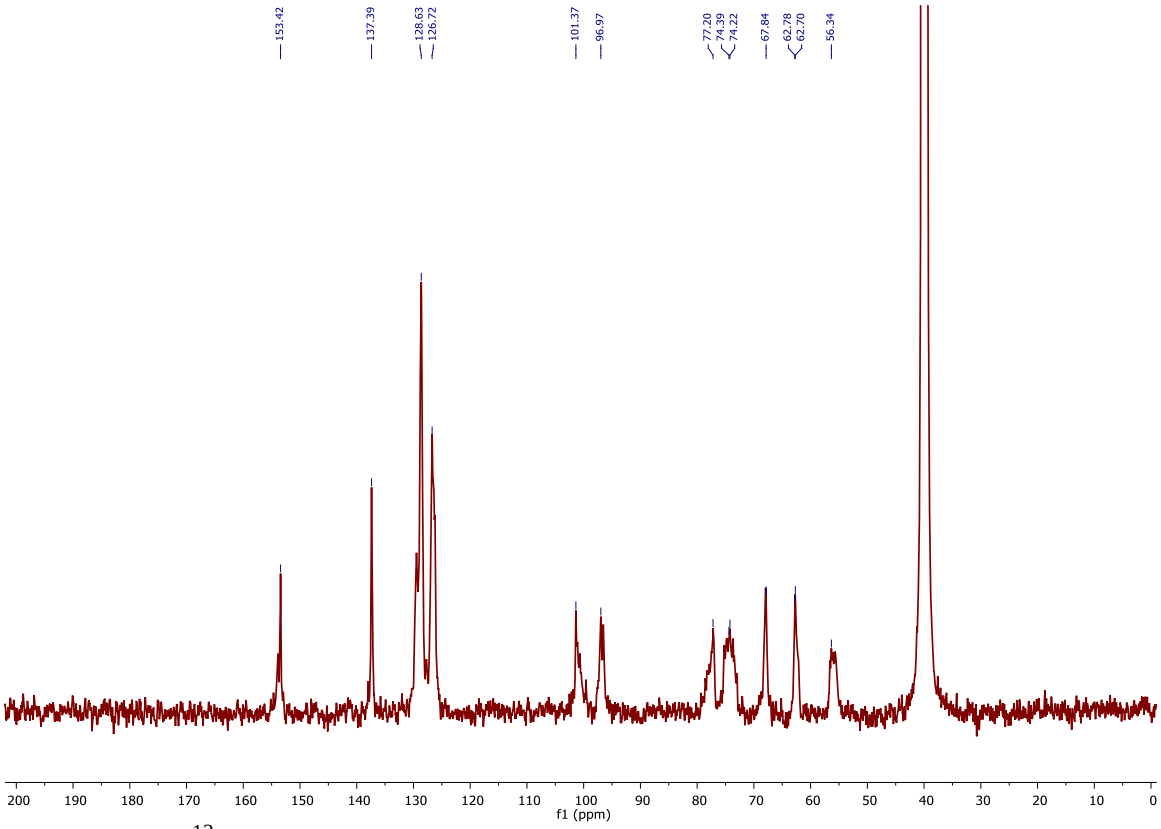

Figure II.22. ^{13}C NMR (125 MHz) spectrum of PMBGC in DMSO-d_6.

General procedure for the synthesis of poly(methyl 2,3-*O*-carbonyl-α-D-glucopyranoside) (PMGC). Aqueous trifluoroacetic acid (200 μL, 88% v/v) was added to a solution of **3** (410.1 mg, 0.038 mmol) in DCM (5.0 mL); the reaction was stirred at RT for 16 h. The reaction mixture was then precipitated three times into cold ether to give **9** as a white powder. FTIR (ATR): 3600–3200, 3050–2850, 1763, 1450, 1281, 1234, 1161, 1038, 980, 910, 779 cm^{-1}. ^{1}H NMR (500 MHz, DMSO-d_6): δ 5.66–5.34 (br), 5.05–4.84 (br), 4.76–4.63 (br), 4.56–4.40 (br), 3.71–3.59 (br), 3.57–3.31 (br) ppm. ^{13}C NMR (125 MHz, DMSO-d_6): δ 153.8, 96.7–94.8, 77.9–75.3, 75.2–73.2, 73.0–71.8, 68.2–67.1, 60.6–59.4, 55.4–53.9 ppm. **8**: 88% yield, M_n(DMF SEC) = 9600 g/mol, $Đ$(DMF SEC) = 1.34, T_g(midpoint) = 132 °C, TGA in Ar: 279–299 °C, 58% weight loss, 6% mass remaining at 500 °C. **9**: 90%

yield, M_n(DMF SEC) = 12 600 g/mol, $Đ$(DMF SEC) = 1.26, T_g(midpoint) = 148 °C, TGA in Ar: 248–277 °C, 57% weight loss, 17% mass remaining at 500 °C. **10**: 78% yield, M_n(DMF SEC) = 16 400 g/mol, $Đ$(DMF SEC) = 1.23, T_g(midpoint) = 158 °C, TGA in Ar: 233–260 °C, 43% weight loss, 25% mass remaining at 500 °C.

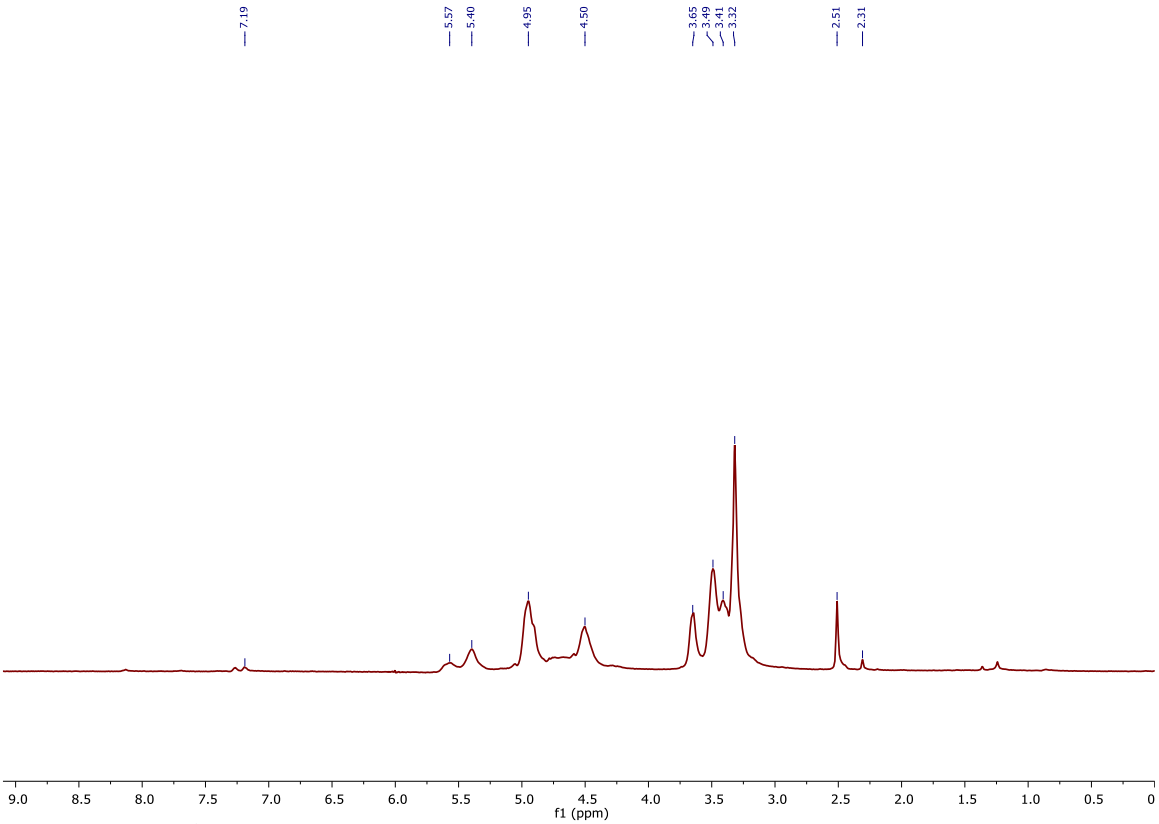

Figure II.23. ^{1}H NMR (500 MHz) spectrum of PMGC in DMSO-d_6.

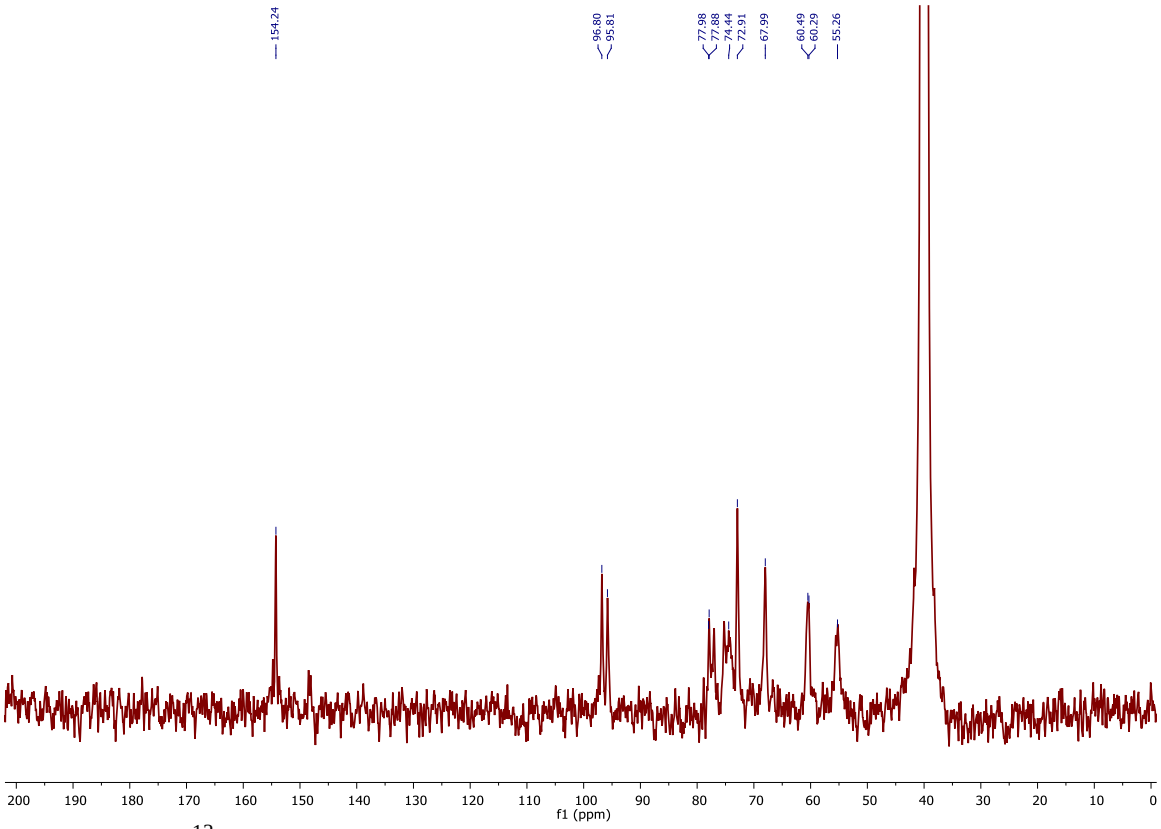

Figure II.24. ^{13}C NMR (125 MHz) spectrum of PMGC in DMSO-d_6.

General procedure for the synthesis of poly(methyl 4,6-di-*O*-acetyl-2,3-*O*-carbonyl-α-D-glucopyranoside) ($PMAc_2GC$). Acetic anhydride (69.0 μL, 0.730 mmol) was added to a mixture of DCM (1.0 mL) and PMGC (41.3 mg, 0.188 mmol with respect to monomeric repeat unit). After stirring for 10 min DMAP (91.8 mg, 0.751 mmol) was added, and the reaction was stirred at RT until all of the solids had dissolved. The reaction mixture was quenched and purified by precipitation into cold methanol from DCM (three times) to give **12** as a white powder. FTIR (ATR): 3030–2820, 1744, 1445, 1368, 1287, 1223, 1169, 1132, 1034, 976, 924, 773, 602 cm^{-1}. ^{1}H NMR (500 MHz, DMSO-d_6): δ 5.15–4.87 (br), 4.87–4.61 (br), 4.24–3.97 (br), 3.97–3.78 (br), 3.43–3.32 (br), 2.17–1.85 (br) ppm. ^{13}C

NMR (125 MHz, DMSO-d_6): δ 170.8–169.1, 154.9–153.1, 97.1–95.0, 76.9–73.5, 68.4–65.9, 62.7–61.5, 55.9–54.6, 21.1–19.8 ppm. **11**: 41% yield, M_n(DMF SEC) = 16 000 g/mol, $Đ$(DMF SEC) = 1.15, T_g(midpoint) = 140 °C, TGA in Ar: 264–330 °C, 74% weight loss, 5% mass remaining at 500 °C. **12**: 56% yield, M_n(DMF SEC) = 17 400 g/mol, $Đ$(DMF SEC) = 1.16, T_g(midpoint) = 149 °C, TGA in Ar: 246–327 °C, 78% weight loss, 4% mass remaining at 500 °C. **13**: 59% yield, M_n(DMF SEC) = 20 700 g/mol, $Đ$(DMF SEC) = 1.19, T_g(midpoint) = 156 °C, TGA in Ar: 290–327 °C, 70% weight loss, 4% mass remaining at 500 °C.

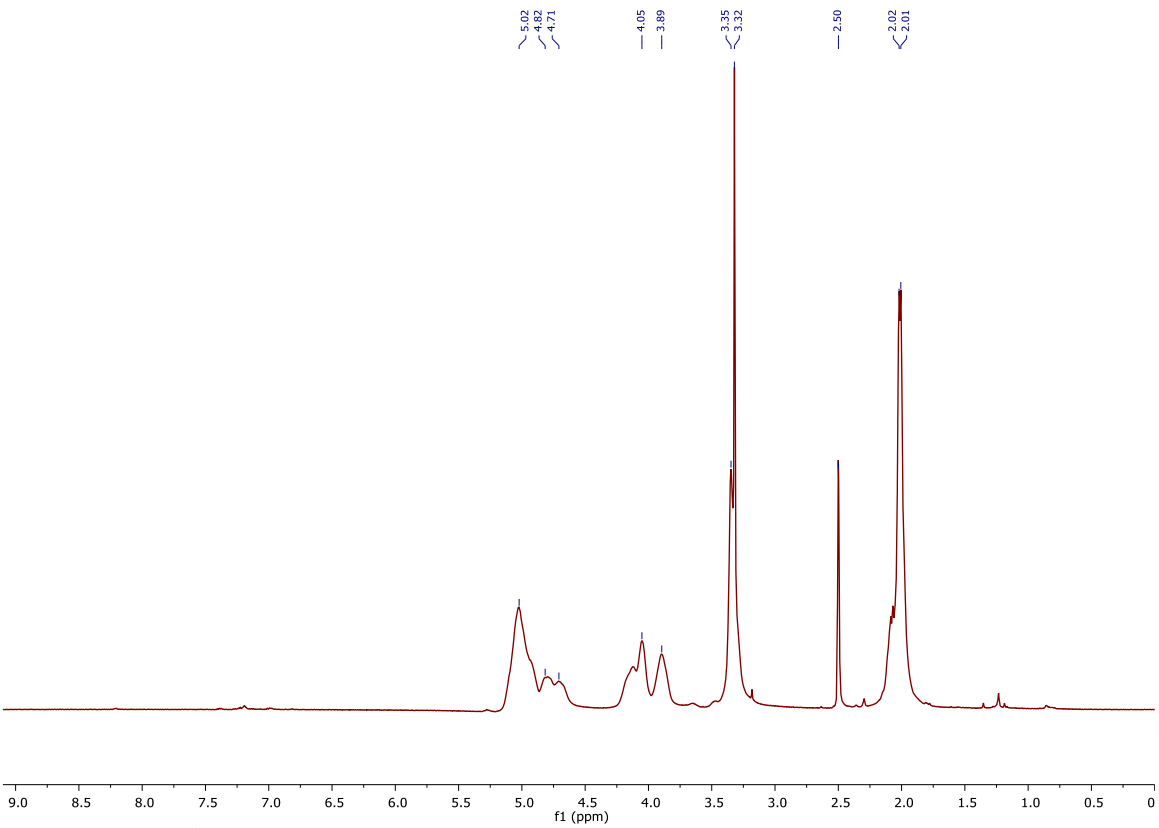

Figure II.25. ^{1}H NMR (500 MHz) spectrum of PMAc$_2$GC in DMSO-d_6.

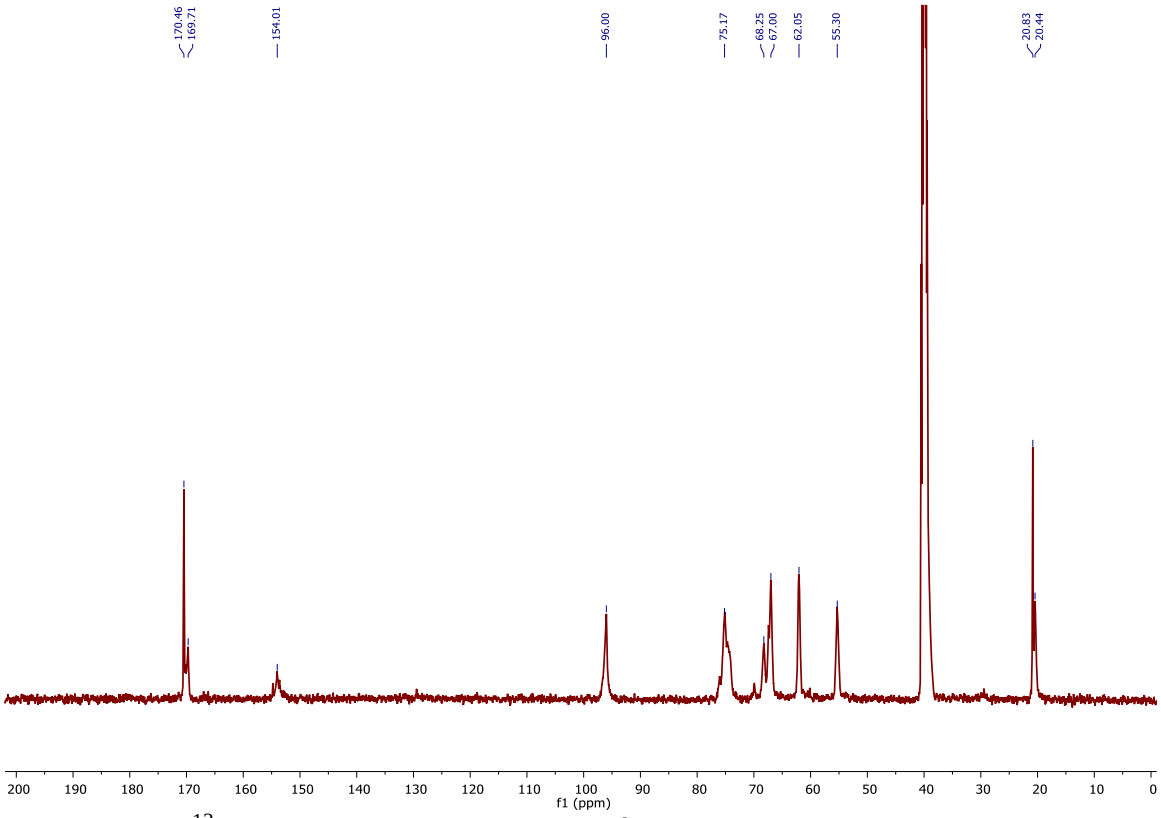

Figure II.26. ^{13}C NMR (125 MHz) spectrum of $PMAc_2GC$ in DMSO-d_6.

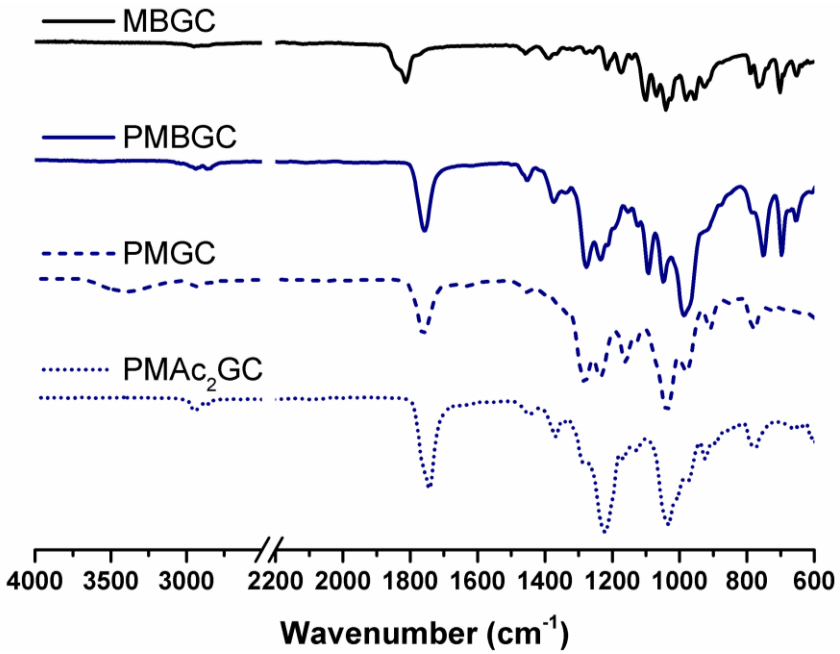

Figure II.27. IR spectra of MBGC (black), PMBGC (blue), PMGC (blue dashed), and $PMAc_2GC$ (blue dotted).

General procedure to determine the plasticization of polymer samples. Polymer samples were weighed into vials, and a solution of THF with 1 %v/v deionized water was added. The THF was allowed to evaporate under atmospheric conditions leaving polymer samples with 5 and 10 wt% of added water. From these, DSC samples were prepared and analyzed

Production of Bulk Polymer Samples. Pellets were produced using a high-pressure hydraulic press heated to 120 °C. Between 13 and 18 mg of polymer was heated in a homemade mold for 15 min under 1/2 ton of pressure, giving cylindrical pellets with a diameter of 4 mm and a height of 2 mm.

Aqueous Degradation Studies. Preweighed pellets of PMBGC were individually submerged in 4 mL of phosphate-buffered saline (PBS, pH = 7), 1 M HCl (pH = 1), or 1 M NaOH (pH = 14) and placed in a heated shaker at 37 °C and 60 rpm. At designated time points, samples were removed from the shaker, and the aqueous solution was withdrawn using a syringe. The pellets were taken from their vials, any large droplets of aqueous solution were blotted with a kimwipe, and a "wet" pellet weight was measured. The pellets were then dried under vacuum at 40 °C for 7–8 h, and their weight was recorded as a "dry" weight. Fresh PBS, HCl(aq), or NaOH(aq) solution was then added to the pellets, and the samples were returned to the shaker. Swelling was measured by comparing the wet vs dry pellet weights, and the mass remaining was measured by comparing the dry pellet weight to the original dry pellet weight (Eqs II.1, 2).

NMR Degradation Studies. Pristine samples of PMBGC and PMGC were added to NMR tubes, and 1 M NaOD or 1 M DCl was added; the samples were stored in a heated

shaker at 37 °C and 60 rpm. At designated time points, the samples were removed from the shaker and analyzed by ^{1}H NMR spectroscopy.

2.4 Conclusions

Our interest in functional polymer materials that lead to biologically benign byproducts upon degradation, whether or not they are meant to degrade, has guided us toward the development of synthetic methodologies that utilize carbohydrates as diverse building blocks. In this current work, we have expanded the scope of glucose as a monomer to generate a series of polymers having varied properties, which coincidentally advances ROP to simple conditions for five-membered cyclic carbonates that are accessible across laboratories. The five-membered cyclic carbonate monomer, methyl 4,6-*O*-benzylidene-2,3-*O*-carbonyl-α-D-glucopyranoside, was synthesized in high yields (99%) through well-established carbonylation techniques. The investigation of this monomer under various organocatalytic conditions revealed the high potential of this *trans*-fused bicyclic monomer to undergo controlled, pseudo-first-order ROP. The optimized polymerization conditions using TBD as the organocatalyst were applied toward the preparation of different molar masses of the protected polymer, PMBGC, which were then deprotected under acidic conditions to give polyhydroxyl polymers (PMGCs). These deprotected polymers were then functionalized with acetyl groups to yield PMAc$_2$GCs. MALDI-TOF MS analysis gave significant insight into the chemistries of the polymerization and post-polymerization modification. For the synthesis of PMBGC, mass spectral analysis revealed the inclusion of the entire monomeric repeat unit during the polymerization with no elimination of CO_2 as well as an undesired transcarbonation reaction that occurred during purification with

methanol. This better understanding of the polymerization chemistry allowed for the improvement of experimental procedures in future studies. Additionally, during the deprotection to generate PMGC, unexpected changes in the molar masses were shown to be caused in part by transcarbonation during the acid-catalyzed reaction.

The effects of the polymer length and protecting group presence on the thermophysical properties were investigated. As expected, a significant change in the water contact angle was observed between the protected polymers (hydrophobic material) vs the deprotected polymer (hydrophilic material). The polymer length had a direct effect on the T_d; the benzylidenated and acetylated polymers had higher T_ds as the polymer length increased while the deprotected polymers had a decrease in the T_d with increasing molar mass. The T_g of the benzylidenated materials rose as the polymer length increased, while for the deprotected and acetylated polymers, no significant changes were observed in the T_g with varying the molar mass over a narrower range.

Consequently, these natural product-derived versatile materials give access to a wide range of thermophysical properties through a robust polymerization technique and simple post-polymerization modifications. The potential optimization of the desired polymer properties to a specific target application makes these materials suitable for biomedical and engineering applications, such as orthopedic devices or drug delivery vehicles. Moreover, the ability of the polymers to degrade hydrolytically into methyl α-D-glucopyranoside and carbon dioxide, as benign small molecules, with the additional degradation product of benzaldehyde or acetic acid in the protected forms, creates possibilities in applications using engineering polymers, in general. The mechanical properties of these polymers as well as their biological interactions are currently under investigation.

2.5 Supplemental Information

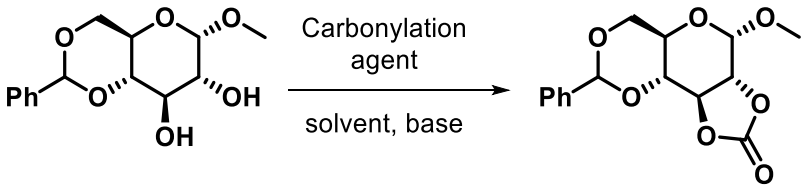

Figure II.28. Synthesis of MBGC monomer.

Table II.3. Reagents and catalysts evaluated for the synthesis of MBGC.

Carbonylation Agent	Equivalents with respect to diol	Temperature (°C)	Solvent	Base	Yield (%)
Ethyl chloroformate	1.3	0, RT, 50, 80	DCM, THF, dioxane	NEt_3, pyridine	<10
4-Nitrophenyl chloroformate	1.7	RT, 50, 80			10
1,1'-Carbonyldiimidazol	1.6	RT, 50, 80			20
Diethyl carbonate	1.2	120	xylene	NaOMe, KOEt	<10
Triphosgene	1.0	RT	DCM	pyridine	30
	0.52	RT			19
	0.34	RT			99.6

Table II.4. Conversion and MW for the kinetic analysis of the MBGC polymerization

Reaction time (min)	Conversion (%)	M_n (Da)	Error M_n (%)	$Đ$	Error $Đ$ (%)	$ln\frac{[M]_0}{[M]}$	Error $ln\frac{[M]_0}{[M]}$
0	0.0	308	1	1.05	1	0.00	0.0
15	19.0	551	2	1.12	11	0.22	0.1
30	23.2	1675	8	1.17	8	0.27	0.2
45	41.1	1951	15	1.17	7	0.57	0.3
60	32.4	2479	15	1.23	2	0.39	0.1
90	50.9	3267	19	1.25	2	0.72	0.1
180	84.8	5477	13	1.29	0	1.95	0.4

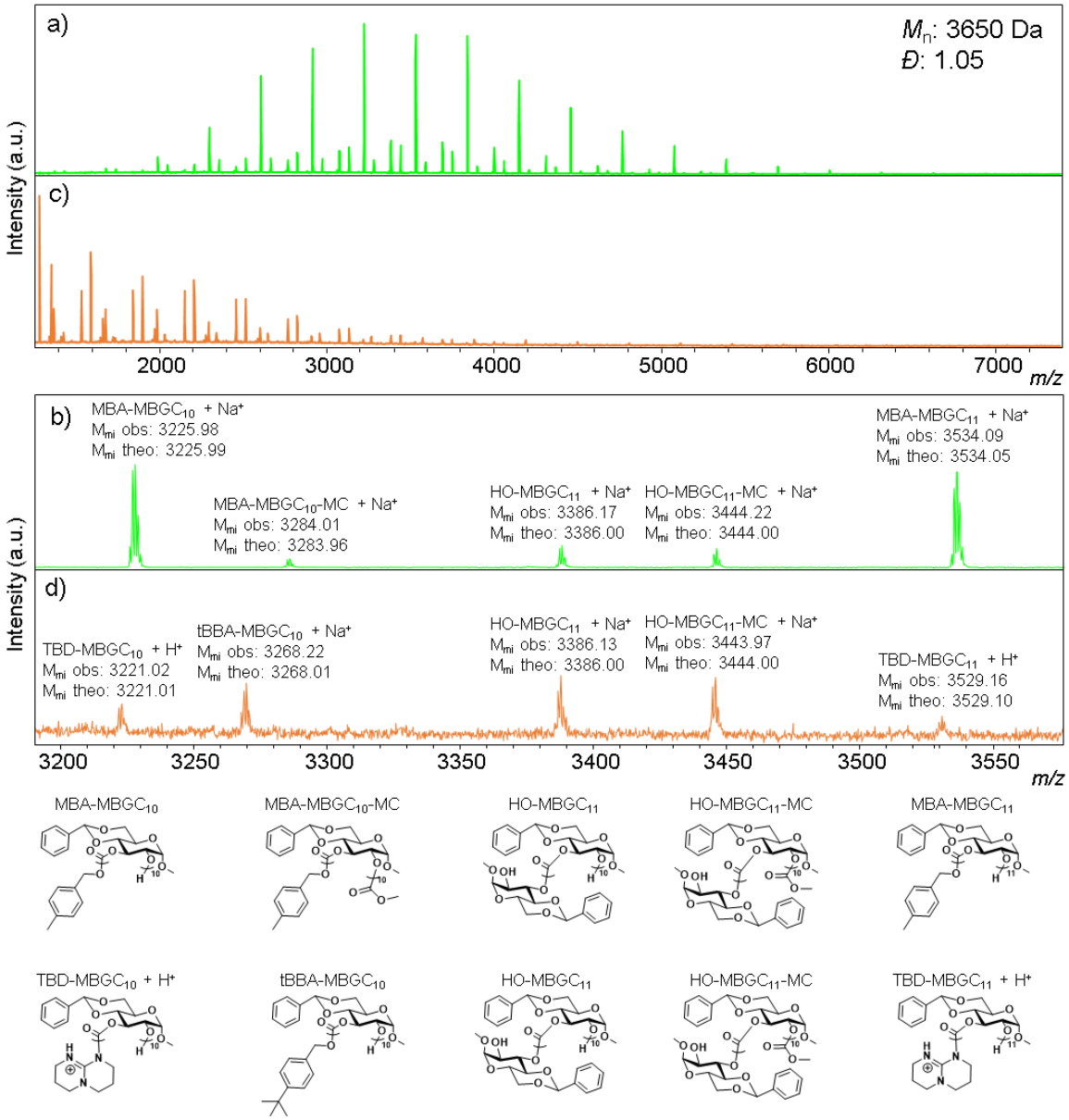

Figure II.29. The monoisotopic masses (M_{mi}) observed in the MALDI-TOF MS spectrum of PMBGC, precipitated into methanol with the proposed chemical structures of each of the identified species. Initiated by both MBA (a, b), and tBBA (c, d). Analysis of PMBGC by matrix-assisted laser desorption ionization time-of-flight mass spectrometry (MALDI-TOF MS) revealed four populations, each with a spacing of 308 m/z equal to that of the expected monomer repeat unit Structurally, these four sets of signals corresponded to populations with distinct end groups, a major population initiated by MBA and three minor populations corresponding to initiation by water, and two populations with a methyl carbonate chain ends caused by an undesired side reaction during the purification of the polymer (Figures II.30, 31 for mechanistic explanation of minor populations). There is no evidence for loss of CO_2 as a side reaction during polymerization.

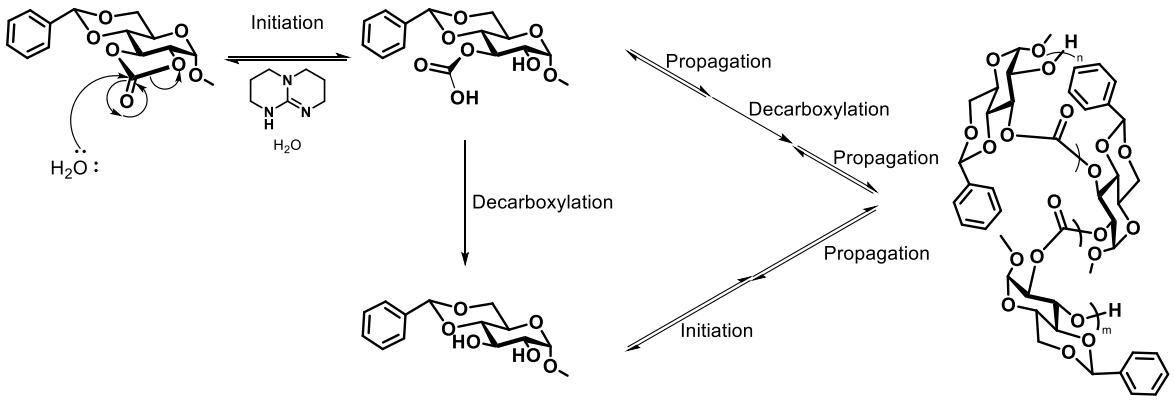

Figure II.30. Mechanistic explanation of MALDI-TOF MS data for H_2O initiated PMBGC population

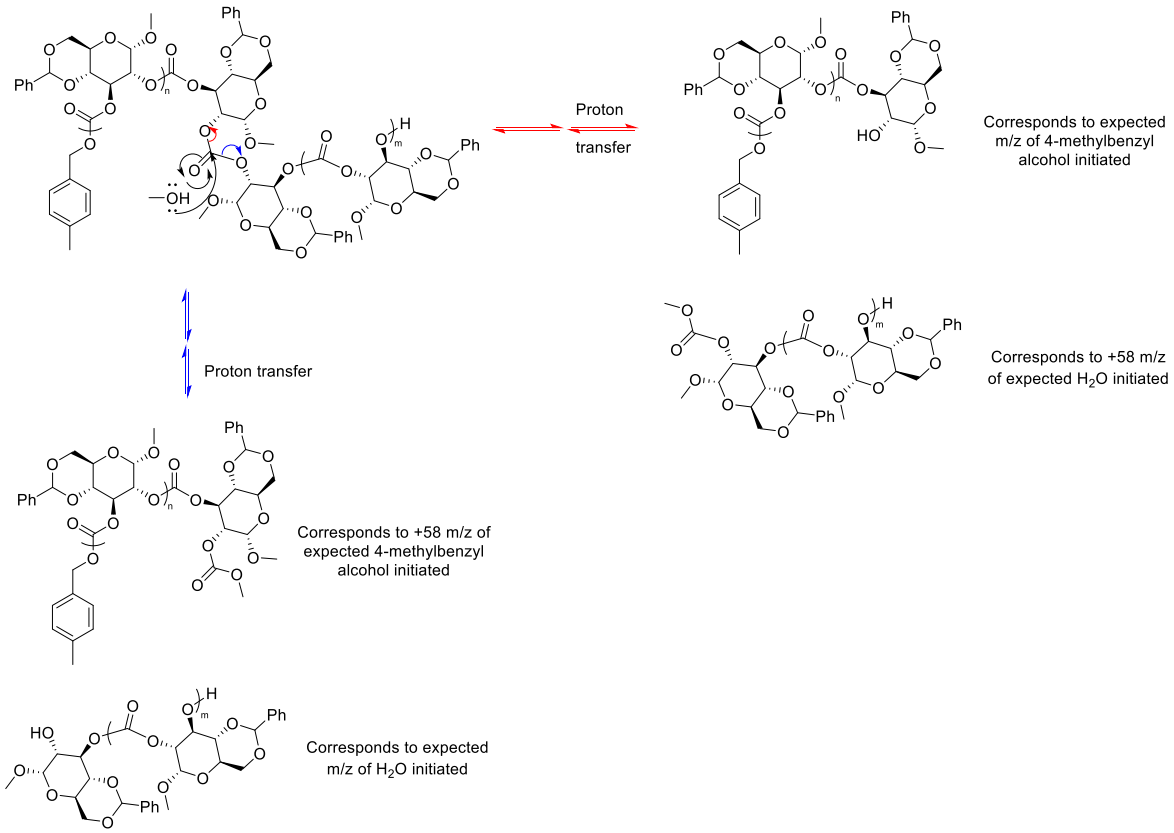

Figure II.31. Mechanistic explanation of MALDI-TOF MS data for methyl carbonate chain end populations. Arrow color indicates the directionality of the elimination after the addition of methanol.

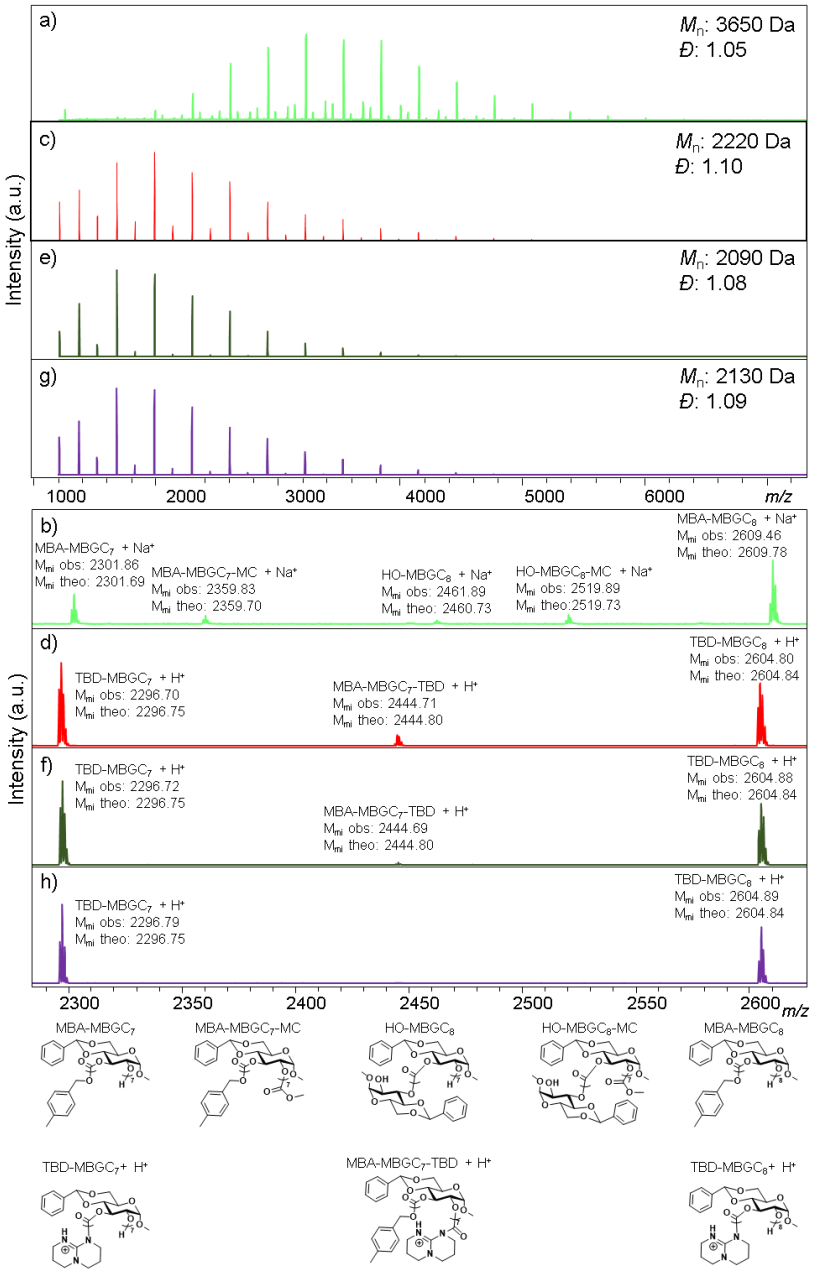

Figure II.32. The monoisotopic masses (M_{mi}) observed in the MALDI-TOF MS spectrum of PMBGC, when precipitated into methanol (a,b) and precipitated into ether, but with varying MALDI-TOF MS sample preparations, namely, with lithium cation (c,d), sodium cation (e, f), and potassium cation (g, h). The proposed chemical structures of each of the individual species identified are provided below. Analysis of PMBGC by MALDI-TOF MS revealed two populations, each with a spacing of 308 m/z equal to that of the expected monomer repeat unit. Structurally, these two sets of signals corresponded to populations with distinct end groups, a major population initiated by TBD and minor populations corresponding to both TBD and MBA chains. There is no evidence for loss of CO_2 as a side reaction during polymerization.

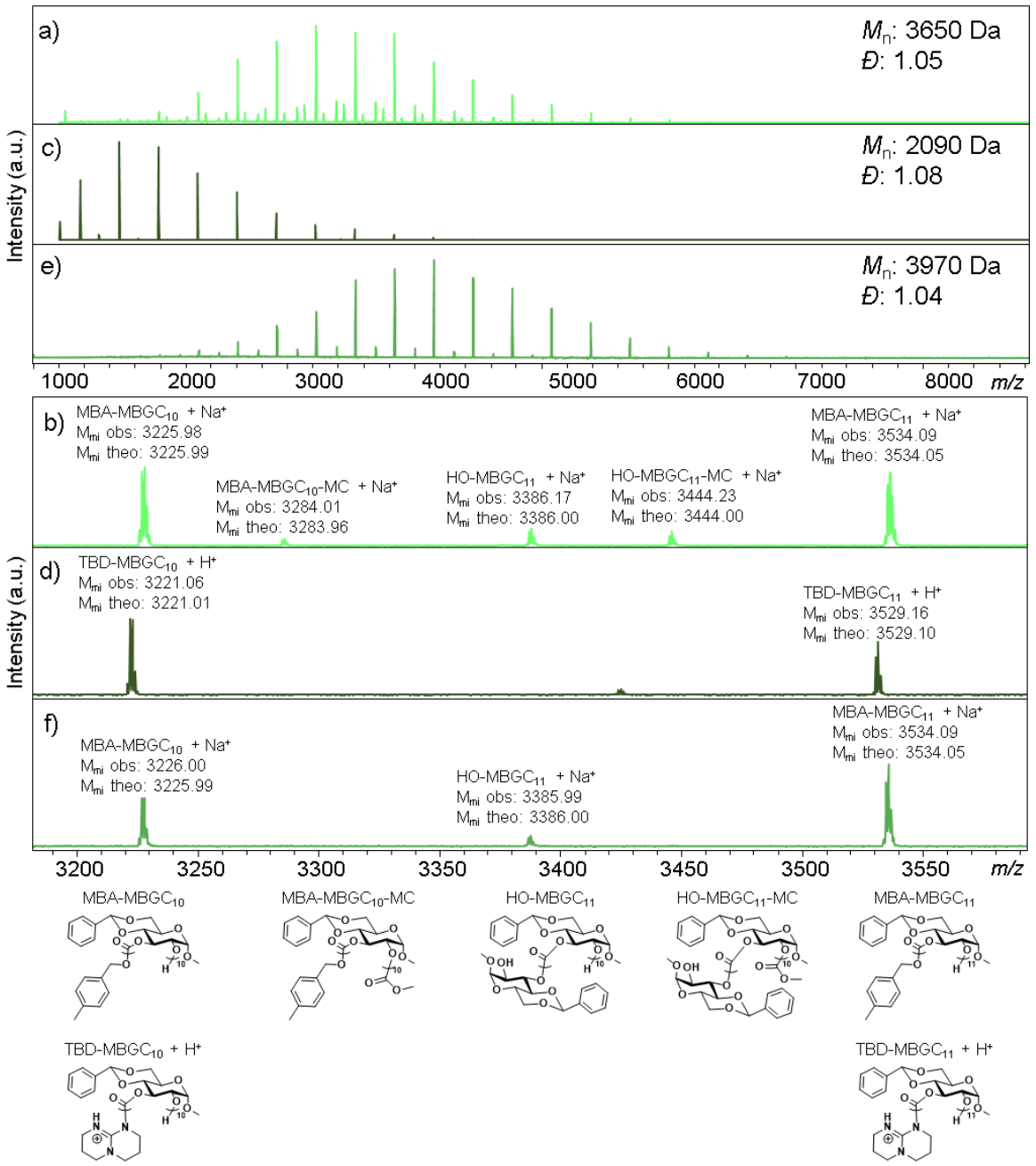

Figure II.33. The monoisotopic masses (M_{mi}) observed in the MALDI-TOF MS comparison of PMBGC purification methods. Methanol (a, b), ether (c, d), and ether followed by methanol (e, f) with the proposed chemical structures of each of the individual species identified. Analysis of PMBGC by MALDI-TOF MS revealed two populations, each with a spacing of 308 m/z equal to that of the expected monomer repeat unit. Structurally, these two sets of signals corresponded to populations with distinct end groups, a major population initiated by MBA and a minor population corresponding to initiation by water. There is no evidence for loss of CO_2 as a side reaction during polymerization.

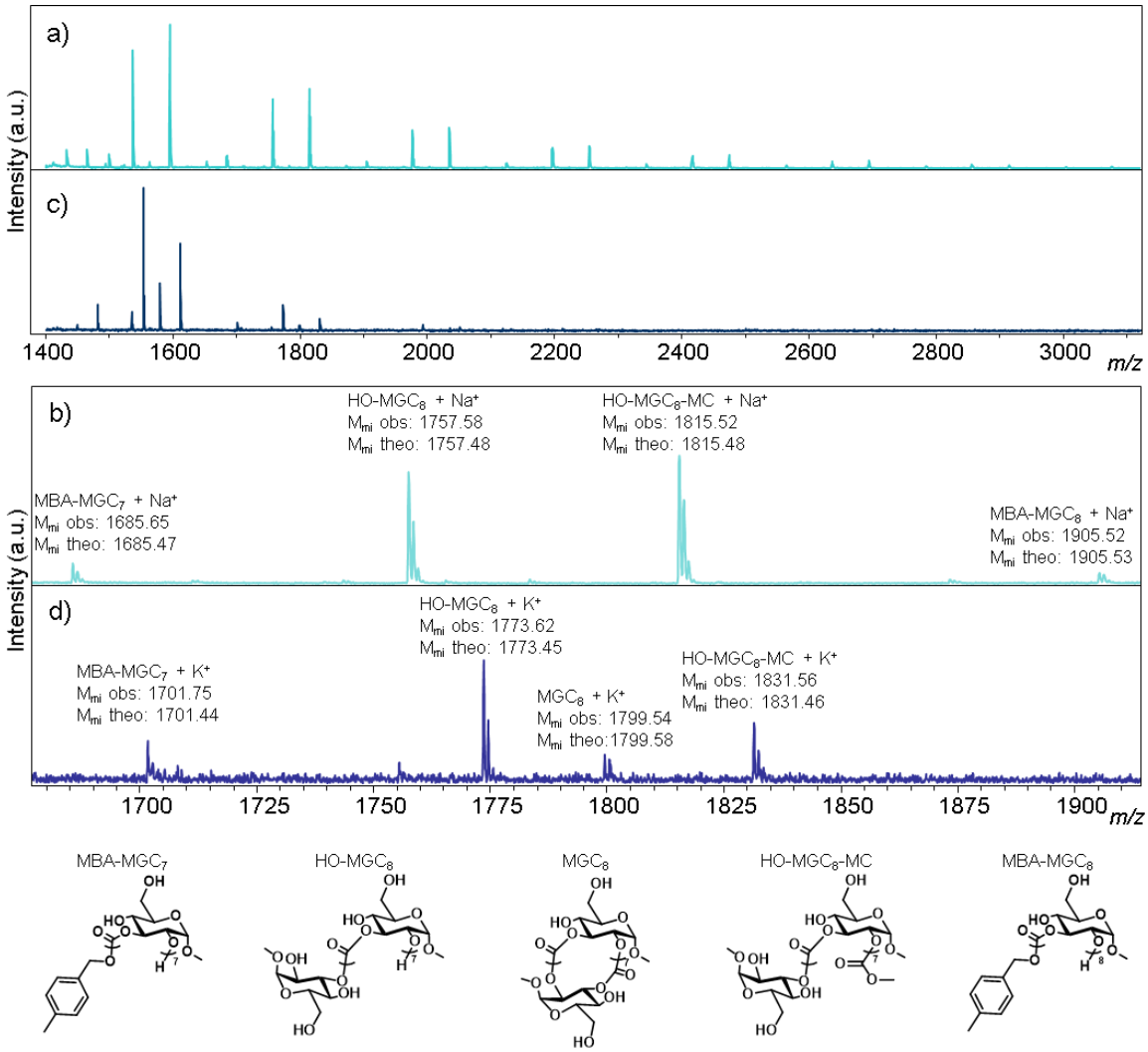

Figure II.34. The monoisotopic masses (M_{mi}) observed in the MALDI-TOF MS spectrum of PMGC, synthesized from PMBGC precipitated into methanol (with sodium cation (a, b), and potassium cation (c, d)) with the proposed chemical structures for each of the individual species identified. Analysis of PMGC by MALDI-TOF MS revealed four populations, each with a spacing of 220 m/z equal to that of the expected monomer repeat unit. Structurally, these sets of signals corresponded to populations with distinct end groups, a population initiated by MBA, a populations initiation by water, two populations with the methyl carbonate chain ends, these four populations are caused by the structure of the PMBGC precursor, and a fifth population corresponding to a cyclic species caused by transcarbonation during the deprotection reaction (Figure II.35, for mechanistic explanation of the transcarbonation reactions that occur during the deprotection).

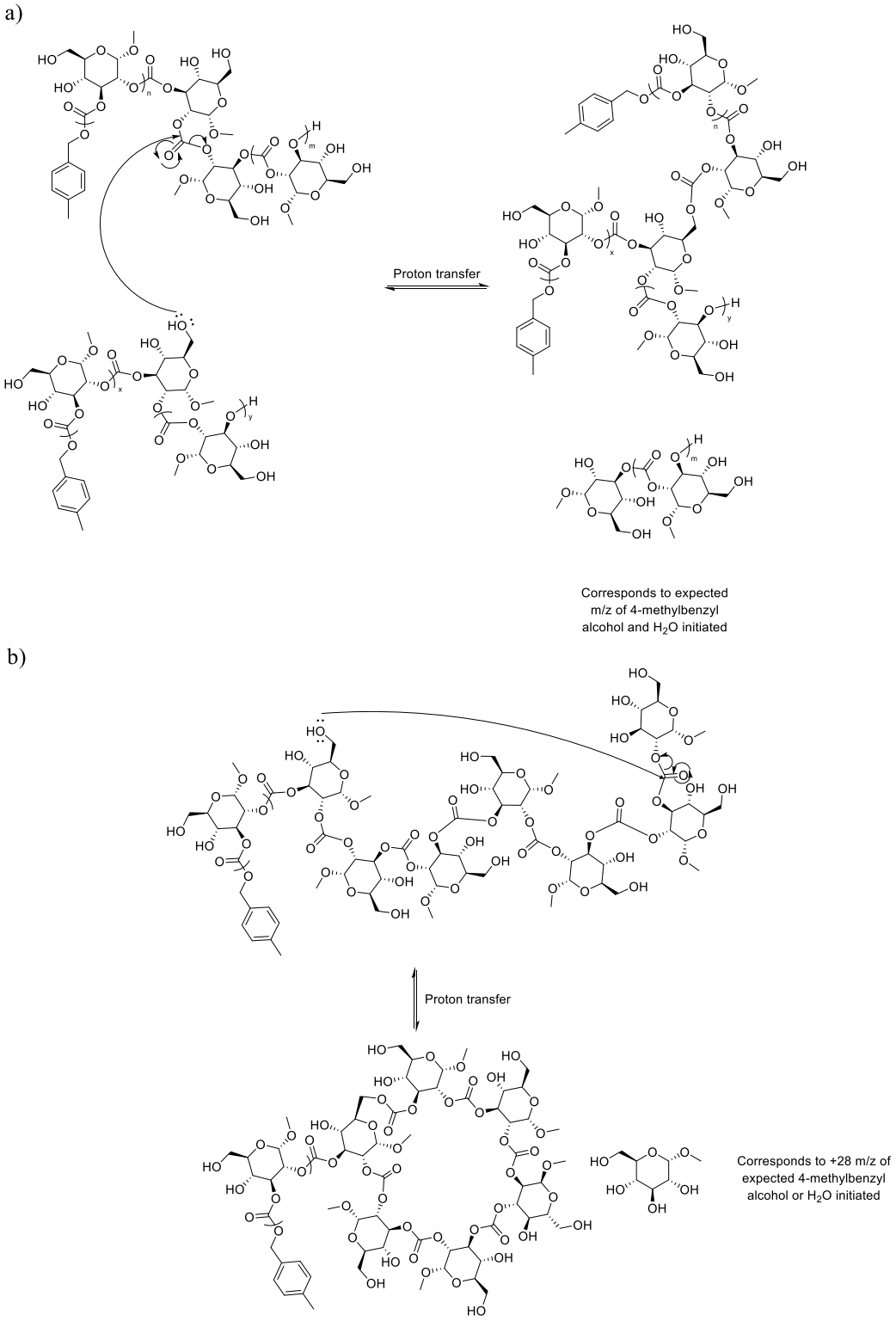

Figure II.35. Mechanistic explanation of transcarbonation reactions occurring during the synthesis of PMGC from PMBGC to form a) branched chains b) cyclic species.

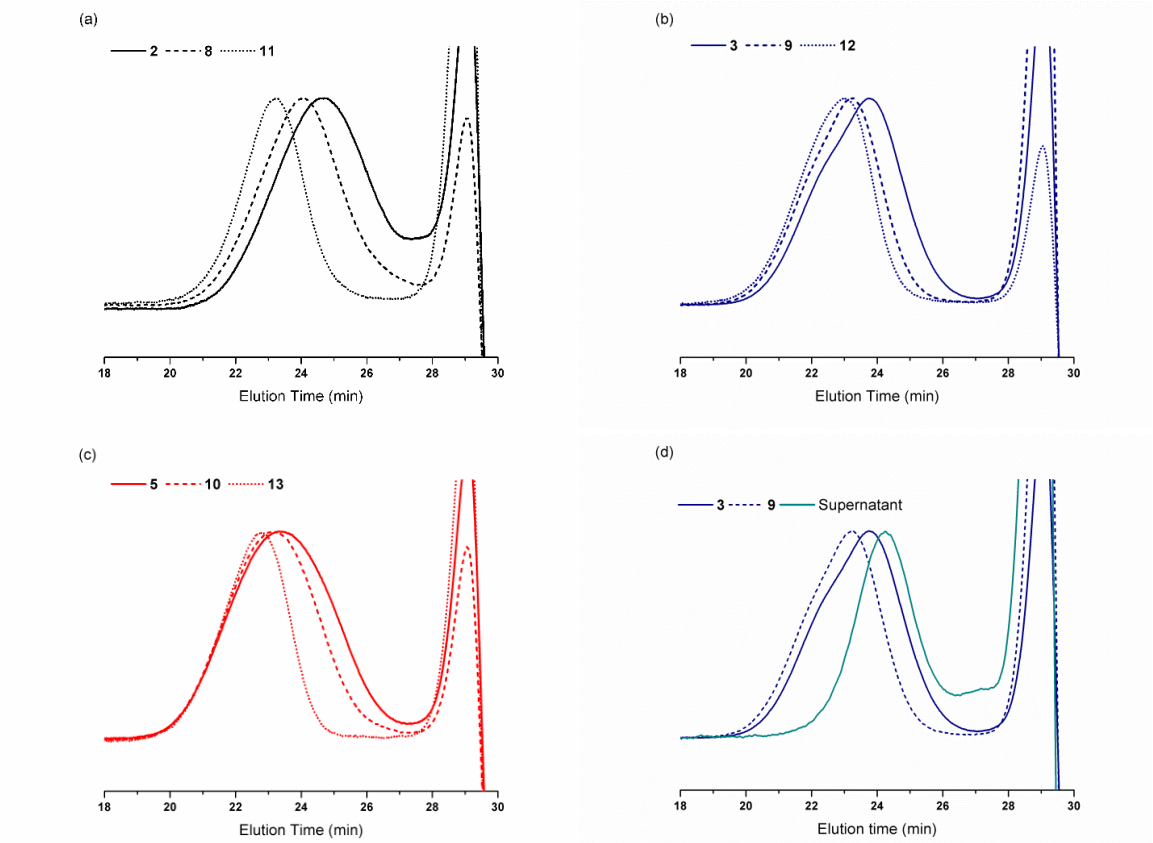

Figure II.36. SEC (DMF eluent) traces of PMBGC (solid lines), PMGC (dashed lines), and $PMAc_2GC$ (dotted lines). The PMGC and $PMAc_2GC$ polymers were synthesized from (a) **2**, (b) **3**, (c) **5**, and (d) **3** with comparison to the supernatant from the reaction of **3** to afford the PMGC sample **9** (teal solid line).

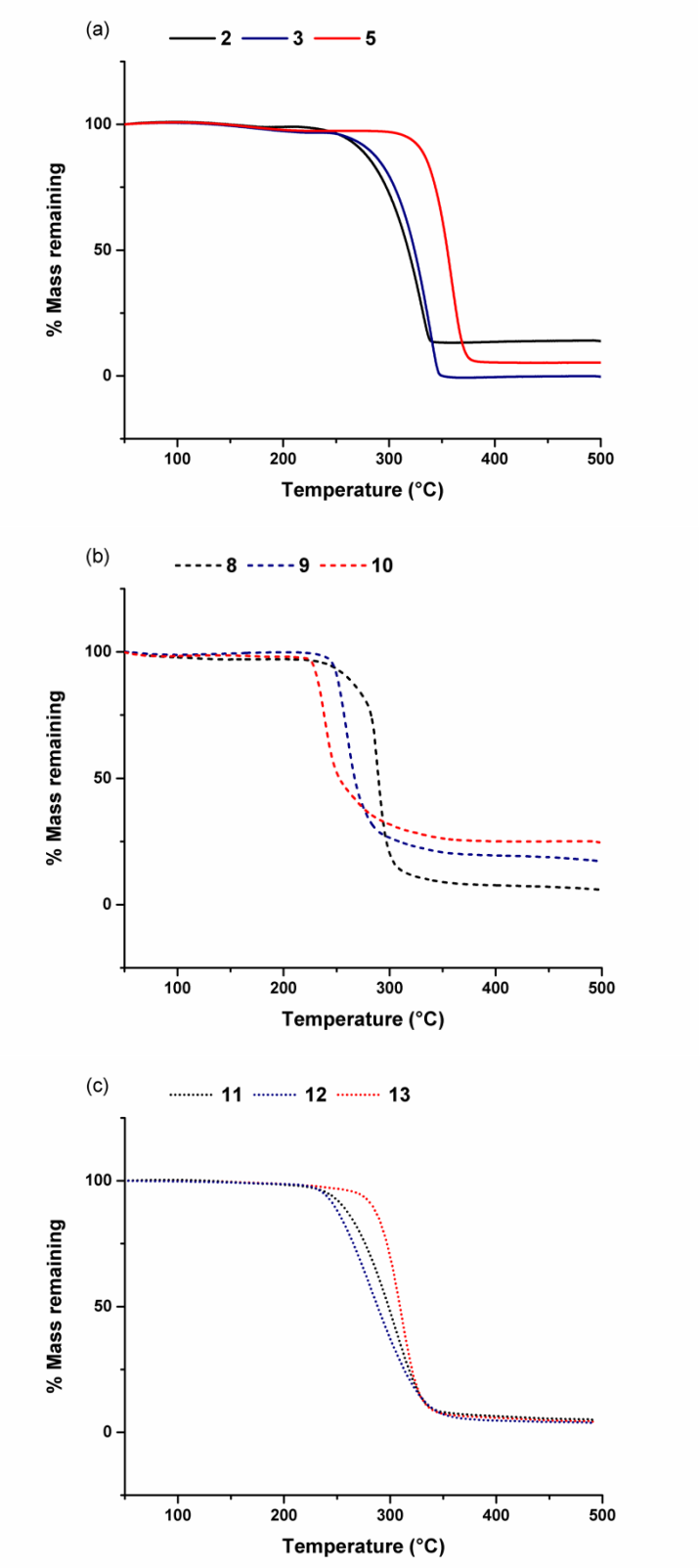

Figure II.37. Thermogravimetric analysis of (a) PMBGC, (b) PMGC, and (c) $PMAc_2GC$.

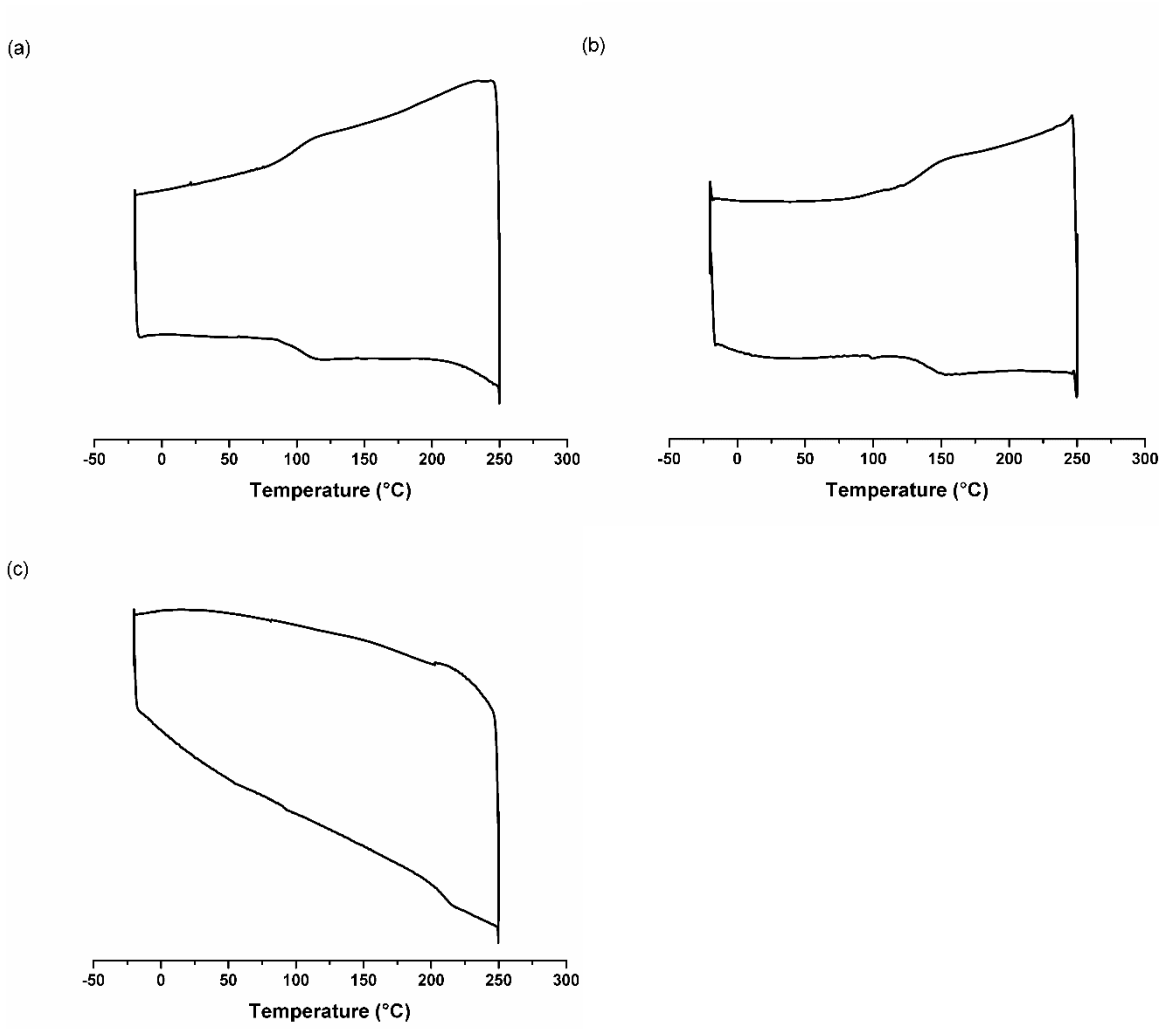

Figure II.38. Differential scanning calorimetry. The heating traces are on the bottom and the cooling traces on the top. An instrumental z-shaped glitch appears in some traces between 90-110 °C; the true T_g is seen in both the heating and cooling traces: (a) **2**, (b) **3**, and (c) **5**.

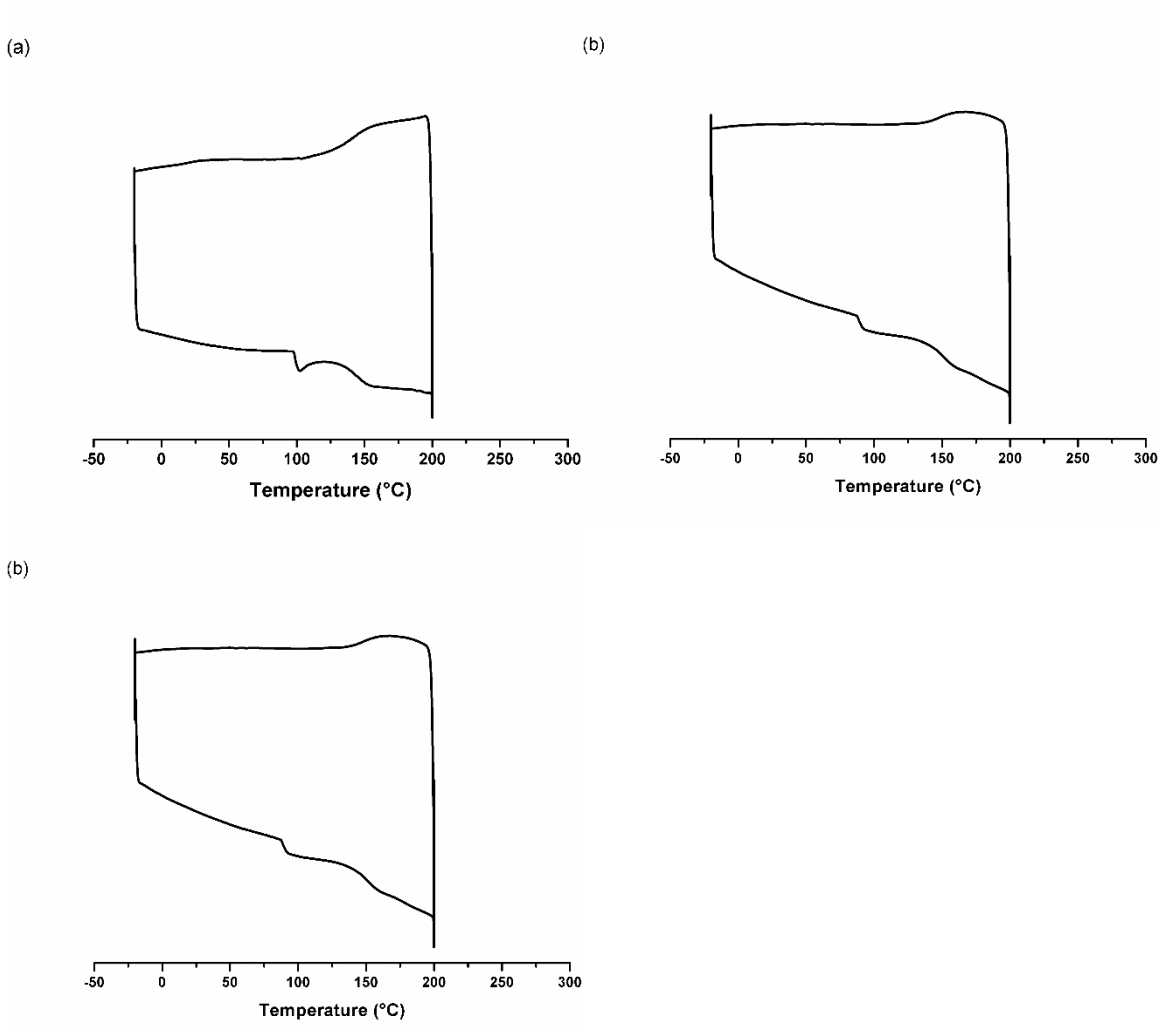

Figure II.39. Differential scanning calorimetry. The heating traces are on the bottom and the cooling traces on the top. An instrumental z-shaped glitch appears in some traces between 90-110 °C; the true T_g is seen in both the heating and cooling traces: (a) **8**, (b) **9**, and (c) **10**.

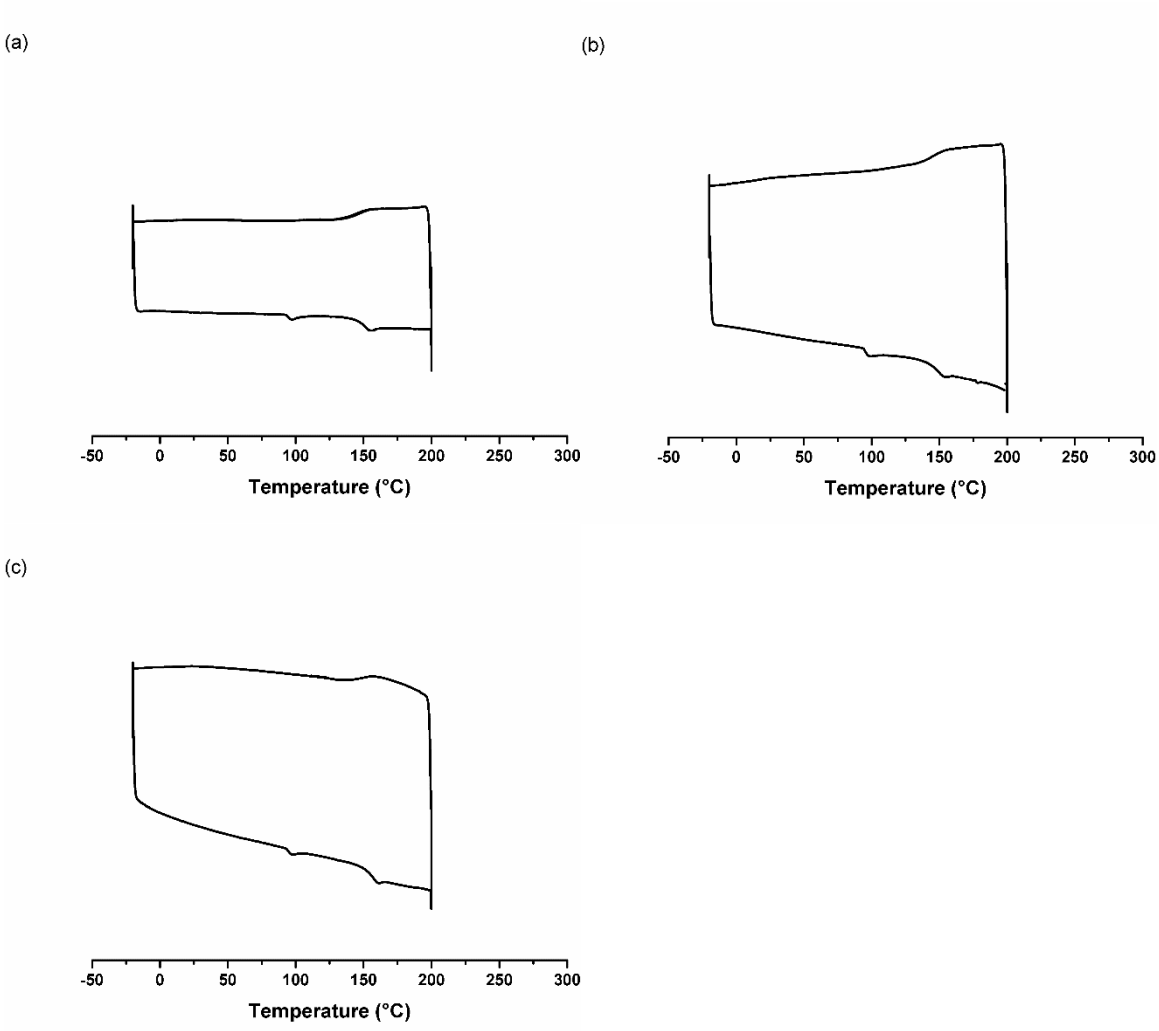

Figure II.40. Differential scanning calorimetry. The heating traces are on the bottom and the cooling traces on the top. An instrumental z-shaped glitch appears in some traces between 90-110 °C; the true T_g is seen in both the heating and cooling traces: (a) **11**, (b) **12**, and (c) **13**.

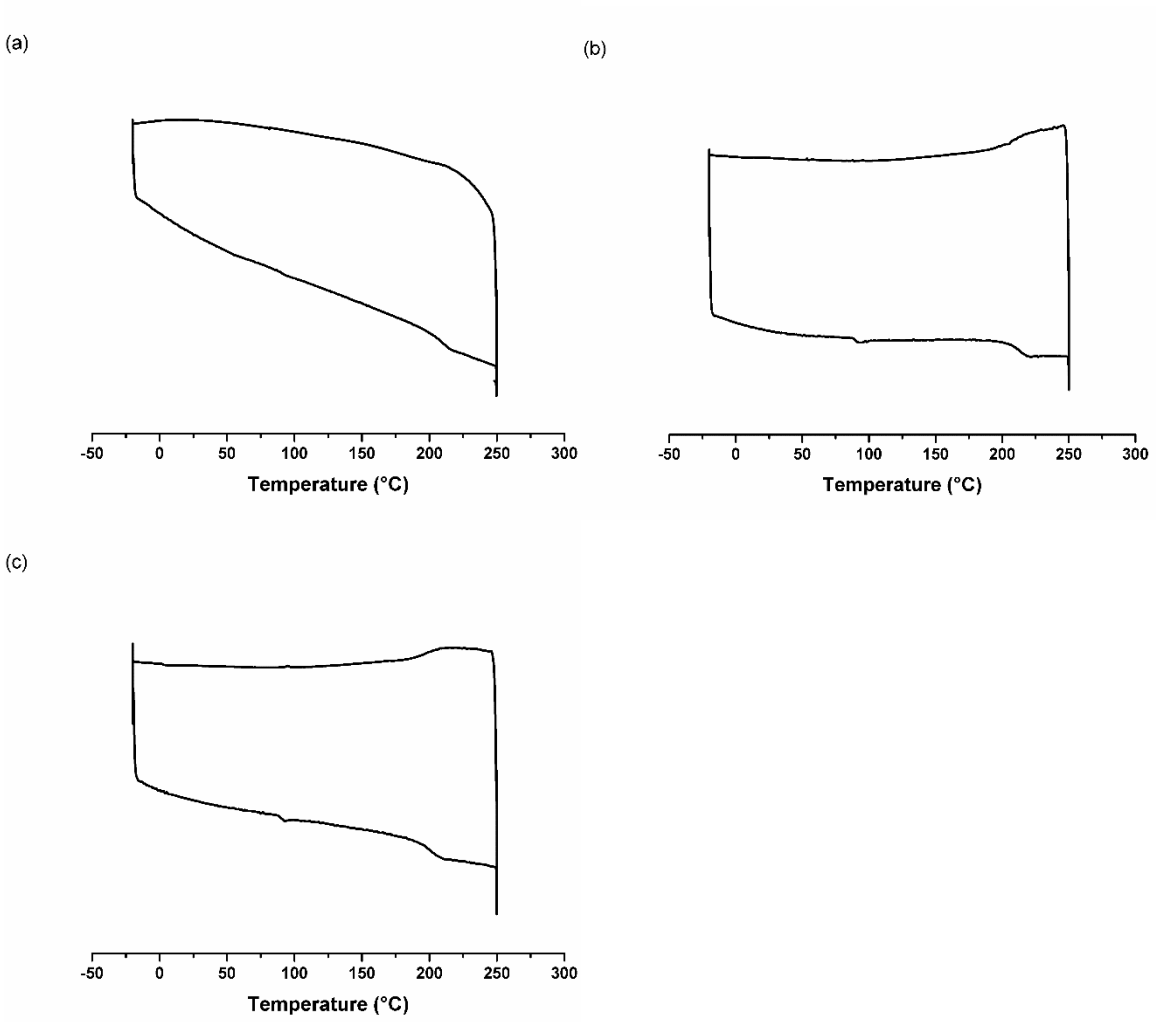

Figure II.41. DSC traces of PMBGC as a function of the wt% of added H_2O. The heating traces are on the bottom and the cooling traces on the top. An instrumental z-shaped glitch appears in some traces between 90-110 °C; the true T_g is seen in both the heating and cooling traces. The wt% of water added to **5** increased: (a) 0 wt%, (b) 5 wt%, and (c) 10 wt%.

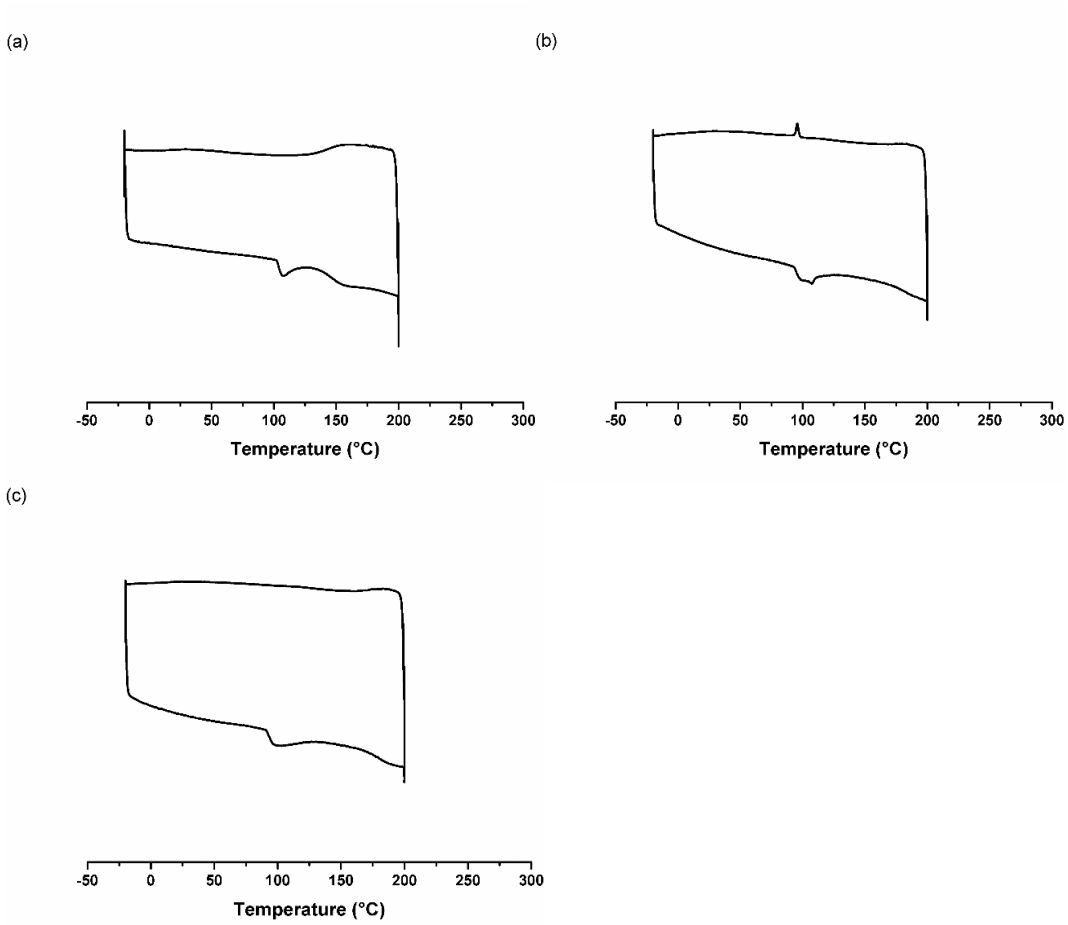

Figure II.42. DSC traces of PMGC as a function of the wt% of added H_2O. The heating traces are on the bottom and the cooling traces on the top. An instrumental z-shaped glitch appears in some traces between 90-110 °C; the true T_g is seen in both the heating and cooling traces. The wt% of water added to **10** increased: (a) 0 wt% (equilibrated in air), (b) 5 wt%, and (c) 10 wt%.

Table II.5. T_g values of polymer samples as a function of the wt% of added H_2O.

Polymer Sample	Water added (wt%)	T_g (°C)	ΔT_g (°C)
5	0 (vacuum dried)	222	0
	0 (equilibrated in air)	211	-11
	5	212	-10
	10	202	-20
10	0 (vacuum dried)	158	0
	0 (equilibrated in air)	136	-22
	5	108 or 178*	-50 or +20*
	10	94 or 180*	-64 or +22*

* Because of the instrumental "glitch" in the DSC, measurements of the T_g values for these samples were inconclusive - either decreasing to the point of overlapping with the "glitch" or increasing in an unusual inverse plasticization phenomenon

(a) (b)

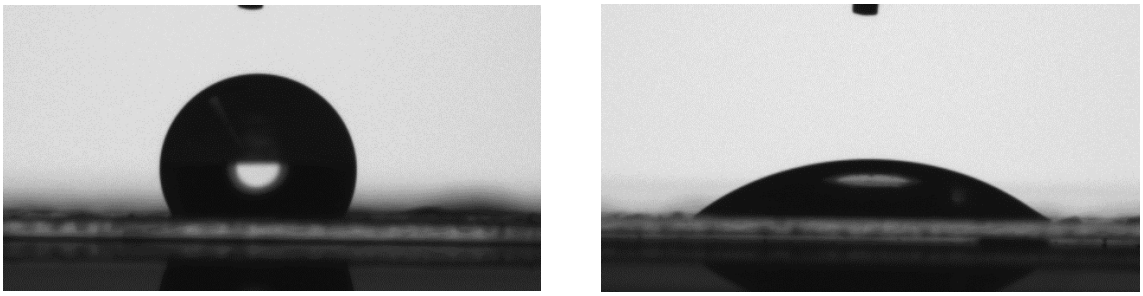

(c)

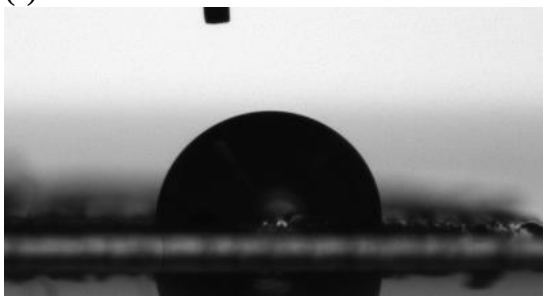

Figure II.43. Static contact angle images of water droplets on (a) **3**, (b) **9**, and (c) **12**.

Equation II.1. Aqueous bulk degradation mass remaining calculation.

$$\%\ mass\ remaining = \left[1 - \frac{W_0 - W_d}{W_0}\right] \times 100$$

$$W_0 = initial\ weight$$

$$W_d = dry\ weight$$

Equation II.2. Aqueous bulk degradation swelling calculation.

$$\%\ swelling = \left[\frac{W_w - W_d}{W_d}\right] \times 100$$

$$W_w = wet\ weight$$

$$W_d = dry\ weigh$$

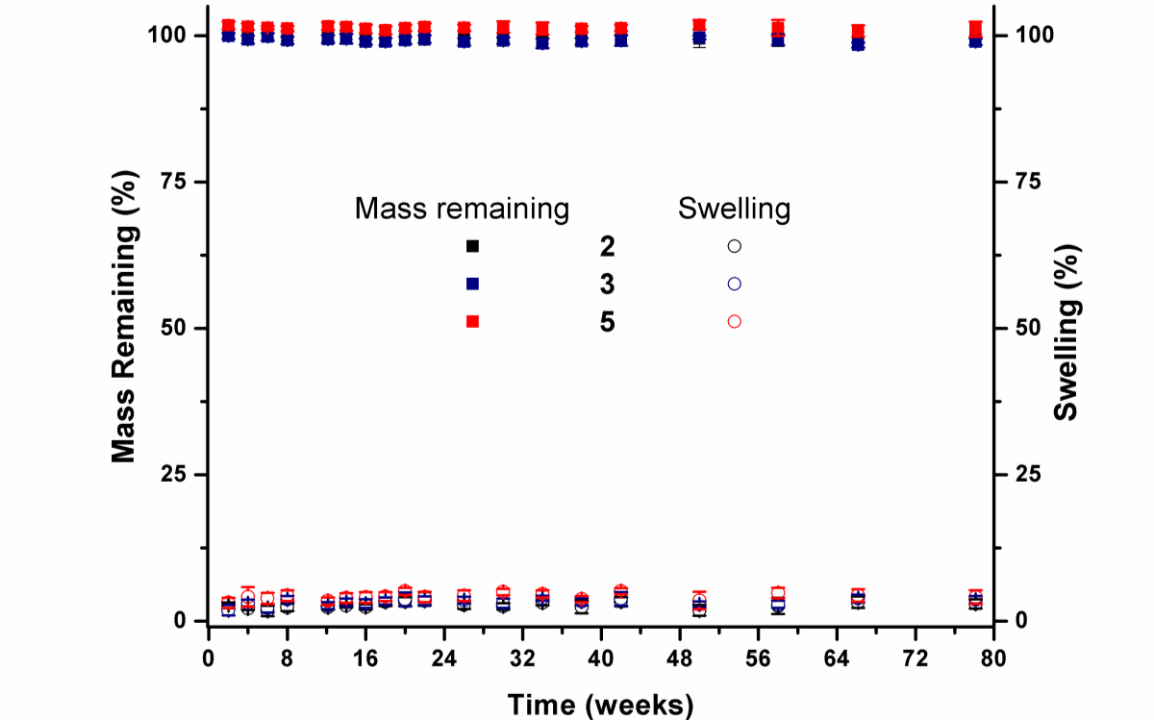

Figure II.44. Aqueous bulk degradation, PBS pH = 7, profile of **2** (black), **3** (blue), and **5** (red). Left axis/squares percent mass remaining of the bulk polymer samples. Right axis/open circles weight percent of buffer swelling in the polymer samples prior to drying, n = 8.

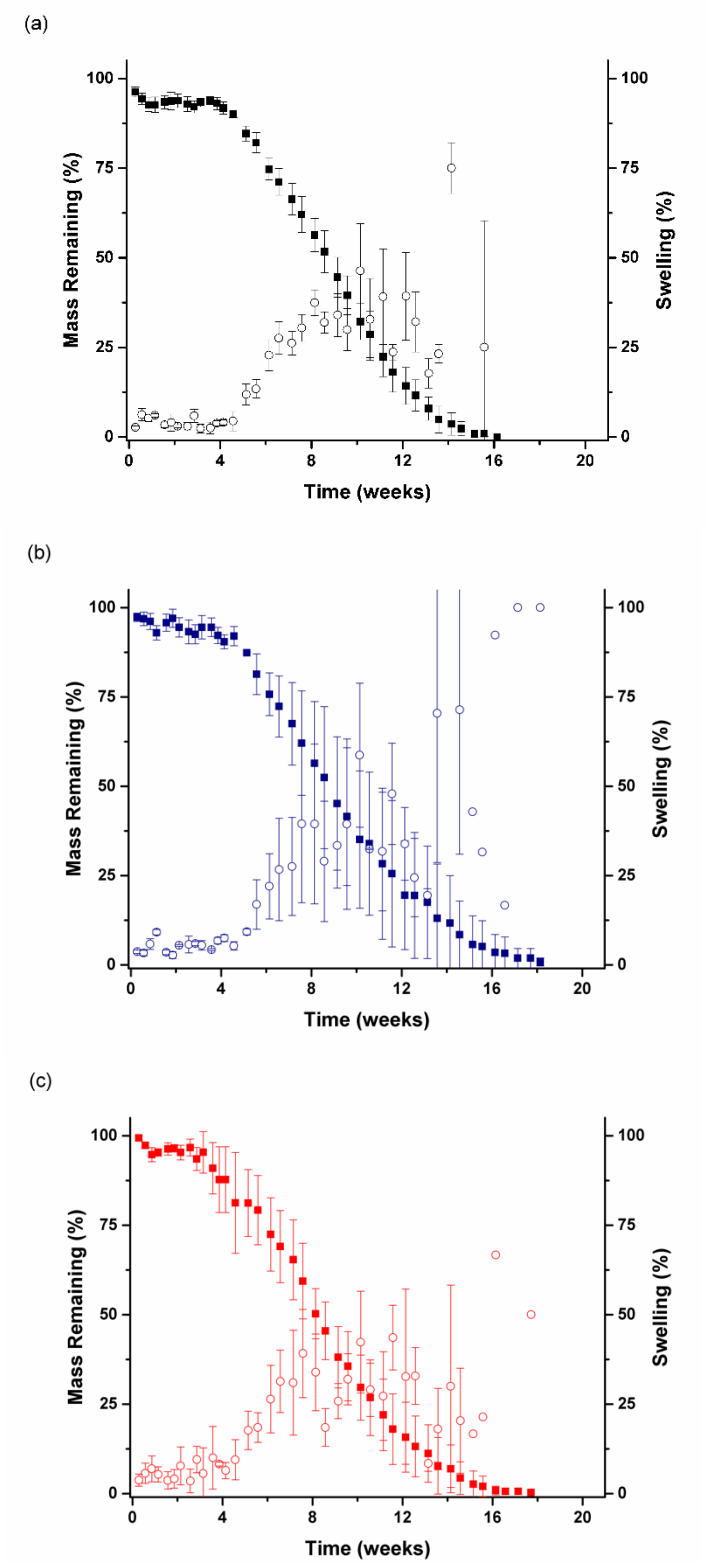

Figure II.45. Aqueous bulk degradation, 1 M HCl pH = 1, profile of (a) **2**, (b) **3**, and (c) **5**. Left axis/squares percent mass remaining of the bulk polymer samples. Right axis/open circles weight percent of aqueous swelling in the polymer samples prior to drying, n = 3.

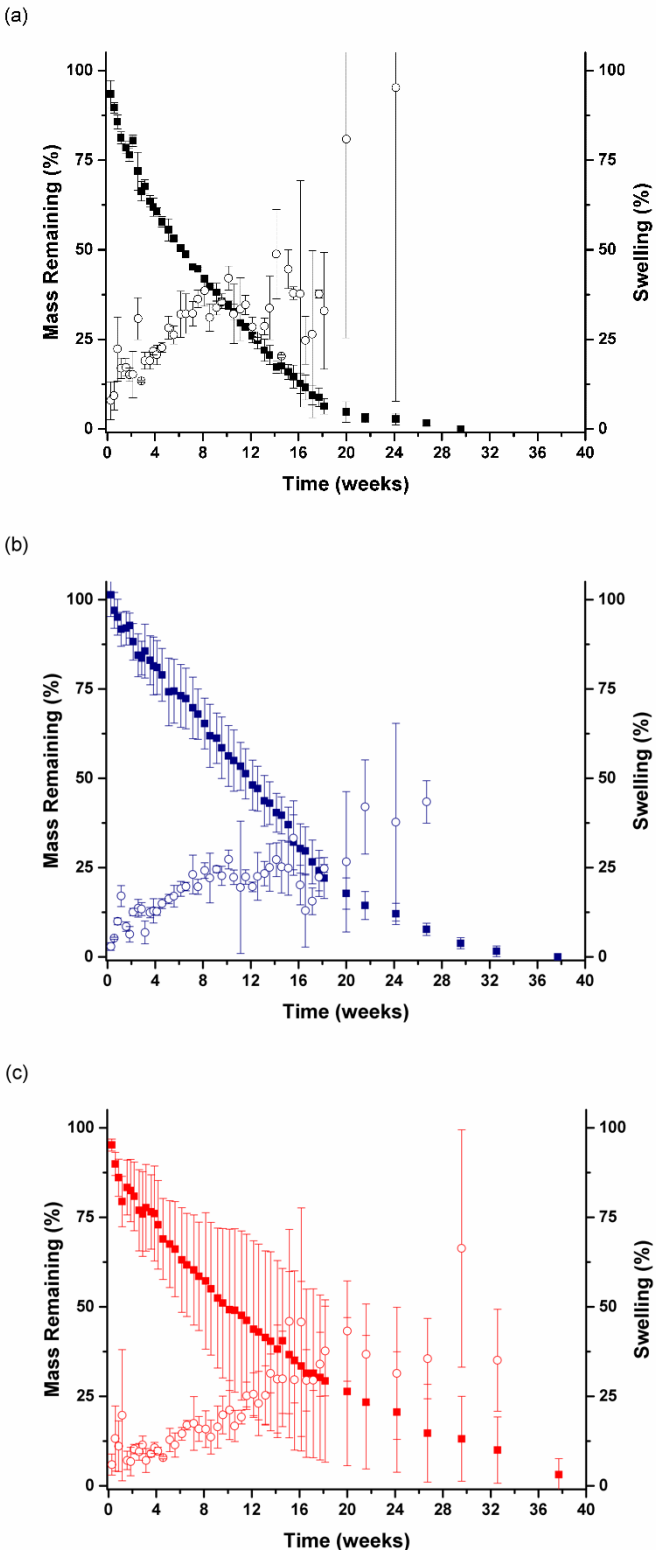

Figure II.46. Aqueous bulk degradation, 1 M NaOH pH = 14, profile of (a) **2**, (b) **3**, and (c) **5**. Left axis/squares percent mass remaining of the bulk polymer samples. Right axis/open circles weight percent of aqueous swelling in the polymer samples prior to drying, n = 3.

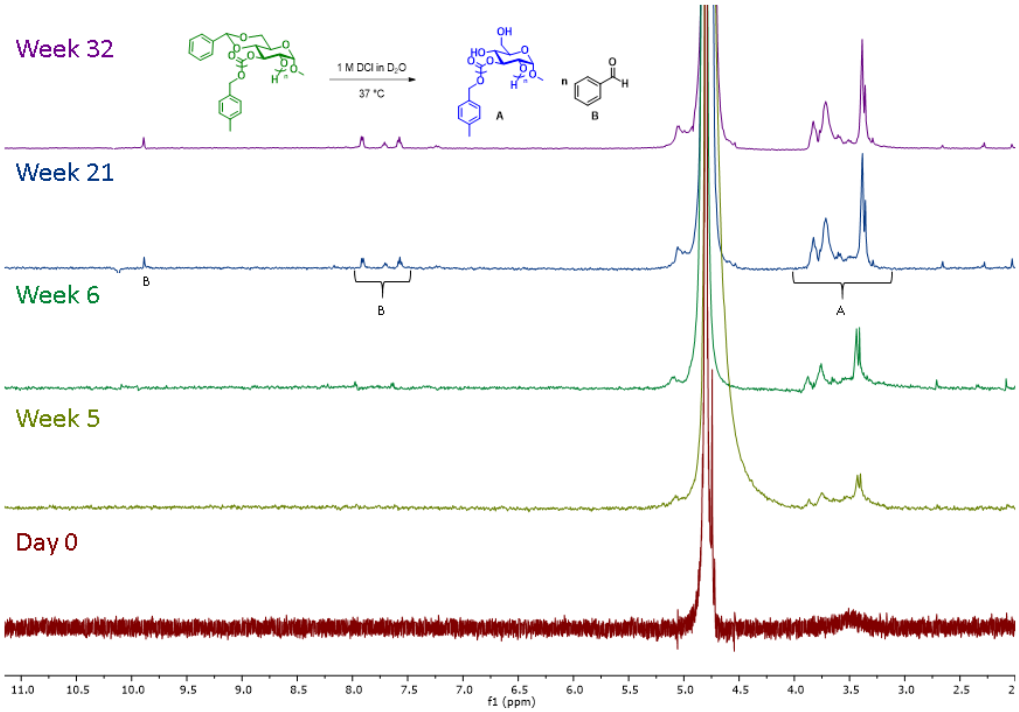

Figure II.47. Aqueous degradation, ^{1}H NMR spectra of **2** in 1.0 M DCl/D_2O at 0, 5, 6, 21, and 32 weeks.

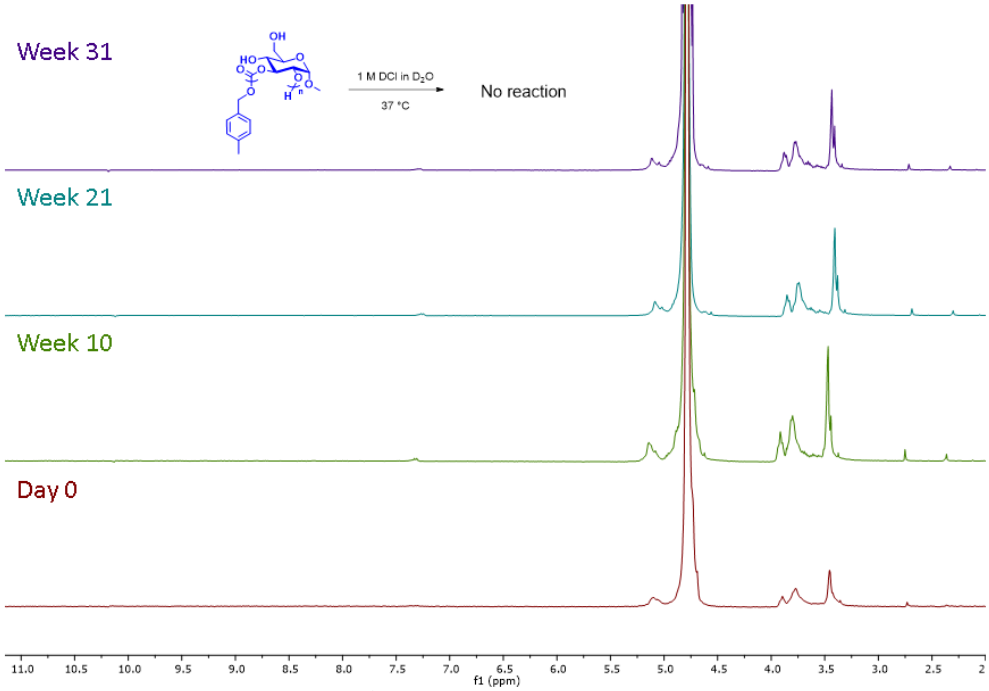

Figure II.48. Aqueous degradation, ^{1}H NMR spectra of **8** in 1.0 M DCl/D_2O at 0, 10, 21, and 31 weeks.

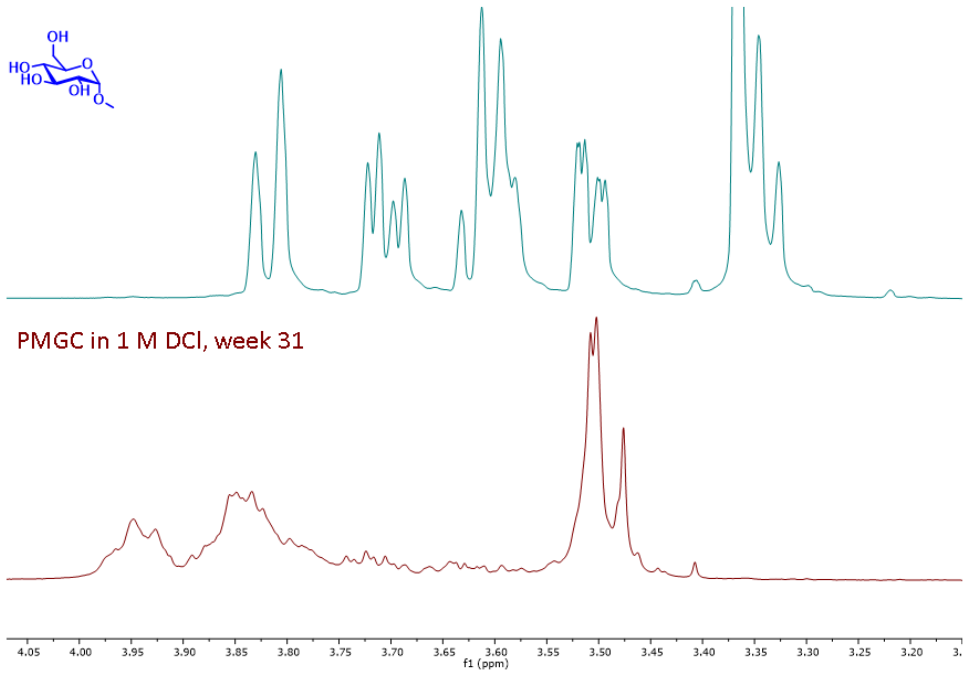

Figure II.49. ^{1}H NMR spectra of methyl α-D-glucopyranoside and PMGC in acidic media, 1 M DCl/D_2O at week 31.

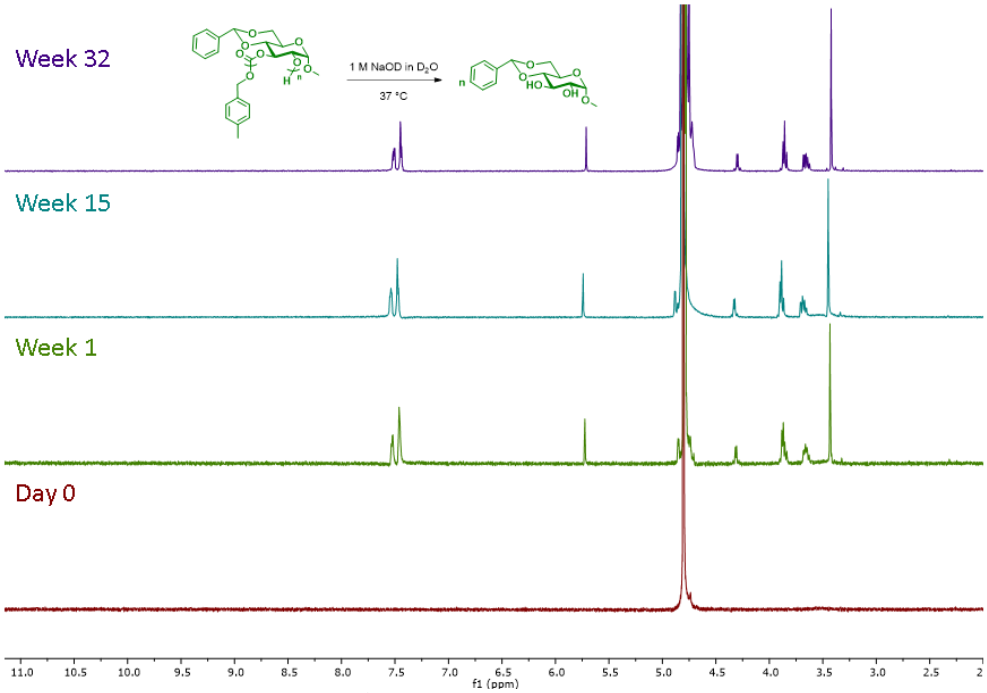

Figure II.50. Aqueous degradation, ^{1}H NMR spectra of **2** in 1.0 M NaOD/D_2O at 0, 1, 15, and 32 weeks.

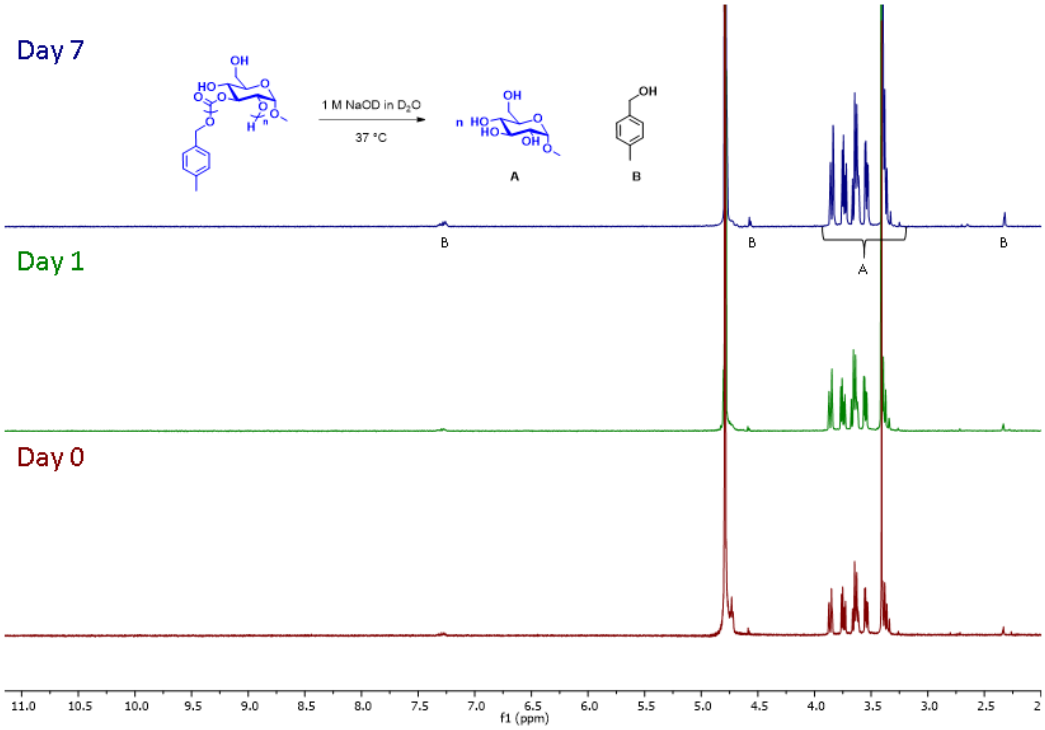

Figure II.51. Aqueous degradation, ^{1}H NMR spectra of **8** in 1.0 M NaOD/D_2O at 0, 1, and 7 days.

CHAPTER III

CONSTRUCTION OF NANOSTRUCTURES IN AQUEOUS SOLUTION FROM AMPHIPHILIC GLUCOSE-DERIVED POLYCARBONATES[2]

3.1 Introduction

In the past several decades, there has been a significant effort in polymer science to develop and synthesize functional polymeric materials from natural starting materials. These new materials have focused on using various lignins, fatty acids, carbohydrates, and other natural products as the building blocks for functional materials.[23,25-27,32,99] Carbohydrates (sugars) are of significant interest within this field, based on their structural diversity and significant bioavailability. The wealth of research that has been done into the placement of precise functionalities on carbohydrates in a regiospecific manner, as well as their high degrees of chemical functionality and bioactivities has allowed for the inclusion of sugars in the backbones and side chains of a variety of different polymeric architectures.[24,33-40] The Wooley lab has a significant interest in the development of synthetic methodologies for the preparation of well-defined poly(glucose carbonate)s, with tuning of their properties and investigation of their translation across a diverse range of applications.[48,75-78] Recently, we reported the straightforward synthesis of a family of poly(glucose carbonate) homopolymers from a single 5-membered cyclic carbonate

[2]Adapted with permission from "Construction of nanostructures in aqueous solution from amphiphilic glucose-derived polycarbonates" by Osumi, S. O.[§;] Felder, S. E. [§]; Wang, H.; Lin, Y.-N.; Dong, M.;Wooley, K. L., *Polym. Sci., Part A: Polym. Chem.* **2018**, DOI:10.1002/pola.29229. Copyright 2018 John Wiley and Sons

monomer, methyl 4,6-*O*-benzylidene-2,3-*O*-carbonyl-α-D-glucopyranoside (MBGC).[76] This system demonstrated a transferable and high yielding (>95%) monomer synthesis with the ability to undergo a controlled organocatalyzed ring-opening polymerization. This polymeric system was also designed to undergo a post-polymerization deprotection that allowed for a switching of the hydrophilicity of the polymers from a hydrophobic to a hydrophilic material. The slight water solubility demonstrated by the hydrophilic poly(glucose carbonate) polymer, drove our interest in the overall ability of this system to undergo self-assembly under aqueous conditions.

Morphological control over the supramolecular assembly of amphiphilic polymers has been studied widely in the bulk and solution states.[100-105] A key advantage for amphiphilic polymers and block polymers is their ability to undergo assembly in water. The self-assembly of amphiphilic block copolymers into micelles or other nanostructures in aqueous solution allows for investigation of their use as nanoscopic objects with potential implementation in a range of vital applications from biomedical to engineering applications.[103-113] Degradable polymers are of great interest as they can enable straightforward end-of-use options for polymeric systems, and a tunable cargo release based on the degradation rate of the polymeric scaffold.[46,114,115] Significant efforts have been directed towards the development of amphiphilic degradable polymers and the study of their self-assembly behaviors.[46,75,77,78,112] It is our premise that, in the design of these types of polymeric materials, monomers should be chosen that allow for the corresponding polymers to degrade into benign, or optimally, beneficial degradation products. Therefore, we have focused for the past decade on the transformation of natural products, particularly sugars, into functional polymer materials.[24,34,75,76,78] Moreover, we harness the regiochemical and

stereochemical sophistication that is inherent to carbohydrates to study effects on chemical reactivity, *e.g*. monomer synthesis and polymerizability, and on physicochemical properties of the resulting polymers. Based on the attractive qualities of the MBGC synthesis and polymerization, we herein extend the study of this polymer to the synthesis and self-assembly behavior of amphiphilic copolymers and block copolymers. Polymers of different molar masses were produced *via* the organocatalytic ring-opening polymerization of MBGC initiated with a small molecule initiator (to afford homopolymers) or a hydrophilic polymer macroinitiator (to afford block copolymers). The acid sensitivity of the benzylidene acetal protecting group was used to generate copolymers with different degrees of benzylidene remaining as a side chain, from 50 to 0%, as a method to modulate the amphiphilicity of the polymers. The self-assembly behavior of these polymers was then examined under aqueous assembly conditions. Comparisons of the assembly behaviors were made between the original block copolymers and the deprotected block polymers, as well as copolymers made from the acidic deprotection of PMBGC homopolymer.

3.2 Results and Discussion

Based on our interest in the development of well-defined poly(glucose carbonate)s, we investigated the synthesis of amphiphilic block copolymers from mPEG and a glucose-based 5-membered cyclic carbonate monomer *via* organocatalytic ring-opening polymerization, and the post-polymerization modification of these polymers to increase their hydrophilicity. The aqueous self-assembly characteristics of these materials were investigated and compared to the corresponding glucose carbonate homopolymer.

3.2.1 Polymer synthesis and post-polymerization modification

Amphiphilic degradable diblock copolymers, mPEG-*b*-PMBGC, were synthesized *via* organocatalytic ring-opening polymerization of MBGC with TBD as a catalyst and $mPEG_{113}$ as a macroinitiator (Figure III.1). The shift of the copolymer to lower retention volumes in SEC than the $mPEG_{113}$ macroinitiator confirmed the successful chain extension to afford the anticipated copolymers (Figure III.1). The polymerization was able to produce well-defined polymers based on the monomodal molar mass distributions and the low dispersity values of the synthesized polymers. The molar mass and glucose carbonate content of the final block copolymer were controllable by the monomer-to-initiator ratio used in the polymerization, and this control was utilized to synthesize a series of block polymers with differing molar masses, hydrophilic-hydrophobic ratios, and glucose contents (Table III.1). The series of amphiphilic diblock copolymers **14**, **15**, and **16** with increasing PMBGC block lengths and correspondingly decreasing hydrophilicity was synthesized. The degree of polymerization was estimated by both SEC and ^{1}H NMR of the polymer following purification by precipitation into diethyl ether. Although SEC requires a calibration, polystyrene in this case, both methods were in agreement with the theoretical molar mass expected from the monomer-to-initiator ratios. Monomer conversion was not monitored quantitatively during these polymerizations because of challenges associated with its measurement,[76] SEC was used to qualitatively determine the presence of residual monomer and monitor the relative evolution of the molar mass distributions.

We then sought to take advantage of the acid labile benzylidene protecting group on the glucose carbonate repeat unit to transform **14** and **16** into block polymers **17**, **18**, and **19**

having increasing hydrophilicity by partial or full benzylidene removal. From the previously reported acidic deprotection of the PMBGC homopolymer, it was found that a transcarbonation reaction between the newly revealed hydroxyl groups along the polymer side chains and the carbonate backbone of the polymer occurred during the benzylidene removal. To reduce this undesired side reaction, the acidic deprotection of PMBGC was further examined. Under the previously reported conditions, within 4 h approximately 95% of the benzylidene residues had been removed from the PMBGC homopolymer. This reaction time was then applied to the mPEG-*b*-PMBGC polymers and in 4 h, less than 25% of the benzylidene residues had been removed, suggesting that the addition of mPEG to the system significantly altered the kinetics of the deprotection. Initially, we hypothesized that the change in kinetics was caused by the formation of assemblies during the reaction because of the unfavorable solubility of the hydroxyl side chains in DCM. To combat this potential shielding of the benzylidene groups, DMSO or DMF was added as a cosolvent. This addition resulted in 0% removal of the benzylidene groups over 14 h. These same conditions were then applied to the PMBGC homopolymer and the same phenomenon was observed, indicating that DMSO and DMF have a significant negative effect on the deprotection reaction. The equivalences of acid and water to the sugar repeat units were then varied, and it was determined that higher equivalences of each, relative to the homopolymer, were required for the reaction to proceed efficiently. Following this study of the deprotection, copolymers were produced having different degrees of benzylidene removed, by reaction with 67 vol% TFA in H_2O at 3 molar equivalents TFA relative to benzylidene acetals along the polymer backbone. The effect of the mPEG on the deprotection of the sugar block was still observed under these conditions. For instance, **14** was not able to be fully deprotected,

whereas **16**, which has a significantly lower mPEG content, was able to reach full deprotection. The overall success of these deprotections (>85% yield) was confirmed through the disappearance or reduction in the ^{1}H (7.55-7.18, 5.72-5.44 ppm) and ^{13}C (137.5-136.4, 129.6-127.4, 126.9-125.1, 101.6-99.0 ppm) NMR signals corresponding to the benzylidene groups (Figures III.9-12). Additionally, an IR absorbance appeared at 3675-3100 cm^{-1} (Figure III.13), corresponding to the O-H stretch, with increasing relative intensity as the amount of deprotection increased.

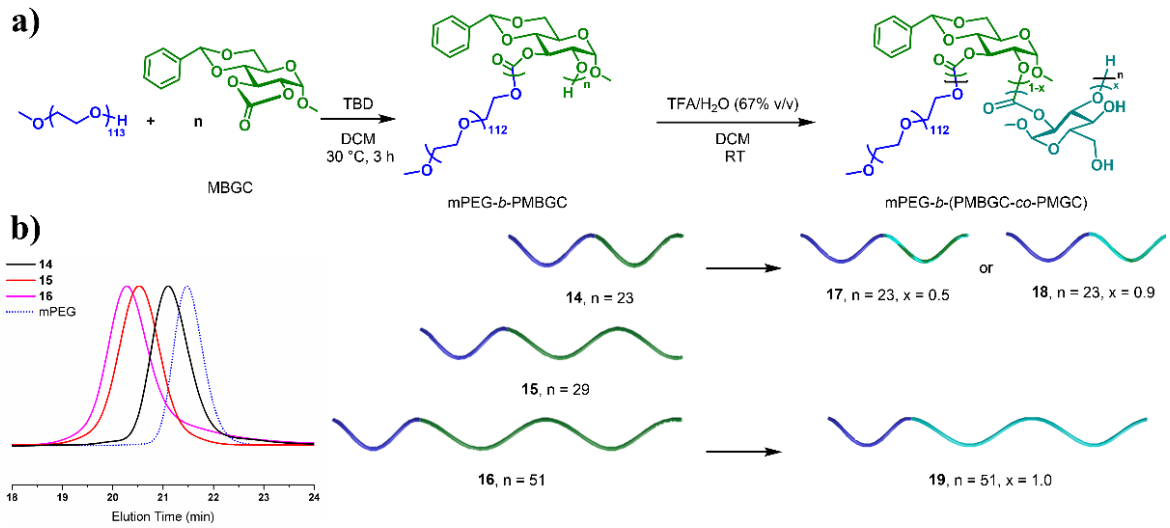

Figure III.1. a) Synthesis and post-polymerization deprotection of mPEG-*b*-PMBGC to afford mPEG-*b*-(PMBGC-*co*-PMGC) and schematic illustrations of the polymer lengths and architectures; b) SEC (THF eluent) traces of mPEG-*b*-PMBGC compared to the mPEG$_{113}$ macroinitiator.

Table III.1. Properties of mPEG-*b*-PMBGC, and mPEG-*b*-(PMBGC-*co*-PMGC).

Polymer	Sample	[M]:[I][a]	Theoretical M_n (kDa)[b]	Hydrophilic-hydrophobic ratio (mass/mass)	M_n[c] (kDa)	M_n[d] (kDa)	$Đ$[d]
$mPEG_{113}$-*b*-$PMBGC_{23}$	**14**	20	11.2	41:59	12.1	12.0	1.06
$mPEG_{113}$-*b*-$PMBGC_{29}$	**15**	30	14.2	36:64	13.9	14.8	1.15
$mPEG_{113}$-*b*-$PMBGC_{51}$	**16**	50	20.4	24:76	20.7	18.9	1.05
$mPEG_{113}$-*b*-($PMBGC_{0.5}$-*co*-$PMGC_{0.5}$)$_{23}$	**17**[e]	-	10.2	32:68	N/A[g]	N/A[h]	N/A[h]
$mPEG_{113}$-*b*-($PMBGC_{0.1}$-*co*-$PMGC_{0.9}$)$_{23}$	**18**[e]	-	9.6	93:7	N/A[g]	N/A[h]	N/A[h]
$mPEG_{113}$-*b*-$PMGC_{51}$	**19**[f]	-	16.0	100:0	N/A[g]	N/A[h]	N/A[h]

[a] MBGC:PEG. [b] Calculated as M_n = 5000 Da + [M]:[I] ratio (308.29 Da) + 1 Da for the $mPEG_{113}$ molar mass, PMBGC DP_n, MBGC repeat unit molar mass and proton terminator molar mass, respectively, given *ca*. complete conversion, and rounded to appropriate significant figures. [c] Measured by ^{1}H NMR comparing the aromatic signals of the polymer to the methylene signal of the $mPEG_{113}$. [d] Measured with SEC (THF eluent) calibrated with polystyrene standards. [e] Synthesized from **14**. [f] Synthesized from **16**. [g] NMR indicates transcarbonation occurred making comparisons of sugar to mPEG signals inaccurate. [h] Not soluble in THF.

Thermal analysis of the polymers by both TGA and DSC was complicated by the hygroscopic nature of the polymers, making the identification of the thermal degradations and transitions difficult. All the polymers demonstrated reasonable thermal stabilities >220 °C, and slightly decreased thermal stability upon deprotection (Figure III.15). The thermal degradation for **14** underwent a single stage mass loss, while **15-19** underwent dual stage mass losses. The block of the polymer degrading in each stage was not quantitatively identifiable by the percent mass loss. However, based on the homopolymer thermal stabilities, the first mass loss was likely predominately the sugar block, whereas the second block was likely predominantly thermal degradation related to the mPEG block. Under DSC analysis, a glass transition for each block of the polymer was not identifiable. The polymers gave traces with different extents of observable glass and melting transitions on subsequent heating cycles. The reported transitions are, therefore, measured from the second heating

and cooling cycle. Both the first and second heating cycle traces are available in the Supporting Information (Figures III.16-21).

3.2.2 Self-assembly of mPEG-*b*-PMBGC

The self-assembly behavior of the amphiphilic diblock copolymers mPEG-*b*-PMBGC were evaluated by the suspension of the polymer in nanopure water with acetone as a cosolvent to allow for complete dissolution, followed by allowing the acetone to evaporate from the solutions to give aqueous solutions with a final polymer concentration of 1 mg/mL. The morphological influence of varying the PMBGC block lengths on the self-assembled nanostructures derived from **14**, **15**, and **16**, with increasing PMBGC block lengths, was characterized by TEM, AFM, and DLS (Figures III.2, 3, Table III.2). The formation of micellar structures was expected with the hydrophobic PMBGC block aggregating in the particle core, being shielded from the aqueous medium by the hydrophilic mPEG block as the particle shell. For the assembly of **14**, both the TEM and AFM images showed micellar structures and revealed the number-average diameter (D_{av}) and average height (H_{av}) of the nanoparticles were *ca*. 17 nm and *ca*. 6 nm, respectively. DLS showed unimodal size distributions of the particles and the number-average hydrodynamic diameter value [$D_{h(number)}$] was 20 ± 5 nm. For the assemblies of **15** and **16**, as the PMBGC block length increased, vesicular structures were observed for TEM images with D_{av} of *ca*. 50 nm and *ca*. 44 nm, respectively, along with micellar structures. The switch in the morphologies observed for the different polymers from micelles to vesicles can be attributed to the increase in the sugar block length, which caused a corresponding decrease in the hydrophilic-hydrophobic ratio of the polymers. The size of the vesicle morphologies (**15** and **16**) were

consistently larger as measured by TEM and DLS, than those of the micelle assemblies (**14**). Further support of the vesicle morphologies observed by TEM was given by the decrease in the average heights observed by AFM for vesicles *vs* micelles. It is expected that the reduced heights for the vesicles is due to disruption of their assembled state under the spin-casting conditions used for preparation of AFM samples, as is suggested by the images of Figure III.3b and 3c *vs* 3a.

Table III.2. Morphological characterization of mPEG-*b*-PMBGC, PMBGC-*co*-PMGC, mPEG-*b*-(PMBGC-*co*-PMGC).

Polymer	Sample	D_{av}[a] (nm)	H_{av}[b] (nm)	$D_{h(number)}$[c] (nm)	Morphology
$mPEG_{113}$-*b*-$PMBGC_{23}$	**14**	17 ± 3	5.8 ± 0.7	20 ± 5	micelle
$mPEG_{113}$-*b*-$PMBGC_{29}$	**15**	50 ± 6	4.0 ± 1.9	40 ± 10	micelle + vesicle
$mPEG_{113}$-*b*-$PMBGC_{51}$	**16**	44 ± 7	3.4 ± 1.5	60 ± 20	micelle + vesicle
$PMBGC_{23}$	**20**	N/A	N/A	N/A	precipitate
$(PMBGC_{0.1}$-*co*-$PMGC_{0.9})_{23}$	**21**	46 ± 8	2.1 ± 0.5	50 ± 20	micelle + vesicle
$PMGC_{23}$	**22**	27 ± 4	2.4 ± 0.4	N/A	micelle
$mPEG_{113}$-*b*-$(PMBGC_{0.5}$-*co*-$PMGC_{0.5})_{23}$	**17**[d]	22 ± 6	2.0 ± 0.4	20 ± 10	micelle
$mPEG_{113}$-*b*-$(PMBGC_{0.1}$-*co*-$PMGC_{0.9})_{23}$	**18**[d]	31 ± 5	2.7 ± 0.6	50 ± 20	micelle
$mPEG_{113}$-*b*- $PMGC_{51}$	**19**[e]	25 ± 4	2.4 ± 0.8	30 ± 10	micelle

[a] Measured by TEM. [b] Measured by AFM [c] Measured by DLS. [d] Synthesized from **14**. [e] Synthesized from **16**.

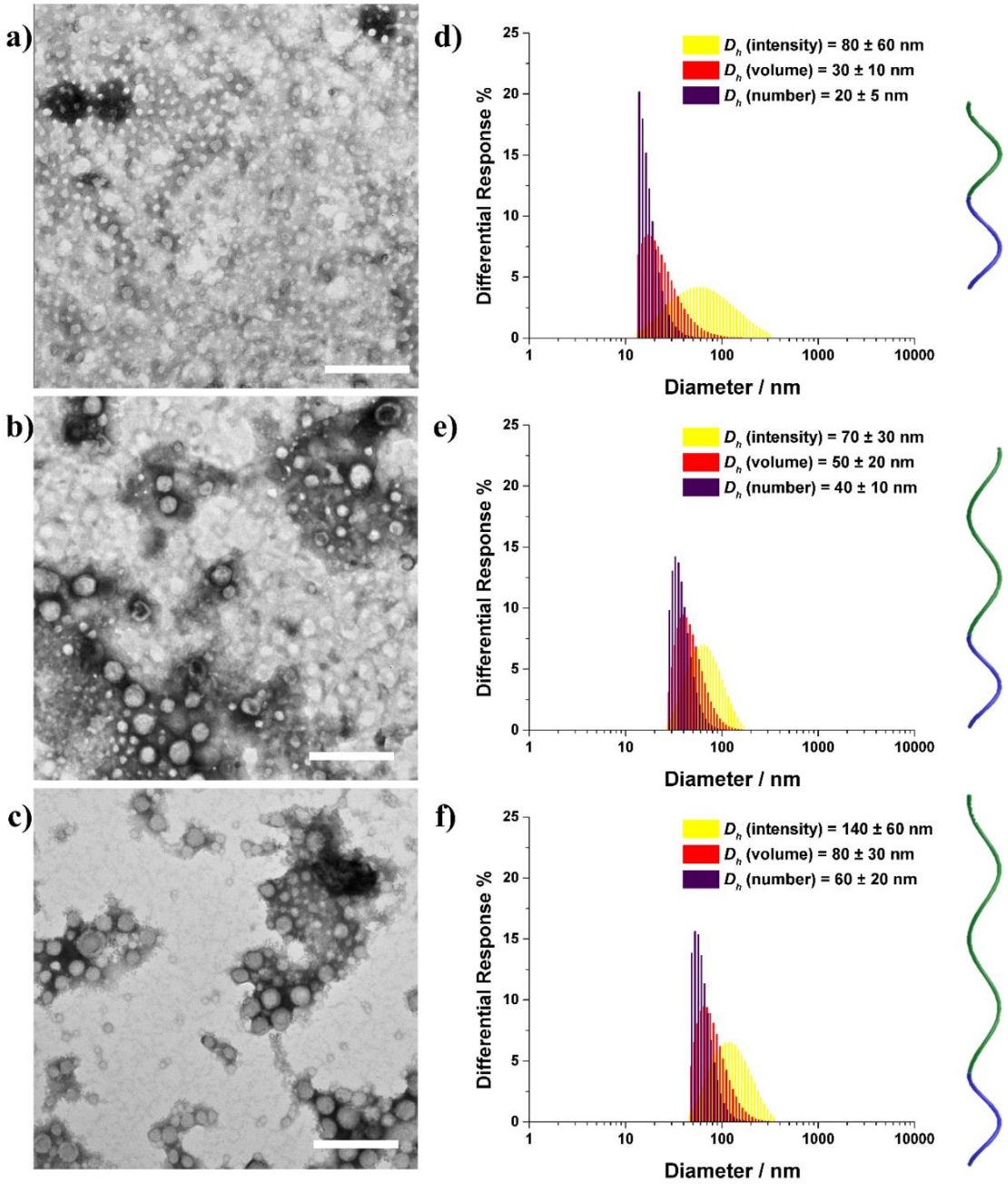

Figure III.2. TEM images of nanoparticles negatively stained by 1 wt % phosphotungstic acid (PTA) aqueous solution (10 μL) of **14** (a), **15** (b), and **16** (c). Number-, intensity- and volume-based hydrodynamic diameters in nanopure water measured by DLS of **14** (d), **15** (e), and **16** (f). The scale bar on the TEM images represents 200 nm. The schematics are a representation of the polymeric architecture being analyzed.

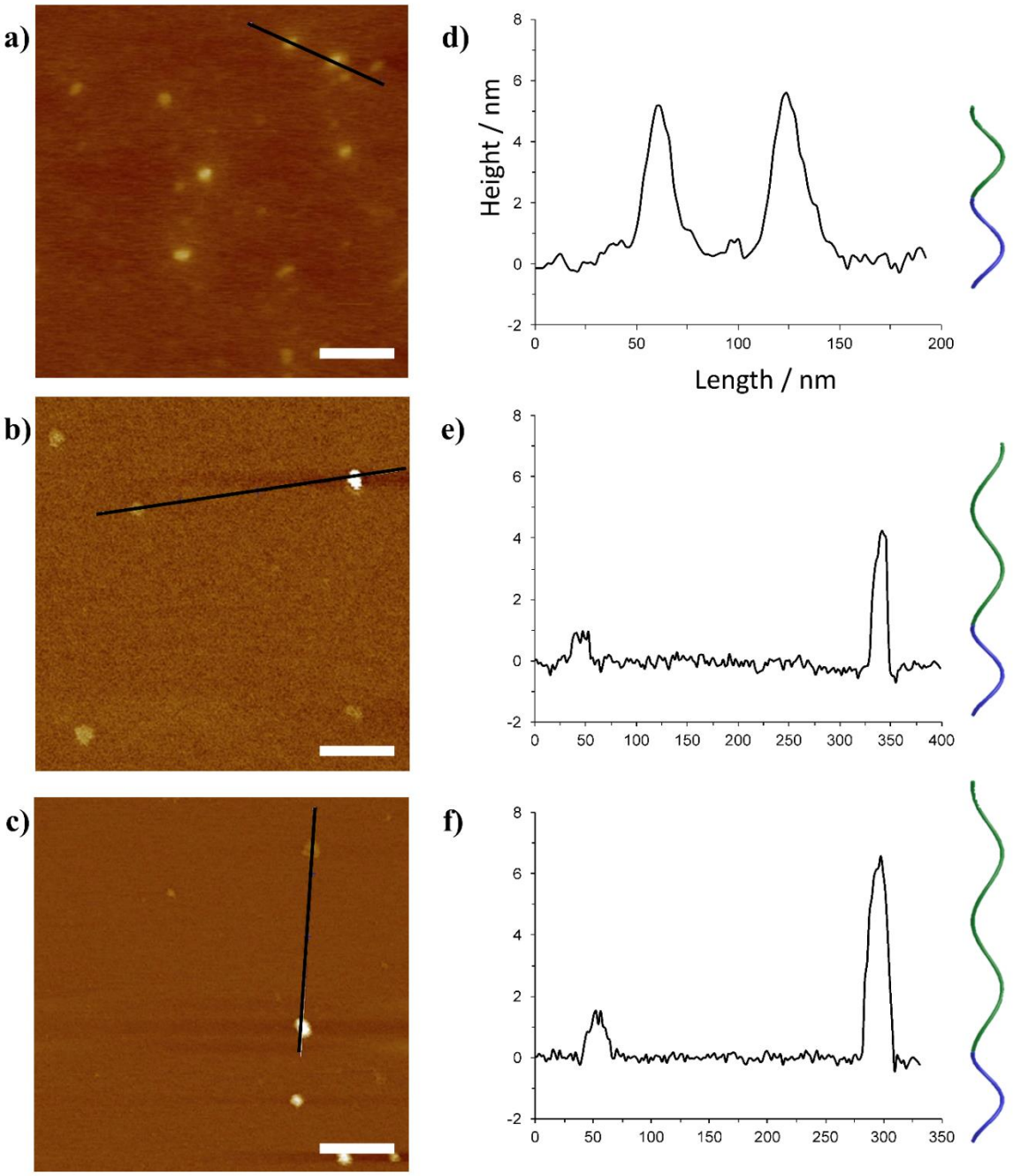

Figure III.3. AFM micrographs (a-c) and height profiles (d-f) from aqueous solutions of mPEG-*b*-PMBGC, **14** (a and d), **15** (b and e), and **16** (c and f) deposited on to freshly cleaved mica, and then allowed to dry in air, **14** was spin coated prior to being allowed to air dry. The height profiles were measured along the black line shown on the micrographs, the scale bars on the micrographs represent 100 nm. The schematics are a representation of the polymeric architecture being analyzed.

3.2.3 Self-assemblies of PMBGC-*co*-PMGC and PMGC

The acidic deprotection of the homopolymer PMBGC to remove the benzylidene side chains was utilized to produce partially-deprotected PMBGC-*co*-PMGC or fully-deprotected homopolymer PMGC. These structures were attractive amphiphilic materials, as the newly formed hydroxyls introduced hydrophilicity while the sugar backbone, as well as any residual benzylidene groups, provided hydrophobicity (Figure III.14). The self-assembly behaviors of PMBGC, PMBGC-*co*-PMGC, and PMGC were studied by suspension of the polymer in nanopure water with acetone as a cosolvent, followed by allowing the acetone to evaporate from the solutions to give aqueous solutions with a final polymer concentration of 1 mg/mL. Different polymers originating from the same PMBGC, with the same sugar block length as **14**, and decreasing percentages of benzylidene at 100%, 10%, and 0% were prepared and named as $PMBGC_{23}$, **20**, $(PMBGC_{0.1}$-*co*-$PMGC_{0.9})_{23}$, **21**, and $PMGC_{23}$, **22**, respectively. The morphological influence of varying the benzylidene percentage on the self-assembled nanostructures was evaluated by TEM, AFM and DLS (Figures III.4, 5, Table III.2). The solubility of **20** was much less than 1 mg/mL with macroscopic precipitation and suspension observed (Figure III.6). With the increase of hydrophilic MGC content, the solubility of the polymer increased and **21** had fully dispersed into aqueous solution at 1 mg/mL, with a strong Tyndall effect observed, indicating the formation of nanoassemblies. Both the TEM and AFM images of assemblies derived from **21** showed vesicular structures of the nanoparticles with D_{av} and H_{av} of *ca*. 46 nm and *ca*. 3 nm respectively, along with micellar structures. DLS showed unimodal size distributions with $D_{h(number)}$ of 50 ± 20 nm. As there was no MBGC content remaining in **22**, the polymer

dispersed readily into aqueous solution at 1 mg/mL and a relatively weak Tyndall effect was observed. Laser light scattering intensity was insufficient so that DLS was not achieved for **22** at this concentration. However, TEM and AFM images showed micellar nanoparticle structures with D_{av} and H_{av} of *ca*. 27 nm and *ca*. 2 nm, respectively. Overall, these data support the moderate water solubility of the hydroxyl-presenting PMGC polymer system, despite the hydrophobic rigid nature of the polymeric backbone.

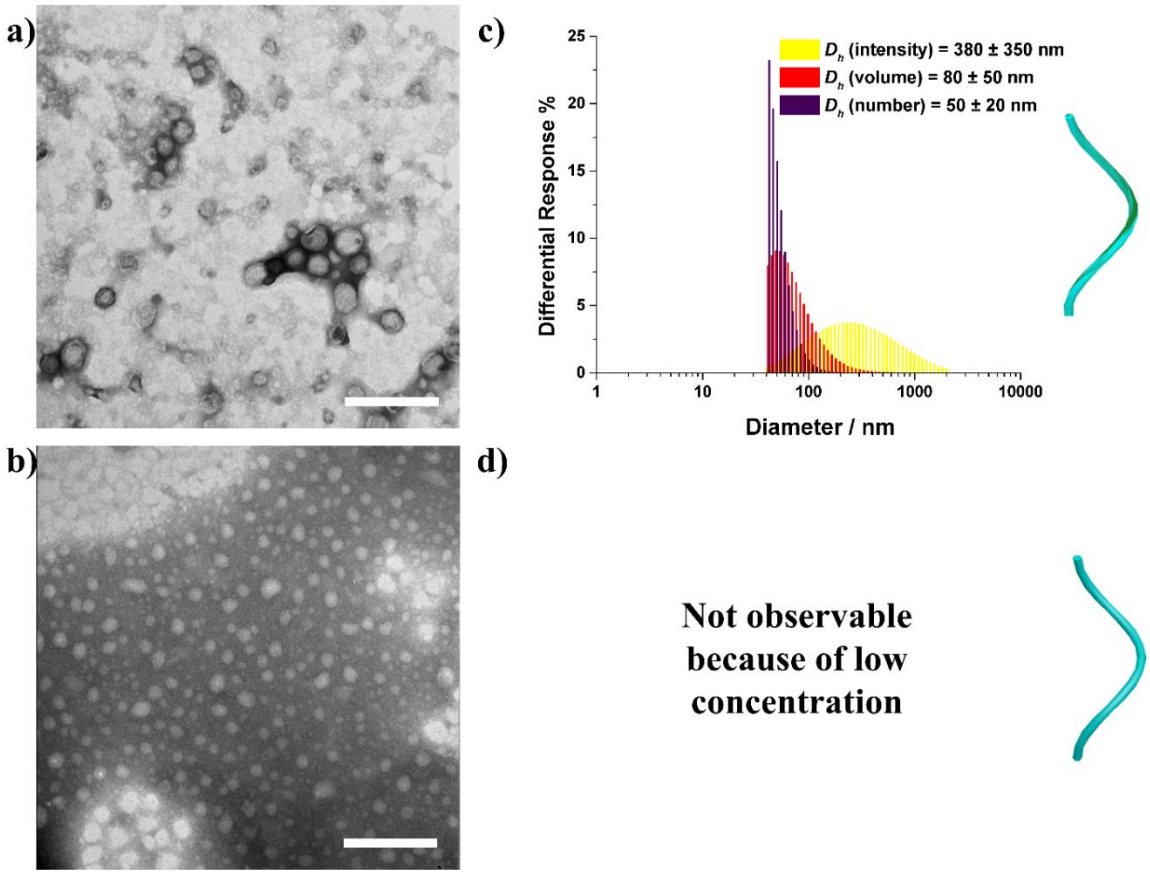

Figure III.4. TEM images of nanoparticles negatively stained by 1 wt % phosphotungstic acid (PTA) aqueous solution (10 μL) of $PMBGC_{0.1}$-*co*-$PMGC_{0.9}$ (a), PMGC (b). Number-, intensity- and volume-based hydrodynamic diameters in nanopure water measured by DLS of $(PMBGC_{0.1}$-*co*-$PMGC_{0.9})_{23}$ (c), $PMGC_{23}$ (d). The scale bar on the TEM images represents 200 nm. The schematics are a representation of the polymeric architecture being analyzed.

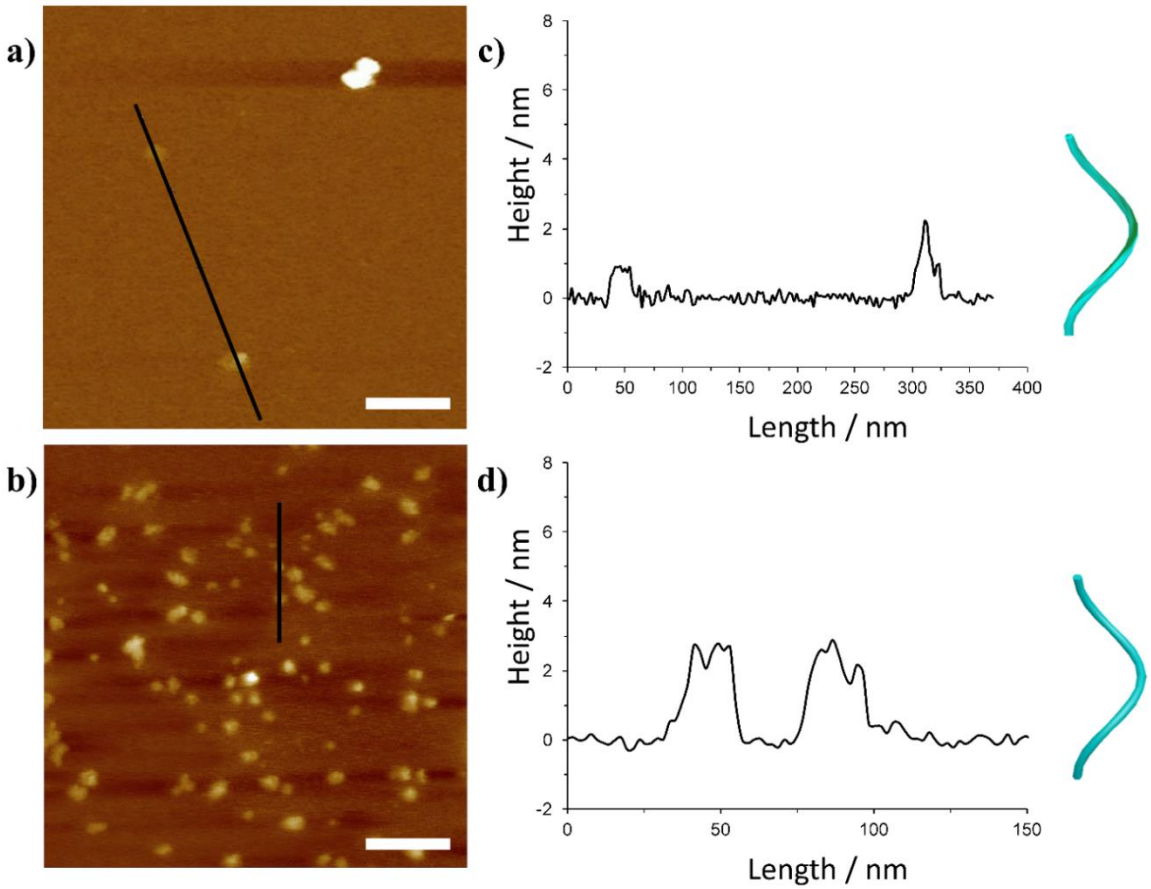

Figure III.5. AFM micrographs (a and b) and height profiles (c and d), from aqueous solutions of $(PMBGC_{0.1}$-*co*-$PMGC_{0.9})_{23}$ (a and c), $PMGC_{23}$ (b and d) deposited on to freshly cleaved mica, spin coated, and then allowed to dry in air, $PMGC_{23}$ was spin coated prior to being allowed to air dry . The height profiles were measured along the black line shown on the micrographs, the scale bars on the micrographs represent 100 nm. The schematics are a representation of the polymeric architecture being analyzed.

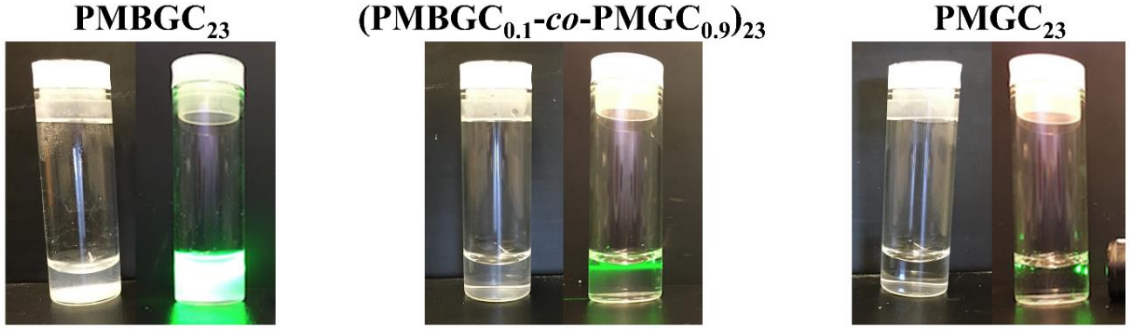

Figure III.6. Fully sugar-based polymers, $PMBGC_{23}$, $(PMBGC_{0.1}$-*co*-$PMGC_{0.9})_{23}$, and $PMGC_{23}$ in aqueous solution. The left side is under ambient light conditions, the right side is with a laser being used to demonstrate the Tyndall effect.

3.2.4 Self-assemblies of mPEG-*b*-(PMBGC-*co*-PMGC) and mPEG-*b*-PMGC

Based on the self-assembly behaviors of **14**, **15**, **16** and **20**, **21**, **22**, the self-assembly behaviors of mPEG-*b*-(PMBGC-*co*-PMGC) and mPEG-*b*-PMGC were studied by suspension of the polymer in nanopure water with acetone as a cosolvent, followed by allowing the acetone to evaporate from the solutions to give aqueous solutions with a final polymer concentration of 1 mg/mL. The morphological influence of introducing mPEG to the sugar block and varying the percentage of benzylidene residues on the self-assembled nanostructures derived from **17**, **18** and **19** was evaluated by TEM, AFM and DLS (Figures III.7, 8, Table III.2). TEM and AFM images showed micellar structures of the nanoparticles derived from **17** with D_{av} and H_{av} of *ca*. 22 nm and *ca*. 2 nm, respectively, in agreement with the $D_{h(number)}$ of 20 ± 10 nm achieved by DLS. Compared to micelles derived from **14** (D_{av} = 17 ± 3 nm, H_{av} = 5.8 ± 0.7 nm, $D_{h(number)}$ = 20 ± 5 nm), micelles derived from **17** had a similar $D_{h(number)}$ while the D_{av} was slightly larger. This was likely due to the decreased rigidity of the sugar block, upon switching from a bicyclic repeat unit to a monocyclic repeat unit, potentially promoting the flattening of the micellar structures in the dry state on TEM grids, which was further supported by the significantly decreased H_{av}. For the mostly deprotected **18**, TEM and AFM images showed micellar structures with D_{av} of the nanoparticle of *ca.* 31 nm and H_{av} of *ca* 2 nm with $D_{h(number)}$ of 50 ± 15 nm. Compared to the observation from **17**, decreasing the percentage of benzylidene to 10% increased the D_{av}, which may have been caused by inefficient core packing brought on by the increased hydrophilicity of the sugar block after further benzylidene removal. When compared to the fully sugar based polymer **21** (D_{av} = 46 ± 8 nm, H_{av} = 2.4 ± 0.4 nm, $D_{h(number)}$ = 50 ± 20 nm),

introduction of the mPEG block switched the vesicular structure to micelles, corresponding to the increased hydrophilic–hydrophobic ratio. TEM and AFM images for nanoparticles derived from **19** showed micellar structures with D_{av} and H_{av} of *ca*. 25 nm and *ca*. 2 nm respectively, in agreement with the $D_{h(number)}$ of 30 ± 10 nm achieved by DLS. Comparing this fully deprotected block polymer to its parent copolymer, **16**, removing the benzylidene units from the backbone caused a morphological change in the assemblies from vesicles to micelles (Table 2) with a decrease in particle size, corresponding to the increased hydrophilic–hydrophobic ratio.

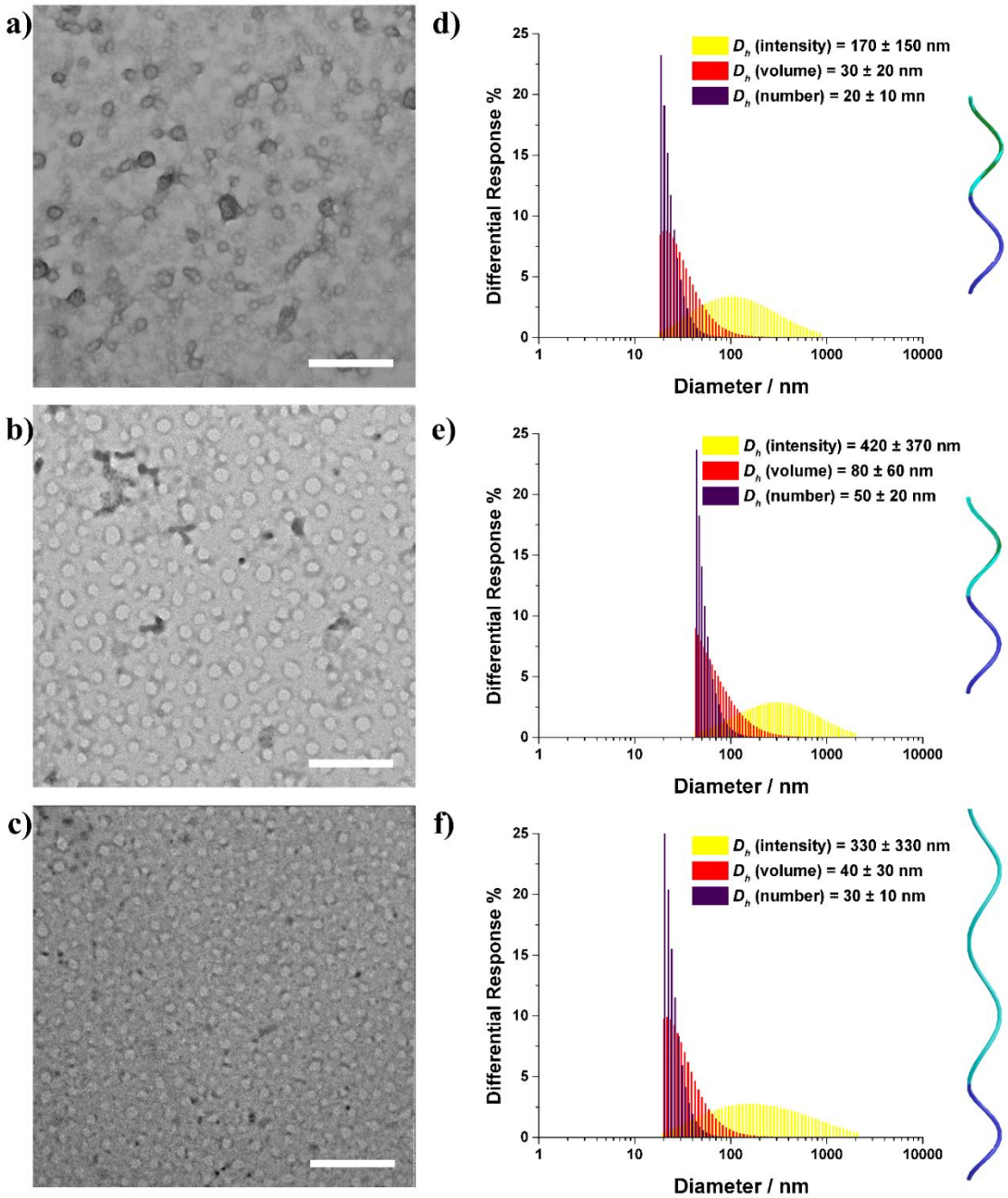

Figure III.7. TEM images of nanoparticles negatively stained by 1 wt % phosphotungstic acid (PTA) aqueous solution (10 μL) of **17**(a), **18** (b), and **19** (c). Number-, intensity- and volume-based hydrodynamic diameters in nanopure water measured by DLS of **17** (d), **18** (e), and **19** (f). The scale bar on the TEM images represents 200 nm. The schematics are a representation of the polymeric architecture being analyzed.

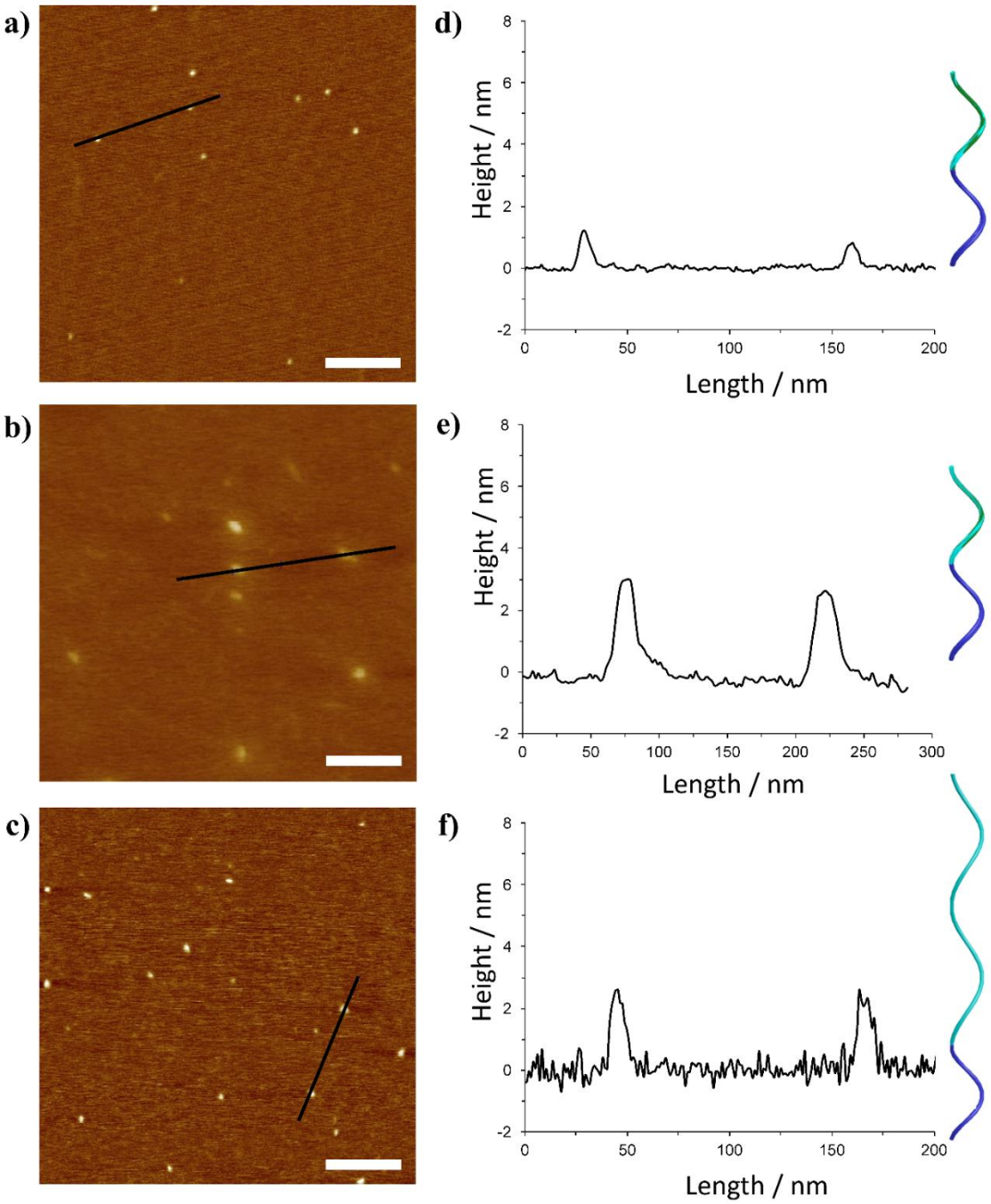

Figure III.8. AFM micrographs (a-c) and height profiles (d-f) from aqueous solutions of mPEG-*b*-(PMBGC-*co*-PMGC), **17** (a and d), **18** (b and e), and **19** (c and f) deposited on to freshly cleaved mica, spin coated, and then allowed to dry in air. The height profiles were measured along the black line shown on the micrographs, the scale bars on the micrographs represent 100 nm. The schematics are a representation of the polymeric architecture being analyzed.

3.3 Experimental Section

3.3.1 Materials

All materials were purchased from VWR or Sigma-Aldrich, unless otherwise noted. Monomethoxy-monohydroxy-terminated poly(ethylene glycol) ($mPEG_{113}$-OH, M_n = 5000 g mol^{-1}) was purchased from Rapp Polymere (Germany). Unless noted, all reagents were used as received. Dichloromethane (DCM) was purified and dried by a solvent purification system (J. C. Meyer Solvent System). 1,5,7-Triazabicyclo[4.4.0]dec-5-ene (TBD) was dried over CaH_2, dried under vacuum, and stored under an argon atmosphere. MBGC, PMBGC, and PMGC were synthesized as previously reported,[76] MBGC was dried under reduced pressure over P_2O_5 and stored under an atmosphere of argon prior to use in polymerizations. mPEG was dried by azeotropic distillation with toluene.

3.3.2 Instrumentation

^1H and ^{13}C NMR spectra were recorded on an Inova500 spectrometer, chemical shifts were referenced to the resonance signals of the deuterated solvent.

IR spectra were recorded on a Shimadzu IR Prestige attenuated total reflectance Fourier-transform infrared spectrophotometer and analyzed using IR solution v. 1.40 software.

Size exclusion chromatography was performed on a Waters Chromatography, Inc. (Milford, MA) system equipped with an isocratic pump (model 1515), a differential refractometer (model 2414), and column set comprised of a PLgel™ 5 μm guard column (50 × 7.5 mm), a PLgel™ 5 μm Mixed C column (300 × 7.5 mm, Agilent Technologies) and

two Styragel® columns (500 Å and 104 Å, 300 × 7.5 mm, Waters Chromatography, Inc.) with THF as the eluent (1.0 mL/min) at 40 °C. Data were analyzed using Breeze software (Waters Chromatography, Inc., Milford, MA). Molar masses were determined relative to polystyrene standards (300-467,000 Da) purchased from Polymer Laboratories, Inc. (Amherst, MA). Polymer solutions were prepared at a concentration of *ca*. 3 mg/mL with 0.05 vol% toluene added as a flow marker, and an injection volume of 200 μL was used.

Melting (T_m) and glass (T_g) transition temperatures were measured by differential scanning calorimetry (DSC) on a Mettler-Toledo DSC3/700/1190 (Mettler-Toledo, Inc., Columbus, OH) under a nitrogen gas atmosphere. Measurements were performed with a heating rate of 10 °C/min and the data were analyzed using Mettler-Toledo STAR^e v. 15.00a software. The T_g was taken as the midpoint of the inflection tangent and the T_m was taken as the peak maximum, with reported values obtained for transitions observed in the second heating scan. The DSC traces collected during the first and second heating scans are included in the Supporting Information (Figures III.16-21).

Thermogravimetric analysis (TGA) was performed under an Ar atmosphere using a Mettler-Toledo model TGA2/1100/464, with a heating rate of 10 °C/min. Measurements were analyzed using Mettler-Toledo Star^e v.15.00a software. Percentage mass values as a function of temperature were determined from the derivative of the TGA traces.

Transmission electron microscopy (TEM) images were collected on a JEOL 1200EX operated at 100 kV, and micrographs were recorded using a SIA-15C CCD camera. Samples for TEM were prepared as follows: 10 μL of the dilute polymer solution in nanopure water was deposited onto a carbon-coated copper grid, and after 1 min, excess solution was quickly wicked away by a piece of filter paper. The samples were then negatively stained with a 1

wt% phosphotungstic acid (PTA) aqueous solution (10 µL). After 30 s, excess staining solution was quickly wicked away by a piece of filter paper and the samples were left to dry under ambient conditions overnight.

Atomic force microscopy (AFM) was performed using a Multimode 8 system (Bruker) using a ScanAsyst-Air Silicon Nitride probe (k = 0.4 N/m, f_0 = 70 kHz, Bruker). AFM images were assessed with Nanoscope Analysis (Bruker). For AFM sample preparation, expect for vesicle samples, the solution of nanoparticles in nanopure water (20 µL) at 0.5 mg/mL was deposited on the mica surface, followed by spin coating. The mica surface was allowed to dry in an air flow. Sample preparation for vesicle containing samples the solution of nanoparticles in nanopure water (4 µL) at 0.1 mg/mL was deposited onto the mica surface and was allowed to dry in air flow.

Dynamic light scattering (DLS) measurements were conducted using a Delsa Nano C instrument from Beckman Coulter, Inc. (Fullerton, CA) equipped with a laser diode operating at 658 nm. Scattered light was detected at 165° and analyzed using a log correlator over 70 accumulations for a 0.5 mL of sample in a glass size cell (0.9 mL capacity). The photomultiplier aperture and attenuator were adjusted automatically to obtain a photon counting rate of *ca*. 10 kcps. The particle size distribution and distribution averages were calculated using CONTIN particle size distribution analysis routines in Delsa Nano 2.31 software. The peak averages of intensity, volume and number distributions from 70 accumulations were reported as the average diameter of the particles. All measurements were repeated 10 times.

3.3.3 Synthesis

General procedure for the synthesis of monomethoxy-terminated poly(ethylene glycol)-*block*-poly(methyl 4,6-*O*-benzylidene-2,3-*O*-carbonyl-α-D-glucopyranoside) (mPEG-*b*-PMBGC). This example includes reagent amounts for the preparation of **14**. In a glovebox, MBGC (40 mg, 0.13 mmol) and $mPEG_{113}$ (32 mg, 0.0065 mmol) were dissolved in DCM (420 μL). A solution of TBD (0.9 mg, 0.0065 mmol) in 90 μL of DCM was then added. The reaction was quenched after 2-3 h by adding Amberlyst 15 H-form resin. The reaction mixture was purified by precipitation into diethyl ether twice, followed by precipitation into methanol to give $mPEG_{113}$-*b*-$PMBGC_{23}$ as a white powder. FTIR (ATR): 3010-2755, 1757, 1643, 1454, 1373, 1360, 1342, 1279, 1240, 1215, 1192, 1146, 1103, 1047, 991, 962, 843, 787, 754, 700, 656 cm^{-1}. ^{1}H NMR (500 MHz, DMSO-d_6): δ 7.55-7.18 (br), 5.72-5.44 (br), 5.27-4.90 (br), 4.88-4.65 (br), 4.39-4.08 (br), 4.03-3.61 (br), 3.62-3.39 (br), 3.39-3.16 (br) ppm. ^{13}C NMR (125 MHz, DMSO-d_6): δ 153.9-152.5, 137.5-136.4, 129.6-127.4, 126.9-125.1, 101.6-99.0, 97.2-95.5, 78.7-75.6, 75.2-72.2, 70.7-69.0, 68.4-66.6, 63.1-61.1, 56.6-54.0 ppm. **14**: 78% yield, M_n (THF SEC) = 12000 g mol^{-1}, $Đ$ (THF SEC) = 1.06, T_m = 56 °C, T_g (midpoint) = 144 °C, TGA in Ar: 279-365 °C, 67% mass loss, 3% mass remaining at 500 °C. **15**: 74% yield, M_n (THF SEC) = 14800 g mol^{-1}, $Đ$ (THF SEC) = 1.15, T_m = 45 °C, T_g (midpoint) = -31 °C, TGA in Ar: 251-324 °C, 43% mass loss, 324-398 °C, 43% mass loss, 6% mass remaining at 500 °C. **16**: 87% yield, M_n (THF SEC) = 18900 g mol^{-1}, $Đ$ (THF SEC) = 1.05, T_m = 52 °C, T_g (midpoint) = 166 °C, TGA in Ar: 267-338 °C, 41% mass loss, 338-397 °C, 41% mass loss, 0.5 % mass remaining at 500 °C.

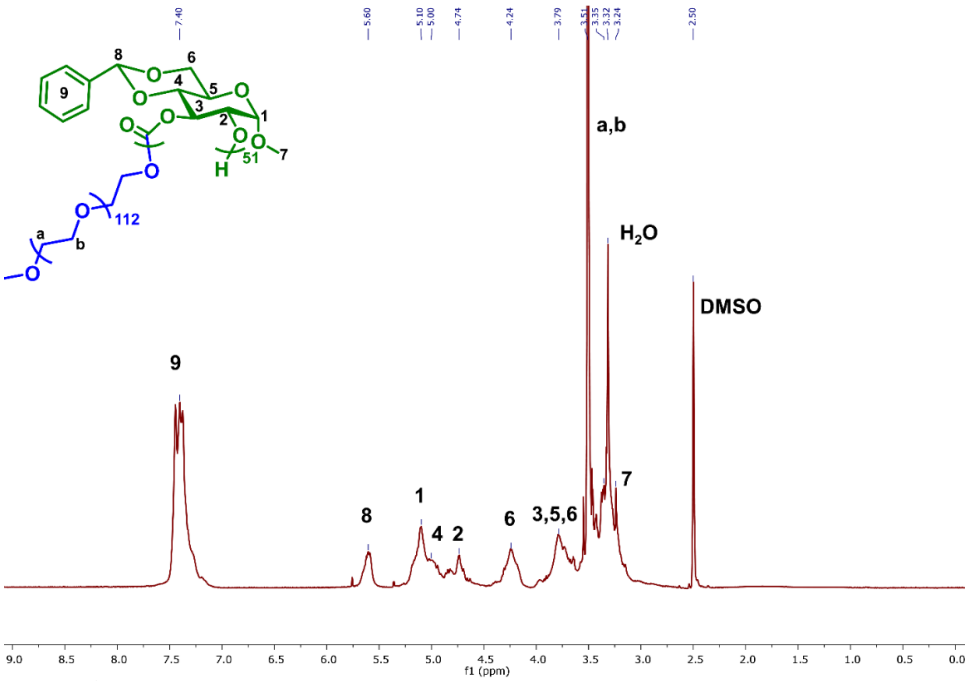

Figure III.9. ^{1}H NMR (500 MHz) spectrum of mPEG$_{113}$-*b*-PMBGC$_{51}$, **16**, in DMSO-d_6. Assignments were made based on 2D analysis of **20** (figures III.22, 23), as the PEG signal caused oversaturation of the block polymer 2D analysis.

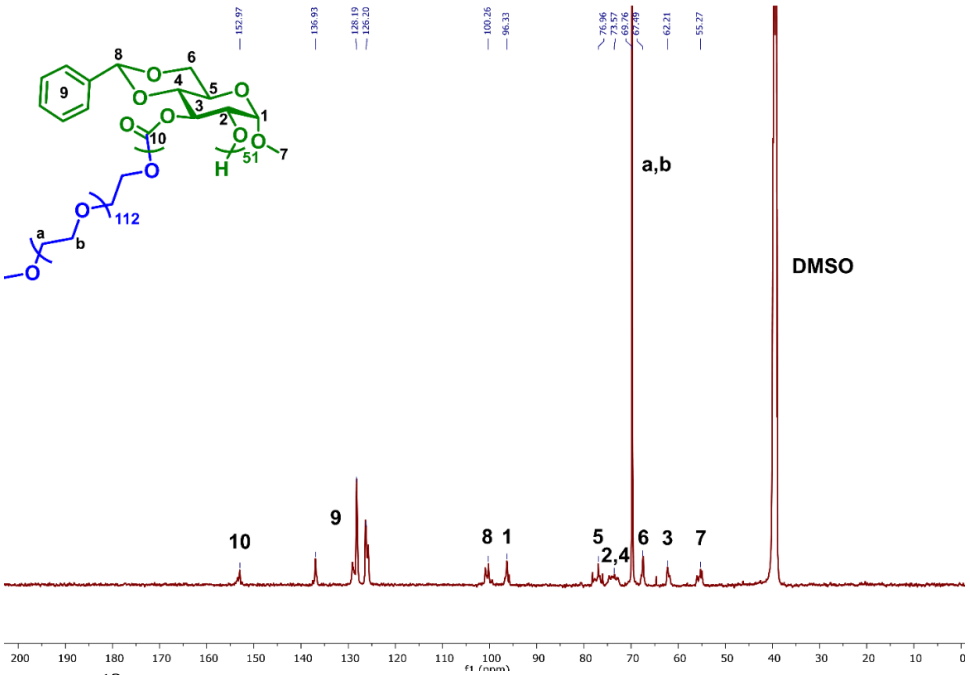

Figure III.10. ^{13}C NMR (125 MHz) spectrum of mPEG$_{113}$-*b*-PMBGC$_{51}$, **16**, in DMSO-d_6. Assignments were made based on 2D analysis of **20** (figures S18-S19), as the PEG signal caused oversaturation of the block polymer 2D analysis.

General procedure for the synthesis of monomethoxy-terminated poly(ethylene glycol)-*block*-poly[(methyl 4,6-*O*-benzylidene-2,3-*O*-carbonyl-α-D-glucopyranoside)-*co*-poly(methyl 2,3-*O*-carbonyl-α-D-glucopyranoside)], mPEG-*b*-(PMBGC-*co*-PMGC). This example includes reagent amounts for the preparation of **18** from **14**. Trifluoroacetic acid (TFA, 20.2 μL) and DI H_2O (10.1 μL) were added to a solution of mPEG-*b*-PMBGC (49.3 mg, 55 wt% sugar, 0.088 mmol sugar repeat units) in DCM (640 μL). The reaction was allowed to proceed at RT for 12.5 h. The reaction was then purified by precipitation into ether three times to give $mPEG_{113}$-*b*-$(PMBGC_{0.1}$-*co*-$PMGC_{0.9})_{23}$. The percent of benzylidene units remaining on the polymer backbone was estimated by comparing the aromatic signal in the ^{1}H NMR spectrum to the combined signals from both sugar repeat units present. FTIR (ATR): 3675-3100, 3017-22752, 1765, 1460, 1454, 1358, 1342, 1279, 1236, 1144, 1101, 1038, 980, 962, 910, 841, 781, 654 cm^{-1}. ^{1}H NMR (500 MHz, DMSO-d_6): δ 5.66-5.45 (br), 5.47-5.27 (br), 5.10-4.78 (br), 4.78-4.58 (br), 4.56-4.36 (br), 3.74-3.55 (br), 3.57-3.44 (br), 3.43- 3.20 (br) ppm. ^{13}C NMR (125 MHz, DMSO-d_6): δ 154.8-153.2, 96.7-94.6, 77.6-75.8, 75.2-73.6, 73.0-71.2, 70.7-68.8, 68.3-66.4, 61.0-58.9, 55.8-53.9 ppm. **17**: synthesized from **14**, 53% PMBGC:47% PMGC, 94% yield, T_m = 50 °C, T_g (midpoint) = -23 °C TGA in Ar: 221-306 °C, 37% mass loss, 306-410 °C, 48% mass loss, 8% mass remaining at 500 °C. **18**: synthesized from **14**, 10% PMBGC:90% PMGC, 88% yield, T_m = 30 °C, T_g (midpoint) = -48 °C TGA in Ar: 244-322 °C, 33% mass loss, 322-412 °C, 40% mass loss, 12% mass remaining at 500 °C. **19**: synthesized from **16**, 0% PMBGC:100% PMGC, 93% yield, T_m = 44 °C, TGA in Ar: 246-293 °C, 50% mass loss, 293-380 °C, 24% mass loss, 2% mass remaining at 500 °C.

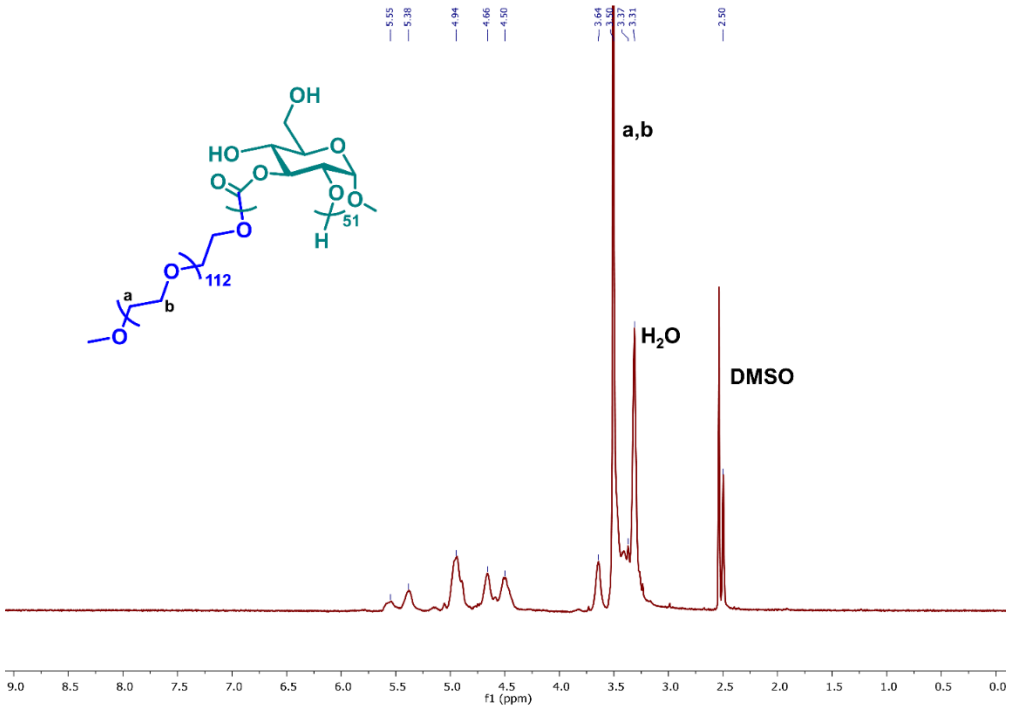

Figure III.11. ^{1}H NMR (500 MHz) spectrum of mPEG$_{113}$-*b*-PMGC$_{51}$, **19**, in DMSO-d_6. Assignments were not made for the sugar signals because of complications caused by transcarbonation during the deprotection reaction and an unavoidable water signal.

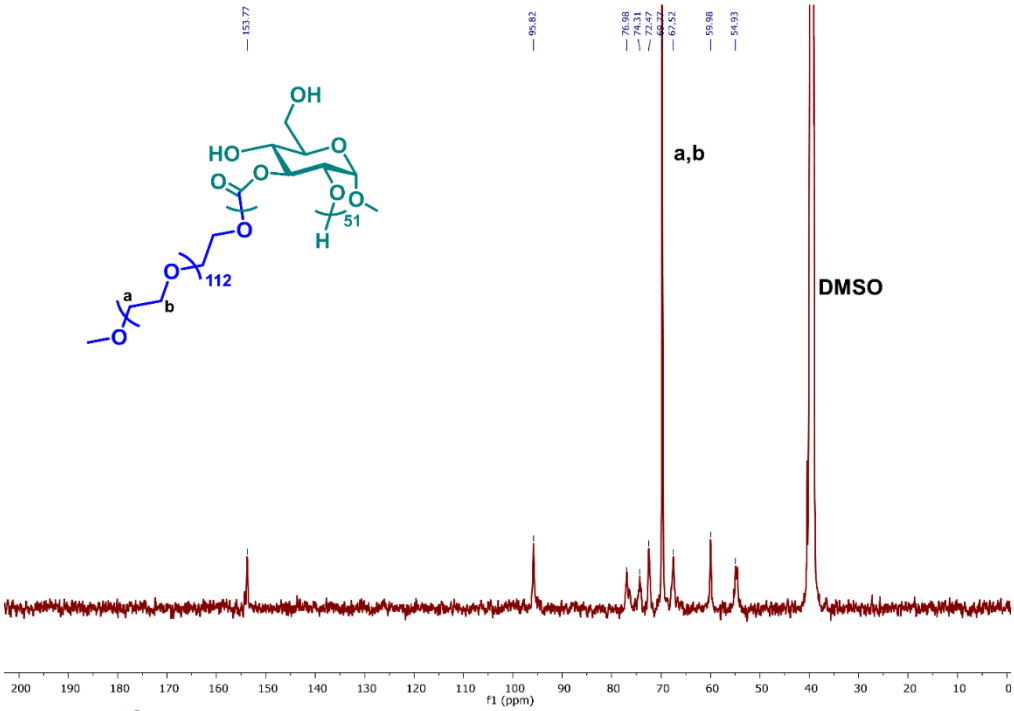

Figure III.12. ^{13}C NMR (125 MHz) spectrum of mPEG$_{113}$-*b*-PMGC$_{51}$, **19**, in DMSO-d_6.

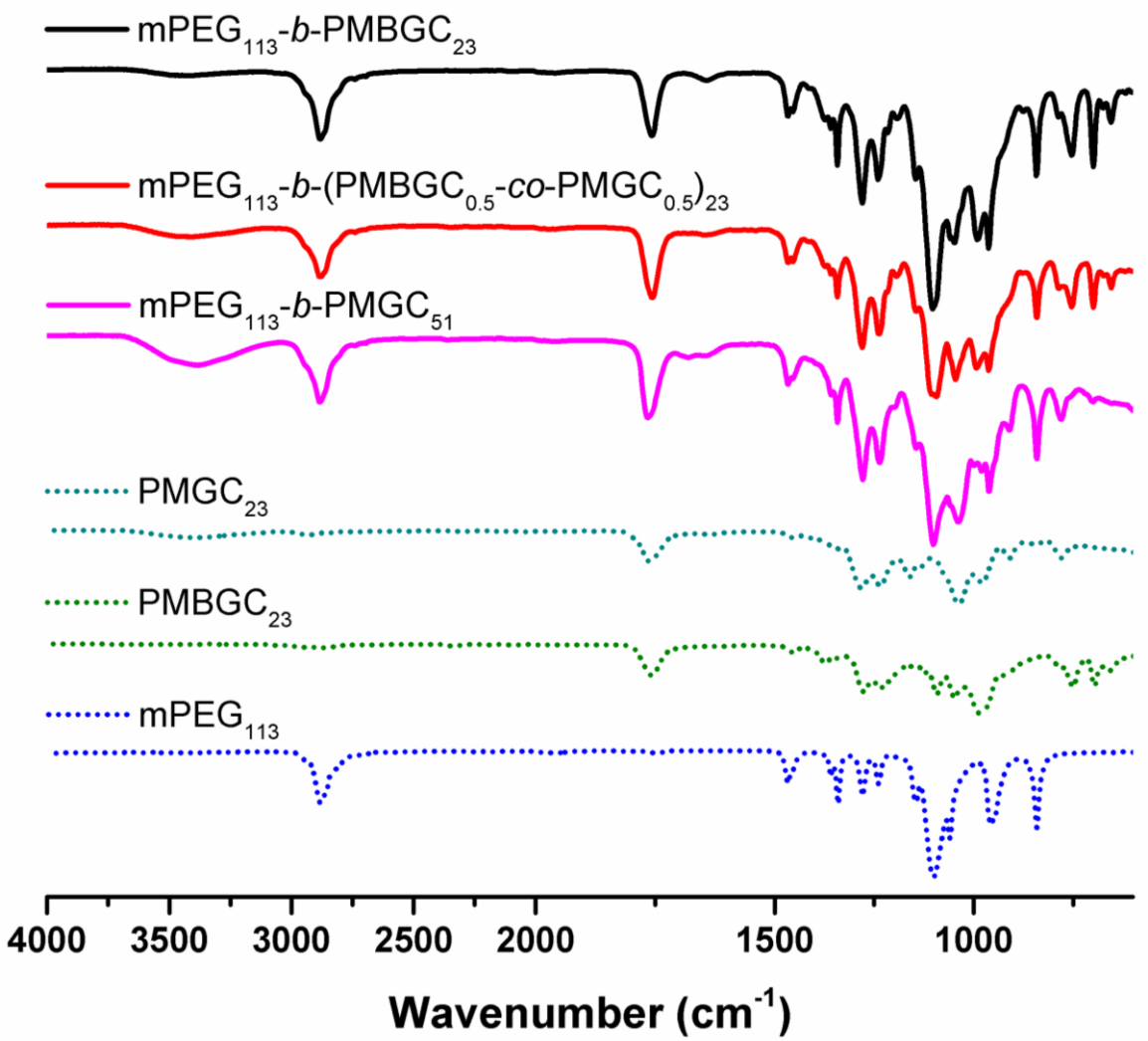

Figure III.13. IR spectra of $mPEG_{113}$-*b*-$PMBGC_{23}$ (black), $mPEG_{113}$-*b*-($PMBGC_{0.5}$-*co*-$PMGC_{0.5}$)$_{23}$ (red), $mPEG_{113}$-*b*-$PMGC_{51}$ (magenta), $PMGC_{23}$ (teal dashed), $PMBGC_{23}$ (green dashed), $mPEG_{113}$ (blue dashed).

Preparation of polymeric nanoparticle assemblies. Because the PMGC homopolymer was not soluble in acetone, an unconventional assembly procedure was followed for all samples. In a typical experiment, the polymer was added as a solid to water at an amount that would give a 1 mg/mL concentration, and acetone was then added until a 2:1 water:acetone mixture was produced. This solution was then sonicated until the macroscopically-visible solid polymer had fully dispersed into solution. Acetone was then

allowed to evaporate for 12 h to afford a series of poly(glucose carbonate) based nanoparticles. The sizes and morphologies were characterized by DLS, AFM, and TEM

3.4 Conclusions

Our interest in the development and understanding of amphiphilic polymers which undergo assembly into interesting morphologies, and can potentially undergo degradation into environmentally-benign by-products after their useful lifetime has driven this investigation into the synthesis and self-assembly of carbohydrate-based polycarbonates. Amphiphilic copolymers, mPEG-*b*-PMBGC, were synthesized by the organocatalytic ROP of a hydrophobic glucose-based bicyclic monomer platform, using a hydrophilic mPEG initiator, to produce block polymers having benzylidene protecting groups along a segment of the side chains. The ability of this system to undergo an acidic post-polymerization deprotection to tune the compositions of the system was then examined, demonstrating the significant influence of the overall polymeric architecture on the efficacy of the benzylidene removal. The self-assembly behavior of these polymers was studied to determine the changes in morphology caused by varying the hydrophilic-hydrophobic ratio and the compositions of the copolymers. It was revealed that a mixture of vesicles and micelles were formed by the starting mPEG-*b*-PMBGC polymers. Upon partial or complete removal of the benzylidene protecting group the subsequent polymers produced micelles. Overall, it was observed that the polymers with lower hydrophilic-hydrophobic ratios gave predominately vesicle morphologies, whereas when the hydrophilic ratio increased micellar morphologies were preferred, as expected. This change in morphologies driven by the acidic deprotection endow these materials with significant potential as delivery vehicles that can

both release cargo and change morphology under a stimulus. The conditions and polymeric architectures required to form only vesicular structures and *in situ* benzylidene removal is under current investigation to probe the practicality of this change under relevant biomedical and environmental conditions.

3.5 Supplemental Information

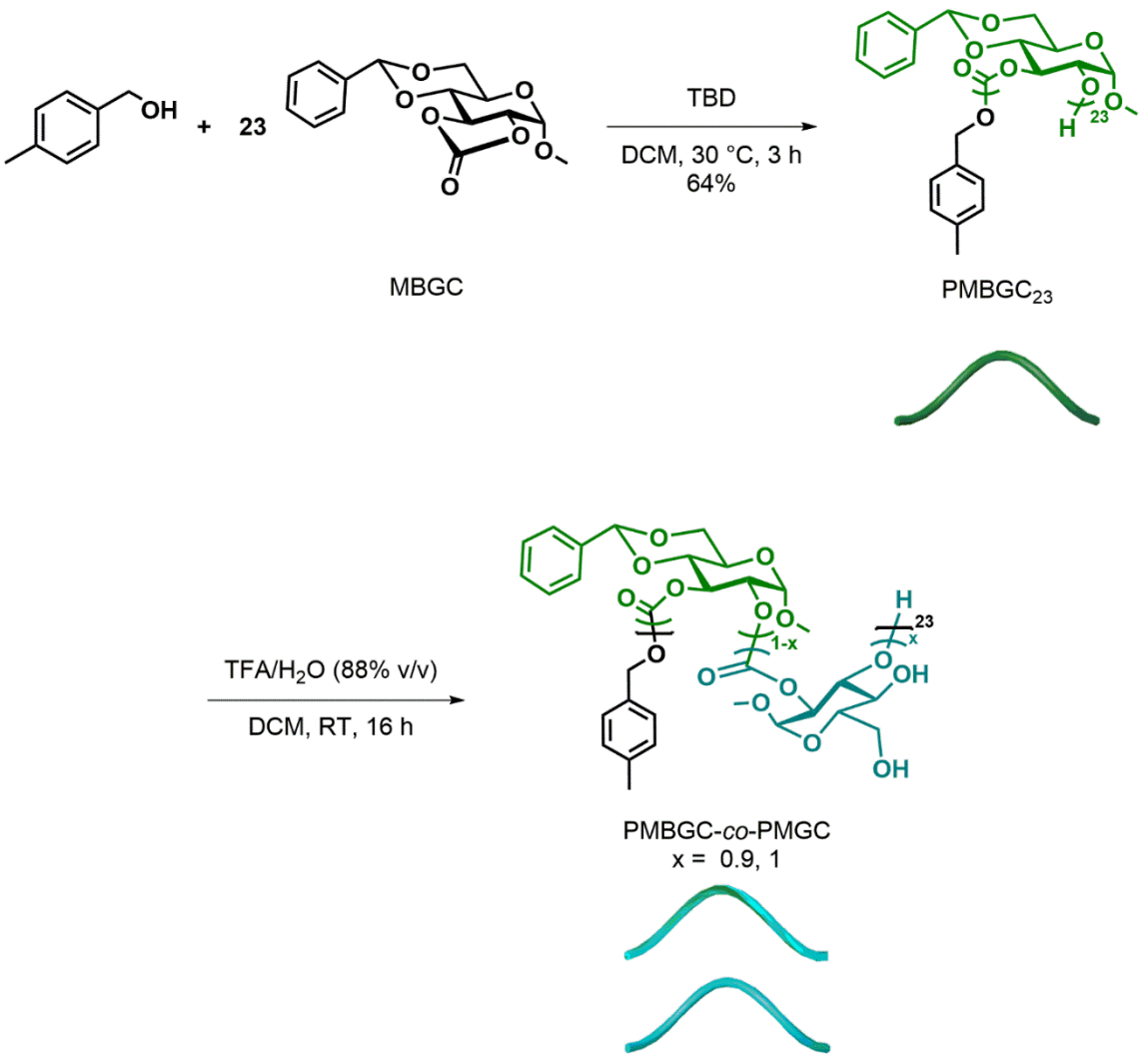

Figure III.14. Synthesis of $PMBGC_{23}$ and $(PMBGC_{1-x}\text{-}co\text{-}PMGC_x)_{23}$ and schematic illustrations of the polymer architecture.

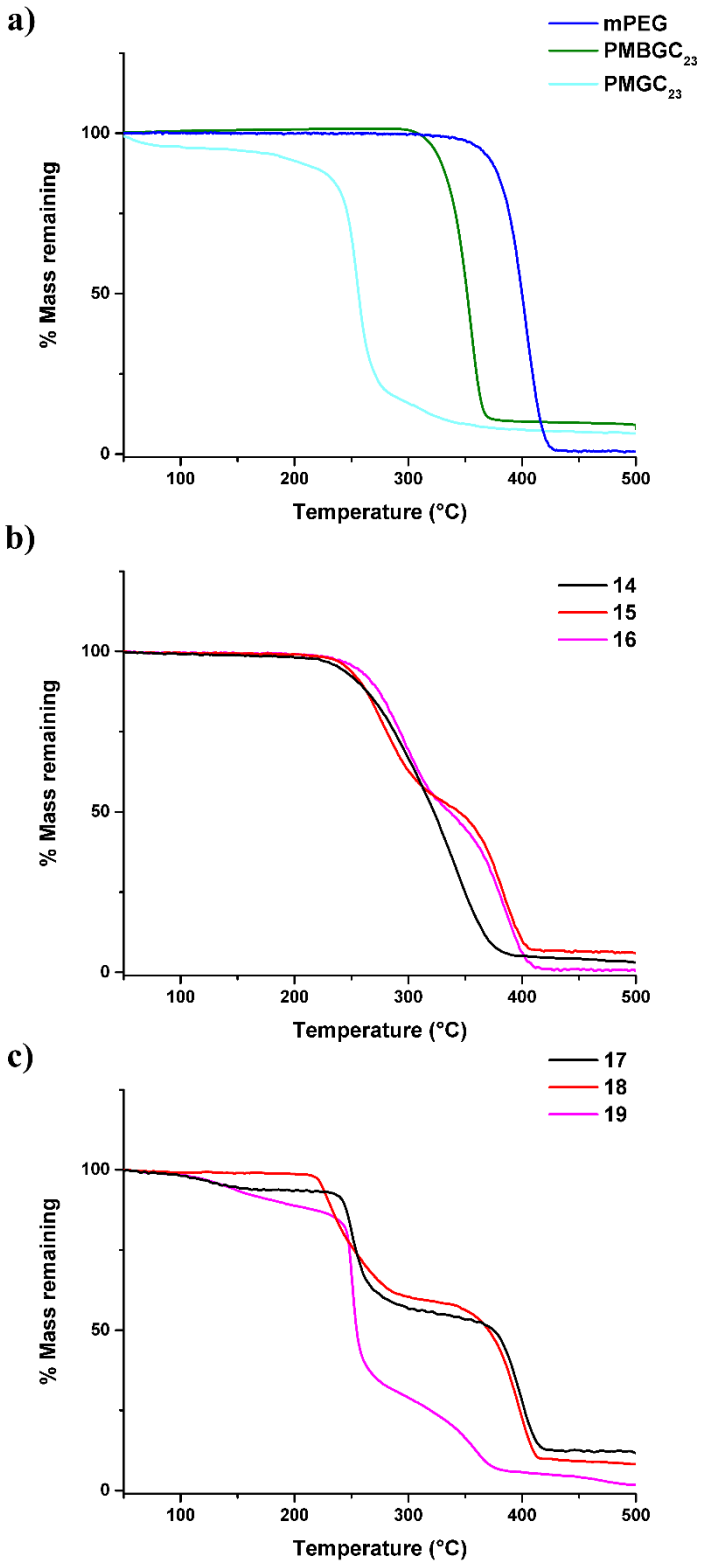

Figure III.15. Thermogravimetric analysis traces of (a) homopolymers mPEG, PMBGC, and PMGC, (b) a series of mPEG-*b*-PMBGC block polymers, (c) a series of mPEG-*b*-(PMBGC-*co*-PMGC) deprotected block polymers.

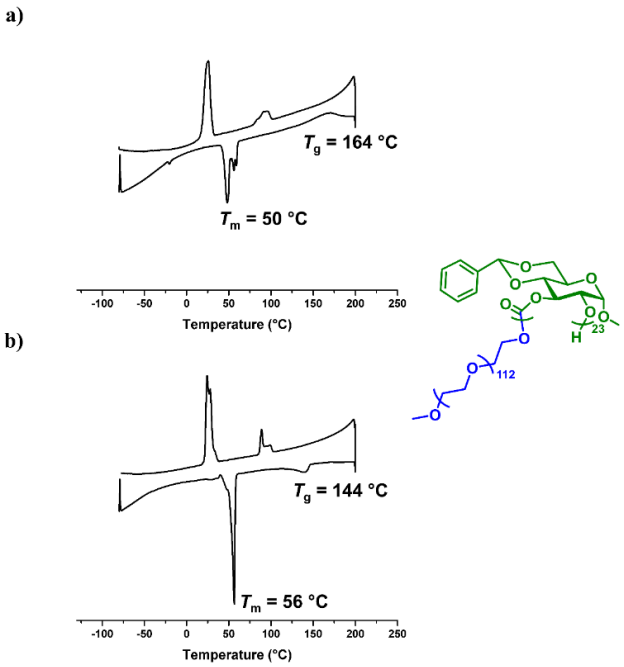

Figure III.16. Differential scanning calorimetry of **14**, (a) first heating and cooling cycle, (b) second heating and cooling cycle. The heating traces are on the bottom and the cooling traces on the top. The various transitions and their temperatures are identified on the traces.

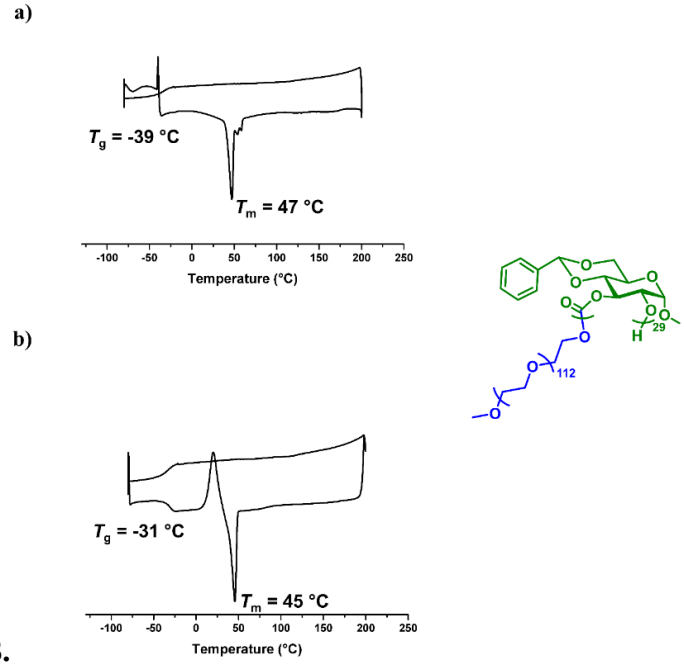

3.

Figure III.17. Differential scanning calorimetry of **15**, (a) first heating and cooling cycle, (b) second heating and cooling cycle. The heating traces are on the bottom and the cooling traces on the top. The various transitions and their temperatures are identified on the traces.

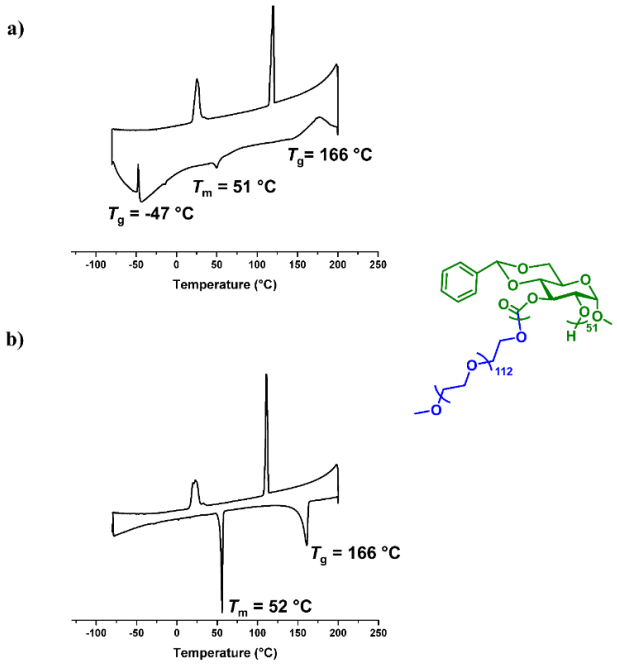

Figure III.18. Differential scanning calorimetry of **16**, (a) first heating and cooling cycle, (b) second heating and cooling cycle. The heating traces are on the bottom and the cooling traces on the top. The various transitions and their temperatures are identified on the traces.

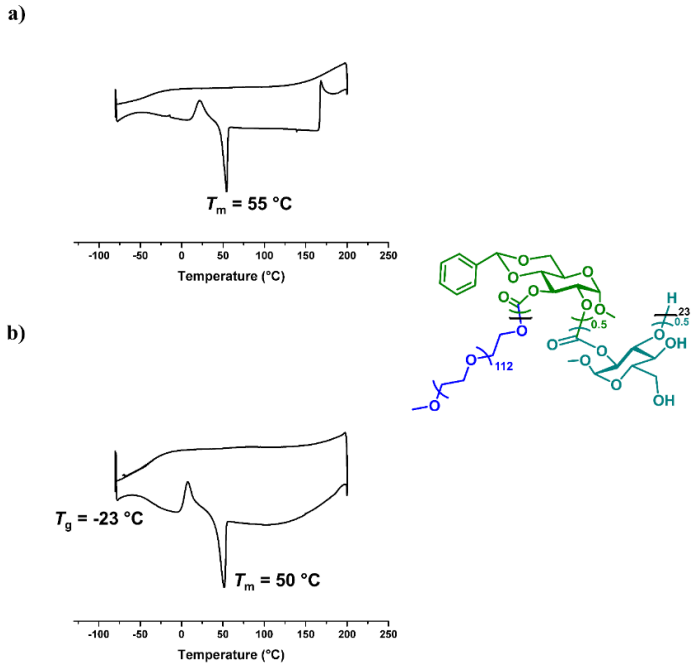

Figure III.19. Differential scanning calorimetry of **17**, (a) first heating and cooling cycle, (b) second heating and cooling cycle. The heating traces are on the bottom and the cooling traces on the top. The various transitions and their temperatures are identified on the traces.

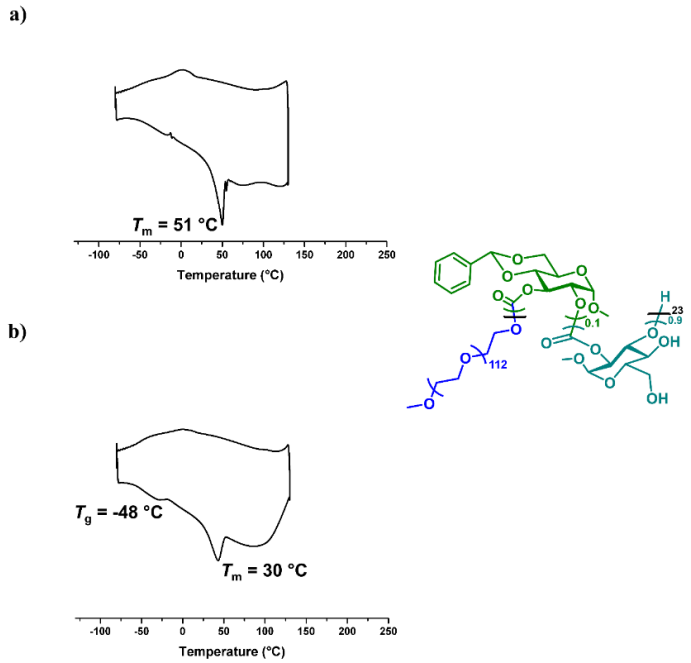

Figure III.20. Differential scanning calorimetry of **18**, (a) first heating and cooling cycle, (b) second heating and cooling cycle. The heating traces are on the bottom and the cooling traces on the top. The various transitions and their temperatures are identified on the traces.

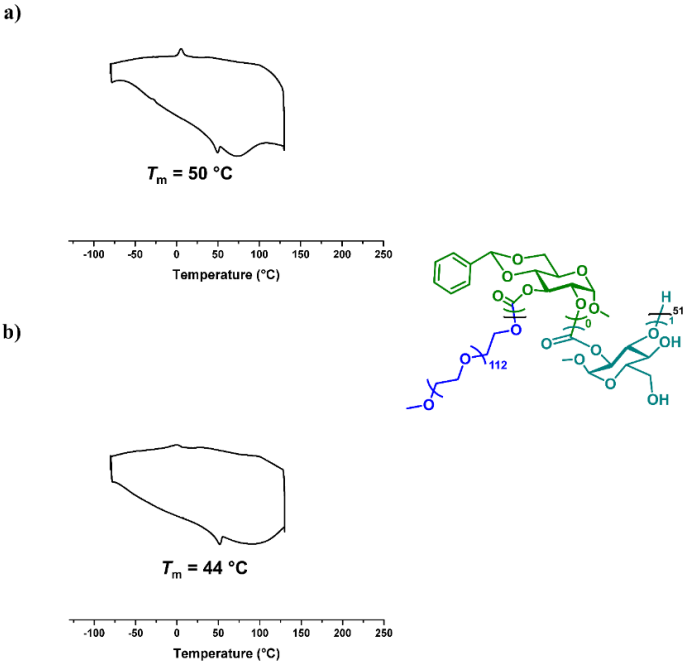

Figure III.21. Differential scanning calorimetry of **19**, (a) first heating and cooling cycle, (b) second heating and cooling cycle. The heating traces are on the bottom and the cooling traces on the top. The various transitions and their temperatures are identified on the traces.

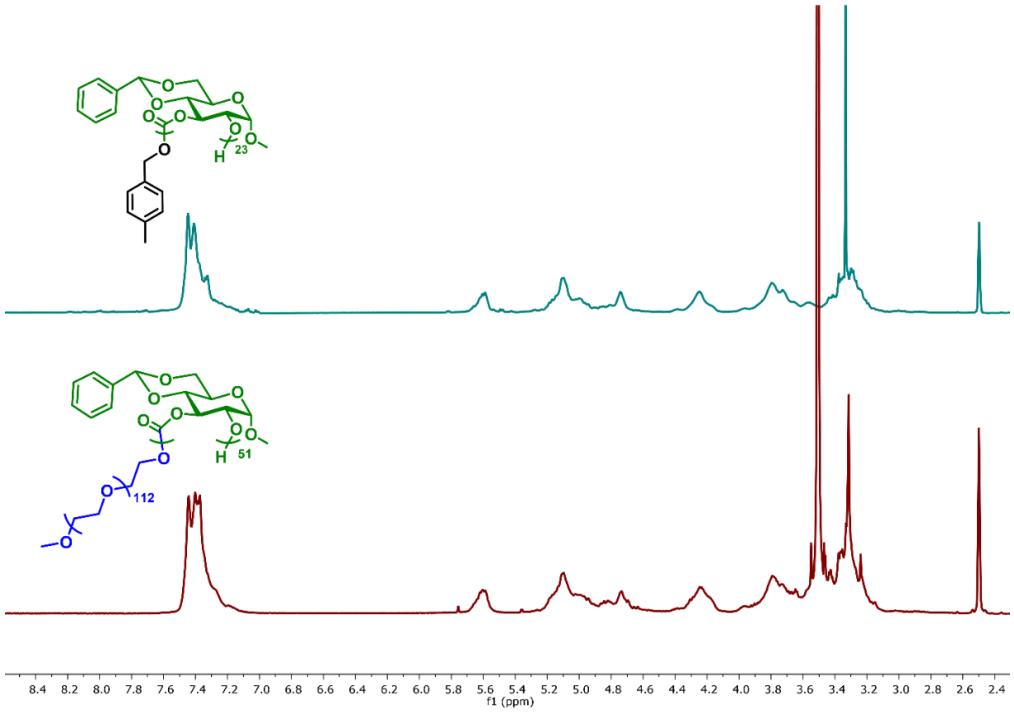

Figure III.22. ^{1}H NMR (500 MHz) spectra of PMBGC$_{23}$ (**20**, top, teal) and mPEG$_{113}$-*b*-PMBGC$_{51}$ (**16**, bottom, maroon) in d_6-DMSO.

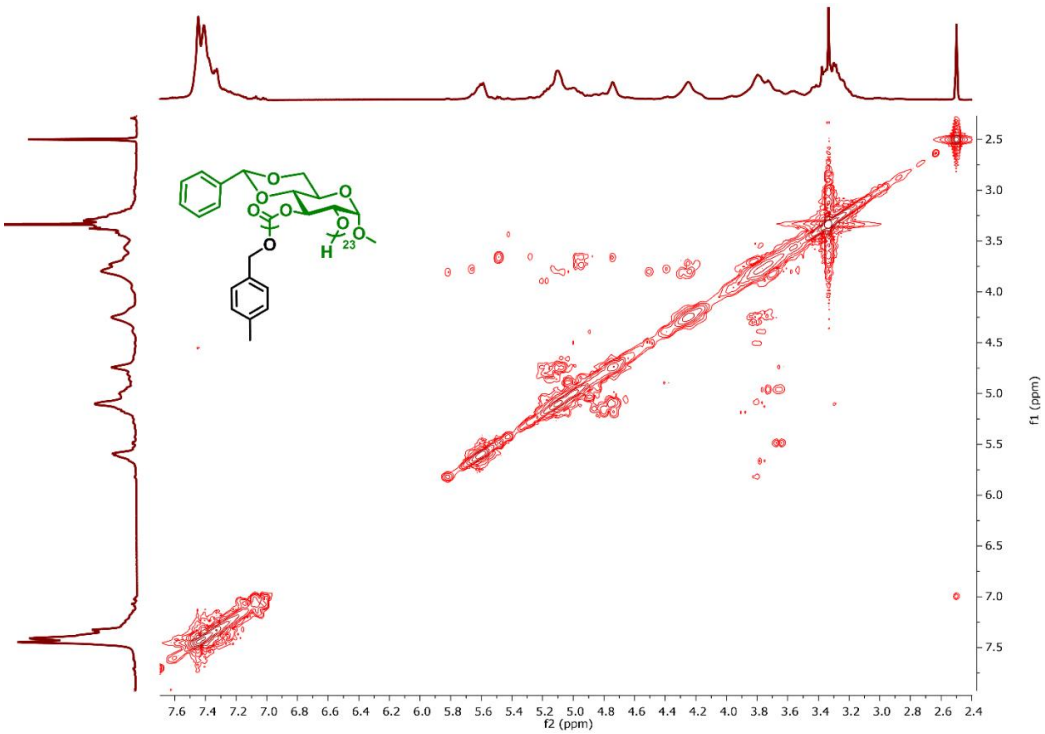

Figure III.23. COSY NMR spectrum of PMBGC$_{23}$, **20**, in d_6-DMSO.

CHAPTER IV

THE DEVELOPMENT OF A MULTIFUNCTIONAL GLUCOSE-BASED MONOMER FOR ROP

4.1 Introduction

Natural polysaccharides play vital roles in a wide range of cellular functions such as adhesion, differentiation, and infection. Mimicking the bioactivities of natural saccharides is of significant interest in polymer chemistry, to this end many polymeric systems have been developed to include sugars in their side chains and backbone repeat units.[24,70,74,116-119] These polymers can be produced using several different polymerization techniques, with those that include the sugar unit in the polymeric backbone being the most attractive mimics of the structures of natural polysaccharides. Generally polymers containing saccharides in their backbone are synthesized *via* ROP or condensation of a saccharide-based monomer, allowing for the inclusion of a wide range backbone linkages such as ester, carbamate, or carbonate linkages.[24,70,74,119] Using these different backbone linkages is expected to combine the advantageous properties of both the saccharide repeat units and the backbones linkages. Monomers and polymerization techniques have been developed that offer control over the orientation and functionality of the sugar repeat units with the aim of optimizing the overall polymer properties for a specific application with predominantly linear polymeric architectures.[33-38,40,48,56,71,75,120,121] However many of the important biological activities of carbohydrates are driven by having multiple interactions with biological receptors.[122-124] Nature allows for these interactions through polysaccharides with a variety of different

branching units and architectures. Synthetic polymers are able to achieve a wide range of architectures, such as linear, cyclic, star, branched, and crosslinked.[125-127] Branched structures are synthetically interesting as they can combine some of the benefits of dendritic materials with the ease of synthesis of one pot linear polymers. In addition the thermal, solution, and mechanical properties of branched polymers tend to be different from their linear analogs.

Due to their high degree of functionality sugars have been used as branching points in a variety of polymers,[128-130] and several examples of branched sugar-based polymers exist,[24,118,126] there are relatively few examples of using ROP to produce sugar-based branched architectures being investigated.[40,120] Several synthetic methodologies have been developed for the synthesis of naturally-derived polycarbonate materials,[24,47,49,53,60,66-68,74,131-134] especially using glucose as a monomer precursor.[48,56,69,71-73,75-77] These synthetic methodologies offer exquisite control of the polymers produced, and allow for a vast range of thermal, physical, mechanical, and degradation properties. Polycarbonates are of particular interest because of their ability to be used in multiple applications from engineering to biomedical material, and their benign degradation products. The monomers for the production of linear poly(glucose carbonate)s *via* ROP have two general structural motifs either a 5-membered cyclic carbonate between the 2 and 3 positions of the sugar,[69,72,73,76] or a 6-membered cyclic carbonate between the 4 and 6 positions of the sugar,[37,38,56,68,71,75,78] with the hydroxyls on the other position protected by a non-reactive functional group. The studies into these cyclic carbonate monomers have demonstrated significant differences in the reactivities of the differently sized rings. The driving force in most ROPs is the release of strain energy upon the opening of the cyclic monomer, generally

in 5-membered rings the strain energy is not significant enough to drive the reaction, the fusing of the ring in *trans* configuration is likely what favors the polymerization in the case of the glucose carbonate monomers.[79-87,89-91] A multifunctional glucose monomer with both a 5- and 6-membered cyclic carbonates may be able to take advantage of the observed differences in polymerization kinetics to produce linear and branched architectures.

Herein, we report the synthesis of a multifunctional glucose-based monomer, methyl 2,3:4,6-di-*O*-carbonyl-α-D-glucopyranoside (MGDC), with a 5- and 6-membered cyclic carbonate for ROP. A range of organocatalytic polymerization conditions were examined to determine if any selectivity existed in the opening of the 5- vs. 6-membered carbonates of MGDC. From these optimized conditions a series of PMGDCs were synthesized. Finally, the ability of MGDC to be used as a comonomer/crosslinker with a monofunctional monomer to produce branched structures was investigated.

4.2 Results and Discussion

4.2.1 Monomer synthesis

A direct synthesis of a dicarbonate glucose monomer MGDC monomer was initially attempted from methyl α-D-glucopyranoside however the high degree of hydroxyl functionality of methyl α-D-glucopyranoside caused significant side reactions to occur and did not allow for reasonable isolated yields. Therefore, MGDC was synthesized in three steps from a partially protected methyl 4,6-*O*-benzylidene-α-D-glucopyranoside (Figure IV.1). The first step was the establishment of a 5-membered cyclic carbonate through the hydroxyl groups at positions 2 and 3 to produce methyl 4,6-*O*-benzylidene-2,3-*O*-carbonyl-

α-D-glucopyranoside (MBGC) as previously described.[76] The benzylidene protecting group was removed in the next step, where a variety of conditions were examined (Table IV.3). These conditions gave two major products, the desired methyl 2,3-*O*-carbonyl-α-D-glucopyranoside ($MGC_{2,3}$), and the over deprotected methyl α-D-glucopyranoside. Hydrogenolysis with 10 wt% Pd/C catalyst was able to produce the desired $MGC_{2,3}$ as the major product in a good yield (>80%) following purification *via* column chromatography. The success of this reaction was confirmed through the disappearance of all ^{1}H (7.50, 7.39, 5.75 ppm) and ^{13}C NMR (138.3, 129.8, 128.9, 122.2, 101.9 ppm) resonances corresponding to the benzylidene group (Figures IV.4, 5), as well as the appearance of both protons on position 6 of the sugar as a single signal (3.81 ppm), the hydroxyl groups on the 4 (5.08 ppm) and 6 (3.82 ppm) positions of the sugar, and OH stretch in the IR (3500-3300 cm^{-1}, Figure IV.6). MGDC was then synthesized by installing the second cyclic carbonate through the hydroxyl groups on the 4 and 6 positions. Triphosgene was utilized as the carbonylation agent as in the synthesis of MBGC as alternatives to phosgene derivatives gave very low isolated yields. Initial attempts at the synthesis of MGDC were made using the conditions that were used to synthesize MBGC. Using these conditions a mixture of products was produced, purification of this mixture using silica gave less than 5% yield of the desired product. It was then determined that MGDC degraded on silica and alumina, likely caused by additional strain from the tricyclic structure. The instability of MGDC to common purification methods drove the need for conditions that were able to provide high levels of conversion to the cyclic product and very few side reactions as the desired product cannot be purified *via* column chromatography. A range of conditions were examined, the concentration and equivalences of base used in the synthesis were determined to have the

greatest effect on the isolated yield. Upon optimization of the conditions good yields (>70%) were obtained for the desired MGDC product. The success of this reaction was verified by the disappearance of the ^{1}H NMR resonance (5.08, 3.82 ppm) and IR stretch (3500-3300 cm^{-1}) of the hydroxyl groups on $MGC_{2,3}$. Additionally the two protons on position 6 of the sugar appear as two resonances in the ^{1}H NMR spectrum (4.63, 4.49 ppm) because of their diastereotopic nature, and the appearance of a second carbonyl signal in both the ^{13}C NMR (146.6 ppm) and IR (1807 cm^{-1}, Figures IV.4-6) further supports the success of the ring-closure.

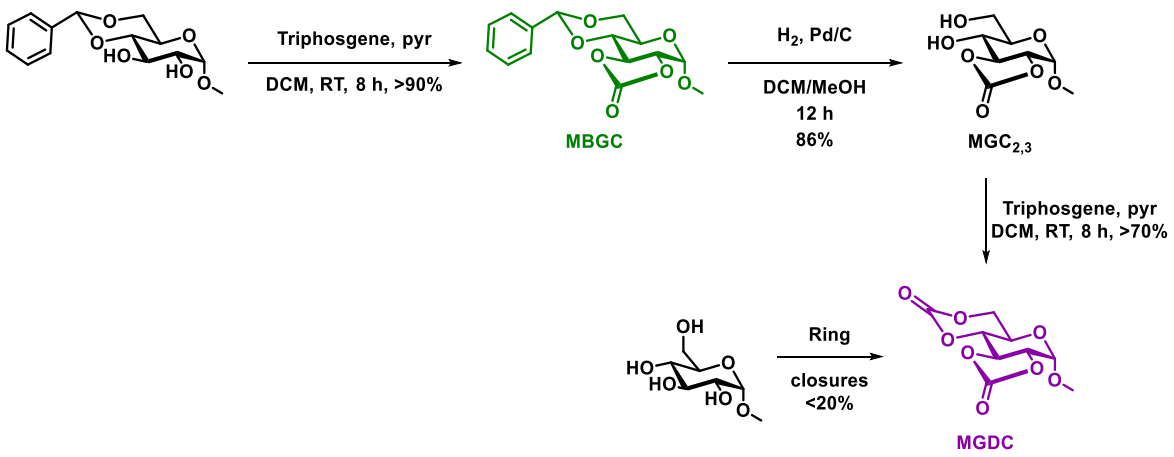

Figure IV.1. Synthesis of MGDC and synthetic precursors.

4.2.2 Homopolymerization of MGDC

Previous experiments with the isolated 5- and 6-membered cyclic glucose carbonates suggested that the kinetics of the ring-openings would be significantly different. The 5-membered carbonate requires several hours at 30 °C with TBD as a catalyst to reach high

levels of conversion, whereas the 6-membered carbonate reaches high conversion at -78 °C within 20 minutes using the same catalyst. We sought to take advantage of these apparent different reactivities between the two different rings to produce both linear and branched polymeric architectures (Figure IV.2). Initially the isolated 5-membered carbonate monomer MBGC was examined under reaction conditions known to allow for the polymerization of the 6-membered cyclic glucose carbonates. Under these conditions at both -78 ° and -5 °C there was a complete recovery of unreacted MBGC following the attempted polymerization. These conditions were then applied to the polymerization of MGDC, immediately upon adding the organocatalyst, TBD, an opaque intractable white gel was formed, suggesting the uncontrolled rapid opening of both 5- and 6-membered rings. Small molecule studies were completed to analyze the initiation step of the mechanism however in these experiments the major products were crosslinked networks rather than the desired single ring-opened product.

Following this initial attempt at polymerizing MGDC, a range of conditions were attempted (Table IV.4) to gain better control of the ring-opening. Initially the strength of the organocatalyst was varied by replacing TBD with the less basic DBU or DMAP while maintaining the other conditions. Using DBU as the organocatalyst also produced a precipitate during the polymerization, while DMAP gave recovery of unreacted MGDC. Optimization of several parameters found that low temperatures, concentrations, and a weaker organocatalyst (< -40 °C, < 0.25 M, DBU) proved successful at synthesizing oligomers and polymers that were suitable for further analyses, demonstrating the inhibition of the crosslinking reactions. Using these conditions, a series of MGDC oligomerizations and polymerizations were performed to measure the progress of the polymerization (Table

IV.1, Figures IV.7, 8, 11, 12). From these polymerizations it was seen that as higher degrees of monomer conversion were reached higher levels of branching occurred. Branching was not calculable *via* a ^{1}H NMR analysis because no unique signals for the branching *versus* linear units of the polymer chains could be identified. MALDI-TOF MS analysis was used to evaluate the presence of a branched population. Branching was first estimated by comparing the molar mass measured by NMR and MALS SEC, although the molar mass measured by MALS SEC is an absolute mass, there is inherent error in both molar mass measurements, the branching calculated from these methods should be considered as only an estimate not an absolute value. For the polymerization with the highest conversion achieved (**23**) branching was estimated at 7-17% whereas for the lowest conversion polymerizations branching >5% could be achieved. This branching trend was further evaluated by MALDI-TOF MS analysis of the polymers. In the samples with estimated low degrees of branching a single major population was seen matching with the expected end groups (Figures IV.13, 14), whereas the samples with higher estimated degrees of branching have 2 main populations, 1 matching to the expected end groups and the second being +122 Da indicating an additional initiator on the polymer, suggesting 1 branching point exists in the polymer backbone. Additionally, although signal intensities are not quantitative in MALDI-TOF MS the relative intensity of the +122 amu distribution decreased in intensity as the extent of branching decreased. The resolution of the current MALDI-TOF MS measurements did not allow for the identification of populations with more than one additional initiator as the mass of the monomeric repeat unit (+246 amu) and two initiators (+244 amu) are too similar meaning that there may be additional populations with more than one branching points in the polymer backbone.

Table IV.1. Properties of PMGDCs.

Polymer	Sample	DP[a]	Conversion (%)	M_w[b] (kDa)	M_n[b] (kDa)	$Đ$[b]	Branching units (%)[c]
PMGDC	**23**	10	100	6.6	4.2	1.55	7-17
	24	14	70	4.5	4.4	1.49	2-6
	25	15	75	6.5	4.8	1.35	1-5
	26	17	57	6.2	4.6	1.36	1-3
	27	17	57	6.6	4.9	1.34	1-4
	28	21	70	8.2	5.6	1.47	1-3
	29	20	50	8.0	5.4	1.46	1-3
	30	23	57	9.7	6.6	1.46	1-3

[a]Measured by comparing the aromatic signal of the initiator to the OMe of the polymer. [b]Measured with SEC (DMF eluent) with a RALS and LALS detectors calibrated with PMMA standards. [c]Estimated by comparing the mass calculated *via* ^{1}H NMR and SEC.

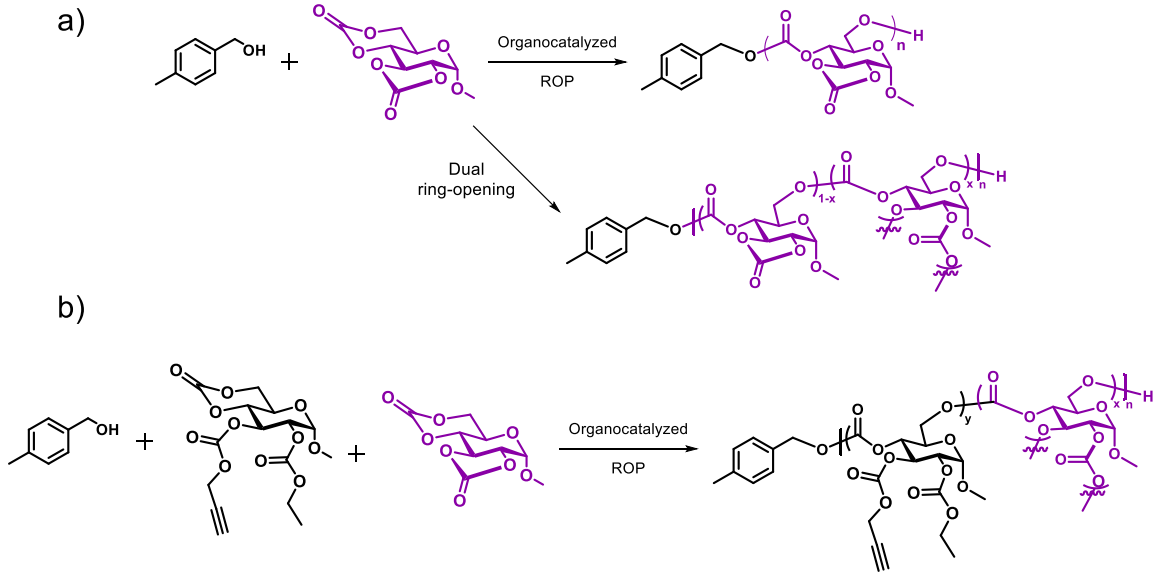

Figure IV.2. Polymerization of MGDC to afford homopolymers (a), and copolymers with GCEPC (b).

4.2.3 Copolymerization of MGDC

As the homopolymerization study had demonstrated the ability of MGDC to undergo ring-opening of both cyclic carbonates under the common conditions used to polymerize the

isolated 6-membered glucose carbonate, MGDC's use as a comonomer/crosslinker to produce branched structures was investigated. Methyl 4,6-*O*-carbonyl-2-*O*-ethyloxycarbonyl-3-*O*-propargyloxycarbonyl-α-D-glucopyranoside (GCEPC) was chosen as a comonomer based on its versatility and straightforward ability to undergo post-polymerization modification. Copolymerizations of GCEPC and MGDC were completed using 4-methylbenzyl alcohol as initiator and TBD as organocatalyst. These reaction conditions were chosen to allow for both rings of the MGDC to open making each MGDC monomer incorporated into the polymer chain a branching point in the chain. The targeted total number of sugar repeat units was kept constant and the target percentage of MGDC used as a comonomer was gradually increased from 0 to 50 mol% (Table IV.2). Starting with 14% intended incorporation of MGDC into the copolymer, organogels formed during the polymerizations. These gels were transparent, stable overnight, intractable in organic solvents, and qualitatively the gels formed with higher MGDC incorporation were more mechanically robust, however a full mechanical analysis is needed to fully understand these materials. For the polymerizations with a lower incorporation of MGDC, the polymers remained in solution for the entirety of the polymerization and were soluble for further analyses. The actual incorporation of MGDC was estimated *via* ^{1}H NMR by comparing the methyl group of the ethyloxycarbonyl side chain (1.28 ppm) to the OMe (3.48 ppm) of the sugar signals (Figure IV.7, 9). The signal at 1.28 ppm was solely from the GCEPC monomer whereas the OMe signal was from both monomers, so the excess intensity in the OMe signal was used to estimate the amount of MGDC included in the polymer. As the amount of MGDC increased, the molecular mass distributions and *Đ* increased significantly reflecting

the branching in the polymer chain (Figure IV.3). The branching structure was also supported by the increase in intrinsic viscosity as the degree of branching increased.

Table IV.2. Properties of PGCEPC-*co*-PMGDCs.

Polymer[a]	Sample	Target MGDC (%)	Actual MGDC (%)[a]	M_w[b] (kDa)	M_n[b] (kDa)	$Đ$[b]	Intrinsic viscosity[b] (dL/g)
$PGCEPC_{47}$	**31**	0	0	18.2	14.4	1.23	0.089
$PGCEPC_{50}$-*co*-$PMGDC_2$	**32**	2	4	42.5	22.4	1.89	0.11
$PGCEPC_{45}$-*co*-$PMGDC_3$	**33**	4	6	166.9	32.7	5.01	0.14
$PGCEPC_{40}$-*co*-$PMGDC_4$	**34**	6	9	757.6	33.0	23.9	0.18

[a]Measured by comparing the aromatic signal of the initiator to the OMe, and methyl protons of the ethyl carbonate group of the GCEPC repeat unit. [b]Measured with SEC (DMF eluent) with a RALS, LALS, and viscometry detectors calibrated with PMMA standards.

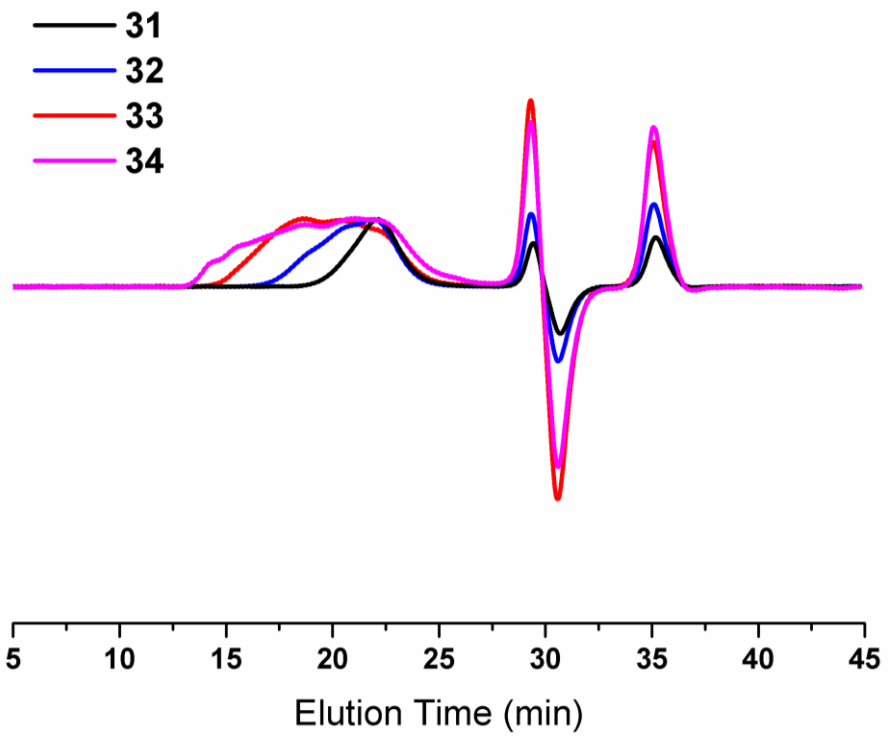

Figure IV.3. SEC (DMF eluent) RI traces of PGCEPC-*co*-PMGDC.

4.3 Experimental Section

4.3.1 Materials

All materials were purchased from VWR or Sigma-Aldrich. Unless noted, all reagents were used as received. Dichloromethane (DCM) was purified and dried by a solvent purification system (J. C. Meyer Solvent System). Anhydrous acetonitrile was stored over molecular sieves under an argon atmosphere. 4-Methylbenzyl alcohol and TBD were dried over CaH_2, dried under vacuum, and stored under an argon atmosphere. DBU was dried over CaH_2, distilled, and stored under an argon atmosphere. MBGC and methyl 4,6-*O*-carbonyl-2-*O*-ethyloxycarbonyl-3-*O*-propargyloxycarbonyl-α-D-glucopyranoside (GCEPC) were synthesized as previously reported. MGDC was dried under reduced pressure over P_2O_5 and stored under an atmosphere of argon. ***Caution***: When working with phosgene precursors, including triphosgene, special precautions should be taken as they are highly toxic by inhalation or ingestion.

4.3.2 Instrumentation

^{1}H, ^{13}C, COSY, and HMQC NMR spectra were recorded on an Inova500 spectrometer, chemical shifts were referenced to the resonance signals of the deuterated solvent.

IR spectra were recorded on a Shimadzu IR Prestige attenuated total reflectance Fourier-transform infrared spectrophotometer and analyzed using IR solution v. 1.40 software.

A Waters Chromatography, Inc. (Milford, MA) system with an isocratic pump model 1515, and a four-column set of 5 μm Guard (50 × 7.5 mm), Styragel HR 4 5 μm DMF (300 × 7.5 mm), Styragel HR 4E 5 μm DMF (300 × 7.5 mm) and Styragel HR 2 5 μm DMF (300 × 7.5 mm) with DMF (0.05 M LiBr) as the eluent (0.75 mL/min) at 70 °C. Polymer solutions were prepared at *ca.* 5 mg/mL, with toluene as a flow marker, and an injection volume of 200 μL was used. The samples were analyzed using a Malvern Panalytical OMNISEC REVEAL (Malvern, UK) with RI, LALS, RALS, and viscometer detectors calibrated against a poly(methyl methacrylate) standard.

4.3.3 Synthesis

Synthesis of methyl 2,3-O-carbonyl-α-D-glucopyranoside ($MGC_{2,3}$). Methyl 4,6-*O*-benzylidiene-2,3-*O*-carbonyl-α-D-glucopyranoside (5.033 g, 16.32 mmol) and palladium on carbon (486.0 mg, 9.9 wt%) were mixed in 100 mL of a methanol/DCM solution. The reaction vessel was evacuated and back-filled to remove oxygen and was then placed under a hydrogen atmosphere. The reaction was allowed to take place at RT for 9 h. The reaction mixture was run through a silica plug to remove the Pd/C catalyst, and then purified *via* column chromatography (3:1 ethyl acetate:hexanes) to produce 2.967 g (82%) of a white foam. FTIR (ATR): 3500-3300, 3000-2900, 1786, 1451, 1418, 1404, 1383, 1364, 1348, 1325, 1275, 1250, 1229, 1204, 1180, 1157, 1119, 1101, 1088, 1066, 1045, 1005, 966, 941, 905, 851, 820, 783, 770, 735, 665 cm^{-1}. ^1H NMR (500 MHz, Acetone-d_6): δ 5.19 (d, J = 3.0 Hz, 1H), 5.08 (d, J = 5.7 Hz, 1H), 4.64 (dd, J = 9.8, 11.6 Hz, 1H), 4.35 (dd, J = 3.0, 11.6 Hz, 1H), 4.11 (dt, J = 5.7, 9.4 Hz, 1H), 3.82 (overlapping multiplet, 3H), 3.54 (multiplet, 1H),

3,49 (s, 3H) ppm. ^{13}C NMR (125 MHz, Acetone-d_6): δ 154.5, 96.5, 80.9, 77.9, 76.2, 69.3, 61.3, 55.7 ppm. MS (ESI+): calculated $[M+Li]^+$ for $C_8H_{12}O_7Li$ 227.0743, found 227.0746.

Synthesis of methyl 2,3:4,6-di-O-carbonyl-α-D-glucopyranoside (MGDC). $MGC_{2,3}$ (2.0661 g, 9.384 mmol) was weighed into preweighed glassware and then dried under vacuum to a constant weight. Anhydrous DCM (120 mL) and pyridine (4.0 mL, 50 mmol) were added to the dried glucopyranoside and mixed until a homogeneous solution was observed. A solution of triphosgene (1.1269 g, 3.797 mmol, 11.391 mmol of carbonylation agent generated *in situ*) in anhydrous DCM (68 mL) was added slowly to the glucopyranoside, and the reaction was allowed to proceed at RT for 14 h. To quench any remaining triphosgene a saturated solution of sodium bicarbonate was added. The organic layer was then washed with saturated sodium bicarbonate, 5% HCl (aq), and DI H_2O, dried over magnesium sulfate, and concentrated to approximately 10% of its original volume. The concentrated organic layer was then purified *via* a celite plug with DCM and was then concentrated to dryness to yield 1.6860 g (73%) of a white powder. FTIR (ATR): 3000-2800, 1807, 1755, 1477, 1429, 1414, 1396, 1381, 1367, 1331, 1260, 1200, 1175, 1146, 1109, 1094, 991, 932, 914, 789, 766, 737, 660 cm^{-1}. ^{1}H NMR (500 MHz, Acetone-d_6): δ 5.44(d, J = 3.0 Hz, 1H), 4.98 (overlapping, 2H), 4.63 (overlapping, 2H), 4.49 (dd, J = 9.5, 10.7 Hz,1H), 4.31 (multiplet, 1H), 3.58 (s, 3H) ppm. ^{13}C NMR (125 MHz, Acetone-d_6): δ 153.5, 146.6, 97.5, 77.6, 76.8, 76.5, 69.8, 62.6, 56.5 ppm. MS (ESI-): calculated $[M+Cl]^-$ for $C_9H_{10}O_8Cl$ 281.0064, found 281.0085.

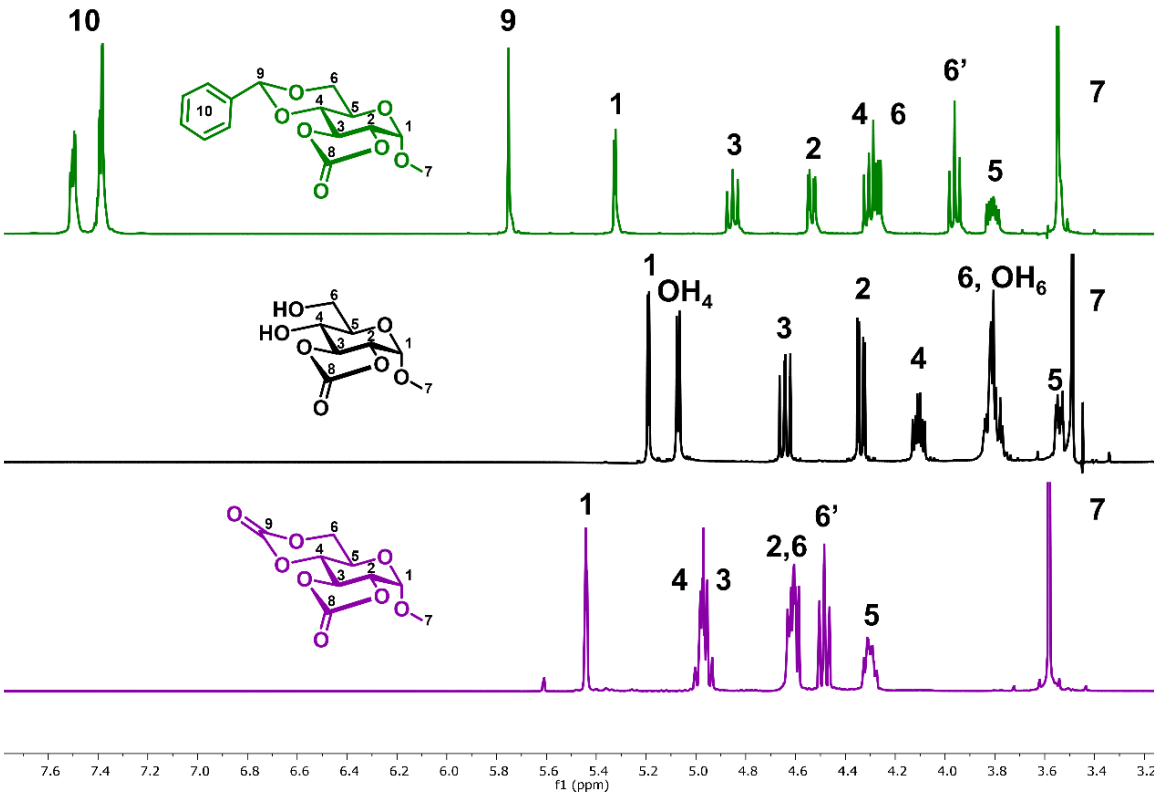

Figure IV.4. Stacked ^{1}H NMR (500 MHz) of MBGC (green), MGC2,3 (black), MGDC (purple) in Acetone-d_6.

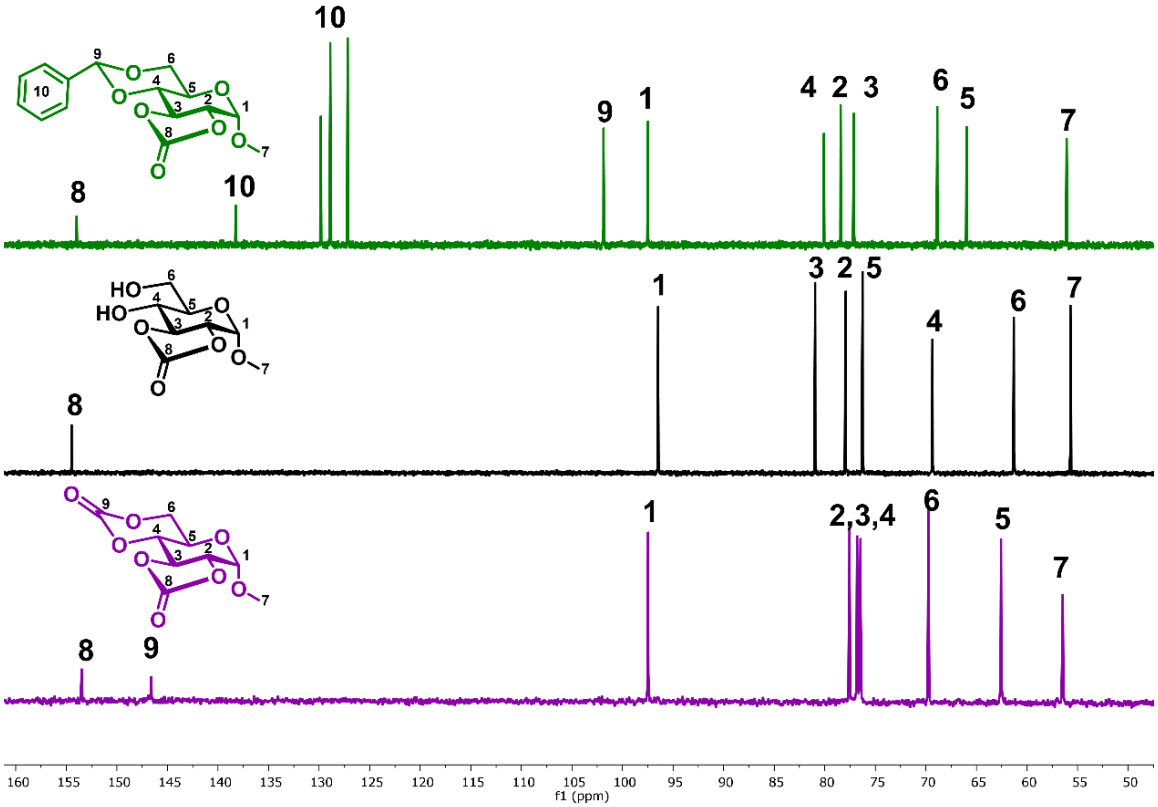

Figure IV.5. Stacked ^{13C} NMR (125 MHz) of MBGC (green), MGC2,3 (black), MGDC (purple) in Acetone-d_6

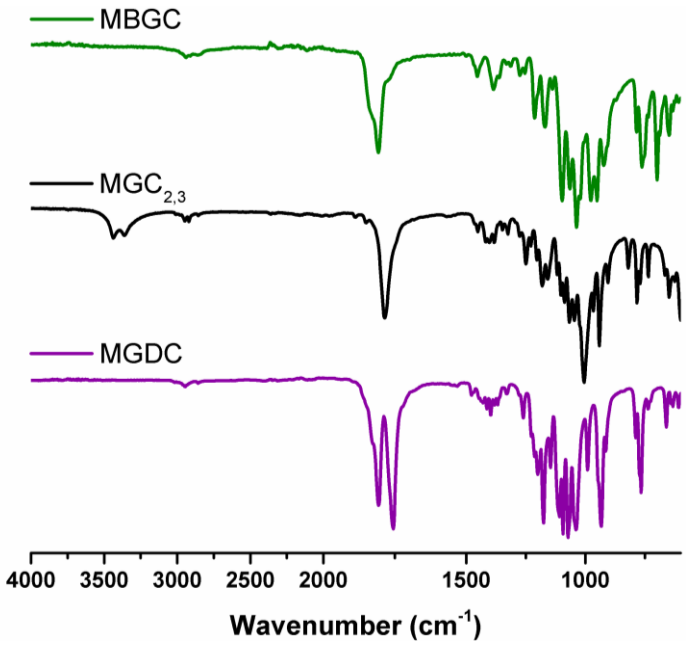

Figure IV.6. IR spectra of MBGC (green), $MGC_{2,3}$ (black), MGDC (purple).

Synthesis of poly(methyl 2,3:4,6-di-O-carbonyl-α-D-glucopyranoside) (PMGDC). All polymerizations were carried out using standard glovebox and Schlenk line techniques. Polymerizations were conducted at -40 °C, the reagents were added to a vial inside a glovebox and the reaction conducted in a fume hood. To a solution of MGDC in acetonitrile (final monomer concentration 0.25 M), 4-methylbenzyl alcohol in acetonitrile was added while stirring. DBU (4 mol% relative to monomer or 1:1 with initiator) in acetonitrile was added to the reaction under Ar atmosphere. After stirring for a certain period of time (1 min to 3 min), the reaction vial was opened to air and quenched by addition of acetic acid in DCM. The polymer was purified by precipitation into ether (2×), followed by precipitation into methanol (1×) and then dried under vacuum to give a white powder (average yield 55%). FTIR (ATR): 3050-2825, 1829, 1755, 1645, 1452, 1240, 1163, 1007, 941, 779, 667 cm^{-1}. ^{1}H NMR (500 MHz, Acetone-d_6): δ 7.33 (d, J = 7.8 Hz, 2H), 7.25 (d, J = 7.8 Hz, 2H), 5.46-5.18 (br), 5.01-4.87 (br), 4.70-4.50 (br), 4.50-4.29 (br), 4.17-4.02 (br), 3.64-3.44 (br), 3.41-3.19 (br), 2.35 (s, 3H) ppm. ^{13}C NMR (125 MHz, Acetone-d_6): δ 153.4, 152.8, 129.1, 128.5, 95.6, 76.5, 72.4, 69.4, 66.0, 55.5, 20.3 ppm.

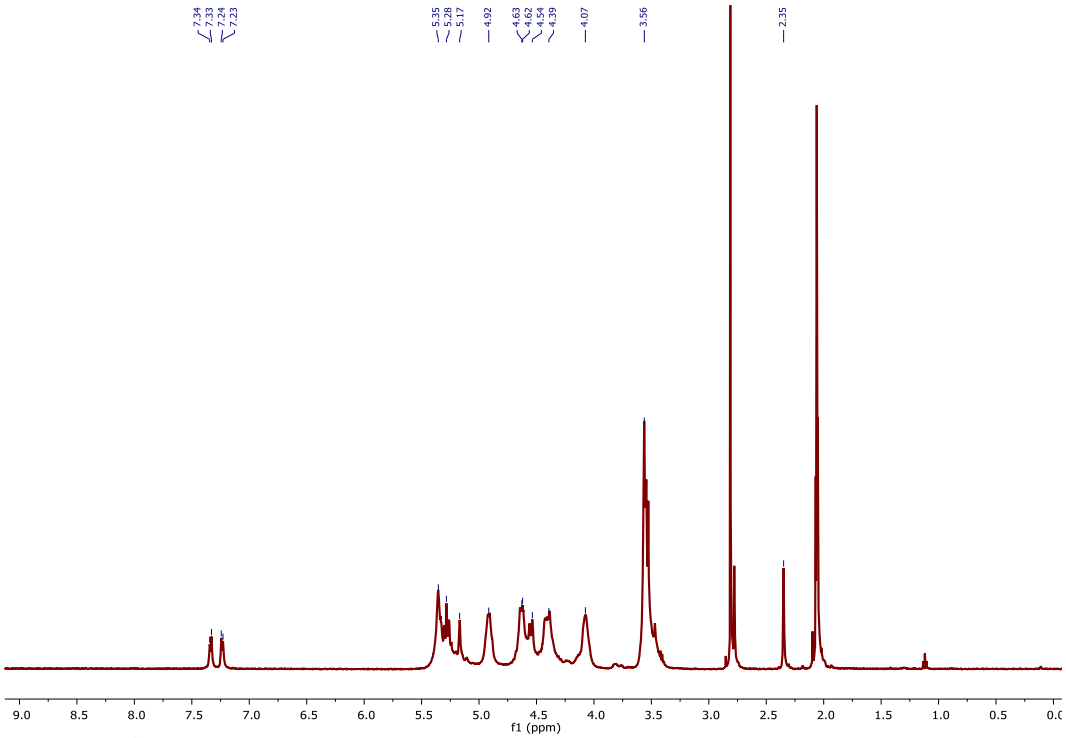

Figure IV.7. ^{1}H NMR (500 MHz) of PMGDC in Acetone-d_6.

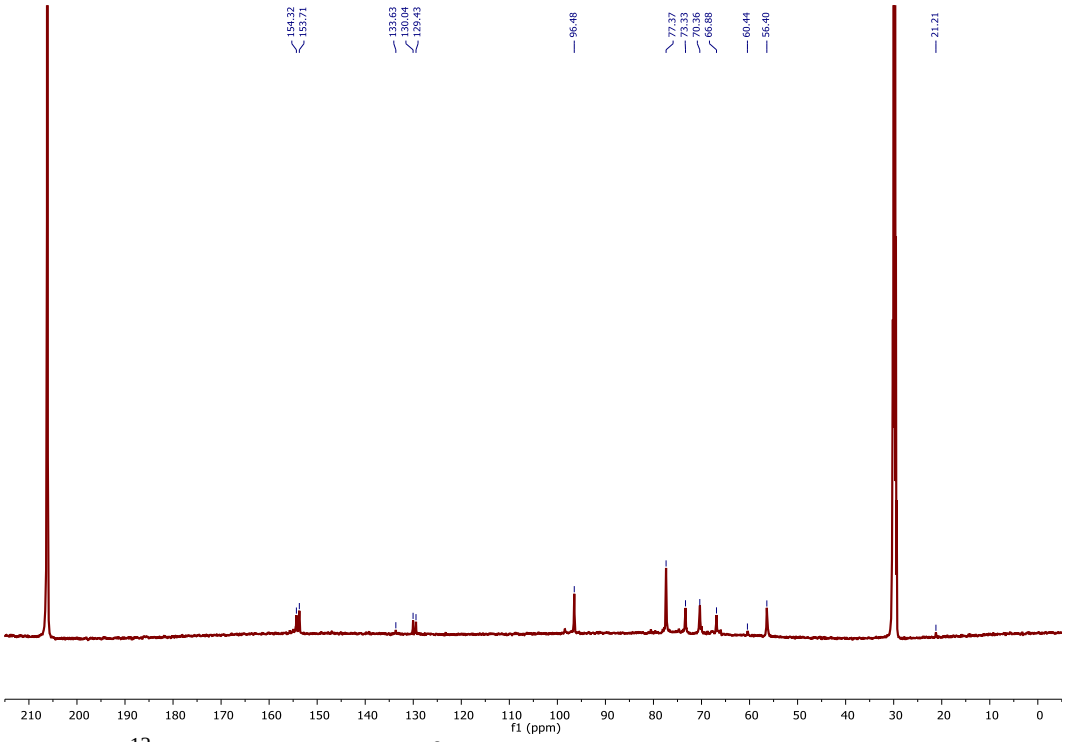

Figure IV.8. ^{13}C NMR (125 MHz) of PMGDC in Acetone-d_6.

Synthesis of poly(methyl 4,6-O-carbonyl-2-O-ethyloxycarbonyl-3-O-propargyloxycarbonyl-α-D-glucopyranoside-*co*-methyl 2,3:4,6-di-O-carbonyl-α-D-glucopyranoside) (PGCEPC-*co*-PMGDC). All polymerizations were carried out using standard glovebox and Schlenk line techniques. Polymerizations were conducted at -40 °C, the reagents were added to a vial inside a glovebox and the reaction conducted in a fume hood. To a solution of GCEPC in acetonitrile (final total monomer concentration 0.50 M), MGDC (0-50 mol%) in acetonitrile was added. 4-methylbenzyl alcohol in acetonitrile was added, followed by TBD (4 mol% relative to total monomer) in acetonitrile under Ar atmosphere. After stirring for 10 min, the reaction vial was opened to air and quenched by addition of acetic acid in DCM. The polymer was purified by precipitation into ether (2×), followed by precipitation into methanol (1×) and then dried under vacuum to give a white powder (average yield 64%). The copolymers with higher than 14 mol% MGDC formed translucent intractable organogels during the polymerization and were not precipitated. FTIR (ATR): 3325-3225, 3050-2850, 1756, 1447, 1373, 1333, 1246, 1171, 1117, 1092, 1018, 986, 907, 878, 781, 671 cm^{-1}. ^{1}H NMR (500 MHz, Acetone-d_6): δ 7.33 (d, J = 7.8 Hz, 2H), 7.23 (d, J = 7.8 Hz, 2H), 5.34 (t, J = 9.7 Hz), 5.13 (d, J = 3.3 Hz), 4.96 (t, J = 9.7 Hz), 4.88-4.74 (br), 4.48-4.41 (br), 4.37-4.28, 4.24-4.09 ppm. ^{13}C NMR (125 MHz, Acetone-d_6): δ 154.0, 153.9, 96.4, 77.2, 76.7, 74.4, 73.4, 72.4, 66.9, 66.0, 64.4, 55.7, 55.1, 13.5 ppm.

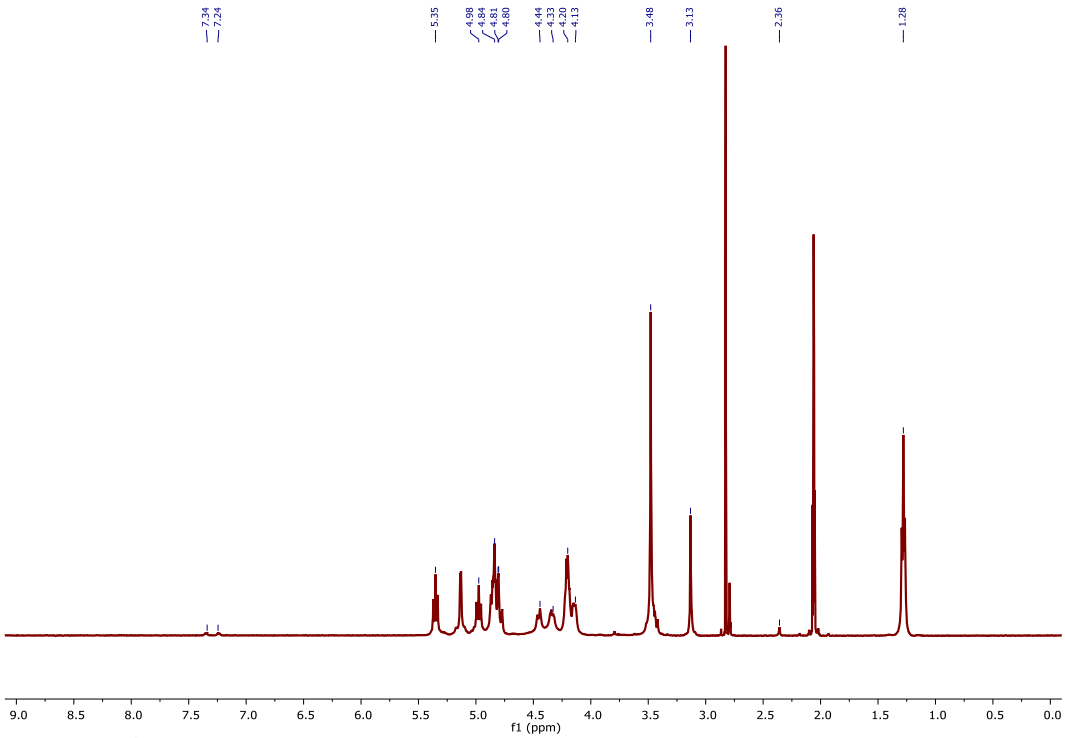

Figure IV.9. ^{1}H NMR (500 MHz) of PGCEPC-*co*-PMGDC in Acetone-d_6.

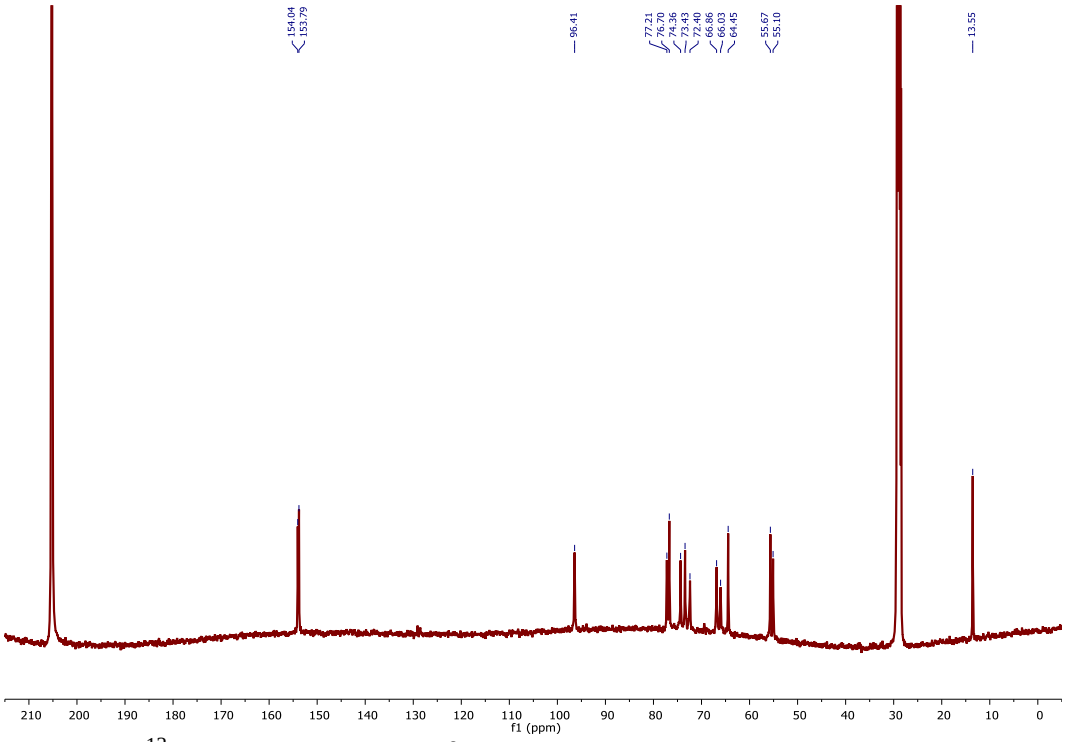

Figure IV.10. ^{13}C NMR (125 MHz) of PGCEPC-*co*-PMGDC in Acetone-d_6.

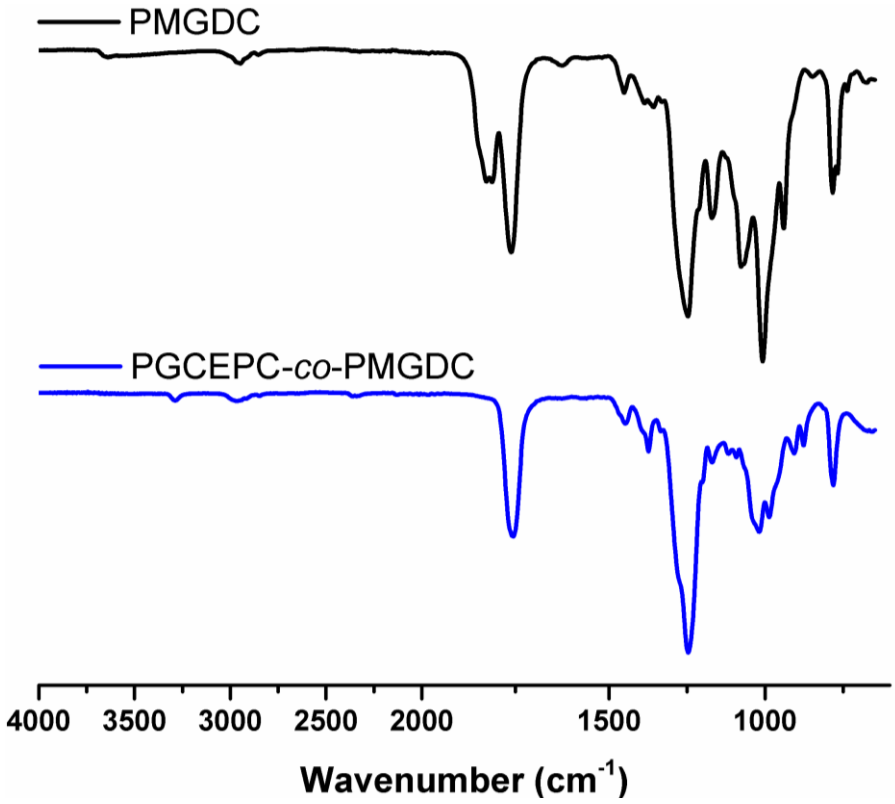

Figure IV.11. IR spectra of PMGDC (black), and PGCEPC-*co*-PMGDC (blue).

4.4 Conclusions

Our interest in functional materials with complex polymeric architectures, that can potentially undergo degradation into benign by-products, has driven this investigation into the development of synthetic methodologies utilizing carbohydrates as diverse building blocks. In this current work the scope of glucose as a monomer was expanded to the production of a difunctional monomer to generate a series of different polymers. The difunctional monomer with a 5- and 6-membered cyclic carbonate, methyl 2,3:4,6-di-*O*-carbonyl-α-D-glucopyranoside (MGDC), was synthesized in 3 steps with good yields (>70%

for each step) from methyl 4,6-*O*-benzylidene-α-D-glucopyranoside using established carbonylation and deprotection chemistries.

The investigation of MGDC under various organocatalytic conditions was undertaken to evaluate changes in reactivity in the differently sized cyclic carbonates in the difunctional monomer to their monofunctional analogs. Based on the monofunctional analogs it was initially hypothesized that the 5- and 6-membered rings would open at significantly different rates allowing for the synthesis of linear or branched polymers from a single monomer. The production of predominantly linear PMGDCs (< 5% estimated branching) was possible by targeting relatively low monomer conversion during the polymerization. The investigation of the homopolymerization of MGDC revealed its high potential to be used as a comonomer to produce highly branched glucose-based polymers. A monofunctional 6-memebered glucose carbonate monomer methyl 4,6-*O*-carbonyl-2-*O*-ethyloxycarbonyl-3-*O*-propargyloxycarbonyl-α-D-glucopyranoside (GCEPC) was polymerized with MGDC under conditions that were expected to open both rings of MGDC. As the percentage of MGDC in the copolymerization was increased, SEC analysis confirmed a more branched structure through the increase of intrinsic viscosity of the polymers, and the molar mass distributions. Incorporation of MGDC ≥ 14% allowed for the production of glucose-based organogels.

Overall, this newly developed difunctional monomer gave access to complex polymeric architectures with fully glucose-based monomers *via* ROP. The ability of the polymers to degrade into methyl α-D-glucopyranoside and carbon dioxide, as benign small molecules, make these materials suitable for biomedical and engineering applications in

general. Studies to probe the properties and further potential applications for these materials, and to produce higher molar mass PMGDCs are ongoing.

4.5 Supplemental Information

Table IV.3. Synthetic conditions examined for synthesis of $MGC_{2,3}$ from MBGC.

Reagent	Loading	Time (h)	Product
Amberlyst	Various	3	Methyl α-D-glucopyranoside
I_2 Et_3SiH	High 0.61, 0.51 equivalents	3	Methyl α-D-glucopyranoside
I_2 Et_3SiH	Catalytic 0.43 equivalents, 5.2 mol%	3	Methyl α-D-glucopyranoside
H_2 Pd/C	20 wt%	12	Major: Methyl 2,3-*O*-carbonyl-α-D-glucopyranoside Minor: Methyl α-D-glucopyranoside
H_2 Pd/C	10.6 wt%	8	86 % yield Methyl 2,3-*O*-carbonyl-α-D-glucopyranoside

Table IV.4. Initial conditions screening for the polymerization of MGDC.

M:I	Catalyst	Temperature (°C)	Concentration (M)	Time (min)	Solubility
25	TBD	-5	0.5	0	intractable
25	DBU	-5	0.5	4	intractable
25	DBU	-5	0.25	5	intractable
10	DBU	-5	0.25	5	intractable
10	DBU	-5	0.25	2.5	intractable
10	DBU	-35	0.25	2	polar organics
10	DBU	-40	0.25	1	polar organics

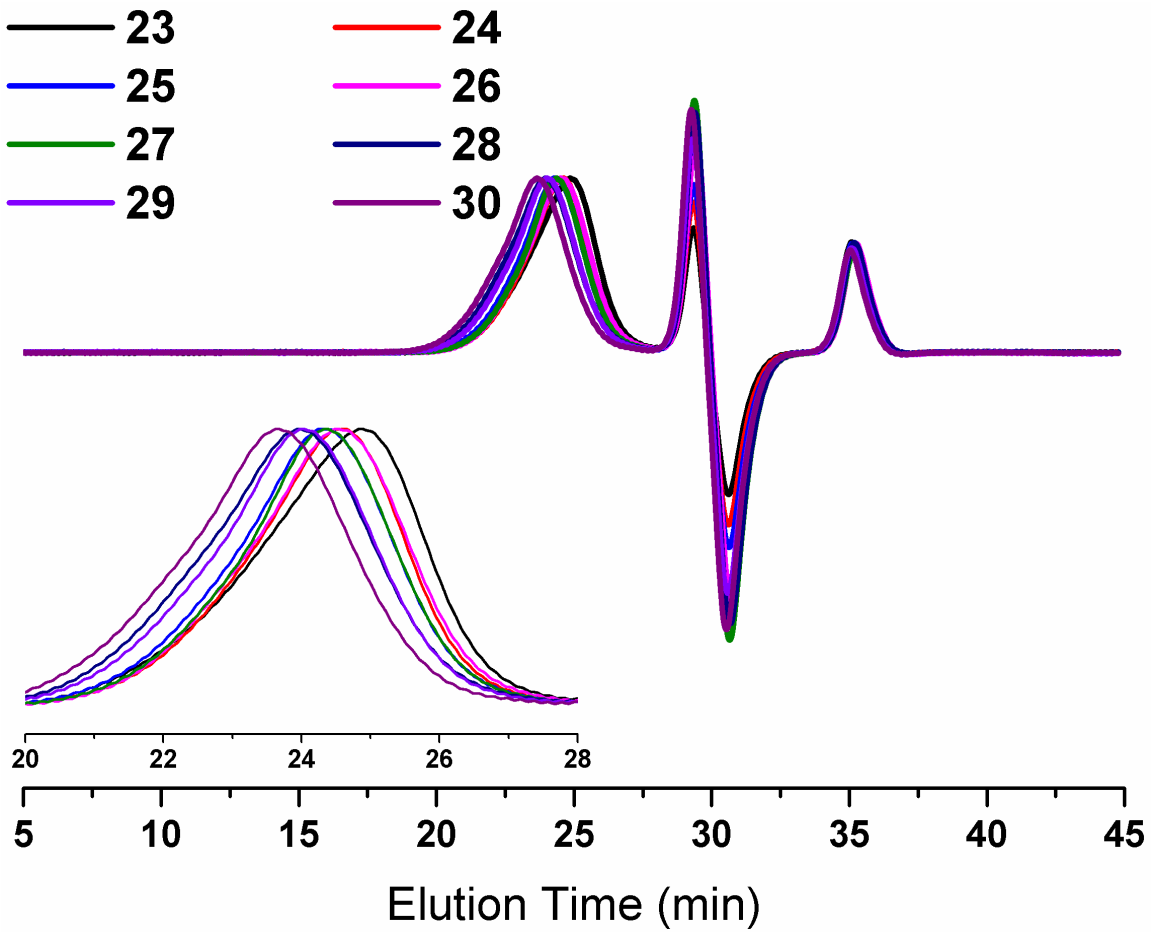

Figure IV.12. SEC (DMF eluent) RI traces of PMGDC, inset shows the same data.

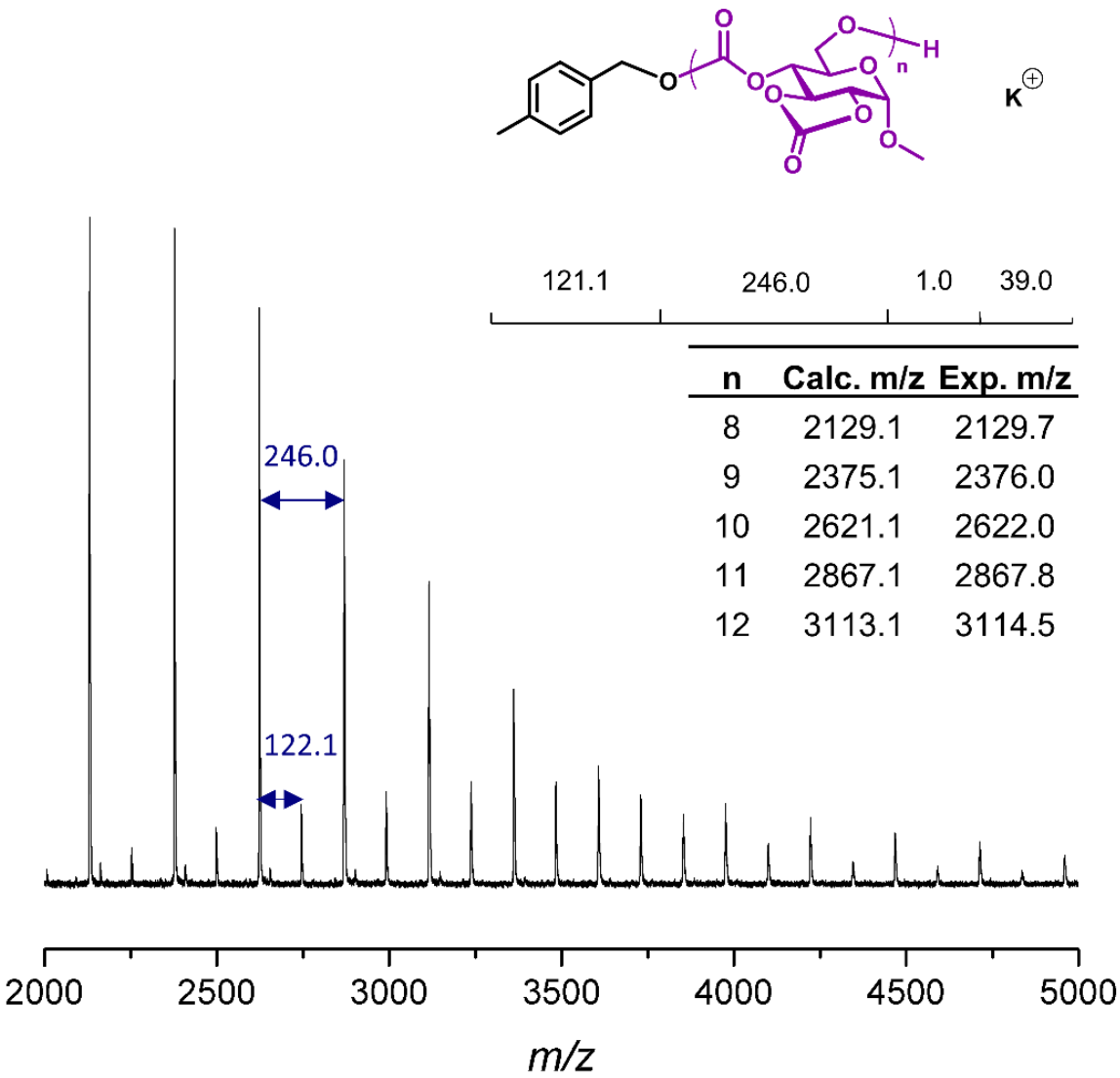

n	Calc. m/z	Exp. m/z
8	2129.1	2129.7
9	2375.1	2376.0
10	2621.1	2622.0
11	2867.1	2867.8
12	3113.1	3114.5

Figure IV.13. MALDI-TOF MS spectrum of PMGDC, **23**, with a high estimated percent of branching units. Analysis of PMGDC revealed two populations, each with a spacing of 246 m/z equal to that of the expected monomer repeat unit. Structurally, these two sets of signals corresponded to populations with distinct end groups, a major population initiated by MBA and a minor population corresponding to branched architectures at +122 m/z of the major population. There is no evidence for loss of CO_2 as a side reaction during polymerization.

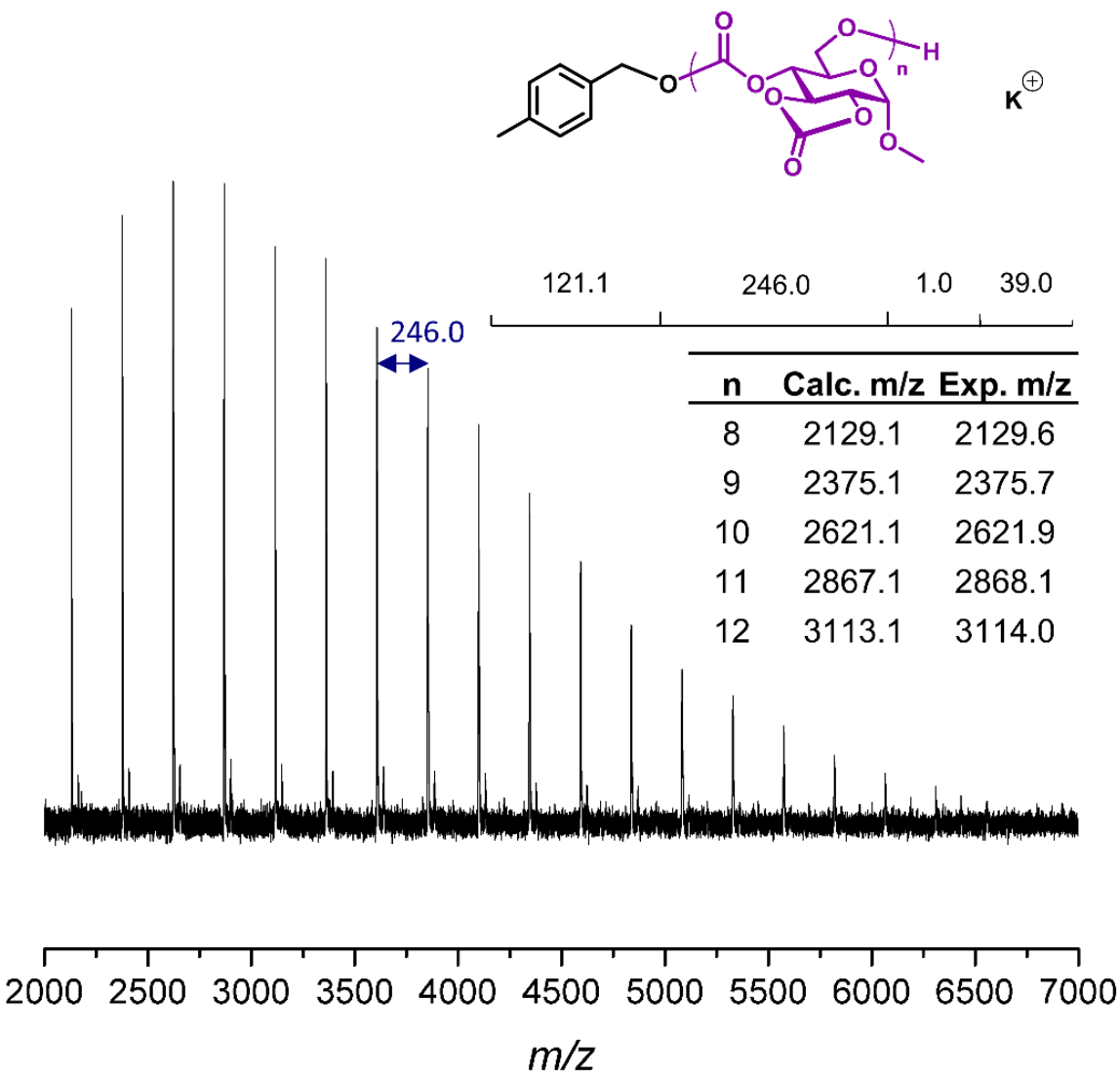

Figure IV.14. MALDI-TOF MS spectrum of PMGDC, **29**, with a low estimated percent of branching units. Analysis of PMGDC revealed one population, with a spacing of 246 m/z equal to that of the expected monomer repeat unit. Structurally this set of signals corresponds to a population initiated by MBA. There is no evidence for loss of CO_2 as a side reaction during polymerization.

CHAPTER V

SYNTHESIS AND CHARACTERIZATION OF POLY(THIOETHER-*CO*-CARBONATE) NETWORKS FROM RAPIDLY GENERATED GLUCOPYRANOSIDE MONOMERS

5.1 Introduction

The accumulation of polymeric materials in the earth's waterways is becoming a significant hazard to aquatic and terrestrial life.[3,8-11] Many of the plastics produced for industrial applications are produced from petrochemical derivatives, and are estimated to take at least 500 years to decompose.[135] When these non-degradable materials are introduced into waterways they accumulate and are unable to break down into small molecules that can potentially be cleared from the environment, and instead breakdown into micro- and nano-particulates that can cause further damage to aquatic environments.[6,7,9] To address this challenge, significant efforts have been undertaken to develop sustainable polymeric materials from novel sources to reduce the reliance of polymers and plastic materials on petrochemical-derived starting materials. Naturally-derived polymers have significant potential as sustainable polymers that retain their usefulness as highly functional and specialized materials.[15,26,27,29,136] Another advantage of naturally sourced materials is their potential to undergo chemical degradation under photochemical, thermal, enzymatic, or hydrolytic pathways. Carbohydrates are of substantial interest as monomer sources to develop synthetic natural product-based materials.[47,70,74] As the fundamental building blocks of many natural polymers, carbohydrates have wide bioavailability, they also possess

high levels of chemical functionality and stereochemical diversity that make them attractive starting materials in the design of functional materials.[24,33,38-40,70,120] Glucose was chosen as the monomeric source for examination in this work. A monomer was designed with hydrolytically degradable carbonate linkages that would allow for the eventual chemical degradation of the polymer into small molecules, rather than only physical degradation into micro- and nano-plastic particulates.

Significant work has been completed in the Wooley lab towards the development of naturally-derived polycarbonate materials, especially using glucose as a monomer precursor.[48,56,71,75-78,131-134] These glucose-based methodologies give exquisite synthetic control of the polymers produced, and allow for a vast range of thermal, physical, mechanical, and degradation properties. However, the synthesis of these polymeric materials can be challenging with significant purification steps being necessary, making them currently ill-suited to adoption in an industrial application. A robust synthetic methodology for a quinic acid-based monomer has been reported by our group, wherein alkenyl units were attached to quinic acid and this monomer then underwent a solvent-free photopolymerization with a range of thiol comonomers to produce poly(thioether-*co*-carbonate) thermoset networks.[132] This monomer synthesis and polymerization were highly scalable and allowed for the rapid generation of polymeric materials with tunable properties based on the thiol comonomer utilized in the polymerization. The scalability and tunability of this system made it extremely attractive for further examination as a translatable polymeric system, however the raw material cost of the quinic acid starting material is a significant disadvantage of the system.

In this work we set out to develop a rapidly producible, straight-forward, scalable synthetic methodology to synthesize a glucose-based functional monomeric platform for use in solvent free thiol-ene photopolymerizations. Further, we were aimed to alleviate some of the translational disadvantages of the previously reported systems by combining our work with glucose and quinic acid to generate alkene functionalized glucose monomers that were able to undergo photopolymerization with a range of thiol comonomers. The thermal and physical properties of the glucose-based poly(thioether-*co*-carbonate) networks were then examined and correlated to the choice of glucose monomer and thiol comonomer. Following this study two network formulations were chosen to examine the addition of different functional additives to increase the overall potential value of the networks. The thermal and physical properties of these networks were also examined to determine if there were any significant changes in the network properties caused by the additives.

5.2 Results and Discussion

This study was driven by a desire to build on the work completed by the Wooley laboratory on the development of polycarbonate containing materials from polyhydroxyl natural products. In an effort to make these networks more commercially accessible, a glucopyranoside derivative was chosen as the monomer source and a robust polymerization technique was used to produce poly(thioether-*co*-carbonate) networks. The effects of using a mixture of functionalized monomers, a range of different crosslinking comonomers, and functional additives on the network properties were also examined.

5.2.1 Monomer Synthesis

The glucose-based allyl monomers can be readily synthesized by the addition of allyl chloroformate (AC) to a commercially available glucopyranoside derivative, methyl α-D-glucopyranoside, with an amine base catalyst (Figure V.1). Glucopyranoside was chosen as the monomer source as the rigidity of the cyclic backbone unit was expected to increase the mechanical strength of the networks. In addition to the potential strength added to the final polymeric networks, the protection of the anomeric position of the saccharide ring also reduced the number of undesired side reactions during the functionalization reaction. The previously reported synthetic methodology used a significant excess (2 equivalents per hydroxyl) of AC to produce a single fully functionalized quinic acid-based monomer. To increase the atom economy of the reaction, lower equivalents of AC per hydroxyl were tested. Lower equivalents of AC were also examined to determine the effect of mixtures of differently functionalized glucopyranosides on the thermal and mechanical properties of the final polymer network. The success of this reaction (>95% yield) was confirmed by the appearance of signals for the alkene group in both the ^{1}H (6.00-5.84, 5.41-5.31, 5.30-5.20) and ^{13}C NMR (131.5-130.9, 119.5-118.7) spectra, as well as the carbonate signal in the ^{13}C NMR (156.1-152.6, Figures V.4, 5) spectrum. The high number of signals in the ^{1}H and ^{13}C NMR confirm the production of multiple differently substituted products observed by thin layer chromatography. The average alkene functionality of the allyl monomer was controllable by the equivalents of AC per hydroxyl used in the synthesis, eleven of the potential alkenyl monomer structures produced are shown in Figure V.6. When a "low" allyl functionality was targeted (3.5 equivalents of AC added per glucopyranoside, 0.87 equivalents per alcohol), 70% of the available AC reacted with the glucopyranoside to give an average functionality of 2.5 alkene units per glucopyranoside. As higher average

functionalities were targeted the percentage of AC that reacted with glucopyranoside decreased, to reach an average functionality of 3.6 alkenes per glucopyranoside 6 equivalents of AC, 1.5 equivalents per alcohol, were needed (60% of the ACs were reacted). This synthesis was also easily replicated on a larger scale (>100 mmol) with no loss of yield. The mixtures of allyl functionalized glucopyranoside were used without column purification in the production of polymeric networks.

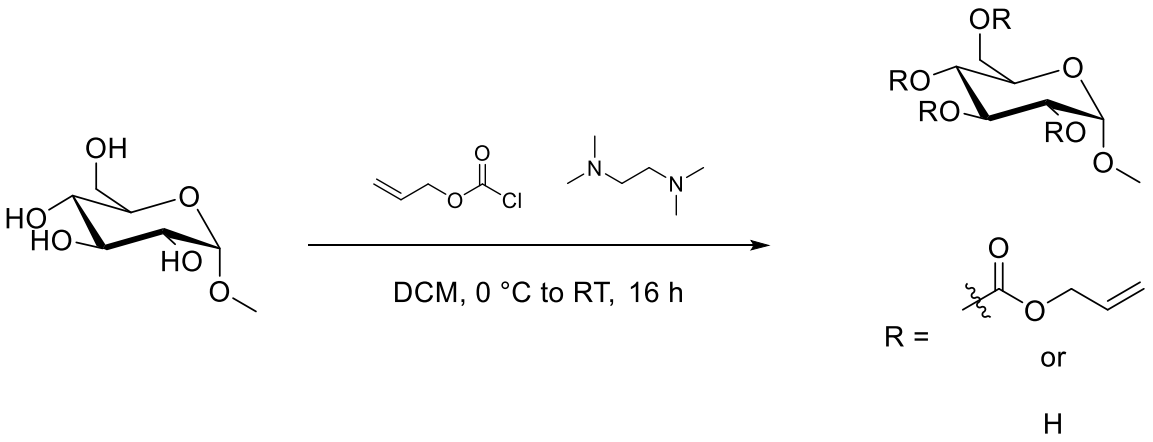

Figure V.1. General synthesis of allyl functionalized glucopyranoside monomers.

5.2.2 Generation of Poly(thioether-*co*-carbonate) Networks and their Thermal and Physical Properties

Polymeric networks were produced *via* a thiol-ene radical addition in a solvent-free crosslinking copolymerization of the alkene functionalized glucopyranoside monomers and various multifunctional thiol monomers. Allyl functionalized glucopyranosides were mixed with a range of multifunctional thiols (Figure V.2), based on a molar equivalence of functional groups (alkene to thiol) to produce homogeneous resins. Thiol comonomers included 1,2-ethane dithiol (EDT), 2,3-butanedithiol (BDT), 1,6-hexanedithiol (HDT), 1,4-

butanediol bis(mercaptoacetate) (BDBMA), tetraethylene glycol bis(3-mercaptoproprionate) (TEGBMP), trimethylolpropanyl tris(3-mercaptopropionate) (TMPTMP), pentaerythritol tetrakis(3-mercaptopropionate) (PETMP), and dipentaerythritol hexakis(3-mercaptoproprionate) (DPEHMP). A radical initiator, 2,2-dimethoxy-2-phenylacetophenone (DMPA, 1 wt%), was then added to the resin which was cast into a mold making various geometries possible (Figures V.3, 6). Crosslinking/polymerization was initiated through exposure to UV irradiation to produce uniform bulk materials, although heat can be explored in future studies. These materials were then postcured at 120 ˚C for at least 4 h to vulcanize any remaining thiol groups.

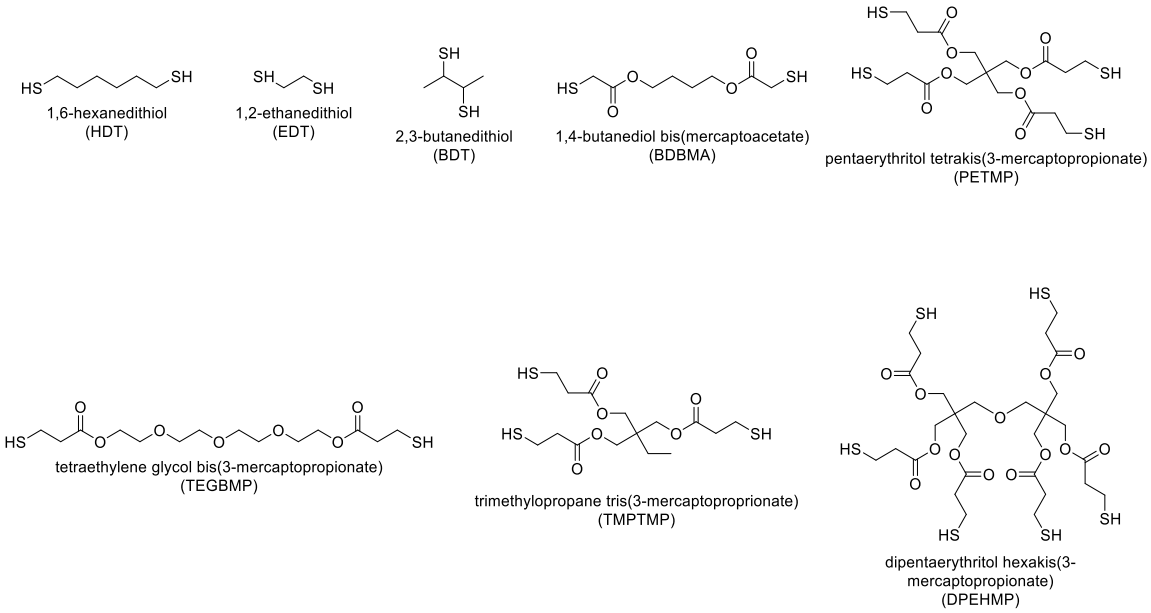

Figure V.2. Thiol comonomers utilized in the productions of polymeric networks.

The properties of the bulk materials were modulated by varying the comonomer formulations used in the photopolymerization. For example, the number of allyl

functionalities on the glucopyranoside monomer, as well as the length and rigidity of the thiol comonomer, affected the crosslink density of the final materials. The thermal and physical properties were examined by thermogravimetric analysis (TGA), differential scanning calorimetry (DSC), and dynamic mechanical analysis (DMA) (Table V.1, Figures V.7, 8, 10-13). All of the networks produced gave good thermal stabilities (>280 °C), with the thermal stability increasing slightly (<20 °C) when the glucose comonomer had higher amounts of allyl functionality. This increase in T_d correlates with an increase in the crosslinking density of the networks as each glucose unit is covalently bound to more of the surrounding network. By varying the thiol comonomer and the degree of functionality of the glucose comonomer materials, a wide range of glass transition temperatures (T_gs) spanning over 75 °C were achieved. When examining material made with the same thiol comonomer and different glucose comonomers, the change in T_g follows a similar trend as T_d wherein as the alkene character of the glucose comonomer increased the T_g also generally increased. However, to achieve significant differences in the T_gs varying the thiol comonomer was significantly more effective.

The thiol structure correlated to the T_gs achieved in the final network, materials synthesized with EDT, PETMP, and DPEHMP gave materials with the highest T_gs. Chemically these T_gs, trends correlated to increased crosslinking density for the PETMP and DPEHMP-based networks, whereas in the EDT-based networks their T_gs were high because these networks had the highest weight fraction of the rigid cyclic glucose comonomer in the final networks. Networks synthesized with thiols containing longer more flexible spacers between the thiols, TEGBMP and BDBMA, achieved much lower T_gs because of the increased free volume caused by the additional flexibility between crosslinks. The storage

moduli (*E*') for the different networks were measured at 5 and 25 °C, and the values determined followed the same general trend as the T_g analysis wherein more flexible thiols gave networks with lower *E*'s and the more rigid comonomers gave higher *E*'s, with the system being able to achieve *E*' into the tens of MPa. As expected for the networks with T_g below 25 °C there was a 1-20 MPa change in the *E*' at 5 *vs*. 25 °C as the networks had undergone a switch from glassy to rubbery, whereas the networks with T_g above 25 °C gave negligible changes in their *E*' at the temperatures examined. Networks were also made using glucose comonomers with similar levels of allyl functionalities from different monomer syntheses and TEGBMP thiol comonomer to probe the reproducibility of the network generation. The thermal transitions and moduli measured were similar (Table V.3), demonstrating the reliability of the network production.

Table V.1. Thermal transition data and moduli exhibited by the poly(thioether-*co*-carbonate) networks. For the glucose monomers low allyl has average functionalities of 2.5 while high allyl has average functionalities of 3.6 allyl groups per glucopyranoside.

Comonomer	Number of Thiols	Glucose Monomer	$T_{d,\ onset}$ (˚C)	T_g (˚C)	*E*' at 5 ˚C (MPa)	*E*' at 25 ˚C (MPa)
EDT	2	Low allyl	287	35	25.8 ± 1.5	24.1 ± 2.0
		High allyl	295	45	17.4 ± 2.7	17.1 ± 2.7
BDT	2	Low allyl	290	29	32.2 ± 4.0	30.8 ± 3.8
		High allyl	298	32	19.4 ± 0.97	17.6 ± 0.57
HDT	2	Low allyl	310	-	-	-
		High allyl	318	29	20.2 ± 1.6	19.1 ± 1.0
BDBMA	2	Low allyl	315	2	21.6 ± 12.7	5.44 ± 4.32
		High allyl	325	1	37.8 ± 1.6	2.87 ±1.4
TEGBMP	2	Low allyl	304	-11	2.84 ± 2.5	0.482 ± 0.0069
		High allyl	320	-17	1.17 ± 1.1	0.387 ± 0.0019
TMPTMP	3	Low allyl	310	35	28.0 ± 6.3	26.4 ±6.0
		High allyl	312	32	24.2 ± 9.4	23.4 ± 8.4
PETMP	4	Low allyl	301	51	15.0 ± 1.0	14.8 ± 1.0
		High allyl	313	51	18.8 ± 2.4	18.3 ± 2.3
DPEHMP	6	Low allyl	279	33	13.9 ± 1.1	13.6 ± 1.2
		High allyl	309	58	13.2 ± 1.5	11.5 ± 0.87

5.2.3 Addition of Functional Additives to Poly(thioether-*co*-carbonate) Networks

To further tune the characteristics of the networks a range of functional additives can be introduced into the resins prior to crosslinking to produce composite materials with various mechanical, physical, and aesthetic properties. As the properties did not vary significantly with different degrees of allyl functionalities, the more efficiently synthesized glucose monomer with lower allyl functionality was examined with EDT and TEGBMP as thiol comonomers. These thiols were chosen as they had similar degrees of functionality and gave networks with the high and low thermal transitions and moduli. Three additives with different desired properties were chosen – a glitter and a dye were chosen as aesthetic

modifiers, an oil-based scent was also chosen. In these experiments a single resin was generated and was then divided into different samples to ensure the differences in the properties measured were caused by the additives, rather than different comonomer ratios. Following the addition of the additives to the resin, DMPA was then added to the resin which was cast into a mold making various geometries possible. Crosslinking/polymerization was initiated through exposure to UV irradiation (365 nm) to produce uniform bulk materials. These materials were then postcured at 120 ˚C for at least 4 h to vulcanize any remaining thiol groups (Figure V.3)

The thermal and physical properties of the networks with functional additives were examined by TGA, DSC, DMA (Table V.2, Figures V.9, 14, 15). The additives were added in small quantities to ensure that they were <5 wt% of the total network, therefore the properties of the network were not expected to vary significantly, although the overall potential value of the network was increased. The T_ds and T_gs of both network types did not vary significantly with the addition of the various additives, as the majority of the network remained as the poly(thioether-*co*-carbonate). There were slight variations in the moduli measured for the networks with the different additives, although the changes observed were not consistent across the different resin formulations. In the TEGBMP-based networks no significant differences were seen in the moduli values for any resin or additive mixture with each value being within the experimental error, except for the *E*' at 25 °C for the network with glitter. The *E*' at room temperature for the glitter containing network was lower than the other networks, this may have been caused by the creation of macroscopic separation in the networks as the resin was unable to penetrate the glitter flake. In the EDT-based networks there were significant differences in the moduli values for the different additives,

however as the T_g of that resin is above 25 °C temperature did not have an effect on the *E*' at the values examined. The EDT formulation containing scent gave an almost 5 MPa decrease in the *E*' measured, we hypothesize this was caused by poor solubility of the scent within the polymer resin. Following the post cure step for that formulation, a layer of oil-sheen was visible on the outside of the sample, this migration of the oil may have created an internal pore structure that reduced the *E*' of the material, although there were no visible air bubbles in the sample. In contrast the dye containing formulation had a 4 MPa increase in its *E*'.

Table V.2. Thermal transition data and moduli exhibited by the poly(thioether-*co*-carbonate) networks with functional additives.

System	Additive	$T_{d,\ onset}$ (˚C)	T_g (˚C)	*E*' at 5 ˚C[a] (MPa)	*E*' at 25 ˚C (MPa)
Low allyl-*co*- EDT	None	286	41	12.0 ± 0.25	11.7 ± 0.34
	Dye	284	36	16.2 ± 0.96	15.6 ± 0.67
	Scent	285	35	7.14 ± 0.31	7.10 ± 0.048
	Glitter	287	37	-[b]	-[b]
	All Three	288	34	17.5 ± 0.84	16.4 ± 0.65
Low allyl-*co*- TEGBMP	None	309	-12	1.41 ± 1.4	0.307 ± 0.025
	Dye	307	-13	1.68 ± 1.4	0.331 ± 0.021
	Scent	320	-13	1.63 ± 1.4	0.372 ± 0.010
	Glitter	324	-10	2.46 ± 2.4	0.243 ± 0.011
	All Three	321	-15	1.83 ± 1.7	0.320 ± 0.020

[a]Modulus values at 5 ˚C for low allyl-*co*-TEGBMP varied widely based on the starting temperature of the measurements, resulting in the large observed error. [b]During the curing process the glitter did not remain suspended in the resin and formed a mostly separated layer at the bottom of the mold.

Figure V.3. Image of poly(thioether-*co*-carbonate) networks with various functional additives.

5.3 Experimental Section

5.3.1 Materials

All materials were purchased from VWR, Sigma-Aldrich, or Wako Chemical. Unless noted, all reagents were used as received. Dichloromethane (DCM) was purified and dried by a solvent purification system (J. C. Meyer Solvent System).

5.3.2 Instrumentation

^{1}H and ^{13}C NMR spectra were recorded on an Inova500 spectrometer, chemical shifts were referenced to the resonance signals of the deuterated solvent.

Glass transition temperatures were measured by differential scanning calorimetry with a Mettler-Toledo DSC822^{e} under N_2, as the midpoint of the inflection tangent on the third heating scan, with a 10 °C/min heating and cooling rate. Measurements were analyzed using Mettler-Toledo Star^{e} v.10.00 software.

Thermogravimetric analysis (TGA) was performed under an Ar atmosphere using a Mettler-Toledo model TGA/DSC 1, with a heating rate of 10 °C/min. Measurements were analyzed using Mettler-Toledo Star^{e} v.10.00 software.

Moduli values were measured on a TT-DMA dynamic mechanical analyzer from Triton Laboratories with a heating rate of 3 °C/min.

5.3.3 Synthesis

General Procedure for the Synthesis of allyl functionalized glucopyranosides. This example includes reagent amounts for the preparation of the "low" allyl functionality monomer. A solution of methyl α-D-glucopyranoside (20.0085 g, 103.0 mmol) and tetramethylethylenediamine (70.0 mL, 467 mmol) in anhydrous dichloromethane (135 mL) was cooled to 0 °C. Allyl chloroformate (39.0 mL, 367 mmol), in 43 mL of anhydrous DCM, was added dropwise to the glucopyranoside solution. The reaction was allowed to warm to room temperature over 16 hours. The reaction mixture was then filtered to remove any precipitates, the filtrate was diluted with additional DCM and was washed with a saturated sodium bicarbonate, 5% HCl aqueous solution, and deionized water. The organic layer was then dried with sodium sulfate and concentrated to yield a mixture of differently protected glucopyranosides (43.81 g, 2.4 average allyl groups per glucopyranoside).

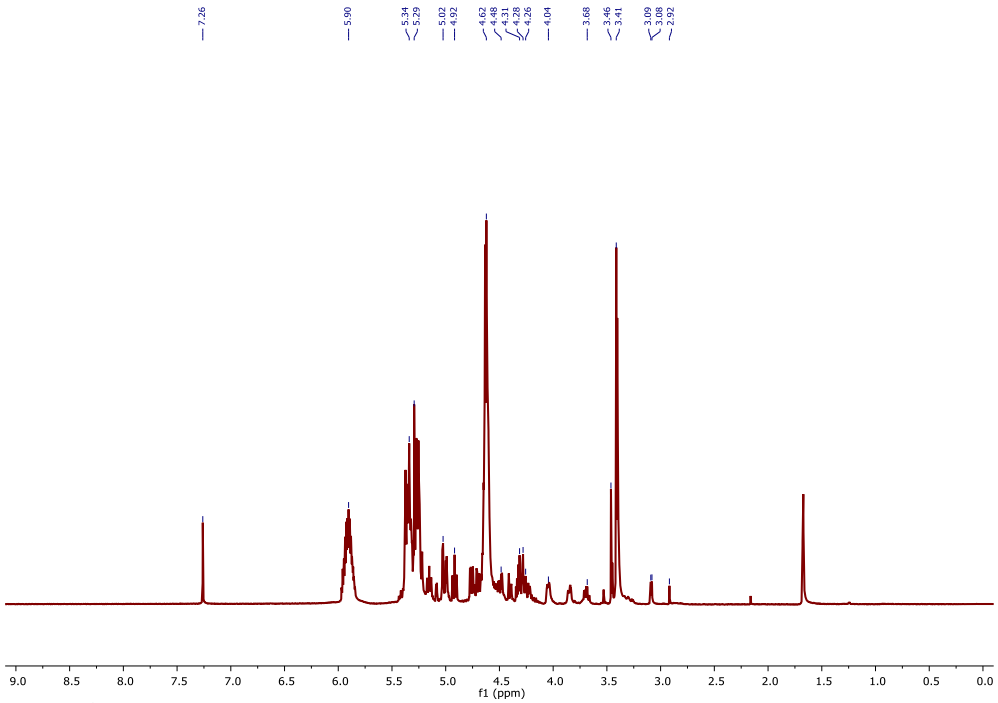

Figure V.4. ^{1}H NMR (500 MHz) spectrum of the high allyl glucopyranoside monomer in $CDCl_3$.

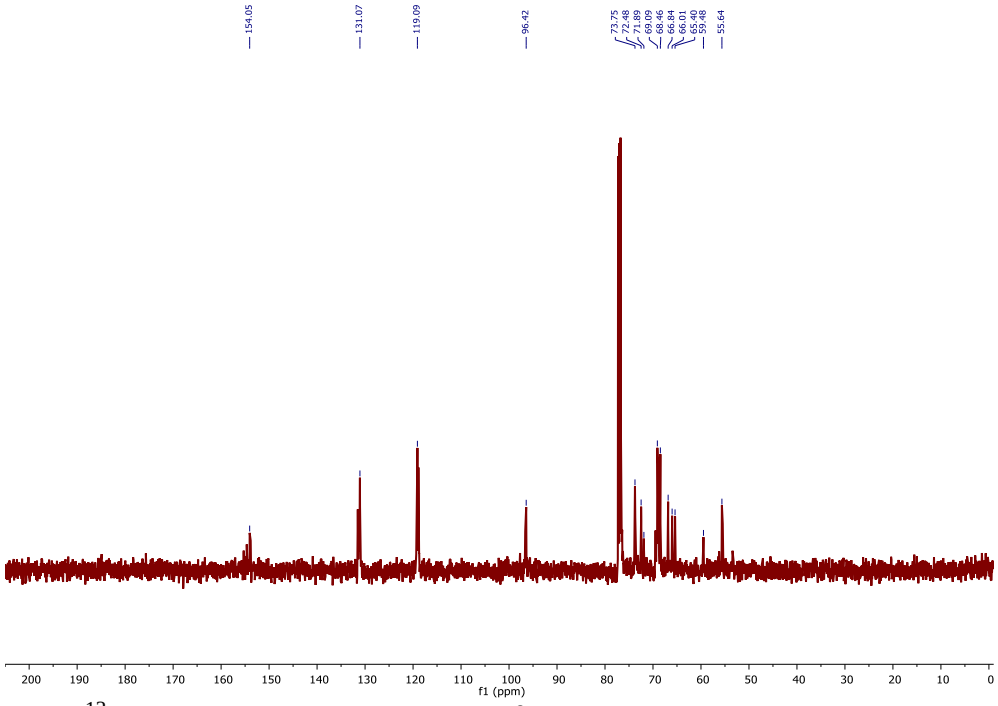

Figure V.5. ^{13}C NMR (125 MHz) spectrum of the high allyl glucopyranoside monomer in $CDCl_3$.

General procedure for fabricating thiol-glucopyranoside networks. In a vial, allyl glucopyranoside monomer and the desired thiol (1:1 alkene:thiol) were mixed by sonication/vortexing until a homogeneous mixture was achieved, any desired additives can be incorporated at this reaction step. The radical initiator, 2,2-dimethoxy-2-phenylacetophenone (1 wt%), was added and mixed into the resin by sonication/vortexing. The resins were loaded into two molds, one pellet and one thin film, and exposed to UV light (365 nm) for 1 minute per side. The materials were post-cured at 120 ˚C overnight to remove any remaining thiols.

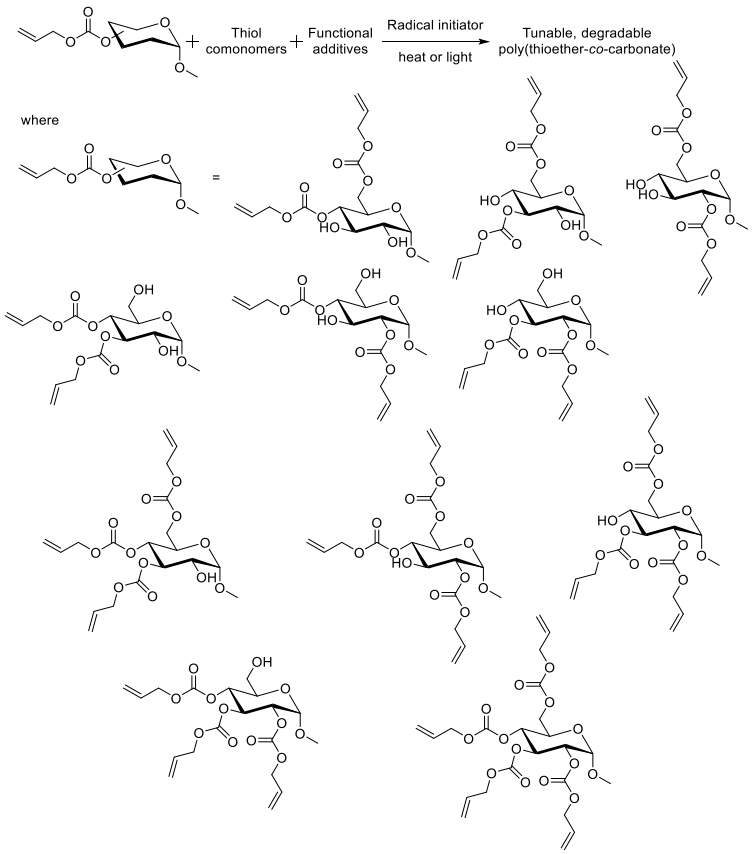

Figure V.6. General scheme for the synthesis of poly(thioether-*co*-carbonate networks and the inclusion of functional additives (top). Possible different glucose monomers present in the mixtures used in the polymerizations (bottom).

5.4 Conclusions

The development of bulk polymeric materials from naturally-derived chemicals is of significant academic and industrial interest. Towards this end, a robust scalable synthesis was developed to produce a glucose-based monomer with side chains containing both carbonate and allyl functionalities. The carbonate linkages were incorporated to allow for the eventual chemical degradation of the networks, while the alkenes were incorporated to allow for the rapid generation of poly(thioether-*co*-carbonate) networks. The glucose-based monomer was mixed with a variety of different thiol comonomers to produce polymeric networks with a range of thermal and physical properties. The various networks were able to span T_gs from -17 to 58 °C, and achieve E's from 0.4 to 30 MPa, with the properties of the network being controlled by the comonomers chosen. More rigid thiol comonomers gave materials with higher T_gs and E', and the glucose monomers with higher alkene functionality demonstrated the same trend. The addition of functional additives to the networks during formation was also examined and the functional additives were found to generally have no significant effect on the thermal and physical properties of the networks formed. Studies involving different carbohydrate starting materials and naturally-sourced thiol comonomers are currently ongoing to determine effects of different carbohydrates on the monomer synthesis, subsequent polymerization, and the properties that can be achieved by the networks.

5.5 Supplemental Information

Table V.3. Thermal transition data and moduli exhibited by the low allyl-*co*-TEGBMP system with glucopyranoside monomers from different batches.

Monomer	$T_{d,\ onset}$ (˚C)	T_g (˚C)	E' at 5 ˚C[a] (MPa)	E' at 25 ˚C (MPa)
Original batch (2.5 avg. functionality)	309	-12	1.41 ± 1.4	0.307 ± 0.025
New batch (2.4 avg. functionality)	300	-21	0.868 ± 0.65	0.208 ± 0.004

[a]Moduli values at 5 ˚C for low allyl-*co*-TEGBMP varied widely based on the starting temperature of the measurements, resulting in the large observed error.

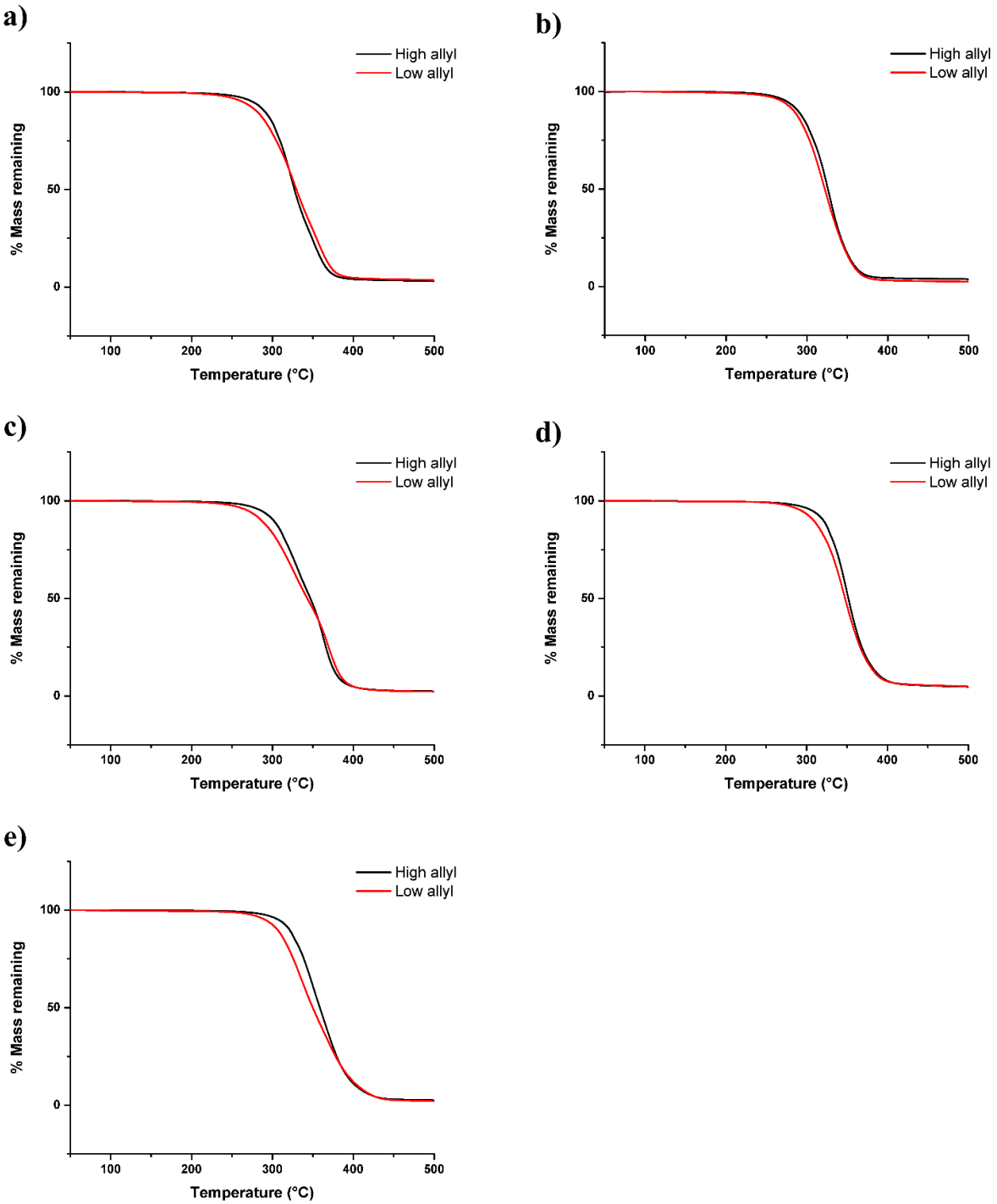

Figure V.7. Thermogravimetric analysis traces of networks synthesized with the high allyl (black) or low allyl (red) glucose monomer and difunctional thiol comonomers EDT (a), BDT (b), HDT (c), BDBMA (d), or TEGBMP (e).

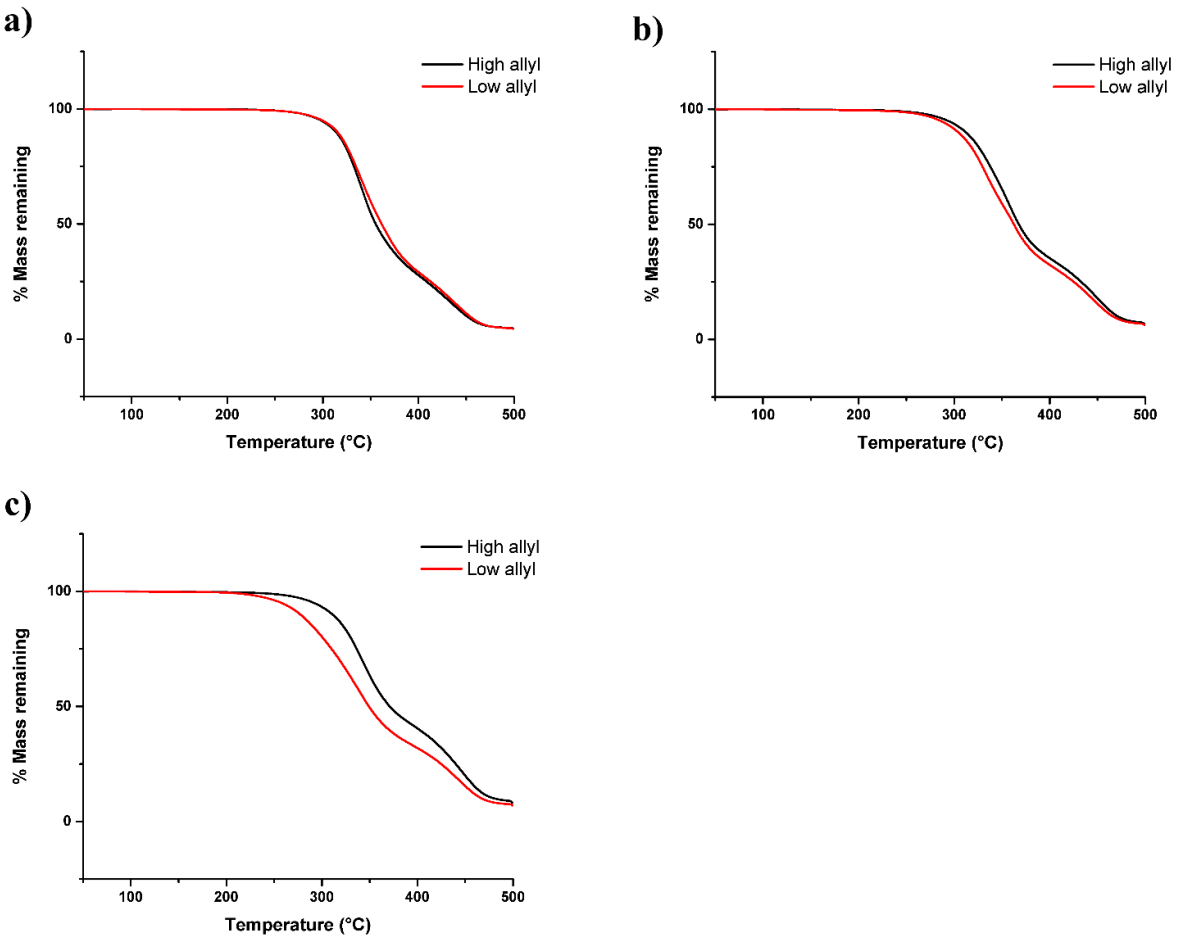

Figure V.8. Thermogravimetric analysis traces of networks synthesized with the high allyl (black) or low allyl (red) glucose monomer and multifunctional thiol comonomers TMPTMP (a), PETMP (b), or DPEHMP (c).

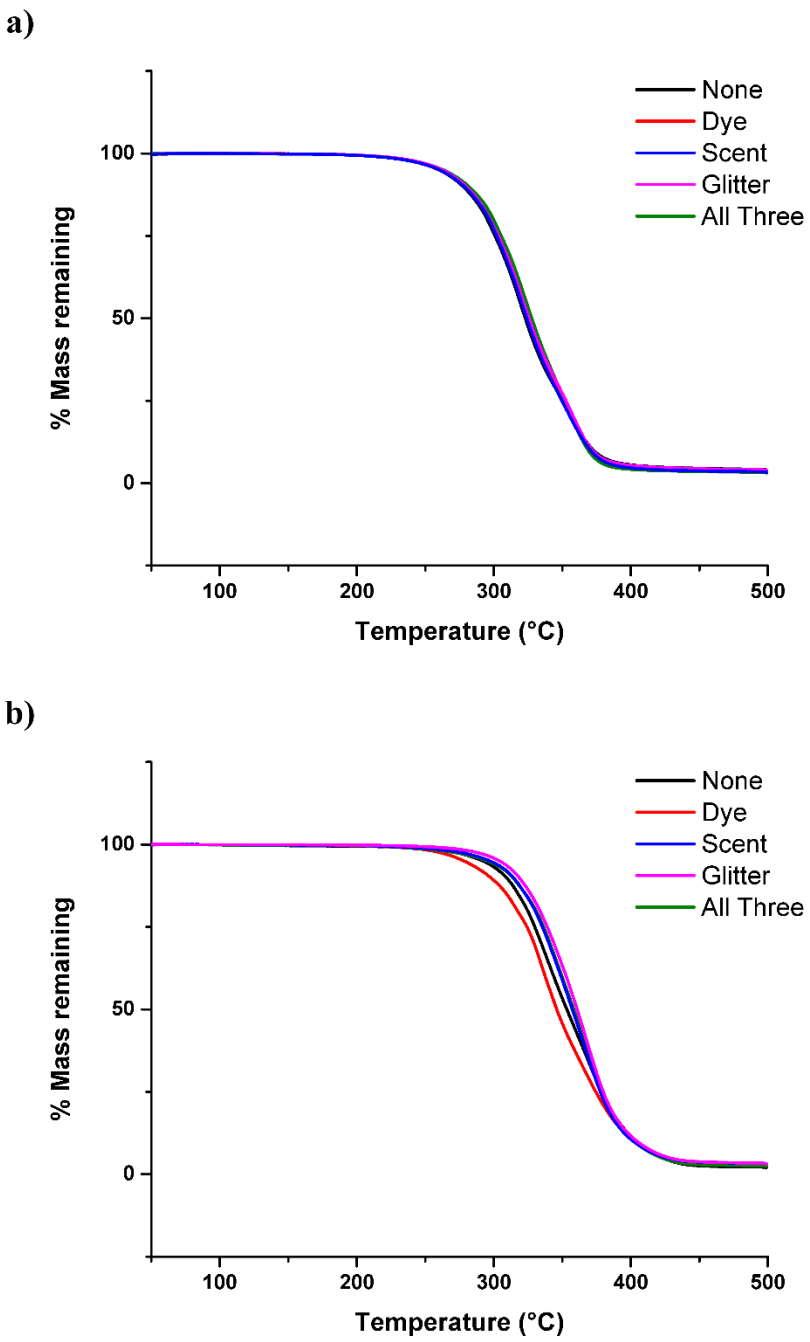

Figure V.9. Thermogravimetric analysis traces of networks synthesized with the low allyl glucose monomer and difunctional thiol comonomers EDT (a) or TEGBMP (b) with functional additives. Networks with no additives (black), dye (red), scent (blue), glitter (pink), or a combination of dye, scent, and glitter (green).

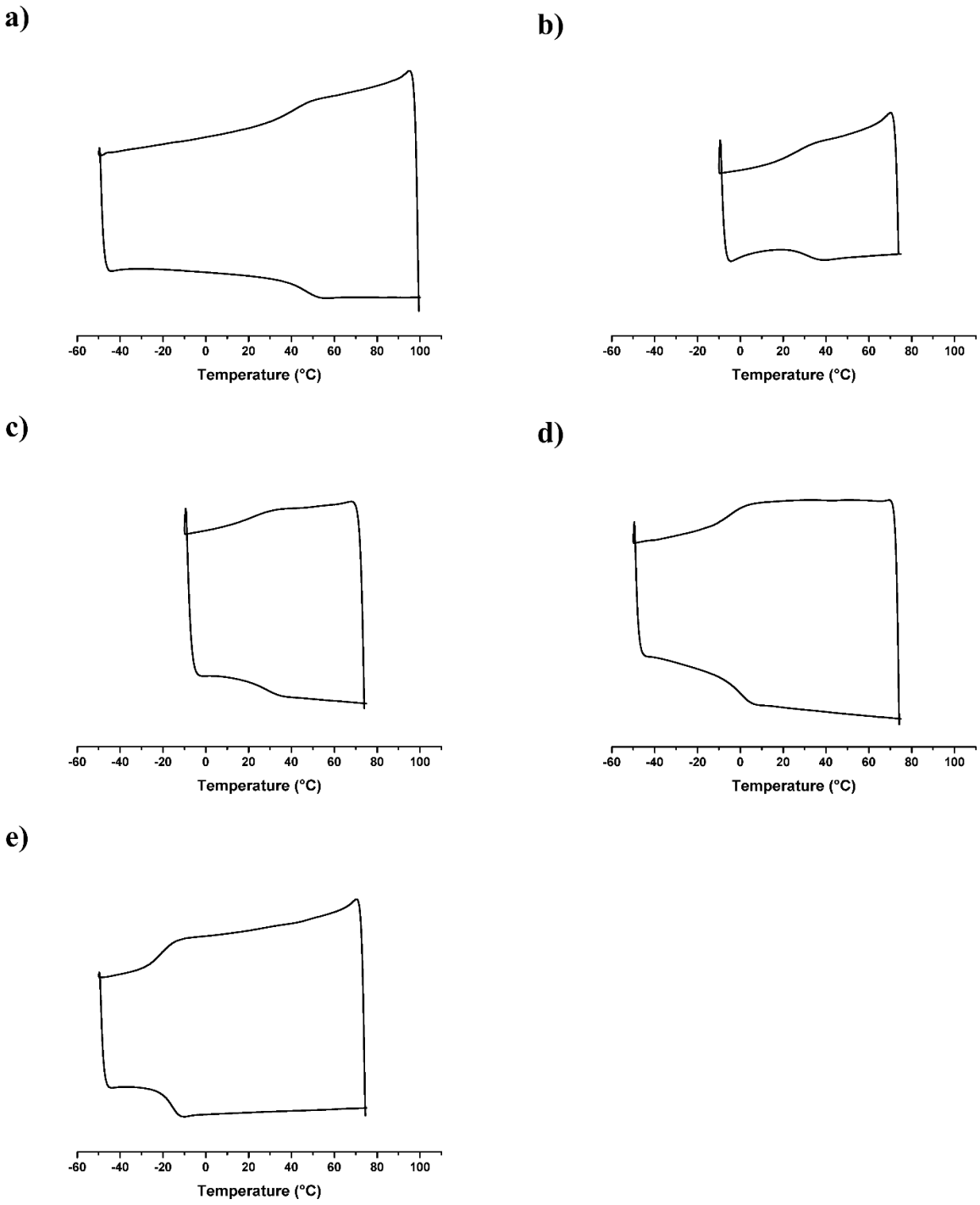

Figure V.10. Differential scanning calorimetry of networks synthesized with the high allyl glucose monomer and difunctional thiol comonomers EDT (a), BDT (b), HDT (c), BDBMA (d), or TEGBMP (e). The heating traces are on the bottom and the cooling traces on the top.

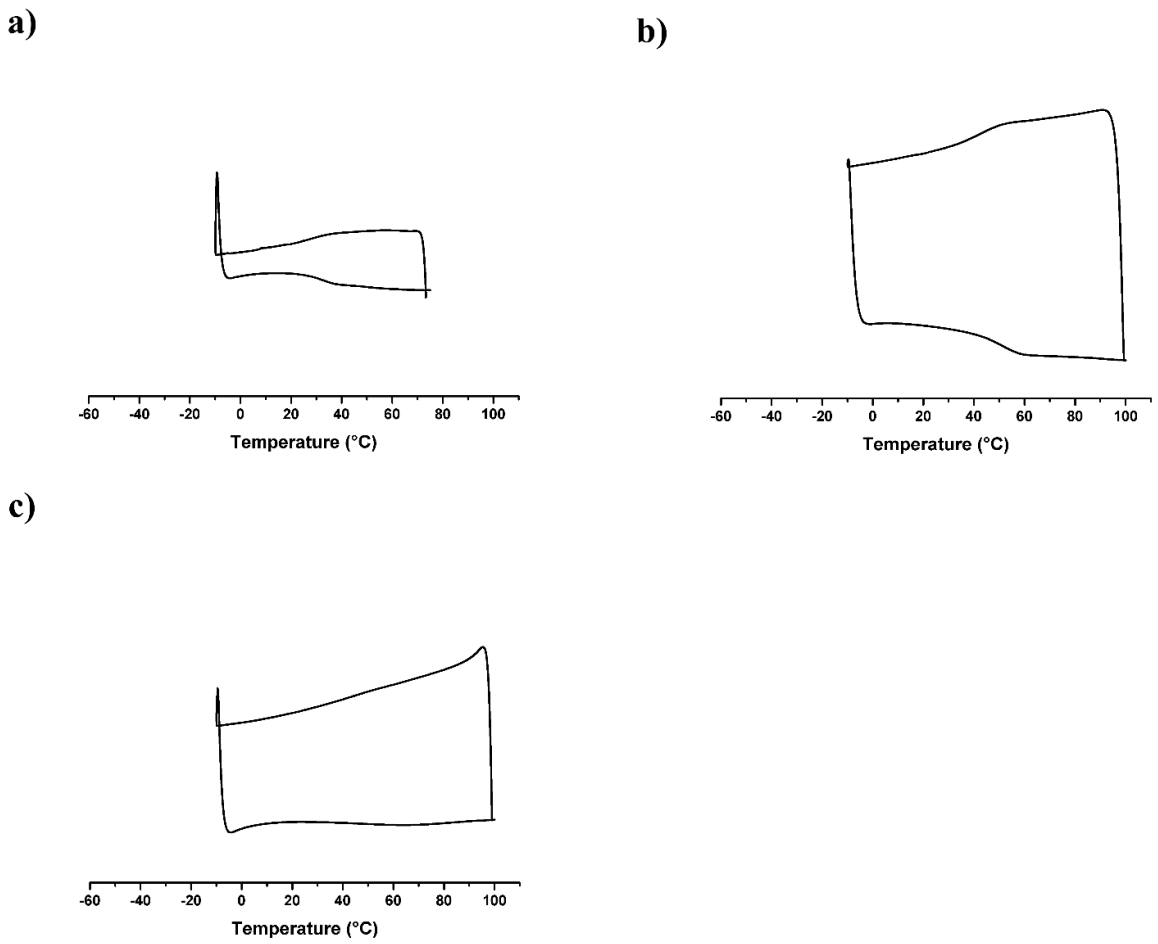

Figure V.11. Differential scanning calorimetry of networks synthesized with the high allyl glucose monomer and multifunctional thiol comonomers TMPTMP (a), PETMP (b), or DPEHMP (c). The heating traces are on the bottom and the cooling traces on the top.

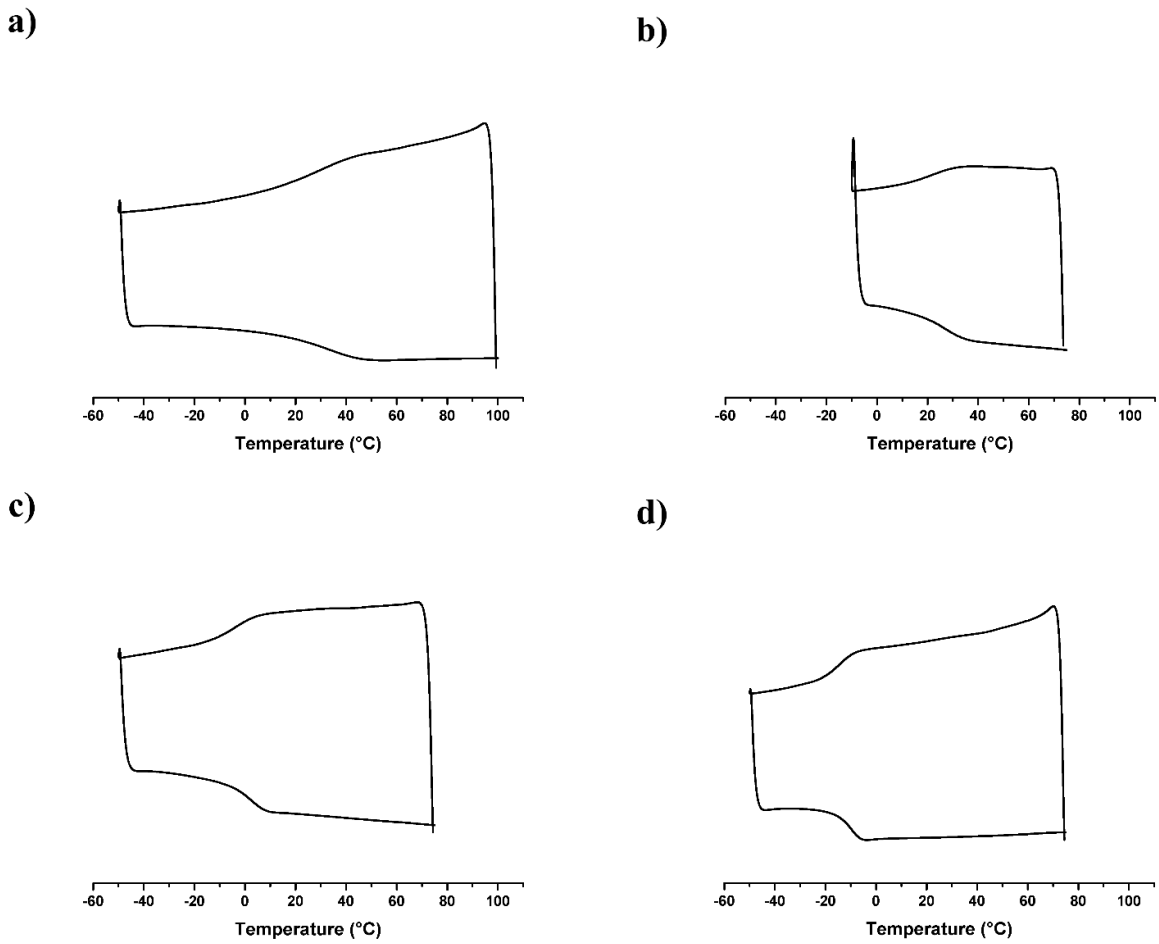

Figure V.12. Differential scanning calorimetry of networks synthesized with the low allyl glucose monomer and difunctional thiol comonomers EDT (a), BDT (b), BDBMA (c), or TEGBMP (d). The heating traces are on the bottom and the cooling traces on the top.

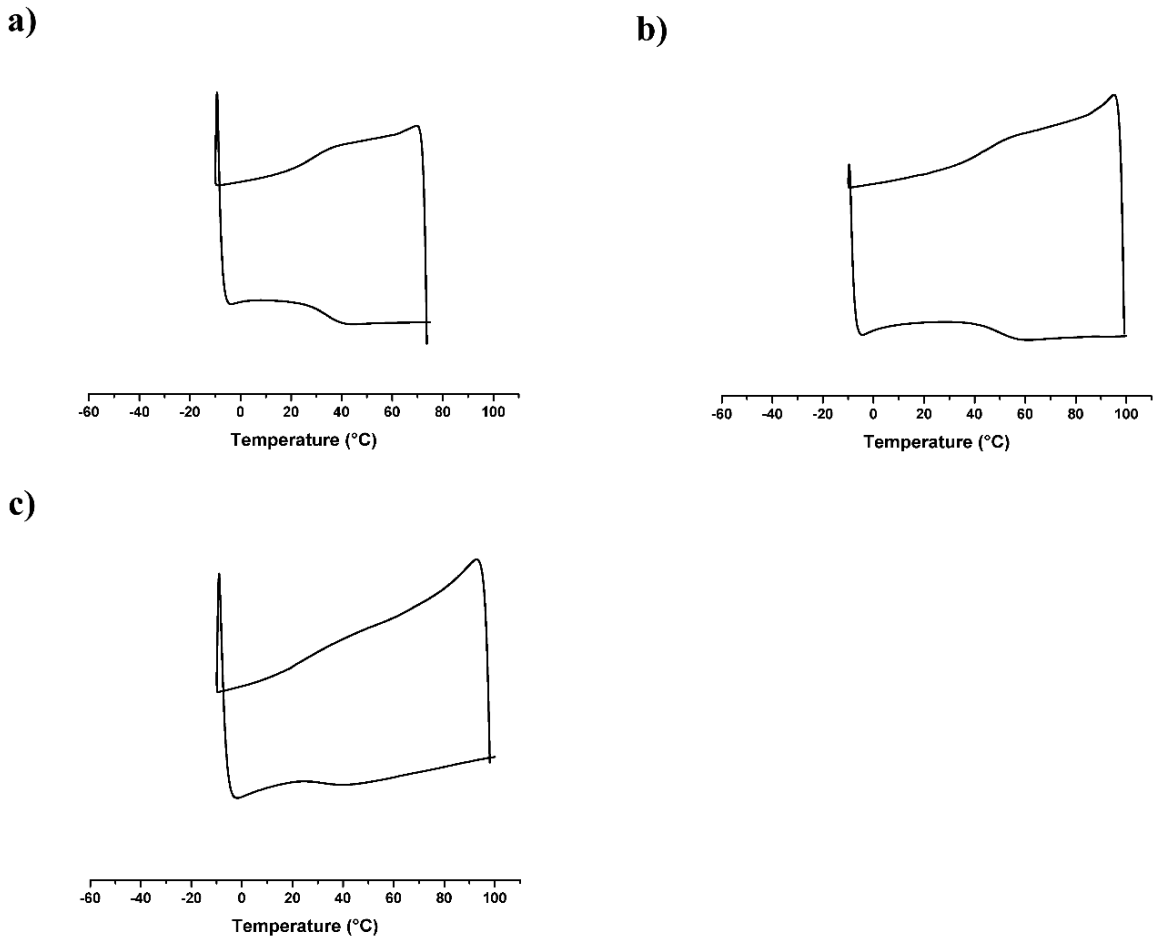

Figure V.13. Differential scanning calorimetry of networks synthesized with the low allyl glucose monomer and multifunctional thiol comonomers TMPTMP (a), PETMP (b), or DPEHMP (c). The heating traces are on the bottom and the cooling traces on the top.

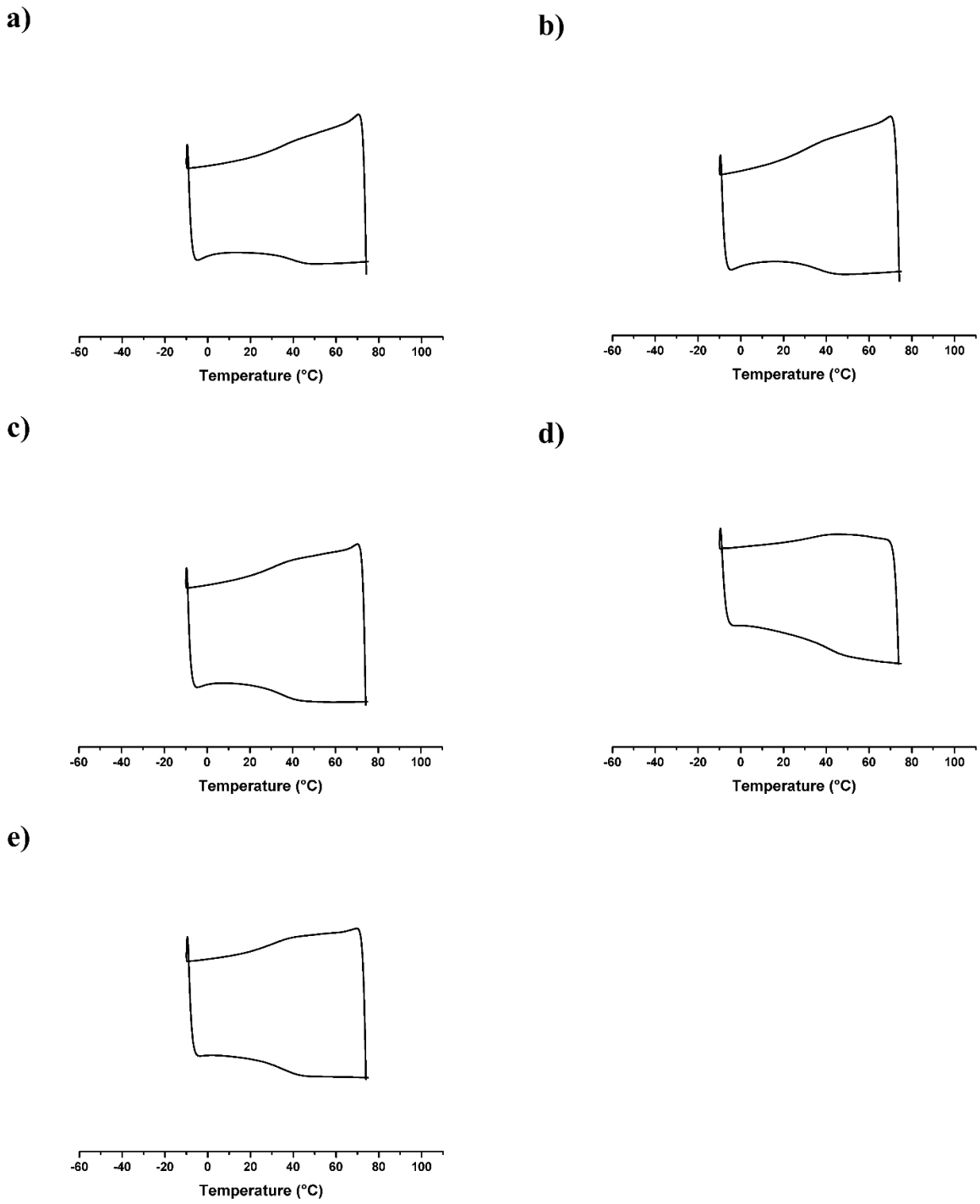

Figure V.14. Differential scanning calorimetry of networks synthesized with the low allyl glucose monomer and difunctional thiol comonomer EDT thiol comonomers and functional additives. Networks with no additives (a), dye (b), scent (c), glitter (d), or a combination of dye, scent, and glitter (e). The heating traces are on the bottom and the cooling traces on the top.

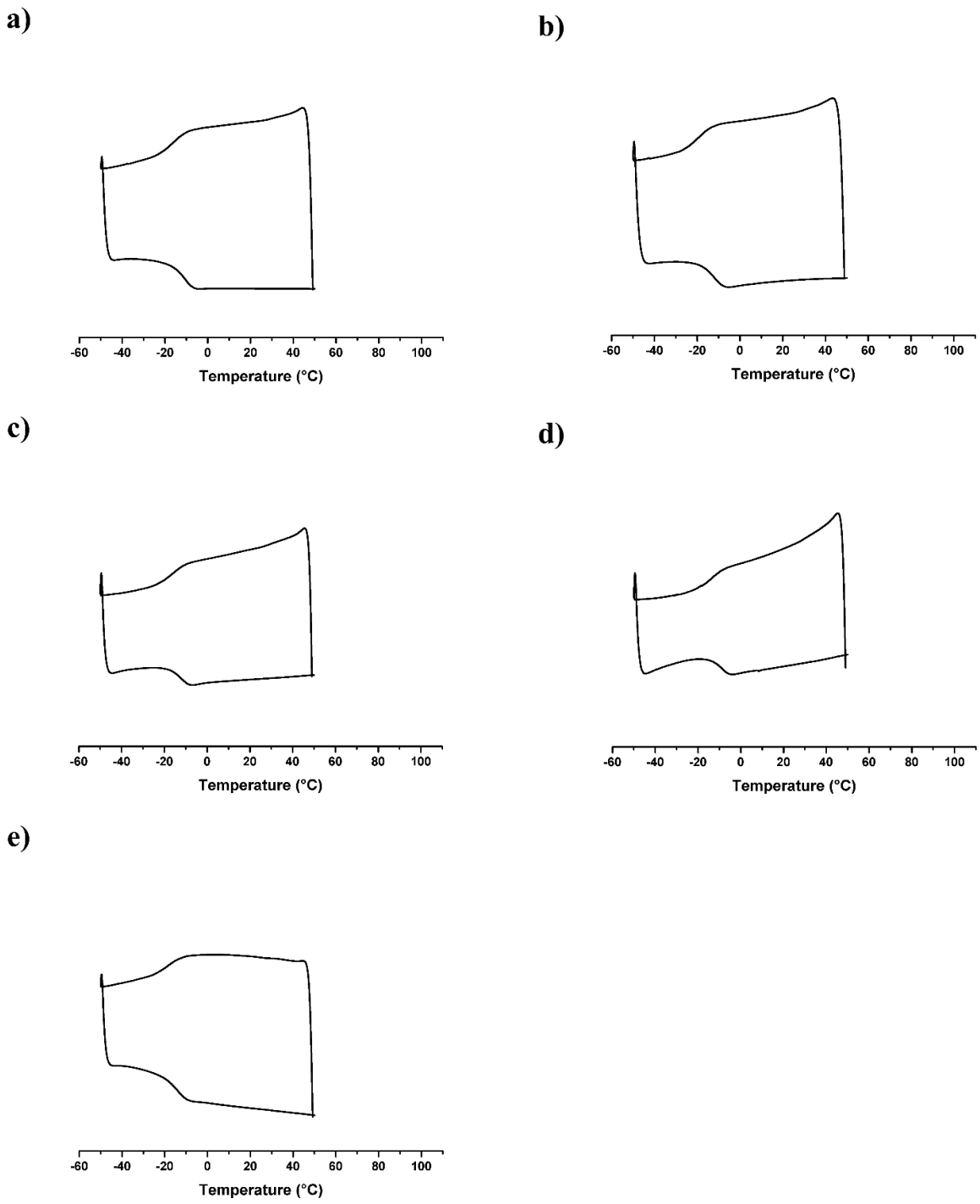

Figure V.15. Differential scanning calorimetry of networks synthesized with the low allyl glucose monomer and difunctional thiol comonomer TEGBMP thiol comonomers and functional additives. Networks with no additives (a), dye (b), scent (c), glitter (d), or a combination of dye, scent, and glitter (e). The heating traces are on the bottom and the cooling traces on the top.

CHAPTER VI

CONCLUSIONS AND FUTURE WORK

6.1 Conclusions

This dissertation has presented the design, synthesis, and characterization of a range of glucose-derived polycarbonates for biomedical and engineering applications. Glucose as the main component of cellulose, is of keen interest as a renewable resource to produce polymeric materials. This work has laid a foundation for the production of varied glucose-based polymers with different functionalities, properties, and architectures. Polymer properties were controlled through the design of the monomer by the incorporation of various chemical functionalities or by the optimization of synthetic conditions employed in the polymer synthesis or post-polymerization reaction.

Chapter II focused on the synthesis of a series of glucose-based polycarbonates, from a single monomer, methyl 4,6-*O*-benzylidene-2,3-*O*-carbonyl-α-D-glucopyranoside (MBGC). Straightforward conditions for the polymerization of 5-membered cyclic carbonates were developed and a series of PMBGCs were synthesized. These PMBGCs underwent two post-polymerization functionalizations to produce hydroxyl or acetyl side chain bearing polymers. The properties of these various polymers were tunable based on the molar mass and repeat unit composition. A wide range of thermal decomposition temperatures (233-347 °C), glass transition temperatures (87-233 °C), and water contact angles (38-128 °) was achieved by this series of polymers. The hydrolytic degradability of these polymers was also examined, demonstrating differing degradation mechanisms and

kinetics based on the acidic vs. basic conditions used. Consequently, these natural product-derived versatile materials give access to a wide range of thermophysical properties through a robust polymerization technique and simple post-polymerization modifications.

In Chapter III, MBGC was further utilized to synthesize amphiphilic copolymers and block copolymers. Organocatalyzed ROP was utilized with 4-methylbenzyl alcohol and methoxy poly(ethylene glycol) as initiator and macroinitiator, to afford glucose-based copolymers. To vary the hydrophilic-hydrophobic ratios of these polymers acidic benzylidene cleavage reactions were performed to deprotect the sugar repeat units and present hydrophilic hydroxyl side chain groups. Assembly of the polymers under aqueous conditions revealed interesting morphological differences, based on the polymer molar mass and repeat unit composition. The initial polymers, prior to the removal of the benzylidenes, underwent a morphological change from micelles to vesicles as the sugar block length was increased, causing a decrease in the hydrophilic-hydrophobic ratio. Deprotection of the sugar block increased the hydrophilicity and gave micellar morphologies. This tunable polymeric platform holds promise for the production of advanced materials for implementation in a diverse range of applications

Chapter IV explored the development of a multifunctional carbonate monomer, methyl 2,3:4,6-di-*O*-carbonyl-α-D-glucopyranoside (MGDC), for the synthesis of complex polymeric architectures *via* ROP. The homopolymerization and copolymerization of MGDC was investigated with a range of organocatalysts to control the openings of the two cyclic carbonates of MGDC to produce polymers with different percentages of branching along the polymeric backbones. These results provide an outlook to the synthesis of polymeric architectures that can mimic the branching of natural polysaccharides, and

therefore allow for future studies utilizing the multivalent characteristics of polysaccharide bioactivities.

In Chapter V, thermosets were synthesized using alkene and carbonyl functionalized glucose monomers with multifunctional thiol comonomers in thiol-ene photopolymerizations. The synthesis of the glucose monomers was designed to allow for a mixture of differently functionalized monomers to be used in the photopolymerization reducing the number of synthetic steps needed to produce the functional polymers. The thermomechanical properties of the materials could be tuned by the comonomers used in the polymerization to give access to a wide range of T_gs (-17 to 58 °C) and E's (0.4 to 30 MPa). These results demonstrated that future use in a range of applications is feasible given the straightforward synthetic methodology and solvent-free polymerization technique employed.

6.2 Future Work

There is significant future potential for new monomers and polymers derived from saccharides and the subset of work completed here with glucose has new avenues of research to undertake. Future work on these polymeric systems should and will include developing a deeper understanding of the polymers and methodologies already developed and exploring new specific applications in which they may have potential. There are also other polymer types and polymerization methods that glucose is highly amenable to for future studies.

The cyclic carbonate monomers discussed in this dissertation were all synthesized using phosgene derivatives to establish the carbonate moiety. Phosgene and its derivatives have severe hazards associated with their use and storage. For this dissertation triphosgene,

a solid, was used in place of gaseous phosgene to mitigate the hazards as much as possible, but stringent chemical hygiene protocols are still necessary to ensure its safe usage. Replacing phosgene-based carbonylation chemistries with non-toxic reagents would allow for more straightforward reaction safeties, and also follows the principles of renewable and green chemistries. In the past few years there have been exciting new synthetic methods developed that allow for the direct usage of CO_2 as a carbonylation reagent to produce cyclic carbonates, or polycarbonates *via* condensation polymerizations. There is also significant potential in the production of glucose-based polycarbonates through the copolymerization of CO_2 and an epoxide. New synthetic methodologies are needed to develop monomers that can be polymerized using these alternative carbonylation agents, but they hold significant promise for more renewable syntheses using natural product starting materials. Further, in future studies undertaken towards the use of these polymeric materials in a biocompatible application, controls and comparisons to known biomaterials are needed. Especially in degradation and mechanical analyses, commercially available materials, such as PLA and PLGA, should be used as controls to provide a more complete understanding of the properties of these novel materials relative to the current state-of-the-art.

In the characterization of the PMBGCs produced for Chapter II unexpected and intriguing results were generated. While examining the toxicity of the polymers it was noted that thin films generated from the PMBGCs appeared to be antibiofouling (Figure VI.1), with cells settling readily in defects of the films. PMBGC has a very high T_g based on its rigid bicyclic repeat unit, and this high T_g causes significant drying patterns to form in the thin films produced. Attempts were made to optimize the solvent casting of PMBGC films, and the defects could be reduced, but were never fully eliminated. Additionally, blends of

PMBGC with other biocompatible polymers was attempted but had similar challenges with film defects. Further study is needed to allow for the production of homogeneous films, these materials would have significant potential in biomedical applications. The block copolymers synthesized in Chapter III hold potential in this area, as do other types of copolymers both block, random, and branched. There is also a need to study fundamentally what about the polymer structure is causing the antibiofouling properties, and whether a glucose-based polymer can be designed that would capture that property while being better suited to the production of thin films and bulk materials.

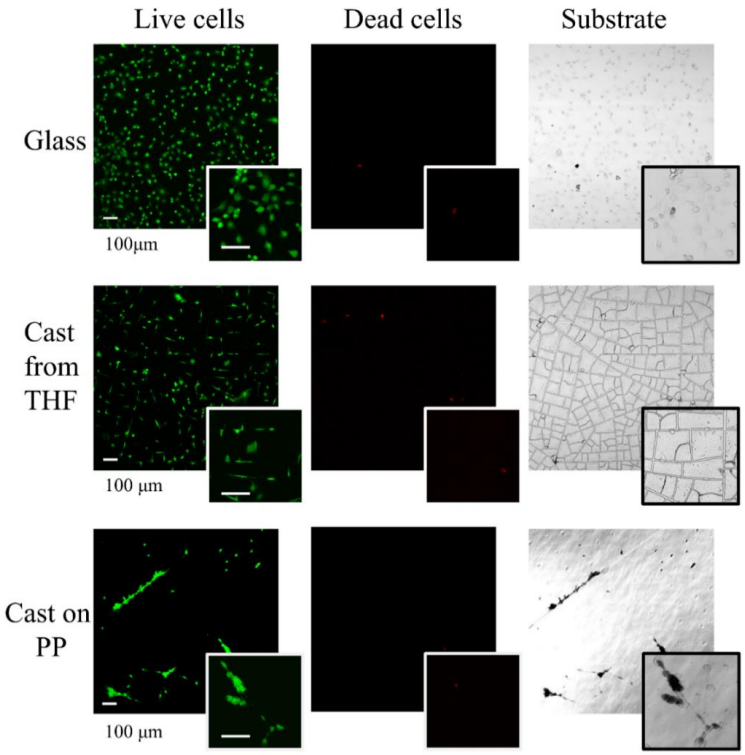

Figure VI.1. Fluorescence images of preosteoblast cells (MC3T3) grown on glass, a PMBGC thin film cast from THF onto glass, and a PMBGC thin film cast from THF onto polypropylene (PP). 24 h after cell placement, cells were tested with Live/Dead assay. Green fluorescence from live cells and red fluorescence from dead cells were imaged with a confocal microscope. Bright field images were also presented to show the morphology of the substrates. Scale bar 100 μm.

Chapter III demonstrated that PMGC, the hydroxyl side chain bearing derivative of PMBGC, was water soluble and can be used in the self-assembly of copolymers into 3D structures. There is significant interest in the production of water-soluble glucose carbonates. Towards this end another glucose monomer was developed (Figure VI.2) with a 6-membered cyclic carbonate, and the 2 and 3 positions being protected by benzyl groups. This monomer was able to undergo ROP to produce polymers, but the deprotection reaction was not realized, hydrogenolysis experiments should be undertaken to determine if these materials have potential as hydrophilic materials. A monomer with the 2 and 3 positions of glucose in a cyclic acetal group was also attempted in the pursuit of a deprotectable polymer, but initial synthetic attempts were not successful. The overall water solubility of PMGC and its ability to be used as a hydrophilic repeat unit in a copolymer should also be examined with different comonomers.

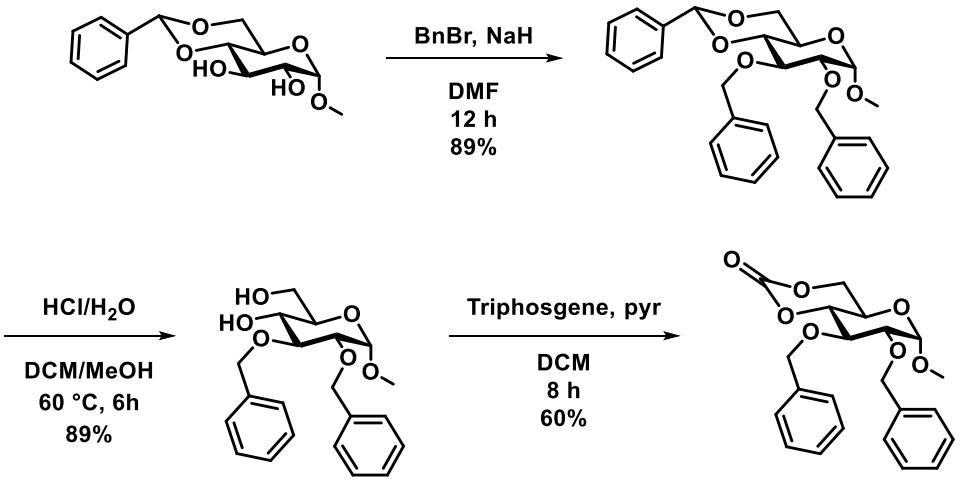

Figure VI.2. Synthesis of methyl 2,3-*O*-dibenzyl-4,6-*O*-carbonyl-α-D-glucopyranoside.

The dicarbonate materials of Chapter IV are currently the least exploited from this dissertation. Further studies into the kinetics of the polymerizations, the production of polymers with higher molar mass, and the accurate determination of branching would be useful. Examination of the changes in thermal and bulk properties of polymers and copolymers incorporating the MGDC monomer are also of interest to better demonstrate the structure property relationships within this system. Based on the production of organogels during the polymerizations of MGDC. A study of this monomer and hydrophilic polymers with reactive alcohol or amine side chains could be of interest towards the production of functional gel materials and hydrogels. Beyond this specific application MGDC holds great potential as a general crosslinking reagent for a variety of applications. Additionally there are several literature examples of using dicarbonate monomers to synthesize poly(hydroxyl urethane)s *via* condensation with a multifunctional amine, initial small molecule studies with MGDC demonstrated its potential but a more complete small molecule study that is then extended to the production of polymers is needed.

REFERENCES

(1) The new plastics economy rethinking the future of plastics http://www3.weforum.org/docs/WEF_The_New_Plastics_Economy.pdf (accessed 08/01/2018).

(2) Laura Parker, J. T. Fast Facts About Plastic Pollution. https://news.nationalgeographic.com/2018/05/plastics-facts-infographics-ocean-pollution/ (accessed 08/01/2018).

(3) Barnes, D. K. A.; Galgani, F.; Thompson, R. C.; Barlaz, M., Accumulation and fragmentation of plastic debris in global environments *Phil. Trans. R. Soc. B* **2009**, *364*, 1985-1998.

(4) Jambeck, J. R.; Geyer, R.; Wilcox, C.; Siegler, T. R.; Perryman, M.; Andrady, A.; Narayan, R.; Law, K. L., Plastic waste inputs from land into the ocean *Science* **2015**, *347*, 768-771.

(5) Great Pacific Garbage Patch. https://www.nationalgeographic.org/encyclopedia/great-pacific-garbage-patch/ (accessed 08/01/2018).

(6) Gewert, B.; Plassmann, M. M.; MacLeod, M., Pathways for degradation of plastic polymers floating in the marine environment *Environ. Sci.: Processes Impacts* **2015**, *17*, 1513-1521.

(7) Lambert, S.; Wagner, M., Formation of microscopic particles during the degradation of different polymers *Chemosphere* **2016**, *161*, 510-517.

(8) Andrady, A. L., Microplastics in the marine environment *Mar. Pollut. Bull.* **2011**, *62*, 1596-1605.

(9) Galloway, T. S.; Cole, M.; Lewis, C., Interactions of microplastic debris throughout the marine ecosystem *Nat. Ecol. Evol.* **2017**, *1*, 0116.

(10) Wright, S. L.; Kelly, F. J., Plastic and Human Health: A Micro Issue? *Environ. Sci. Technol.* **2017**, *51*, 6634-6647.

(11) Lusher, A., Microplastics in the Marine Environment: Distribution, Interactions and Effects. In *Marine Anthropogenic Litter*, Bergmann, M.; Gutow, L.; Klages, M., Eds. Springer International Publishing: Cham, 2015; pp 245-307.

(12) Luckachan, G.; Pillai, C. K. S., Biodegradable Polymers- A Review on Recent Trends and Emerging Perspectives *J. Polym. Environ.* **2011**, *19*, 637-676.

(13) Nair, L. S.; Laurencin, C. T., Biodegradable polymers as biomaterials *Prog. Polym. Sci.* **2007**, *32*, 762-798.

(14) Doppalapudi, S.; Jain, A.; Khan, W.; Domb, A. J., Biodegradable polymers—an overview *Polym. Adv. Technol.* **2014**, *25*, 427-435.

(15) Miller, S. A., Sustainable Polymers: Opportunities for the Next Decade *ACS Macro Lett.* **2013**, *2*, 550-554.

(16) Hill, M. R.; Kubo, T.; Goodrich, S. L.; Figg, C. A.; Sumerlin, B. S., Alternating Radical Ring-Opening Polymerization of Cyclic Ketene Acetals: Access to Tunable and Functional Polyester Copolymers *Macromolecules* **2018**, *51*, 5079-5084.

(17) Tardy, A.; Nicolas, J.; Gigmes, D.; Lefay, C.; Guillaneuf, Y., Radical Ring-Opening Polymerization: Scope, Limitations, and Application to (Bio)Degradable Materials *Chem. Rev.* **2017**, *117*, 1319-1406.

(18) Steinbach, T.; Wurm, F. R., Poly(phosphoester)s: A New Platform for Degradable Polymers *Angew. Chem. Int. Ed.* **2015**, *54*, 6098-6108.

(19) Li, Z.-L.; Zeng, F.-R.; Ma, J.-M.; Sun, L.-H.; Zeng, Z.; Jiang, H., Precision Aliphatic Polyesters with Alternating Microstructures via Cross-Metathesis Polymerization: An Event of Sequence Control *Macromol. Rapid Commun.* **2017**, *38*, 1700050.

(20) Maeda, T.; Kamimura, S.; Ohishi, T.; Takahara, A.; Otsuka, H., Synthesis of polyethylene/polyester copolymers through main chain exchange reactions via olefin metathesis *Polymer* **2014**, *55*, 6245-6251.

(21) Dove, A. P., Metal-Free Catalysis in Ring-Opening Polymerization. In *Handbook of Ring-Opening Polymerization*, Wiley-VCH Verlag GmbH & Co. KGaA: 2009; pp 357-378.

(22) Dove, A. P., Organic Catalysis for Ring-Opening Polymerization *ACS Macro Lett.* **2012**, *1*, 1409-1412.

(23) Gandini, A.; Lacerda, T. M.; Carvalho, A. J. F.; Trovatti, E., Progress of Polymers from Renewable Resources: Furans, Vegetable Oils, and Polysaccharides *Chem. Rev.* **2016**, *116*, 1637-1669.

(24) Xiao, R. Q.; Grinstaff, M. W., Chemical synthesis of polysaccharides and polysaccharide mimetics *Prog. Polym. Sci.* **2017**, *74*, 78-116.

(25) Ricapito, N. G.; Ghobril, C.; Zhang, H.; Grinstaff, M. W.; Putnam, D., Synthetic Biomaterials from Metabolically Derived Synthons *Chem. Rev.* **2016**, *116*, 2664-2704.

(26) Isikgor, F. H.; Becer, C. R., Lignocellulosic biomass: a sustainable platform for the production of bio-based chemicals and polymers *Polym. Chem.* **2015**, *6*, 4497-4559.

(27) Kristufek, S. L.; Wacker, K. T.; Tsao, Y. T.; Su, L.; Wooley, K. L., Monomer design strategies to create natural product-based polymer materials *Nat. Prod. Rep.* **2017**, *34*, 433-459.

(28) Philp, J. C.; Ritchie, R. J.; Allan, J. E. M., Biobased chemicals: the convergence of green chemistry with industrial biotechnology *Trends Biotechnol.* **2013**, *31*, 219-222.

(29) Rabnawaz, M.; Wyman, I.; Auras, R.; Cheng, S., A roadmap towards green packaging: the current status and future outlook for polyesters in the packaging industry *Green Chem.* **2017**, *19*, 4737-4753.

(30) Yao, K.; Tang, C., Controlled Polymerization of Next-Generation Renewable Monomers and Beyond *Macromolecules* **2013**, *46*, 1689-1712.

(31) Mülhaupt, R., Green Polymer Chemistry and Bio-based Plastics: Dreams and Reality *Macromol. Chem. Phys.* **2013**, *214*, 159-174.

(32) Holmberg, A. L.; Reno, K. H.; Wool, R. P.; Epps, I. I. I. T. H., Biobased building blocks for the rational design of renewable block polymers *Soft Matter* **2014**, *10*, 7405-7424.

(33) Xiao, R.; Dane, E. L.; Zeng, J.; McKnight, C. J.; Grinstaff, M. W., Synthesis of Altrose Poly-amido-saccharides with beta-N-(1-->2)-d-amide Linkages: A Right-Handed Helical Conformation Engineered in at the Monomer Level *J. Am. Chem. Soc.* **2017**, *139*, 14217-14223.

(34) Gregory, G. L.; Lopez-Vidal, E. M.; Buchard, A., Polymers from sugars: cyclic monomer synthesis, ring-opening polymerisation, material properties and applications *Chem. Commun.* **2017**, *53*, 2198-2217.

(35) Lopez-Vidal, E. M.; Gregory, G. L.; Kociok-Kohn, G.; Buchard, A., Polymers from sugars and CS2: synthesis and ring-opening polymerisation of sulfur-containing monomers derived from 2-deoxy-D-ribose and D-xylose *Polym. Chem.* **2018**, *9*, 1577-1582.

(36) Gregory, G. L.; Kociok-Kohn, G.; Buchard, A., Polymers from sugars and CO_2: ring-opening polymerisation and copolymerisation of cyclic carbonates derived from 2-deoxy-D-ribose *Polym. Chem.* **2017**, *8*, 2093-2104.

(37) Gregory, G. L.; Jenisch, L. M.; Charles, B.; Kociok-Kohn, G.; Buchard, A., Polymers from Sugars and CO_2: Synthesis and Polymerization of a D-Mannose-Based Cyclic Carbonate *Macromolecules* **2016**, *49*, 7165-7169.

(38) Pati, D.; Feng, X. S.; Hadjichristidis, N.; Gnanou, Y., Hydrophobic, Hydrophilic, and Amphiphilic Polyglycocarbonates with Linear and Macrocyclic Architectures from Bicyclic Glycocarbonates Derived from CO2 and Glucoside *Macromolecules* **2017**, *50*, 1362-1370.

(39) Pati, D.; Feng, X.; Hadjichristidis, N.; Gnanou, Y., CO_2 as versatile carbonation agent of glycosides: Synthesis of 5- and 6-membered cyclic glycocarbonates and investigation of their ring-opening *J. CO_2 Util.* **2018**, *24*, 564-571.

(40) Pati, D.; Chen, Z. L.; Feng, X. S.; Hadjichristidis, N.; Gnanou, Y., Synthesis of polyglycocarbonates through polycondensation of glucopyranosides with CO_2 *Polym. Chem.* **2017**, *8*, 2640-2646.

(41) Miura, Y., Design and synthesis of well-defined glycopolymers for the control of biological functionalities *Polym. J.* **2012**, *44*, 679-689.

(42) Pramudya, I.; Kim, C.; Chung, H., Synthesis and adhesion control of glucose-based bioadhesive via strain-promoted azide-alkyne cycloaddition *Polym. Chem.* **2018**, *9*, 3638-3650.

(43) Xu, J.; Feng, E.; Song, J., Renaissance of aliphatic polycarbonates: New techniques and biomedical applications *J. Appl. Polym. Sci.* **2014**, *131*, 39822.

(44) Wang, J.; He, Y.; Maitz, M. F.; Collins, B.; Xiong, K.; Guo, L.; Yun, Y.; Wan, G.; Huang, N., A surface-eroding poly(1,3-trimethylene carbonate) coating for fully biodegradable magnesium-based stent applications: Toward better biofunction, biodegradation and biocompatibility *Acta Biomater.* **2013**, *9*, 8678-8689.

(45) Fukushima, K.; Pratt, R. C.; Nederberg, F.; Tan, J. P. K.; Yang, Y. Y.; Waymouth, R. M.; Hedrick, J. L., Organocatalytic Approach to Amphiphilic Comb-Block Copolymers Capable of Stereocomplexation and Self-Assembly *Biomacromolecules* **2008**, *9*, 3051-3056.

(46) Brannigan, R. P.; Dove, A. P., Synthesis, properties and biomedical applications of hydrolytically degradable materials based on aliphatic polyesters and polycarbonates *Biomater. Sci.* **2016**, *5*, 9-21.

(47) García-Martín, M. G.; Pérez, R. R.; Hernández, E. B.; Espartero, J. L.; Muñoz-Guerra, S.; Galbis, J. A., Carbohydrate-Based Polycarbonates. Synthesis, Structure, and Biodegradation Studies *Macromolecules* **2005**, *38*, 8664-8670.

(48) Lonnecker, A. T.; Lim, Y. H.; Felder, S. E.; Besset, C. J.; Wooley, K. L., Four Different Regioisomeric Polycarbonates Derived from One Natural Product, D-Glucose *Macromolecules* **2016**, *49*, 7857-7867.

(49) Feng, L.; Zhu, W.; Li, C.; Guan, G.; Zhang, D.; Xiao, Y.; Zheng, L., A high-molecular-weight and high-Tg poly(ester carbonate) partially based on isosorbide: synthesis and structure-property relationships *Polym. Chem.* **2015**, *6*, 633-642.

(50) Taherimehr, M.; Pescarmona, P. P., Green polycarbonates prepared by the copolymerization of CO_2 with epoxides *J. Appl. Polym. Sci.* **2014**, *131*, 41141.

(51) Liu, Y.; Zhou, H.; Guo, J.-Z.; Ren, W.-M.; Lu, X.-B., Completely Recyclable Monomers and Polycarbonate: Approach to Sustainable Polymers *Angew. Chem. Int. Ed.* **2017**, *56*, 4862-4866.

(52) Tsai, F.-T.; Wang, Y.; Darensbourg, D. J., Environmentally Benign CO_2-Based Copolymers: Degradable Polycarbonates Derived from Dihydroxybutyric Acid and Their Platinum–Polymer Conjugates *J. Am. Chem. Soc.* **2016**, *138*, 4626-4633.

(53) Xu, Y.; Lin, L.; Xiao, M.; Wang, S.; Smith, A. T.; Sun, L.; Meng, Y., Synthesis and properties of CO_2-based plastics: Environmentally-friendly, energy-saving and biomedical polymeric materials *Prog. Polym. Sci.* **2018**, *80*, 163-182.

(54) Poland, S. J.; Darensbourg, D. J., A quest for polycarbonates provided via sustainable epoxide/CO_2 copolymerization processes *Green Chem.* **2017**, *19*, 4990-5011.

(55) Mespouille, L.; Coulembier, O.; Kawalec, M.; Dove, A. P.; Dubois, P., Implementation of metal-free ring-opening polymerization in the preparation of aliphatic polycarbonate materials *Prog. Polym. Sci.* **2014**, *39*, 1144-1164.

(56) Mikami, K.; Lonnecker, A. T.; Gustafson, T. P.; Zinnel, N. F.; Pai, P. J.; Russell, D. H.; Wooley, K. L., Polycarbonates derived from glucose via an organocatalytic approach *J. Am. Chem. Soc.* **2013**, *135*, 6826-6829.

(57) Nederberg, F.; Lohmeijer, B. G. G.; Leibfarth, F.; Pratt, R. C.; Choi, J.; Dove, A. P.; Waymouth, R. M.; Hedrick, J. L., Organocatalytic Ring Opening Polymerization of Trimethylene Carbonate *Biomacromolecules* **2007**, *8*, 153-160.

(58) Su, L.; Khan, S.; Fan, J.; Lin, Y.-N.; Wang, H.; Gustafson, T. P.; Zhang, F.; Wooley, K. L., Functional sugar-based polymers and nanostructures comprised of degradable poly(D-glucose carbonate)s *Polym. Chem.* **2017**, *8*, 1699-1707.

(59) Pati, D.; Feng, X.; Hadjichristidis, N.; Gnanou, Y., Hydrophobic, Hydrophilic, and Amphiphilic Polyglycocarbonates with Linear and Macrocyclic Architectures from Bicyclic Glycocarbonates Derived from CO_2 and Glucoside *Macromolecules* **2017**, *50*, 1362-1370.

(60) Gregory, G. L.; Hierons, E. M.; Kociok-Kohn, G.; Sharma, R. I.; Buchard, A., CO_2-Driven stereochemical inversion of sugars to create thymidine-based polycarbonates by ring-opening polymerisation *Polym. Chem.* **2017**, *8*, 1714-1721.

(61) Nuyken, O.; Pask, S., Ring-Opening Polymerization—An Introductory Review *Polymers* **2013**, *5*, 361-403.

(62) Comerford, J. W.; Ingram, I. D. V.; North, M.; Wu, X., Sustainable metal-based catalysts for the synthesis of cyclic carbonates containing five-membered rings *Green Chem.* **2015**.

(63) Kamber, N. E.; Jeong, W.; Waymouth, R. M.; Pratt, R. C.; Lohmeijer, B. G. G.; Hedrick, J. L., Organocatalytic Ring-Opening Polymerization *Chem. Rev.* **2007**, *107*, 5813-5840.

(64) Lin, B.; Waymouth, R. M., Organic Ring-Opening Polymerization Catalysts: Reactivity Control by Balancing Acidity *Macromolecules* **2018**, *51*, 2932-2938.

(65) Pratt, R. C.; Lohmeijer, B. G.; Long, D. A.; Waymouth, R. M.; Hedrick, J. L., Triazabicyclodecene: a simple bifunctional organocatalyst for acyl transfer and ring-opening polymerization of cyclic esters *Journal of the American Chemical Society* **2006**, *128*, 4556-4557.

(66) Shen, Y.; Chen, X.; Gross, R. A., Polycarbonates from Sugars: Ring-Opening Polymerization of 1,2-O-Isopropylidene-D-Xylofuranose-3,5- Cyclic Carbonate (IPXTC) *Macromolecules* **1999**, *32*, 2799-2802.

(67) Shen, Y.; Chen, X.; Gross, R. A., Aliphatic Polycarbonates with Controlled Quantities of D-Xylofuranose in the Main Chain *Macromolecules* **1999**, *32*, 3891-3897.

(68) Suzuki, M.; Sekido, T.; Matsuoka, S.; Takagi, K., Syntheses of Aliphatic Polycarbonates from 2′-Deoxyribonucleosides *Biomacromolecules* **2011**, *12*, 1449-1459.

(69) Haba, O.; Tomizuka, H.; Endo, T., Anionic Ring-Opening Polymerization of Methyl 4,6-O-Benzylidene-2,3-O- carbonyl-α-D-glucopyranoside: A First Example of Anionic Ring-Opening Polymerization of Five-Membered Cyclic Carbonate without Elimination of CO_2 *Macromolecules* **2005**, *38*, 3562-3563.

(70) Galbis, J. A.; García-Martín, M. G., Synthetic polymers from readily available monosaccharides. In *Top. Curr. Chem.*, 2010; Vol. 295, pp 147-176.

(71) Gustafson, T. P.; Lonnecker, A. T.; Heo, G. S.; Zhang, S.; Dove, A. P.; Wooley, K. L., Poly(D-glucose carbonate) block copolymers: a platform for natural product-based nanomaterials with Solvothermatic characteristics *Biomacromolecules* **2013**, *14*, 3346-3353.

(72) Tezuka, K.; Komatsu, K.; Haba, O., The anionic ring-opening polymerization of five-membered cyclic carbonates fused to a cyclohexane ring *Polym. J.* **2013**, *44*, 1183-1187.

(73) Tezuka, K.; Koda, K.; Katagiri, H.; Haba, O., Anionic ring-opening polymerization of five-membered cyclic carbonates derived from aldohexopyranosides *Polym. Bull.* **2015**, 1-12.

(74) Galbis, J. A.; García-Martín, M. G.; de Paz, M. V.; Galbis, E., Synthetic Polymers from Sugar-Based Monomers *Chem. Rev.* **2016**, *116*, 1600-1636.

(75) Su, L.; Li, R.; Khan, S.; Clanton, R.; Zhang, F.; Lin, Y. N.; Song, Y.; Wang, H.; Fan, J.; Hernandez, S.; Butters, A. S.; Akabani, G.; MacLoughlin, R.; Smolen, J.; Wooley, K. L., Chemical Design of Both a Glutathione-Sensitive Dimeric Drug Guest and a Glucose-Derived Nanocarrier Host to Achieve Enhanced Osteosarcoma Lung Metastatic Anticancer Selectivity *J. Am. Chem. Soc.* **2018**, *140*, 1438-1446.

(76) Felder, S. E.; Redding, M. J.; Noel, A.; Grayson, S. M.; Wooley, K. L., Organocatalyzed ROP of a Glucopyranoside Derived Five-Membered Cyclic Carbonate *Macromolecules* **2018**, *51*, 1787-1797.

(77) Su, L.; Khan, S.; Fan, J. W.; Lin, Y. N.; Wang, H.; Gustafson, T. P.; Zhang, F. W.; Wooley, K. L., Functional sugar-based polymers and nanostructures comprised of degradable poly(D-glucose carbonate)s *Polym. Chem.* **2017**, *8*, 1699-1707.

(78) Song, Y.; Chen, Y.; Su, L.; Li, R.; Letteri, R. A.; Wooley, K. L., Crystallization-driven assembly of fully degradable, natural product-based poly(l-lactide)-block-poly(α-d-glucose carbonate)s in aqueous solution *Polymer* **2017**, *122*, 270-279.

(79) Myers, D.; Cyriac, A.; Williams, C. K., Polymer synthesis: To react the impossible ring *Nat. Chem.* **2016**, *8*, 3-4.

(80) Tomita, H.; Sanda, F.; Endo, T., Reactivity comparison of five- and six-membered cyclic carbonates with amines: Basic evaluation for synthesis of poly(hydroxyurethane) *J. Polym. Sci., Part A: Polym. Chem.* **2001**, *39*, 162-168.

(81) Endo, T. K., K.; Ochiai, B.; Nagai, D., Synthesis and Chemical Recycling of a Polycarbonate Obtained by Anionic Ring-Opening Polymerization of a Bifunctional Cyclic Carbonate *Macromolecules* **2005**, *38*, 8177-8182.

(82) Hong, M.; Chen, E. Y. X., Coordination Ring-Opening Copolymerization of Naturally Renewable α-Methylene-γ-butyrolactone into Unsaturated Polyesters *Macromolecules* **2014**, *47*, 3614-3624.

(83) Hong, M.; Chen, E. Y. X., Towards Truly Sustainable Polymers: A Metal-Free Recyclable Polyester from Biorenewable Non-Strained γ-Butyrolactone *Angew. Chem. Int. Ed.* **2016**, *55*, 4188-4193.

(84) Nifant'ev, I.; Shlyakhtin, A.; Bagrov, V.; Lozhkin, B.; Zakirova, G.; Ivchenko, P.; Legon'kova, O., Theoretical and experimental studies of 1,5,7-triazabicyclo[4.4.0]dec-5-ene-catalyzed ring opening/ring closure reaction mechanism for 5-, 6- and 7-membered cyclic esters and carbonates *Reac. Kinet. Mech. Cat.* **2016**, *117*, 447-476.

(85) Lee, J.-C.; Litt, M. H., Ring-Opening Polymerization of Ethylene Carbonate and Depolymerization of Poly(ethylene oxide-co-ethylene carbonate) *Macromolecules* **2000**, *33*, 1618-1627.

(86) Elmér, A. M.; Jannasch, P., Synthesis and characterization of poly(ethylene oxide-co-ethylene carbonate) macromonomers and their use in the preparation of crosslinked polymer electrolytes *J. Polym. Sci., Part A: Polym. Chem.* **2006**, *44*, 2195-2205.

(87) Kapiti, G.; Keul, H.; Möller, M., Organocatalytic polymerization of ethylene carbonate *Mater. Today Commun.* **2015**, *5*, 1-9.

(88) Haba, O.; Furuichi, N.; Akashika, Y., Anionic Ring-Opening Copolymerization of L-Lactide with a Five-Membered Cyclic Carbonate Having a Glucopyranoside Structure *Polym. J.* **2009**, *41*, 702-708.

(89) Diallo, A. K.; Kirillov, E.; Slawinski, M.; Brusson, J.-M.; Guillaume, S. M.; Carpentier, J.-F., Syndioselective ring-opening polymerization and copolymerization of trans-1,4-cyclohexadiene carbonate mediated by achiral metal- and organo-catalysts *Polym. Chem.* **2015**, *6*, 1961-1971.

(90) Diallo, A. K.; Guerin, W.; Slawinski, M.; Brusson, J.-M.; Carpentier, J.-F.; Guillaume, S. M., Block and Random Copolymers of 1,2-Cyclohexyl Cyclocarbonate and L-Lactide or Trimethylene Carbonate Synthesized by Ring-Opening Polymerization *Macromolecules* **2015**, *48*, 3247-3256.

(91) Guerin, W.; Diallo, A. K.; Kirilov, E.; Helou, M.; Slawinski, M.; Brusson, J.-M.; Carpentier, J.-F.; Guillaume, S. M., Enantiopure Isotactic PCHC Synthesized by Ring-Opening Polymerization of Cyclohexene Carbonate *Macromolecules* **2014**, *47*, 4230-4235.

(92) Doane, W. M.; Shasha, B. S.; Stout, E. I.; Russell, C. R.; Rist, C. E., A facile route to trans cyclic carbonates of sugars *Carbohydr. Res.* **1967**, *4*, 445-451.

(93) Doane, W. M.; Shasha, B. S.; Stout, E. I.; Russell, C. R.; Rist, C. E., Ring-opening reactions of trans-carbonates and thionocarbonates *Carbohydr. Res.* **1969**, *11*, 321-329.

(94) Li, Y.; Hoskins, J. N.; Sreerama, S. G.; Grayson, M. A.; Grayson, S. M., The identification of synthetic homopolymer end groups and verification of their transformations using MALDI-TOF mass spectrometry *J. Mass Spectrom.* **2010**, *45*, 587-611.

(95) Fukushima, K.; Lecuyer, J. M.; Wei, D. S.; Horn, H. W.; Jones, G. O.; Al-Megren, H. A.; Alabdulrahman, A. M.; Alsewailem, F. D.; McNeil, M. A.; Rice, J. E.; Hedrick, J. L., Advanced chemical recycling of poly(ethylene terephthalate) through organocatalytic aminolysis *Polym. Chem.* **2013**, *4*, 1610-1616.

(96) Horn, H. W.; Jones, G. O.; Wei, D. S.; Fukushima, K.; Lecuyer, J. M.; Coady, D. J.; Hedrick, J. L.; Rice, J. E., Mechanisms of Organocatalytic Amidation and Trans-Esterification of Aromatic Esters As a Model for the Depolymerization of Poly(ethylene) Terephthalate *J. Phys. Chem. A* **2012**, *116*, 12389-12398.

(97) Leibfarth, F. A.; Moreno, N.; Hawker, A. P.; Shand, J. D., Transforming polylactide into value-added materials *J. Polym. Sci., Part A: Polym. Chem.* **2012**, *50*, 4814-4822.

(98) Grayson, S. M.; Myers, B. K.; Bengtsson, J.; Malkoch, M., Advantages of Monodisperse and Chemically Robust "SpheriCal" Polyester Dendrimers as a "Universal" MS Calibrant *J. Am. Soc. Mass Spectrom.* **2014**, *25*, 303-309.

(99) Wilbon, P. A.; Chu, F.; Tang, C., Progress in renewable polymers from natural terpenes, terpenoids, and rosin *Macromol. Rapid Commun.* **2013**, *34*, 8-37.

(100) Brendel, J. C.; Schacher, F. H., Block Copolymer Self-Assembly in Solution—Quo Vadis? *Chem. - Asian J.* **2018**, *13*, 230-239.

(101) Elsabahy, M.; Wooley, K. L., Design of polymeric nanoparticles for biomedical delivery applications *Chem. Soc. Rev.* **2012**, *41*, 2545-2561.

(102) Epps, I. I. I. T. H.; O'Reilly, R. K., Block copolymers: controlling nanostructure to generate functional materials - synthesis, characterization, and engineering *Chem. Sci.* **2016**, *7*, 1674-1689.

(103) Tritschler, U.; Pearce, S.; Gwyther, J.; Whittell, G. R.; Manners, I., 50th Anniversary Perspective: Functional Nanoparticles from the Solution Self-Assembly of Block Copolymers *Macromolecules* **2017**, *50*, 3439-3463.

(104) Blanazs, A.; Armes, S. P.; Ryan, A. J., Self-Assembled Block Copolymer Aggregates: From Micelles to Vesicles and their Biological Applications *Macromol. Rapid Commun.* **2009**, *30*, 267-277.

(105) Schacher, F. H.; Rupar, P. A.; Manners, I., Functional Block Copolymers: Nanostructured Materials with Emerging Applications *Angew. Chem. Int. Ed.* **2012**, *51*, 7898-7921.

(106) Dararatana, N.; Seidi, F.; Crespy, D., pH-Sensitive Polymer Conjugates for Anticorrosion and Corrosion Sensing *ACS Appl. Mater. Interfaces* **2018**.

(107) Shibata, M.; Matsumoto, M.; Hirai, Y.; Takenaka, M.; Sawamoto, M.; Terashima, T., Intramolecular Folding or Intermolecular Self-Assembly of Amphiphilic Random Copolymers: On-Demand Control by Pendant Design *Macromolecules* **2018**, *51*, 3738-3745.

(108) Imai, S.; Hirai, Y.; Nagao, C.; Sawamoto, M.; Terashima, T., Programmed Self-Assembly Systems of Amphiphilic Random Copolymers into Size-Controlled and Thermoresponsive Micelles in Water *Macromolecules* **2018**, *51*, 398-409.

(109) Voo, Z. X.; Khan, M.; Narayanan, K.; Seah, D.; Hedrick, J. L.; Yang, Y. Y., Antimicrobial/Antifouling Polycarbonate Coatings: Role of Block Copolymer Architecture *Macromolecules* **2015**, *48*, 1055-1064.

(110) Ferji, K.; Venturini, P.; Cleymand, F.; Chassenieux, C.; Six, J.-L., In situ glyco-nanostructure formulation via photo-polymerization induced self-assembly *Polym. Chem.* **2018**, *9*, 2868-2872.

(111) Thomas, A. W.; Dove, A. P., Postpolymerization Modifications of Alkene-Functional Polycarbonates for the Development of Advanced Materials Biomaterials *Macromol. Biosci.* **2016**, *16*, 1762-1775.

(112) Hedir, G. G.; Arno, M. C.; Langlais, M.; Husband, J. T.; O'Reilly, R. K.; Dove, A. P., Poly(oligo(ethylene glycol) vinyl acetate)s: A Versatile Class of Thermoresponsive and Biocompatible Polymers *Angew. Chem. Int. Ed.* **2017**, *56*, 9178-9182.

(113) Doncom, K. E. B.; Blackman, L. D.; Wright, D. B.; Gibson, M. I.; O'Reilly, R. K., Dispersity effects in polymer self-assemblies: a matter of hierarchical control *Chem. Soc. Rev.* **2017**, *46*, 4119-4134.

(114) Zhao, J. Q.; Liu, J. J.; Han, S. C.; Deng, H. Z.; Deng, L. D.; Liu, J. F.; Meng, A. M.; Dong, A. J.; Zhang, J. H., Acid-induced disassemblable nanoparticles based on cyclic benzylidene acetal-functionalized graft copolymer via sequential RAFT and ATRP polymerization *Polym. Chem.* **2014**, *5*, 1852-1856.

(115) Hu, Z.; Chen, Y.; Huang, H.; Liu, L.; Chen, Y., Well-Defined Poly(α-amino-δ-valerolactone) via Living Ring-Opening Polymerization *Macromolecules* **2018**, *51*, 2526-2532.

(116) Okada, M., Molecular design and syntheses of glycopolymers *Prog. Polym. Sci.* **2001**, *26*, 67-104.

(117) Ladmiral, V.; Melia, E.; Haddleton, D. M., Synthetic glycopolymers: an overview *Eur. Polym. J.* **2004**, *40*, 431-449.

(118) Bonduelle, C.; Lecommandoux, S., Synthetic Glycopolypeptides as Biomimetic Analogues of Natural Glycoproteins *Biomacromolecules* **2013**, *14*, 2973-2983.

(119) Galbis, J. A.; García-Martín, M. G., Chapter 5 - Sugars as Monomers. In *Monomers, Polymers and Composites from Renewable Resources*, Gandini, M. N. B., Ed. Elsevier: Amsterdam, 2008; pp 89-114.

(120) Xiao, R.; Zeng, J.; Grinstaff, M. W., Biologically Active Branched Polysaccharide Mimetics: Synthesis via Ring-Opening Polymerization of a Maltose-Based β-Lactam *ACS Macro Lett.* **2018**, 772-777.

(121) Lonnecker, A. T.; Lim, Y. H.; Wooley, K. L., Functional Polycarbonate of a d-Glucal-Derived Bicyclic Carbonate via Organocatalytic Ring-Opening Polymerization *ACS Macro Lett.* **2017**, *6*, 748-753.

(122) Mammen, M.; Choi, S.-K.; Whitesides, G. M., Polyvalent Interactions in Biological Systems: Implications for Design and Use of Multivalent Ligands and Inhibitors *Angew. Chem. Int. Ed.* **1998**, *37*, 2754-2794.

(123) Lundquist, J. J.; Toone, E. J., The Cluster Glycoside Effect *Chem. Rev.* **2002**, *102*, 555-578.

(124) Kiessling, L. L.; Pohl, N. L., Strength in numbers: non-natural polyvalent carbohydrate derivatives *Chemistry & Biology* **1996**, *3*, 71-77.

(125) Hideharu Mori, A. H. E. M., Peter F. W. Simon, Linear Versus (Hyper)branched Polymers. In *Macromolecular Engineering*.

(126) Voit, B. I.; Lederer, A., Hyperbranched and Highly Branched Polymer Architectures—Synthetic Strategies and Major Characterization Aspects *Chem. Rev.* **2009**, *109*, 5924-5973.

(127) England, R. M.; Rimmer, S., Hyper/highly-branched polymers by radical polymerisations *Polym. Chem.* **2010**, *1*, 1533-1544.

(128) Pal, S.; Brooks, W. L. A.; Dobbins, D. J.; Sumerlin, B. S., Employing a Sugar-Derived Dimethacrylate to Evaluate Controlled Branch Growth during Polymerization with Multiolefinic Compounds *Macromolecules* **2016**, *49*, 9396-9405.

(129) Zhang, J.; Schneiderman, D. K.; Li, T.; Hillmyer, M. A.; Bates, F. S., Design of Graft Block Polymer Thermoplastics *Macromolecules* **2016**, *49*, 9108-9118.

(130) Zhang, J.; Li, T.; Mannion, A. M.; Schneiderman, D. K.; Hillmyer, M. A.; Bates, F. S., Tough and Sustainable Graft Block Copolymer Thermoplastics *ACS Macro Lett.* **2016**, *5*, 407-412.

(131) Besset, C. J.; Lonnecker, A. T.; Streff, J. M.; Wooley, K. L., Polycarbonates from the Polyhydroxy Natural Product Quinic Acid *Biomacromolecules* **2011**, *12*, 2512-2517.

(132) Link, L. A.; Lonnecker, A. T.; Hearon, K.; Maher, C. A.; Raymond, J. E.; Wooley, K. L., Photo-cross-linked Poly(thioether-co-carbonate) Networks Derived from the Natural Product Quinic Acid *ACS Appl. Mater. Interfaces* **2014**, *6*, 17370-17375.

(133) Noel, A.; Borguet, Y. P.; Raymond, J. E.; Wooley, K. L., Poly(carbonate–amide)s Derived from Bio-Based Resources: Poly(ferulic acid-co-tyrosine) *Macromolecules* **2014**, *47*, 2974-2983.

(134) Noel, A.; Borguet, Y. P.; Raymond, J. E.; Wooley, K. L., Poly(ferulic acid--tyrosine): Effect of the Regiochemistry on the Photophysical and Physical Properties en Route to Biomedical Applications *Macromolecules* **2014**, *47*, 7109-7117.

(135) Geyer, R.; Jambeck, J. R.; Law, K. L., Production, use, and fate of all plastics ever made *Sci. Adv.* **2017**, *3*.

(136) Arca, H. C.; Mosquera-Giraldo, L. I.; Bi, V.; Xu, D.; Taylor, L. S.; Edgar, K. J., Pharmaceutical Applications of Cellulose Ethers and Cellulose Ether Esters *Biomacromolecules* **2018**, *19*, 2351-2376.